SCIENZE DELL'INGEGNERIA CIVILE

SCUOLA DOTTORALE / DOTTORATO DI RICERCA IN

XXVI CICLO

CICLO DEL CORSO DI DOTTORATO

NONLINEAR STATIC PROCEDURES FOR ANALYSIS AND RETROFITTING OF EXISTING BUILDINGS WITH DISSIPATIVE BRACES

Titolo della tesi

XU LIU _____

Nome e Cognome del dottorando firma

PROF. CAMILLO NUTI _____

Docente Guida/Tutor: Prof. firma

PROF.ALDO FIORI _____

Coordinatore: Prof. firma

Collana delle tesi di Dottorato di Ricerca
In Scienze dell'Ingegneria Civile
Università degli Studi Roma Tre
Tesi n° 45

Abstract

Nonlinear Static Procedures (NSPs), often called pushover analyses, are deemed to be very practical tools to assess the nonlinear seismic performance of structures. The use of NSPs for the seismic assessment of plan regular buildings and bridges is widespread nowadays. The use of NSPs in the case of real existing structures, which are almost always irregular, has so far been studied by a limited number of authors. This fact limits the application of NSPs to assess current existing structures. In order to improve the use of NSPs in practical, the applicability of NSPs for analysis and retrofitting of existing buildings with dissipative braces is evaluated in this thesis. In this work, a more efficient incremental modal pushover analysis (IMPA) to obtain capacity curve of the structure to evaluate the seismic demand is proposed: the procedure allows defining the capacity curve based on the execution of a series of MPAs. The case studies chosen are a benchmark structure as the regular structure and a real existing reinforced concrete building, which shows a strong irregularity in plan and vertical.Comparative evaluation of the different commonly used NSPs, which are Capacity Spectrum Method (CSM) adopted in ATC-40, Displacement Coefficient Method integrated into FEMA356, and N2 method presented in Eurocode 8 and modal pushover analysis (MPA), to describe their relative accurancy and limitations. A displacement based design procedure of dissipative devices for seismic upgrading structures is applied to the exising builidng. The accuracy of the IMPA is evaluated by comparison with IDA curve for the regular and irregular structure. Force-based and displacement design procedure of passive energy dissipation devices are applied to retrofit a school building located in shanghai, the comparisons of the two design methods and the seismic behavior of the retrofitting structure with different passive energy dissipation devices are discussed.

Contents

Figures index

Tables index

Symbol Index

m	mass matrices of the system
c	classical damping matrices of the system
k	lateral stiffness matrices of the system
u	floor displacement
ι	influence vector
$\ddot{u}_g(t)$	ground motion
ϕ	shape vector
u_t	roof/top displacement
u^*	reference displacement of the SDOF system
V_b	Base Shear
u_t	Roof Displacement
V_y	yield strength
Ke	effective elastic stiffness
Ks	hardening/softening stiffness
α	strain-hardening ratio
T_{eq}	initial period of the equivalent SDOF system
d_t^*	trial peak deformation demand
ξ_{eq}	equivalent damping ratio
ξ_0	inherent damping of the structure
k	a damping modification factor
ξ_h	hysteretic damping
Γ	modal participation factor
C_0	the modification factor to relate spectral displacement of an equivalent SDOF system to the roof displacement of the building
C_1	the modification factor to relate expected maximum inelastic displacements to displacements calculated for linear elastic response
C_2	the modification factor to represent the effect of pinched hysteretic shape, stiffness degradation and strength deterioration on maximum displacement response
C_3	the modification factor to represent increased displacements due to dynamic P-Δ effects
S_a	the response spectrum acceleration at the effective fundamental period and damping ratio (5% in this study) of the building
T_e	the effective fundamental period of the building in the direction under consideration
fs	lateral force
s_n	modal inertia force distribution
w_n	natural vibration frequency
ξ_n	the damping ratio for the nth mode
$q_n(t)$	modal coordinate
$r(t)$	response quantity

r_n^{st}	modal static response
$D_n(t)$	movement of linear SDF system
F_i	lateral load applied at floor level i
m_i	he floor mass
h_i	the story height
k	the period-dependent coefficient
ϕ_i	amplitude of the fundamental mode at level i
i	the floor number
j	the mode number
ϕ_{ij}	amplitude of mode j at level i
$Sa_j(\xi_j, T_j)$	the spectral acceleration at the period T_j
I_0	diagonal matrix with I_{0jj}= I_{0j} the polar moment of inertia of jth floor diaphragm
a_λ	non-negative scalar
λ	scale factor (SF)
a_1	unscaled accelerogram
ξ_{ni}	effective damping for nth mode
ξ_0	the inherent damping of the elastic structure
E_{dni}	the energy dissipated in an ideal hysteretic cycle
E_{s0ni}	the maximum strain energy that the structure dissipates
V_{bmmi}	multimodal base shear
u_{rmmi}	multimodal roof displacement
ν_{eq}	equivalent viscous damping
$K'_{b,j}$	the elastic axial stiffness
$F'_{b,j}$	the yield strength
$\beta_{b,j}$	the hardening ratio
θ_b	the inclination of each brace
K_b	the horizontal components of stiffness
F_{by}	the horizontal components of yield strength
D_{by}	the horizontal components of displacement
δ_j	the interstorey drift
$\nu_{eq,s}$	the equivalent viscous damping of the structure
$E_{D,S}$	the energy dissipated in a single cycle of amplitude D
$E_{S,S}$	the elastic strain energy corresponding to the displacement D
D	the displacement reached from the structure
$F_s(D)$	the force corresponding to D (the force is the base shear)
D_{sy}	displacement at yielding
F_{sy}	the yielding force (base shear at yielding)
$E_{D,B}^{bilinear}$	the energy dissipated by the ideal hysteretic cycle of the dissipative brace
χ_S	corrective coefficient for the structure

χ_B	corrective coefficient for the braces
$\nu_{eq,S+B}$	equivalent viscous damping of the braced structure
ν_I	the inherent damping
$E_{D,B,j}^{bilinear}$	the energy dissipated by the dissipative braces placed at level *j*
$E_{D,B,i}^{bilinear}$	the energy dissipated by the *i* braces placed at level *j*
$\nu_{eq,S}$	equivalent viscous damping provided by the original structure
$\nu_{eq,B}$	equivalent viscous damping provided by the braces
ν_{tot}	total damping for the braced structure
$K'_{b,j}$	the equivalent stiffness of the spring series in the plastic range
$K'_{p,i}$	the equivalent stiffness of the spring series in the plastic range
$A_{d,j}$	cross section of BRBs
$f_{dy,j}$	the yielding stress of the device
$E_{d,j}$	the e elastic modulus of the device
$l_{d,j}$	the length of the device
V_R	the reference design life
P_{VR}	probability of exceedance of the seismic action
V_N	the nominal life
T_R	the return period
C_N	the importance coefficient
$\sigma(T_i)$	the standard devisation of the response spectrums of the natutral records in correspondence of the period T_i
$S_{aj}(T_i)$	the pseudo-acceleration of the *j*th spectrum
$\overline{S_a}(T_i)$	the mean pseudo-acceleration,
N	the number of the natural records
F_d	the damping force of a single viscous damper
C	the damping factor
v	the velocity of the viscous damper
a	damper parameter
K	storage stiffness of the damper
β	ratio of post stiffness
u_y	the yield displacement
$Z(t)$	the evolutionary variable
F	the story shearing force

1. Introduction

In recent years, as a result of seismic events occurred in Italy, the safety of buildings has become a topic of considerable interest. Therefore it is very important to develop fast and reliable analysis procedures to identify the safety level of existing structures.

The nonlinear dynamic time-history analysis is considered to be the most accurate method for the seismic assessment/design of structures. Nonlinear dynamic time-history analysis utilizes the combination of ground motion records with a detailed structural model, therefore is capable of producing results with relatively low uncertainty. In nonlinear dynamic analyses, the detailed structural model subjected to a ground-motion record produces estimates of component deformations for each degree of freedom in the model. Since the properties of the seismic response depend on the intensity, or severity, of the seismic shaking, a comprehensive assessment calls for numerous nonlinear dynamic analyses at various levels of intensity to represent different possible earthquake scenarios. This has led to the emergence of methods like the Incremental Dynamic Analysis.

Nonlinear dynamic time-history analyses are very time-consuming, which is a relevant drawback in design offices. Additionally the response derived from such an analysis is generally very sensitive to the characteristics of the ground motions as well as the material models used. All these render it quite impractical for everyday use, especially when overly complex structures need to be considered.

Nonlinear Static Procedures (NSPs) are deemed to be very practical tools to assess the nonlinear seismic performance of structures. In a pushover analysis, a mathematical model of the building, that includes all significant lateral force resisting members, is subjected to a monotonically increasing invariant (or adaptive) lateral force (or displacement) pattern until a pre-determined target displacement is reached or the building is on the verge of incipient collapse. Seismic design codes, like the FEMA273, FEMA356, FEMA440, ATC40 and Eurocode 8, have recommended the use of this type of procedures.

The use of NSPs for the seismic assessment of plan regular buildings and bridges is widespread nowadays. Their good performance in such cases is widely supported by the extensive number of scientific studies described in the previous studies.

However, capability of NSPs to closely correlate results from inelastic dynamic analysis has been checked with reference either to idealized building models or to geometrically simple tested structures. Real structures are almost always irregular as perfect regularity is an idealization that very rarely occurs. Structural irregularities may vary dramatically in their nature and, in principle, are very difficult to define. Actually, irregularity conditions in existing buildings can go far beyond the code definition of plan (and vertical) irregularity and, in any case, it is very likely that vertical and plan irregularities are combined. The use of NSPs in the case of real existing structures has so far been studied by a limited number of authors. This fact limits the application of NSPs to assess current existing structures.

Due to the development of NSP to evaluate the seismic demands of the structure, it is of a great interest to replace the NL_RHA for each given seismic intensity level by NSP to reduce the computational effort required for IDA. Remembering that MPA procedure retains the conceptual simplicity and computational attractiveness of current pushover procedures with invariant force distributions, it is of great interest to obtain capacity curves by replacing the nonlinear response history analysis of the IDA procedure with Modal Pushover Analysis (MPA).

Another important use of NSPs is for the seismic retrofit of existing buildings. A displacement-based procedure to design dissipative bracings for the seismic protection of frame structures was proposed by Bergami & Nuti (2013): the procedure uses the capacity spectrum method, and no dynamic non linear analyses are needed. Two performance objectives have been considered developing the procedure: protect the structure against structural damage or collapse and avoid non-structural damage as well as excessive base shear. The compliance is obtained dimensioning dissipative braces to limit global displacements and interstorey drifts. In the design procedure, the capacity spectrum method is adopted to evaluate the seismic response of the existing or retrofitting buildings in terms of global displacement and interstorey drifts to evaluate the required equivalent viscous damping, valuate the additional equivalent viscous damping contribution due to the naked structure and braces, and check whether the insertion of the dissipative brace could make the structure satisfy performance requirement. In that paper, the procedure was validated through a comparison with nonlinear dynamic response of two 2D R.C. frames and a simple existing structure. In fact, frequently, the characteristics of an existing building (e.g. non regular distribution of

masses and stiffness, presence of a soft story) can compromise the effectiveness of procedures that impose a predefined loading pattern during pushover analyses. Moreover, in case of medium rise building (quite widespread in Italy), it is a matter of fact that the relevance of higher modes depends not only on their level of irregularity but also related to the quite high number of stories. To check such hypothesis of the design procedure has been tested on a medium rise irregular existing R.C. building in this work.
Another important issue in the procedure is the pushover curve in terms of base shear and roof displacement is taken as the capacity curve, and the intersection of capacity spectrum, which is transformed by the capacity curve, and demand spectrum is taken as the performance point (P.P.). There is big error for the capacity curve obtained from the monomodal pushover curve. Incremental dynamic analysis (IDA) is considered to be the most accurate method for the estimation of the seismic response and capacity of structures over the entire range of structural response, from elastic behavior to global dynamic instability. However, its intensive computation of many NL_RHA limits its practical use. It is necessary to improve the capacity evaluation for the structure in the design procedure.
My work starts from the study of these problems and I tried to give a contribute on evaluating the accuracy of current NSPs on the seismic assessment of existing irregular structures, proposing a more efficient incremental modal pushover analysis (IMPA) to obtain capacity curve of the structure, incorporating IMPA into the design procedure of dissipative braces and its application to existing building. I studied these topics, I will describe the state of the art of NSPs, propose a more efficient incremental modal pushover analysis (IMPA) to obtain capacity curve of the structure, incorporate IMPA into the deign procedure of dissipative braces, a regular structure and an irregular structure are introduced and the current NSPs and IMPA are applied to these two buildings to check their accuracy, then the most accurate NSP and IMPA for the irregular structure are incorporated into the design procedure to retrofit the existing irregular structure, finally some other passive energy dissipation devices are selected to retrofit the existing irregular building to investigate their effectiveness.

1.1 Aims of the study

Nonlinear static pushover analysis represents the most attractive

alternative to nonlinear response history analysis tools. Many international seismic design codes, like FEMA440, ATC40, Eurocode 8, Italian Technical Code NTC 2008 (NTC2008) and Chinese seismic code (GB 50011-2010) have recommended the use of this type of procedures.
The use of NSPs is backed by a large number of extensive verification studies that have demonstrated their relatively good accuracy in estimating the seismic response of regular structures. The few studies on the extension of NSPs to the case of 3D irregular structures limit significantly the employment of NSPs to assess actual existing structures. In order to improve the use of NSPs in practical, the applicability of NSPs for analysis and retrofitting of existing buildings with dissipative braces should be checked. Therefore, the primary objectives of this work are:

1. Checking whether the commonly used procedures can be successful even in the case of very complex irregularity conditions: Capacity Spectrum Method (CSM) adopted in ATC-40, Displacement Coefficient Method integrated into FEMA356, and N2 method presented in Eurocode 8 and modal pushover analysis (MPA).
2. Comparative evaluation of the different commonly used NSPs describing their advantages and limitations.
3. During the displacement based design procedure of dissipative braces, NSP is adopted to evaluate the seismic response of the existing and retrofitted structure, the applicability of NSPs to the case of braced irregular structures will be discussed. And The necessity of using a multi modal pushover instead of the standard single mode pushover in the design procedure has been investigated
4. Proposing a more efficient incremental modal pushover analysis (IMPA) to obtain capacity curve of the structure to evaluate the seismic demand: the procedure allows defining the capacity curve based on the execution of a series of MPAs.
5. Evaluating feasibility of force-based and displacement-based approaches for the design of passive energy dissipation devices and investigates the effectiveness of different passive energy devices.

1.2 Thesis layout

In chapter 2, the state of the art is reviewed. Four popular NPSs, which are Capacity Spectrum Method (CSM) adopted in ATC-40, Displacement Coefficient Method integrated into FEMA356, and N2 method presented in Eurocode 8 and modal pushover analysis (MPA), and the commonly

used lateral load distribution, are introduced. The development of extension of NSPs to 3D structure is presented.
In chapter 3, a more efficient incremental modal pushover analysis (IMPA) to obtain capacity curve of the structure to evaluate the seismic demand is proposed. The basic idea of IMPA is presented and the step-by-step computational procedure is summarized.
In chapter 4, a displacement-based procedure to design dissipative bracings for the seismic protection of frame structures is presented and the step by step procedure is summarized.
In chapter 5, the case studies used in this thesis and the modeling options assumed during the work are presented.
In chapter 6, the applicability of commonly used procedures to the very complex irregularity conditions is checked.
In chapter 7, IMPA is applied to existing building to evaluate seismic demand and capacity of structures over the entire range of structural response.
In chapter 8, the design procedure of dissipative bracings for the seismic protection of frame structures is applied to existing irregular structure and steel concentric braced frames (CBF).
In chapter 9, force-based and displacement design procedure of passive energy dissipation devices are applied to retrofit a school building located in shanghai, the comparisons of the two design methods and the seismic behavior of the retrofitting structure with different passive energy dissipation devices are discussed.
At the end, conclusions of the work developed are drawn and future work is outlined.

2. State of the art: NSP

2.1 Introduction

It is well known that the most accurate method of seismic demand prediction and performance evaluation of structures is nonlinear time history analysis. It is usually considered to be 'exact' results to assessment or design problems. The properties of each structural element are properly modeled, including nonlinearities of the materials, with the analysis solution being computed through a numerical step by-step integration of the equilibrium equation:

$$m\ddot{u}+c\dot{u}+ku=-m\iota\ddot{u}_g(t) \tag{2.1}$$

where *m, c* and *k* are the mass, classical damping, and lateral stiffness matrices of the system; each element of the influence vector ι is equal to unity., and $\ddot{u}_g(t)$ is the ground motion.

However, step-by-step integration demands a considerable computational effort and is very time-consuming; which is a relevant drawback especial in design phase.

During the last decade, the Nonlinear Static Procedure (NSP) analysis, often called Pushover Analysis, has been proposed among the structural engineering society as an alternative mean of analysis. The purpose of the pushover analysis is to assess the structural performance by estimating the strength and deformation capacities using static, nonlinear analysis and comparing these capacities with the demands at the corresponding performance levels.

In the pushover analysis, the structural model is subjected to a predetermined monotonic lateral load (forces or displacements) pattern, which approximately represents the relative inertia forces generated at locations of substantial mass. The intensity of the load is increased, i.e. the structure is 'pushed', and the sequence of cracks, yielding, plastic hinge formations, and the load at which failure of the various structural components occurs is recorded as function of the increasing lateral load. This incremental process continues until a predetermined displacement limit.

The static pushover analysis method has no strict theoretical base. Both

the force distribution and target displacement are based on the assumption that the response is controlled by the fundamental mode and that the mode shape remains unchanged after the structure yields. Obviously, after the structure yields both assumptions are approximate, but investigations (Saiidi and Sozen, 1981; Miranda, 1991; Lawson et al., 1994; Fajfar and Fischinger, 1988; Krawinkler and Seneviratna, 1998; Kim and D'Amore, 1999; Maison and Bonowitz, 1999; Gupta and Krawinkler, 1999, 2000; Skokan and Hart, 2000) have led to good estimates of seismic demands. However, such satisfactory predictions of seismic demands are mostly restricted to low- and medium-rise structures in which inelastic action is distributed throughout the height of the structure (Krawinkler and Seneviratna, 1998; Gupta and Krawinkler, 1999).

By assuming a single shape vector, $\{\Phi\}$, which is not a function of time and defining a relative displacement vector, u, of the MDOF system:

$$u=\phi u_t \tag{2.2}$$

where u_t denotes the roof/top displacement, the governing differential equation of the MDOF system will be transformed to:

$$m\phi\ddot{u}_t+c\phi\dot{u}_t+k\phi u_t=-m\iota\ddot{u}_g(t) \tag{2.3}$$

If the reference displacement u^* of the SDOF system is defined as

$$u^*=\frac{\phi^T m\phi}{\phi^T m\iota}u_t \tag{2.4}$$

Pre-multiplying equation (1.3) by $\{\phi^T\}$, and substituting for u_t using equation (2.3) the following differential equation describes the response:

$$\phi^T m\phi\ddot{u}_t+\phi^T c\phi\dot{u}_t+\phi^T k\phi u_t=-\phi^T m\iota\ddot{u}_g(t) \tag{2.5}$$

$$M^*\ddot{u}^*+C^*\dot{u}^*+K^*u^*=-M^*\ddot{u}_g(t) \tag{2.6}$$

where

$$M^*=\phi^T m\iota \tag{2.7}$$

$$C^*=\phi^T c\phi\frac{\phi^T m\iota}{\phi^T m\phi} \tag{2.8}$$

$$K^*=\phi^T k\phi\frac{\phi^T m\iota}{\phi^T m\phi} \tag{2.9}$$

This provides the basis for transforming a dynamic problem to a static problem which is theoretically flawed. Furthermore, the response of a

Multi degree of freedom (MDOF) structure is related to the response of an equivalent Single degree of freedom (SDOF) system, ESDOF, as shown in Figure 2.1.

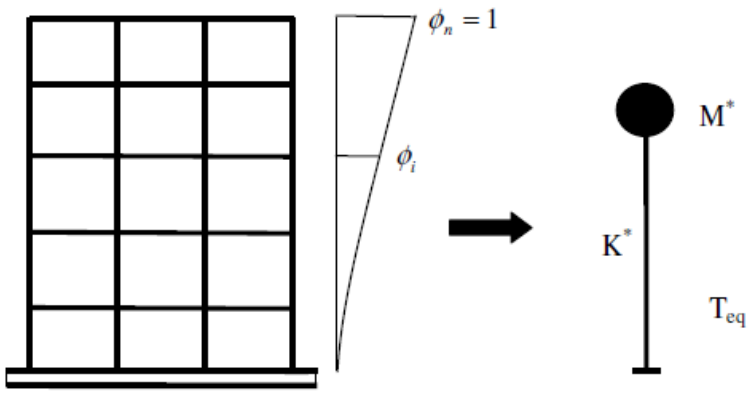

Figure 2.1Conceptual diagram for transformation of MDOF to SDOF system

A nonlinear incremental static analysis of the MDOF structure can now be carried out from which it is possible to determine the force-deformation characteristics of the ESDOF system. The outcome of the analysis of the MDOF structure is a Base Shear, V_b, - Roof Displacement, u_t, diagram, the global force-displacement curve or capacity curve of the structure,as shown in . This capacity curve provides valuable information about the response of the structure because it approximates how it will behave after exceeding its elastic limit. Some uncertainty exists about the post-elastic stage of the capacity curve and the information it can provide since the results are dependent on the material models used (Pankaj et al. 2004) and the modeling assumptions.

For simplicity, the curve is idealized as bilinear from which the yield strength V_y, effective elastic stiffness Ke and a hardening/softening stiffness Ks are defined. The idealised curve can then be used together with Eqs (2.4) and (2.9) to define the properties of the equivalent SDOF system, as shown in

$$Ks = \alpha Ke \tag{2.10}$$

The strain-hardening ratio, α, of the base shear-roof displacement

relationship of the ESDOF system is taken as the same as for the MDOF structure.
Thus the initial period T_{eq} of the equivalent SDOF system will be:

$$T_{eq} = 2\pi\sqrt{\frac{M^*}{K^*}} \tag{2.11}$$

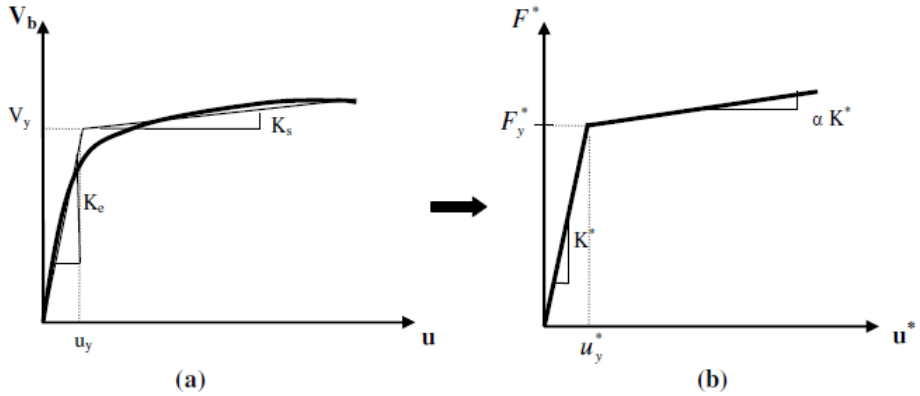

Figure 2.2(a) Capacity curve for MDOF structure, (b) bilinear idealization for the equivalent SDOF system.

The maximum displacement of the SDOF system subjected to a given ground motion can be found from either elastic or inelastic spectra or a time-history analysis. Then the corresponding displacement of the MDOF system can be estimated by re-arranging Eq. (2.4) as follows:

$$u_t = \frac{\phi^{\mathrm{T}} \mathrm{m} \iota}{\phi^{\mathrm{T}} \mathrm{m} \phi} u^* \tag{2.12}$$

The inelastic displacement of the controlled node (u_t) is obtained by making the correspondence of the target displacement of the SDOF system to the MDOF. In order to obtain the peak inelastic deformations of individual structural elements, such as interstorey drifts or chord rotations, one has to go back to the MDOF pushover curve step corresponding to the controlled node inelastic displacement previously calculated, and take the results in the desired elements.
The nonlinear static procedures can be classified as displacement-based evaluation methods for the assessment and rehabilitation of existing structures. However, these methods can be applied together with displacement-based design methods for the seismic design of new structures. In fact, to perform a pushover analysis it is necessary to

develop a nonlinear model of the structure, which includes the nonlinear formulation of the material relationships. In the case of reinforced concrete structures, the reinforcement in the elements must be correctly defined.
The main advantages of the nonlinear static analysis when compared with the linear dynamic and nonlinear dynamic analysis are listed below:
1) The seismic assessment and design using nonlinear static analysis are performed based on the control of structural deformations;
2) The NSPs explicitly consider the nonlinear behaviour of the structure instead of using the behaviour factors applied to the linear analysis results.
3) The nonlinear static analysis allows the definition of the capacity curve of the structure allowing the sequential identification of the structural elements that yield and collapse. This analysis identifies the structural damage distribution along the structure during the loading process, giving important information about the structural elements that first enter the inelastic regime which can turn out to be very useful when performing seismic strengthening of the structure;
4) The nonlinear static analysis is very useful within the performance based design and assessment philosophy, because it allows the consideration of different limit states and the performance check of the structure for the corresponding target displacements.

2.2 Pushover analysis methods

The use of nonlinear static procedures for the seismic assessment of planar frames and bridges has become very popular amongst the structural engineering community. The reason for their success lies in the possibility of gaining an important insight into the nonlinear seismic behaviour of structures in a simple and practical way.
The popular conventional pushover methods are the capacity spectrum method (CSM), Displacement Coefficient Method (DCM), N2 method and modal pushover analysis (MPA). The conventional pushover methods were officially introduced in design codes all over the world. They started to be implemented within the framework of performance-based seismic engineering ATC40, FEMA237 and FEMA356. Recently, the Japanese structural design code for buildings has adopted the capacity spectrum method (CSM) of ATC40 as a seismic assessment tool. In Europe, the N2 method was implemented in Eurocode 8.

2.2.1 Capacity Spectrum Method (CSM)

The Capacity Spectrum Method (CSM) was initially proposed by Freeman (1998) and later included in ATC-40 guidelines (ATC, 1996). This method compares the capacity of a structure to resist lateral forces to seismic demand given by a response spectrum. The response spectrum represents the demand while the pushover curve (or the "capacity curve") represents the available capacity.

The capacity spectrum method is a very practical tool in the evaluation and retrofit of existing concrete buildings. Its graphical representation allows a clear understanding of how a building responds to an earthquake. The CSM was developed to represent the first mode response of a structure based on the idea that the fundamental mode of vibration is the predominant response of the structure. For buildings in which the higher mode effects can be important, the results obtained with the CSM may not be so accurate. A step-by-step summary of the CSM procedure to estimate the seismic demands for building is briefly described following, and the detailed procedure can be found in Appendix A.

1) Perform pushover analysis and determine the capacity curve in base shear (V_b) versus roof displacement of the building (D);
2) Convert the capacity curve to acceleration–displacement terms (AD) using an equivalent Single Degree of System (SDOF);
3) Plot the capacity spectra on the same graph with the 5%-damped elastic response spectrum that is also in AD format;
4) Select a trial peak deformation demand d_t^* and determine the corresponding pseudo-acceleration from the capacity spectrum, initially assuming $\xi = 5\%$;
5) The equivalent damping ratio ξ_{eq} corresponding to d_t^* is evaluated from the following relationship form:

$$\xi_{eq} = \xi_0 + k\xi_h \tag{2.13}$$

   where ξ_0 is inherent damping of the structure, k is a damping modification factor that depends on the hysteretic behavior of the system, and ξ_h is the hysteretic damping.
6) Update the estimate of d_t^* using the elastic demand spectrum for ξ_{eq};

7) Check for convergence the displacement d_t^*. When convergence has been achieved the target displacement of the MDOF system is equal to d_t:

$$d_t = \Gamma d_t^* \tag{2.14}$$

where Γ is the modal participation factor.

2.2.2 Displacement Coefficient Method (DCM)

When DCM is implemented, the target displacement, which is the displacement during a given seismic event of a characteristic node on the top of a structure, typically in the roof, is defined with the following formula:

$$d_t = C_0 C_1 C_2 C_3 S_a \frac{T_e^2}{4\pi^2} g \tag{2.15}$$

where C_0 is the modification factor to relate spectral displacement of an equivalent SDOF system to the roof displacement of the building; C_1 is the modification factor to relate expected maximum inelastic displacements to displacements calculated for linear elastic response; C_2 is the modification factor to represent the effect of pinched hysteretic shape, stiffness degradation and strength deterioration on maximum displacement response; C_3 is the modification factor to represent increased displacements due to dynamic P-Δ effects; S_a is the response spectrum acceleration at the effective fundamental period and damping ratio (5% in this study) of the building in the direction under consideration; and T_e is the effective fundamental period of the building in the direction under consideration.

2.2.3 N2 method

The N2 method was initially proposed by Fajfar (1988, 1996) and was later expressed in a displacement-acceleration format (1999). And, the method has been included in the Eurocode8 (2004).

The basis of the method came from the Q-model proposed by Saiidi and Sozen (1981), which was improved by Fajfar and Gaspersic (1996). The N2 method was extended to bridges in 1997 (Fajfar. etc, 1997). In 1999, the N2 method was formulated in the acceleration-displacement format ((Fajfar, 1999), which combines the advantages of the graphical

representation of the capacity spectrum method developed by Freeman with the practicality of inelastic demand spectra. The method is actually a variant of the capacity spectrum method based on inelastic spectra.
Conceptually the method is a variation of CSM that instead of highly damped spectra using an $R_\mu - \mu - T$ relationship. This method, as implemented in EC8, consists of the following steps:

1) Perform pushover analysis and obtain the capacity curve in $V_b - D$ terms;
2) Convert the pushover curve of the MDOF system to the capacity diagram of an equivalent SDOF system and approximate the capacity curve with an idealized elasto-perfectly plastic relationship to get the period T_e of the equivalent SDOF
3) The target displacement is then calculated:

$$d_{et}^* = S_a(T_e)[\frac{T_e}{2\pi}]^2 \tag{2.16}$$

where $S_a(T_e)$ is the elastic acceleration response spectrum at the period T_e.

To determine the target displacement d_t^* , different expressions are suggested for the short and the medium to long-period ranges ,thus:

- $T^* < T_C$ (short period range): If $F_y^* / m^* \geq S_a(T_e)$, the response is elastic and thus $d_t^* = d_{et}^*$. Otherwise the response is nonlinear and the ESDOF maximum displacement is calculated as $d_t^* = \frac{d_{et}^*}{R_\mu}[1 + (R_\mu - 1)\frac{T_C}{T_e}]$.
- $T^* \geq T_C$ (medium and long period range):The target displacement of the inelastic system is equal to that of an elastic structure, thus $d_t^* = d_{et}^*$.

4) The displacement of the MDOF system is always calculated as $d_t = \Gamma d_t^*$.

2.2.4 Modal Pushover Analysis (MPA)

None of the invariant force distributions can account for the contributions of higher modes to response, or for a redistribution of inertia forces

because of structural yielding and the associated changes in the vibration properties of the structure. To overcome these limitations, several researchers have proposed adaptive force distributions that attempt to follow more closely the time-variant distributions of inertia forces (Fajfar and Fischinger, 1988; Bracci et al., 1997; Gupta and Kunnath, 2000). While these adaptive force distributions may provide better estimates of seismic demands (Gupta and Kunnath, 2000), they are conceptually complicated and computationally demanding for routine application in structural engineering practice.

Chopra and Goel (2002) proposed an improved pushover analysis procedure based on structural dynamics theory, which retains the conceptual simplicity and computational attractiveness of current procedures with invariant force distribution. In this modal pushover analysis (MPA), the seismic demand due to individual terms in the modal expansion of the effective earthquake forces is determined by a pushover analysis using the inertia force distribution for each mode. Combining these 'modal' demands due to the first two or three terms of the expansion provides an estimate of the total seismic demand on inelastic systems. This procedure has been improved, especially in its treatment of P-Δ effects due to gravity loads, by including them in all modes. The improved version of MPA is summarized in Goel and Chopra (2004). This improved accuracy is achieved without any significant increase in computational effort. The MPA procedure estimates seismic demands much more accurately than current pushover procedures used in structural engineering practice (Goel and Chopra 2004, Chopra and Chintanapakdee 2004, Chopra,etc, 2004).

For each structural element of a building, the initial loading curve can be idealized appropriately (e.g. bilinear with or without degradation) and the unloading and reloading curves differ from the initial loading branch. Thus, the relations between lateral forces $\boldsymbol{f_s}$ at the N floor levels and the lateral displacements $\boldsymbol{u}$ are not single-valued, but depend on the history of the displacements:

$$f_s = f_s(u, \text{sign}\dot{u}) \tag{2.17}$$

With this generalization for inelastic systems, Eq. (2.1) becomes:

$$m\ddot{u}+c\dot{u}+f_s(u, \text{sign}\dot{u})=-m\iota\ddot{u}_g(t) \tag{2.18}$$

The standard approach is to directly solve these coupled equations, leading to the 'exact' non-linear RHA.

The right-hand side of Eq.(2.18) can be interpreted as effective

earthquake forces:

$$P_{eff}(t) = -m\iota\ddot{u}_g(t) \tag{2.19}$$

The spatial distribution of these effective forces over the height of the building is defined by the vector $s = m\iota$ and their time variation by $\ddot{u}_g(t)$. This force distribution can be expanded as a summation of modal inertia force distribution s_n:

$$m\iota = \sum_{n=1}^{N} S_n = \sum_{n=1}^{N} \Gamma_n m\phi_n \tag{2.20}$$

$$\Gamma_n = \frac{L_n}{M_n}, L_n = \phi_n^T m\iota, M_n = \phi_n^T m\phi \tag{2.21}$$

Although classical modal analysis is not valid for inelastic systems, it will be used next to transform Eq.(2.18) to the modal coordinates of the corresponding linear system. Each structural element of this elastic system is defined to have the same stiffness as the initial stiffness of the structural element of the inelastic system. Both systems have the same mass and damping. Therefore, the natural vibration periods and modes of the corresponding linear system are the same as the vibration properties of the inelastic system undergoing small oscillations (within the linear range).

Expanding the displacements of the inelastic system in terms of the natural vibration modes of the corresponding linear system, we get

$$u(\mathrm{t}) = \sum_{n=1}^{N} \phi_n q_n(\mathrm{t}) \tag{2.22}$$

Substituting Eq. (2.23) into Eq. (2.18), pre-multiplying by $\phi_n{}^T$, and using the mass and classical damping orthogonality property of modes gives:

$$\ddot{q}_n + 2\xi_n w_n \dot{q}_n + \frac{F_{sn}}{M_n} = -\Gamma_n \ddot{u}_g(t), \qquad n = 1, 2, ..., N \tag{2.23}$$

$$F_{sn} = F_{sn}(q_n, sign\dot{q}_n) = \phi_n^T f_s(u_n, sign\dot{u}_n) \tag{2.24}$$

where w_n is the natural vibration frequency and ξ_n is the damping ratio for the nth mode.

1. UNCOUPLED MODAL RESPONSE HISTORY ANALYSIS

Neglecting the coupling of the N equations in modal coordinates leads to the uncoupled modal response history analysis (UMRHA) procedure. This approximate RHA procedure is the preliminary step in developing a

modal pushover analysis procedure for inelastic systems.
The spatial distribution *s* of the effective earthquake forces is expanded into the modal contributions s_n, where φ_n are now the modes of the corresponding linear system. The equations governing the response of the inelastic system to $p_{eff,n}(t)$ given by:

$$\ddot{q}_n + 2\xi_n w_n \dot{q}_n + \frac{F_{sn}}{M_n} = -\Gamma_n \ddot{u}_g(t), \qquad n = 1, 2, ..., N \tag{2.25}$$

This resisting force depends on all modal coordinates $q_n(t)$, implying coupling of modal coordinates because of yielding of the structure. The solution q_n of Eq.(2.25) is given by:

$$m\ddot{u} + c\dot{u} + f_s(u, sign\dot{u}) = -s_n \ddot{u}_g(t) \tag{2.26}$$

$$q_n(t) = \Gamma_n D_n(t) \tag{2.27}$$

where $D_n(t)$ is governed by the equation of motion for the *n*th-mode linear SDF system, an SDF system with vibration properties—natural frequency w_n and damping ratio ξ_n—of the nth-mode of the MDF system, subjected to $\ddot{u}_g(t)$:

$$\ddot{D}_n + 2\xi_n w_n \dot{D}_n + \frac{F_{sn}}{L_n} = -\ddot{u}_g(t) \tag{2.28}$$

$$F_{sn} = F_{sn}(D_n, sign\dot{D}_n) = \phi_n^T f_s(D_n, sign\dot{D}_n) \tag{2.29}$$

Substituting Equation (2.27) into Equation (2.24) gives the floor displacements

$$u_n(t) = \Gamma_n \phi_n D_n(t) \tag{2.30}$$

Any response quantity *r(t)*—storey drifts, internal element forces, etc.—can be expressed as

$$r_n(t) = r_n^{st} A_n(\mathrm{t}) \tag{2.31}$$

where r_n^{st} denotes the modal static response, the static value of r due to external forces s_n, and

$$A_n(\mathrm{t}) = w_n^2 D_n \tag{2.32}$$

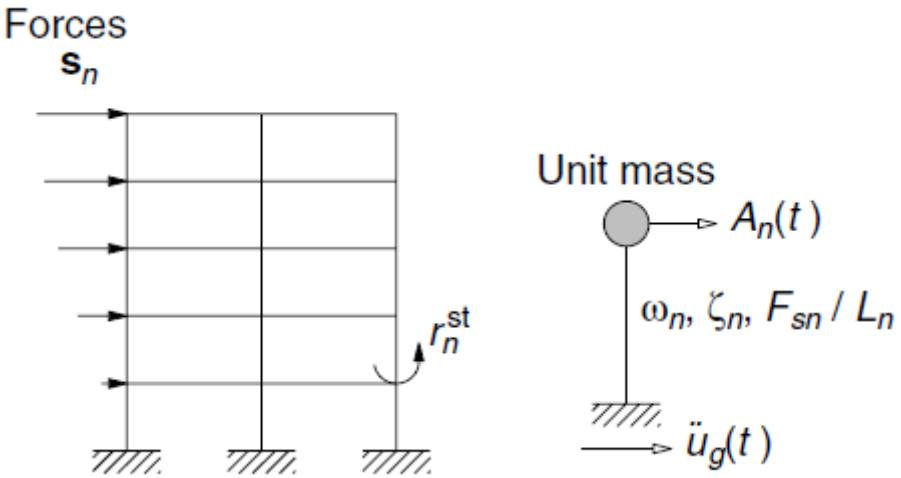

a) Static Analysis of Structure

b) Dynamic Analysis of Inelastic SDF System

Figure 2.3 Conceptual explanation of uncoupled modal response history analysis of inelastic MDF systems

Solution of the nonlinear Eq. (2.29) formulated in this manner provides $D_n(t)$, which substituted into Eq. (2.30) gives the floor displacements of the structure associated with the nth-"mode" inelastic SDF system. Any floor displacement, story drift, or another deformation response quantity $r(t)$ is given by Eqs. (2.13) and (2.14), where $A_n(t)$ is now the pseudoacceleration response of the nth-"mode" inelastic SDF system. The two analyses leading to r_n^{st} and $A_n(t)$ are shown schematically in Fig. 4.3. Eqs. (2.13) and (2.14) represent the response of the inelastic MDF system to $p_{eff}(t)$, the nth-mode contribution to $p_{eff}(t)$. Therefore the response of the system to the total excitation $p_{eff}(t)$ is given by Eqs. (2.15) and (2.16). This is the UMRHA procedure.

What is an appropriate invariant distribution of lateral forces to determine F_{sn}? For an inelastic system no invariant distribution of forces can produce displacements proportional to ϕ_n at all displacements or force levels. However, before any part of the structure yields, the only force distribution that produces displacements proportional to ϕ_n is given by Eq. (2.22). Therefore, this distribution seems to be a rational choice—even

after the structure yields—to determine F_{sn} in Eq. (2.22). When implemented by commercially available software, such non-linear static analysis provides the so-called pushover curve, which is different than the F_{sn}/L_n–D_n curve. The structure is pushed using the force distribution of Eq. (2.22) to some predetermined roof displacement, and the base shear V_{bn} is plotted against roof displacement urn. A bilinear idealization of this pushover curve for the nth-'mode' is shown in Figure 2.4 a). At the yield point, the base shear is V_{bny} and roof displacement is urny. How to convert this V_{bn}–u_{rn} pushover curve to the F_{sn}/L_n–D_n relation? The two sets of forces and displacements are related as follows:

$$F_{sn} = \frac{V_{bn}}{\Gamma_n}, \qquad D_n = \frac{u_{rn}}{\Gamma_n \phi_{rn}} \tag{2.33}$$

Eq.(2.33) enables conversion of the pushover curve to the desired F_{sn}/L_n–D_n relation shown in Figure 5(b), where the yield values of F_{sn}/L_n relation and D_n are

$$\frac{F_{sny}}{L_n} = \frac{V_{bny}}{M_n^*}, \qquad D_{ny} = \frac{u_{rny}}{\Gamma_n \phi_{rn}} \tag{2.34}$$

in which M_n^* is the effective modal mass:

$$M_n^* = L_n \Gamma_n \tag{2.35}$$

The two are related through

$$\frac{F_{sny}}{L_n} = w_n^2 D_{ny} \tag{2.36}$$

implying that the initial slope of the bilinear curve in Figure 2.4 b) is w_n^2 .Knowing F_{sny}/L_n and D_{ny} from Eq. (2.24), the elastic vibration period T_n of the nth-'mode' inelastic SDF system is computed from

$$T_n = 2\pi \left(\frac{L_n D_{ny}}{F_{sny}}\right)^2 \tag{2.37}$$

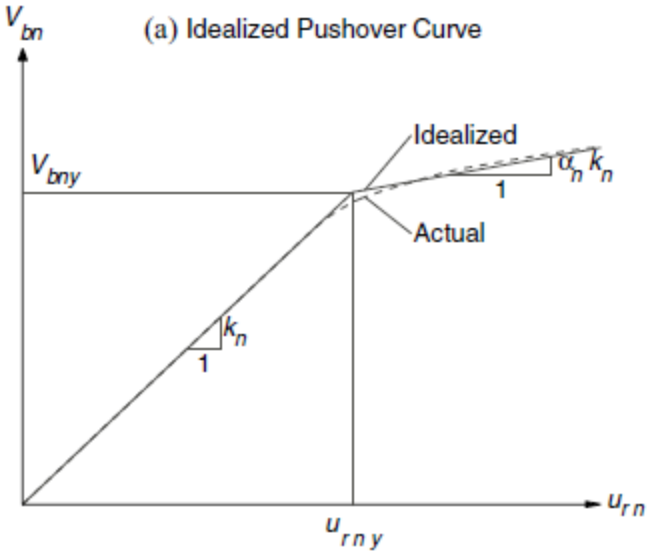

a) idealized Pushover Curve

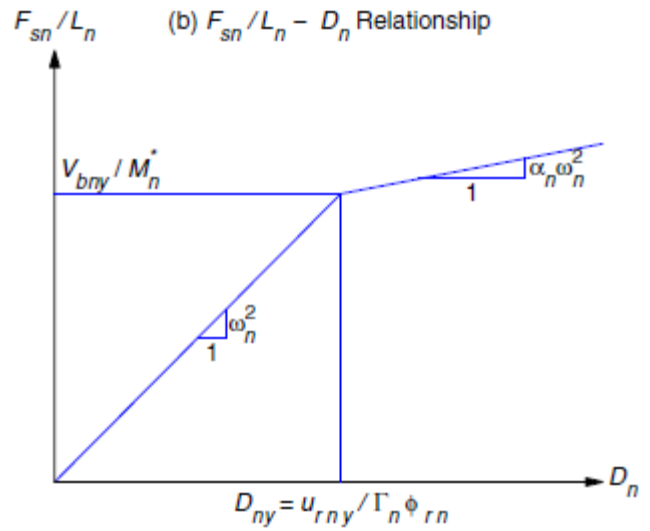

b) F_{sn}/L_n–D_n relation

Figure 2.4Properties of the nth-"mode" inelastic SDF system from the pushover curve

3. Modal pushover analysis

A pushover analysis procedure is presented next to estimate the peak response r_{no} of the inelastic MDF system to effective earthquake forces $p_{eff,n}(t)$. Consider a nonlinear static analysis of the structure subjected to

lateral forces distributed over the building height according to s_n, with the structure is pushed to the roof displacement u_{rno}. This value of the roof displacement is given by Eq. (2.21) where D_n, the peak value of $D_n\ (t)$, is now determined by solving Eq. (2.28); alternatively, it can be determined from the inelastic response (or design) spectrum (Chopra, 2001; Sections 7.6 and 7.12). At this roof displacement, the pushover analysis provides an estimate of the peak value r_{no} of any response $r_n(t)$: floor displacements, storey drifts, joint rotations, plastic hinge rotations, etc.

This pushover analysis, although somewhat intuitive for inelastic buildings, seems rational for two reasons. First, pushover analysis for each 'mode' provides the exact modal response for elastic buildings and the overall procedure, as demonstrated earlier, provides results that are identical to the well-known RSA procedure. Second, the lateral force distribution used appears to be the most rational choice among all invariant distribution of forces.

The response value *rno* is an estimate of the peak value of the response of the inelastic system to $p_{eff,n}(t)$, governed by Eq. (2.26). As shown earlier for elastic systems, *rno* also represents the exact peak value of the nth-mode contribution $r_n(t)$ to response $r(t)$. Thus, we will refer to r_{no} as the peak 'modal' response even in the case of inelastic systems. The peak 'modal' responses r_{no}, each determined by one pushover analysis, is combined using an appropriate modal combination rule, e.g. Eq. (2.17), to obtain an estimate of the peak value r_o of the total response. This application of modal combination rules to inelastic systems obviously lacks a theoretical basis. However, it provides results for elastic buildings that are identical to the well-known RSA procedure described earlier.

2.3 Summary of NSPs

Table 2.1 shows a summary of the methods used in this work pointing out the main differences between the methods in each step of the nonlinear static procedure.

Table 2.1Summary of studied NSPs

	CSM	DCM	N2	MPA
Pushover analysis type	Conventional force-based: invariant load pattern			
Load Pattern	1st mode proportional loading	Any reasonable lateral load patterns	1st mode proportional or uniform loading	All predominate modes proportional loading
Capacity curve	Base shear vs. displacement of a control node			
Demand curve	Elastic viscous damping-based reduced spectrum	Inelastic ductility-based reduced spectrum		Elastic viscous damping-based reduced spectrum
MDOF to SDOF Transformation	Γ	C_0	Γ_1	$\Gamma_1 \dots \Gamma_n$
Target Displacement	Intersecting the SDOF capacity curve with a reduced ADRS	Four modification factors multiply elastic displacement spectrum	Calculates the SDOF equivalent period and obtain target displacement from inelastic spectrum.	Intersecting the SDOF capacity curve with a reduced ADRS
Code	ATC-40	FEMA273	Eurocode 8	

2.4 Lateral load distribution

The load patterns are intended to represent and bound the distribution of inertia forces in a design earthquake. It is clear that the distribution of inertia forces will vary with the severity of the earthquake (extent of inelastic deformations) and with time within an earthquake.

If an invariant load pattern is used, the basic assumptions are that the distribution of inertia forces will be reasonably constant throughout the earthquake and that the maximum deformations obtained from this invariant load pattern will be comparable to those expected in the design earthquake. These assumptions may be close to the truth in some cases, but not in others.

Clearly, none of these invariant load patterns can account for a redistribution of inertia forces, which may occur when a local mechanism forms and the dynamic properties of the structure change accordingly. Adaptive load patterns would follow more closely the time variant distribution of inertia forces. Different suggestions have been made in this regard, including the use of story loads that are proportional to the deflected shape of the structure (Fajfar, 1988), the use of SRSS load patterns based on mode shapes derived from secant stiffnesses at each load step, and the use of patterns in which the applied story loads are proportional to story shear resistances at the previous step (Bracci, etc, 1997). However, adaptive load pattern would makes the pushover procedure be time-consuming, not practical for design offices, so just the invariant load patterns considered in this paper as following:

1) Uniform load

   A uniform lateral load distribution consisting of forces that are proportional to the story masses at each story level:

$$F_i = \frac{m_i}{\sum m_i} \tag{2.38}$$

   where F_i is the lateral load applied at floor level i, m_i is the floor mass.

2) Equivalent Lateral Force (ELF)

   The buildings are subjected to a lateral load distributed across the height of the building based on the following formula specified in FEMA-356:

$$F_i = \frac{m_i h_i^k}{\sum m_i h_i^k} \tag{2.39}$$

where h_i is the story height, and k is the period-dependent coefficient.

$$k = 2.0 \quad \text{for} \quad T > 2.0s$$
$$k = 1.0 \quad \text{for} \quad T > 0.5s \tag{2.30}$$

Linear interpolation shall be used to calculate values of k for intermediate values of T.

3) SRSS
Load Patten is defined by the lateral forces back-calculated from the story shears determined by response spectrum analysis of the structure, which is assumed to be linearly elastic.

4) Fundamental Modal Distribution(FMD)
A vertical distribution proportional to the shape of the fundamental mode in the direction under consideration.

$$F_i = \frac{m_i \phi_i}{\sum m_i \phi_i} \tag{2.31}$$

Where ϕ_i is amplitude of the fundamental mode at level i.

5) Multi-Modal Profile (MMP)
This procedure requires multiple modal profiles. The lateral forces are determined for each independent mode and then combined using an appropriate combination rule such as SRSS:

$$\mathrm{F_i} = \sqrt{\sum_{j=1}^{N} (\Gamma_j m_i \phi_{ij} Sa_j(\xi_j, T_j)^2} \tag{2.32}$$

Where i is the floor number , j is the mode number, ϕ_{ij} is amplitude of mode j at level i, and $Sa_j(\xi_j, T_j)$ is the spectral acceleration at the period T_j and modal damping ξ_j corresponding to mode j.

2.5 Application of NSA to 3D irregular buildings

The use of Nonlinear Static Procedures (NSPs) for the seismic assessment of plan regular buildings and bridges is widespread nowadays. Their good

performance in such cases is widely supported by the extensive number of scientific studies described in the previous pages.
Real structures are almost always irregular as perfect regularity is an idealization that very rarely occurs. Structural irregularities may vary dramatically in their nature and, in principle, are very difficult to define. Regarding buildings, for practical purposes, major seismic codes distinguish between irregularity in plan and in elevation, but it must be realized that quite often structural irregularity is the result of a combination of both types. The tendency to separate irregularity in plan and in elevation also characterizes the scientific literature and, therefore, this state-of-the-art review will follow such distinction.

2.5.1 Multi-storey plan-asymmetric structures

Starting with plan irregularity, assessments of structural performance during past earthquakes demonstrates that this type of irregularity, which is due to asymmetric distributions of mass, stiffness and strength, is one of the most frequent sources of severe damage, since it results in floor rotations (torsional response) in addition to floor translations. However, the applicability of NSPs on plan-irregular 3D buildings has so far been the object of a limited number of papers. This limitation leads to a minor use of these methods to assess current existing structures, the majority of which do tend to be irregular in plan. The most important issue that controls the structural response of this kind of structures is torsion. The aforementioned NSPs are not able to reproduce in a correct manner the torsional response of plan irregular buildings; therefore one should be cautious when using these methods to assess these structures.
In past years, large research efforts were devoted to the study of the seismic response of asymmetric structures and improving torsional provisions of seismic codes. A recent review of research development up to 2001 can be found in Rutenberg (2002).
Early research dates back to the mid 1990s, with the investigations by Kilar and Fajfar (1997). They presented the use of a 3D model for the pushover analysis of plan irregular buildings. They used an invariant force pattern with an inverted triangular shape at the centre of mass of the floors. In this study the authors arrived at the conclusion that the torsional rotation was strongly dependent on the orthogonal structural elements.
Faella and Kilar (1998) tested different location in plan to apply the

lateral forces of the pushover analysis of plan irregular buildings. Three eccentricities, measured from the centre of mass location, were applied. In this study, the target displacement was defined as the maximum response obtained from the nonlinear time-history analysis. The torsional rotation was always underestimated, even when the eccentricity was maximum.

In the same year, De Stefano and Rutenberg (1998) considered in their study the interaction between walls and frames in a pushover analysis of 3D asymmetric multistorey wall-frame structures. The results obtained were generally close to the time-history except at the flexible edges where the pushover analysis overestimated the response.

Moghadam and Tso (2000) proposed a 3D pushover procedure. In this method, the conventional pushover is performed independently in each resisting element using a planar analysis, and the target displacements are calculated considering the equal displacement rule. In fact, the target displacements of each resisting element (planar frames and walls) are calculated with an elastic response spectrum analysis of a 3D model of the building. However, it is generally recognized that the equal displacement rule may lead to small inelastic displacements in the case of: near-fault ground motions; systems with low strength; soft soil conditions; hysteresis behaviour of the elements with considerable pinching or stiffness and strength degradation. Therefore, the use of this method may lead to not so accurate results.

Kilar and Fajfar (2002) proposed an extension to 3D models of the N2 method by applying a height-wise distribution of lateral forces to the floor centre of mass. The method, initially formulated for planar (2D) structures, consists of a simplified nonlinear approach that makes use of pushover analysis, equivalent SDOF system and inelastic response spectrum. The suitability of the extended procedure was demonstrated by investigating both multi-storey steel frame buildings and multi-storey RC buildings with structural walls. A comparison with results obtained by nonlinear dynamic analysis evidenced the ability of the method to predict seismic behavior of torsionally stiff structures. Sources of inaccuracy have also been identified as follows: approximations already present in predicting 2D behavior, no allowance for dynamic effects of lateral–torsional coupling, uncertainties in combining results obtained from independent pushover analyses in the two horizontal directions. However, the N2 method turns out to be conservative, since overestimation of displacement at the center of mass prevails over underestimation of torsional effects.

More recently, an important step forward to properly including torsional

effects has been made by Peruš and Fajfar (2005), who proposed combining the results obtained by pushover analysis of a 3D structural model, based on the N2 method, with the results from a linear dynamic (spectral) analysis. The N2 method controls the target displacements and distribution of deformations along the height of the building, whereas the linear dynamic analysis is used to define the torsional amplifications of lateral displacements. Use of linear dynamic analysis was justified by the assumption that, at the flexible edge, the elastic envelope of lateral displacements is conservative with respect to the inelastic ones.

Chopra and Goel (2004) sought to extend themodal pushover analysis proposed in (Chopraand Goel 2002), by applying torsional moments at each floor (to account for dynamic effects of torsional response) in addition to lateral forces, all of them obtained from modal analysis. A comparison of predictions from the proposed procedure to exact values determined by nonlinear modal response history analysis was conducted for four structural systems with different values of the ratio of uncoupled lateral to torsional vibration periods. Results demonstrate an accuracy in response of the modal pushover analysis similar to that for a symmetric building. However, the results deteriorate for systems with stronger coupling of elastic modes, in part due to underestimation of roof displacement by the CQC modal combination rule, which occurs because the individual modal responses attain their peaks almost simultaneously. Structural plan-asymmetry about both axes and simultaneous action of two horizontal components of ground motion also remain to be investigated. In the extended MPA procedure by Chopra, the seismic demand due to individual terms in the modal expansion of the effective earthquake forces is determined by non-linear static analysis using the inertia force distribution sn for each mode, which for asymmetric buildings includes two lateral forces and torque at each floor level:

$$s_n = \Gamma_n M \phi_n = \Gamma_n \begin{Bmatrix} m\phi_{xn} \\ m\phi_{yn} \\ I_0\phi_{\theta n} \end{Bmatrix} \tag{2.33}$$

$$\Gamma_n = \frac{L_n}{M_n} \quad M_n = \phi_n^T M \phi_n \quad L_n = \begin{cases} \phi_{xn}^T m1 & \text{for direction X} \\ \phi_{yn}^T m1 & \text{for direction Y} \end{cases} \tag{2.34}$$

where Γ_n is the *n*th modal participation factor; M is a diagonal mass matrix of order *3N*, including three diagonal submatrices m , m and I_0; m is a diagonal matrix with $m_{jj}=m_j$, the mass lumped at *j*th floor diaphragm; and I_0 is a diagonal matrix with $I_{0jj}= I_{0j}$ the polar moment of inertia of *j*th

floor diaphragm about a vertical axis through the center of mass (CM); ϕ_n is the nth natural vibration mode of the structure consisting of three subvectors: $\phi_{xn,}$ ϕ_{yn} and $\phi_{\theta n}$; the $N \times 1$ vector $\boldsymbol{1}$ is equal to unit.

Penelis and Kappos (2005) also aimed at modelling the inelastic torsional response of buildings in nonlinear static (pushover) analysis. The proposed method consisted of a 3D pushover analysis, applying spectral load vectors defined from dynamic elastic spectral analysis; moreover, response quantities were obtained through a generalized equivalent SDOF system, which incorporates both translational and torsional modes. The proposed procedure was verified for few case studies: two single-storey and two multi-storey mono-symmetric buildings. In the first case, the deviation of the proposed methodology from the mean response resulting from nonlinear dynamic analysis was around 10%, while in the case of multi-storey buildings the difference in the response was about 20%, also considered acceptable given the uncertainties in the inelastic response of three-dimensional nonlinear models.

Fajfar et al. (2005) proposed an extended version of the N2 method for plan asymmetric buildings. In this proposal the pushover analysis of the 3D model is performed independently in each direction, the target displacement being calculated using the original N2 method procedure. In order to take torsional effects into account, the pushover results are amplified by torsional correction factors. These factors are computed through an elastic response spectrum analysis and a pushover analysis. No de-amplification of displacements due to torsion is considered by the method. In 2009 D'Ambrisi et al.(2009) tested the Extended N2 method in an existing school, and in 2011 Koren and Kilar (2011) tested the method in asymmetric base isolated buildings.

2.5.2 Vertically irregular structures

Design of public buildings such as theatres and museums as well as monuments is commonly dictated by either aesthetic or functional considerations that often preclude the simplicity of less important buildings. As a result, the shape of the majority of such structures is irregular, both in plan and in elevation (Reinhorn et al. 2005).

Das and Nau (2003) investigated a relatively large set of RC buildings with different number of storeys, types and locations of vertical irregularities. Starting from the belief in usefulness of simplified procedures for seismic design, the paper focused on seismic codes, such

as the UBC, which make restrictions on the applicability of simplified design methods—i.e. the equivalent lateral force method (ELF)—for structures with consistent vertical irregularities. To check the suitability of such code limitations, seismic response of building models with lateral resisting elements designed via the ELF method were evaluated by 2D linear and nonlinear dynamic analyses. Results pointed out that most structures performed well when subjected to the design earthquake, suggesting that limitations on the applicability of simplified design procedure are unnecessarily conservative for certain types of vertical irregularities.

Chintanapakdee and Chopra (2004) investigated the accuracy in predicting seismic demands for vertically irregular frames through themodal pushover analysis (MPA) proposed in Chopra and Goel (2002), which includes the higher mode contributions. They considered many 12-storey irregular frames, with strong-columns and weak-beams, designed with three types of irregularity (of stiffness, strength, and their combinations) located differently along the height. Comparison with results from nonlinear dynamic analysis showed that the accuracy of MPA in determining storey drift ratio values did not deteriorate, in spite of irregularity provided in the middle or upper storeys, or in the presence of a soft and/or weak first storey. Conversely, the MPA procedure became less accurate for frames with stiff and strong first storeys, and when the irregularity is in the lower half of the height. Nevertheless, even for these cases, modal pushover analysis was capable of identifying the storeys with the largest drift demands, i.e. detect critical storeys in such frames.

Lignos and Gantes (2005) also investigated the effectiveness of MPA, with reference to various 4-storey and 9-storey steel braced frames with stiffness irregularities. Their study, however, led to the conclusion that for taller structures the modal pushover analysis, though capable of capturing the shape of mechanism, cannot predict collapse. Hence, it should not be used for investigation near collapse.

As an alternative to the modal pushover analysis, Alba et al. (2005) proposed an extension of the N2 method, modified to consider the contribution of higher modes of vibration; with the proposed method, the capacity curve is actually obtained by means of a series of modal spectral analyses. Some case studies suggested to the authors that the method achieves more accuracy than the N2 procedure for structures with a significant contribution of the higher modes, independent of their vertically regular or irregular status.

The aim of Pinho and Antoniou (2005) was to verify the suitability of the Displacementbased Adaptive Pushover procedure (DAP), proposed in a previous work by the same authors in order to overcome limitations identified in the more traditional Force-based Adaptive Pushover methods (Antoniou and Pinho 2004). To this end, the DAP procedure was applied to a 4-storey building (tested at the JRC) characterized by relevant stiffness/strength variations at the third storey level, and yielded more accurate results in terms of deformation profiles and capacity curves.
The work of Bosco et al. (2002) was related to more traditional simplified design procedures. Starting with the premise that real multi-storey asymmetric structures rarely fulfil the strict conditions that characterize the so-called regularly asymmetric systems, they tried to define clear limits for application of simplified methods of analysis, developed rigorously only for such type of buildings. To this purpose, the authors proposed two parameters (Ghersi et al. 2002) that numerically define the vertical irregularity and showed how they are related to the ability of simplified methods to predict the elastic behavior of irregular structures. Moreover, the static analysis procedure seems to cover a wider field of application than the planar modal analysis corrected by torsional response of an equivalent single-storey system, as proposed by Chopra.

3. Proposal of a new method for the evaluation of the capacity of structures

3.1 Introduction

In recent years, as a result of seismic events occurred in Italy, the safety of buildings has become a topic of considerable interest. Therefore it is very important to develop fast and reliable analysis procedures to identify the safety level of existing structures.

Incremental dynamic analysis (IDA) is a method for the estimation of the seismic response and capacity of structures over the entire range of structural response, from elastic behavior to global dynamic instability. The most accurate way to compute seismic demands of a structure under a given seismic action is to carry out a nonlinear response history analysis (NL_RHA) of a detailed three-dimensional (3D) mathematical model of the structure. IDA requires the execution of NL_RHA for an ensemble of ground motions, each scaled to many intensity levels, selected to cover a wide range of structural response, all the way from elastic behaviour to global instability. From the results of such computation, it is possible to determine structural capacities corresponding to various limit states (Vamvatsikos and Cornell, 2002).

However, IDA is onerous for practicing engineers since it requires intensive computation of many NL_RHA. Therefore it is a rigorous procedure but not practical for a professional use.

Hence, Nonlinear Static Procedures (NSPs) attract the attention of both practicing engineers and the research community since it is more practical and faster to be implemented. Different NSPs have been developed and used for their conceptual simplicity, computational attractiveness and capability of providing satisfactory predictions of seismic response for buildings as described in section 2. Among the current nonlinear static analysis methods, modal pushover analysis (MPA) was developed by Chopra and Goel (2002) to take account of the contribution of higher modes to the total response; later, Geol and Chopra (2004), Chintanapakdee and Chopra (2004) reported that MPA yields better results compared to the traditional pushover analysis. However, most of the researches dealing with nonlinear static analysis procedures have been limited to planar structures.

Due to the development of NSP to evaluate the seismic demands of the

structure, it is of a great interest to replace the NL_RHA for each given seismic intensity level by NSP to reduce the computational effort required for IDA. Remembering that MPA procedure retains the conceptual simplicity and computational attractiveness of current pushover procedures with invariant force distributions: Han and Chopra (2006) developed an approximate IDA procedure based on MPA, showing that the MPA-based IDA procedure can provide accurate estimation of capacity for structures. The capacity curve is a plot of the spectral pseudo-acceleration against a seismic demand parameter. The demand parameter may be the peak roof drift ratio, defined as the roof displacement divided by building height, or the maximum over all stories of the peak inter-storey drift ratio, defined as the storey drift divided by the storey height. Therefore, the aim of this paper is to propose a more efficient incremental modal pushover analysis (IMPA) to obtain capacity curve of the structure to evaluate the seismic demand: the procedure allows defining the capacity curve based on the execution of a series of MPAs. The capacity curve defines the relationship between base shear and top displacement of the building and can be used for the prediction of the seismic performance of detected structure. In the following, first, the MPA is discussed referring to asymmetric structures, the basic idea of IMPA is presented and the step-by-step computational procedure is summarized. Secondly, an existing building, which presents both vertical and plan irregularities, is selected as case study to check whether the MPA procedure to asymmetric structures can be successful, even in the case of very complex irregularity conditions and develop the capacity curve for the building through IMPA. Finally the seismic response which are presented in terms of roof displacement and base shear, are compared with NL_RHA. Concluding, capacity curves obtained by IMPA are then presented and discussed.

3.2 Incremental Dynamic Analysis (IDA) theory

The main idea of IDA method is to carry out dynamic time-history analysis under several ground motion inputs with different intensities, which analyzes the whole damage process and collapse resistant capacity of structures through the relation curve of damage measure (DM) and intensity measure (IM).

A monotonic scalable ground motion intensity measure (or simply intensity measure, IM) of a scaled accelerogram, a_λ, is a non-negative

scalar $IM \in [0,+\infty)$ that constitutes a function, $IM = f_{a1}(\lambda)$, that depends on the unscaled accelerogram, a_1, and is monotonically increasing with the Scale Factor (SF), λ .
Damage measure (DM) or structural state variable is a non-negative scalar $DM \in [0,+\infty)$, that characterizes the additional response of the structural model due to a prescribed seismic loading.

3.2.1 Single-record IDA curve

The single-record IDA is to carry out nonlinear dynamic history analysis with a specific seismic action from a ground motion database. An unscaled accelerogram a_1 is referred to as the base, and a simple transformation is introduced by uniformly scaling up or down the amplitudes by a scaler $\lambda \in (0,+\infty) : a_\lambda = \lambda \cdot a_1$ .Every a_λ corresponds to a structural performance parameter, and all DM-IM points plotted in 2D-coordinate are connected to finally form the single-record IDA curve.
Common examples of scalable IMs are the Peak Ground Acceleration (PGA), Peak Ground Velocity, the ξ=5% damped Spectral Acceleration at the structure's first-mode period ($S_a(T_1,5\%)$), and the normalized factor $R = \lambda / \lambda_{yield}$ yield (where λ_{yield} signifies, for a given record and structural model, the lowest scaling needed to cause yielding) which is numerically equivalent to the yield reduction R-factor for, for example, bilinear SDOF systems (see later section). These IMs also have the property of being proportional to the SF as they satisfy the relation $IM = \lambda \cdot f_{a1}$ .On the other hand the quantity $S_{am}(T_1,\xi,b,c,d) = [S_a(T_1,\xi)]^b \cdot [S_a(\mathrm{c}T_1,\xi)]^d$ proposed by Shome and Cornell (1999) and Mehanny and Deierlein (2000) is scalable and monotonic but non-proportional, unless b+d = 1. Some non-monotonic IMs have been proposed, such as the inelastic displacement of a nonlinear oscillator by Luco and Cornell (2007), but will not be focused upon, so IM will implicitly mean monotonic and scalable hereafter unless otherwise stated.
DM is an observable quantity that is part of, or can be deduced from, the output of the corresponding nonlinear dynamic analysis. Possible choices could be maximum base shear, node rotations, peak storey ductilities, various proposed damage indices (e.g., a global cumulative hysteretic energy, a global Park–Ang index (Ang and Leon, 1997) or the stability index proposed by Mehanny and Deierlein (2000)), peak roof drift, the

floor peak interstorey drift angles $\theta_1,...,\theta_n$ of an *n*-storey structure, or their maximum, the maximum peak interstorey drift angle $\theta_{\max} = \max(\theta_1,...,\theta_n)$. Selecting a suitable DM depends on the application and the structure itself; it may be desirable to use two or more DMs (all resulting from the same nonlinear analyses) to assess different response characteristics, limit-states or modes of failure of interest in a Performance Based Earthquake Engineering (PBEE) assessment. If the damage to non-structural contents in a multi-storey frame needs to be assessed, the peak floor accelerations are the obvious choice. On the other hand, for structural damage of frame buildings, $\theta_{\max}$ relates well to joint rotations and both global and local storey collapse, thus becoming a strongDM candidate. The latter, expressed in terms of the total drift, instead of the effective drift which would take into account the building tilt, will be our choice of DM for most illustrative cases here, where foundation rotation and column shortening are not severe.

3.2.2 Multi-Record IDAS

Single-record IDA study cannot fully capture the behavior a building may display in a future event. The IDA can be highly dependent on the record chosen, so a sufficient number of records will be needed to cover the full range of responses. A Multi-Record IDA study is a collection of single-record IDA studies of the same structural model, under different accelerograms. Such a study correspondingly produces sets of IDA curves, which by sharing a common selection of IMs and the same DM, can be plotted on the same graph. An IDA curve set is a collection of IDA curves of the same structural model under different accelerograms, which are all parameterized on the same IMs and DM. While each curve, given the structural model and the ground motion record, is a completely defined deterministic entity, if we wish to take into account the inherent randomness with respect to what record the building might experience, we have to bring a probabilistic characterization into play. The IDA given the structural model and a statistical population of records is no longer deterministic; it is a random line, or a random function $DM=f(IM)$ (for a single, monotonic IM). Then, just as we are able to summarize a suite of records by having, for example, mean, median, and 16%, 84% response spectra, so we can define mean, median and 16%, 84% IDA curves.

3.3 Incremental Modal Pushover Analysis（IMPA）

The incremental modal pushover analysis (IMPA) proposed is a pushover based procedure that requires execution of MPA and evaluation of the performance of the structure for a range of intensity of seismic actions. The database resulting from the application of MPA with the detected range of seismic intensity provides all the response information needed to estimate seismic response due to different intensity levels. For each seismic intensity level, the corresponding Performance Point (P.P.) for the multi-degree-of-freedom (MDOF) system, in terms of roof displacement and corresponding base shear, can be obtained by combining the P.P. determined by applying the Capacity Spectrum Method (CSM) for the significant signle modes: the P.Ps will be combined through Square Root of the Sum of Squares (SRSS) rule. This way it is possible to obtain a range of multimodal performance point (P.P.mm), each one corresponding to a specified seismic intensity level: CSM is applied with Response Spectrum (RS) of the set of intensity. The RS will be scaled up to obatian a set of intensities such as in IDA with the time histories. By connecting all the P.P.mm, a curve can be obtained: this curve has been named "Multimodal Capacity Curve" (MCC). The detailed step-by-step implementation of the IMPA procedure is presented below:

1. Compute the natural frequencies, w_n and modes, ϕ_n for linearly elastic vibration of the building;
2. Select the ground motions and the RS for a range of intensity levels;
3. For the intensity level *i*, which is represented by Peak Ground motion

Acceleration (PGA), CSM is adopted to search for P.P. for the predominate modes: for the *n*th mode, transform capacity curve, which in terms of base shear and roof displacement, into a capacity spectrum and transform the RS into Acceleration Displacement Response spectrum (ADRS) format, plot them on the same chart, their intersection is taken as the P.P., as shown in Figure 3.1 a). Obtain the corresponding P.P. from the capacity curve, as shown in Figure 3.1 b). It is worthy to note that, for the *n*th mode, if the structure enters nonlinear plastic stage, then the demand spectrum should be reduced by the spectral reduction factor which depends on the effective viscous damping of structure ξ_{ni}:

$$\xi_{ni} = \xi_0 + k\frac{1}{4\pi}\frac{E_{dni}}{E_{S0ni}} = \xi_0 + k\xi_{eqni} \tag{3.1}$$

where ξ_{ni} is the effective damping for nth mode, ξ_0 is the inherent damping of the elastic structure, around 5% for reinforced concrete structures; E_{dni} is the energy dissipated in an ideal hysteretic cycle, in the sense which corresponds to the area of enclosed by the hysteresis loop; E_{s0ni} is the maximum strain energy that the structure dissipates, which corresponds to the area of hatched triangle; and k is modification factor of the damping.

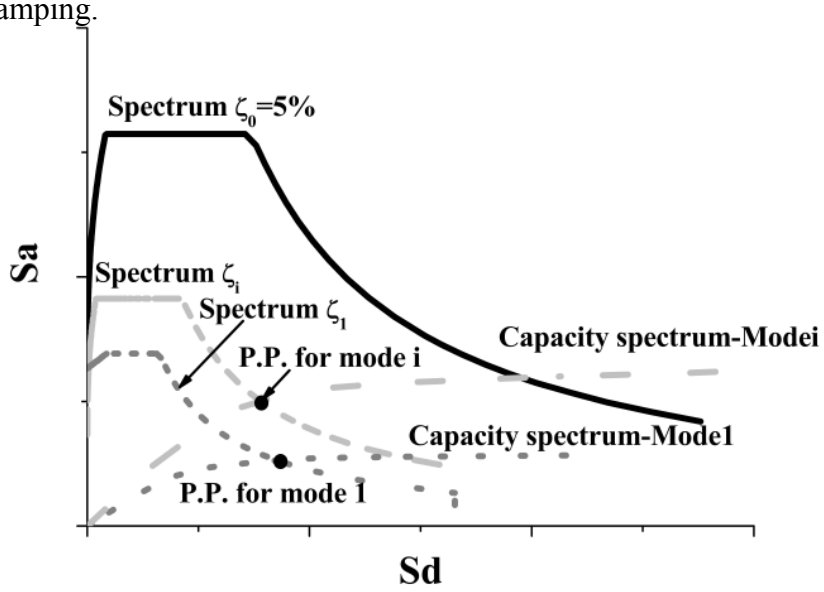

a) for each capacity curve the P.P. is determined via C.S.M.

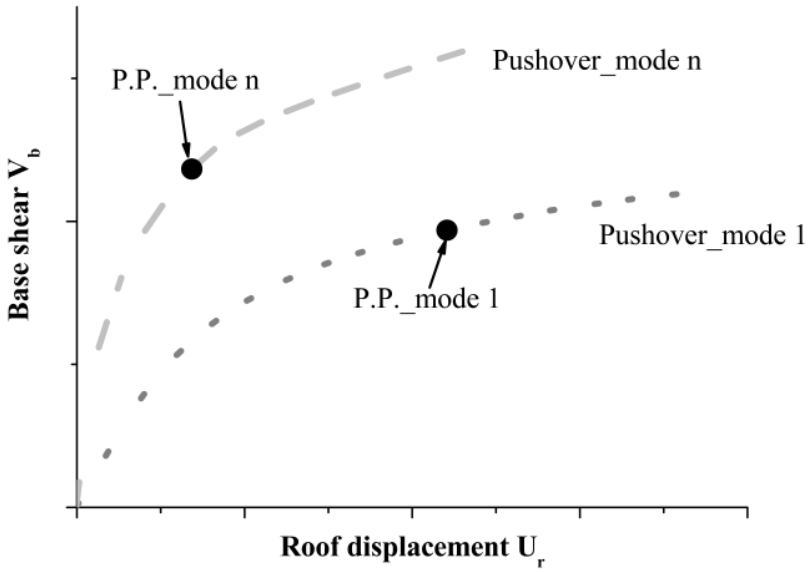

b) P.P. can be plotted in the V-U plane

Figure 3.1 Evaluation of the performance points (P.P.) for each capacity curve that belongs from the pushover analysis with the selected load distributions: proportional to Mode1..Mode n.

4. Determine multimodal performance point (P.P.mm) in terms of multimodal base shear V_{bmmi} and multimodal roof displacement u_{rmmi} for seismic intensity level i by combining the single ‘‘modal’’ base shears ($V_{b1i}…V_{bni}$) and roof displacements ($u_{r1i}…u_{rni}$) using SRSS rule:

$$u_{rmmi} = ((\sum_{n} u_{rni}^{2})^{1/2}) \quad V_{bmmi} = ((\sum_{n} V_{bni}^{2})^{1/2}) \tag{3.2}$$

5. Repeat steps 2–4 for as many intensity levels to form the IMPA curve, as shown in Figure 3.2.

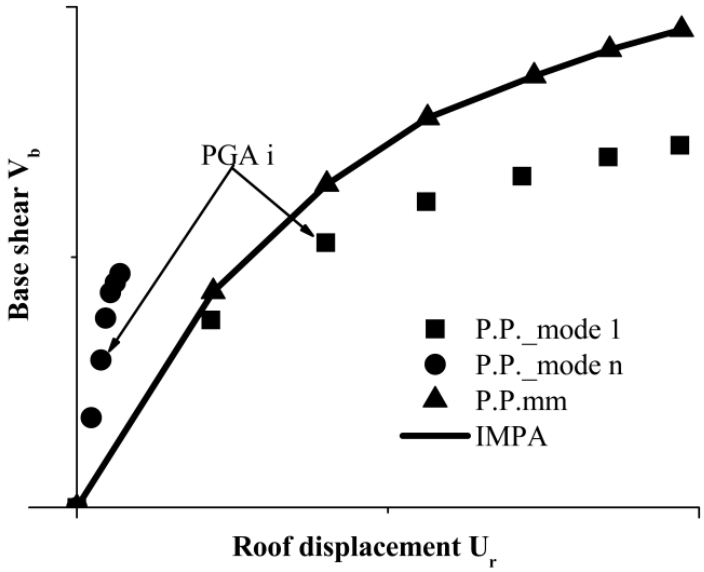

Figure 3.2 Construction multimodal capacity curve (MCC) from the IMPA procedure. By applying SRSS rule with the P.P. obtained with each load distribution (Mode1..Mode n) and for each intensity level (the response spectrum is scaled from lower to higher intensity levels) the MCC) can be obtained.

4. Retrofitting of structure via dissipative braces

4.1 Introduction

Buildings not designed according to modern seismic codes may present structural deficiencies and might suffer damage and collapse when subjected to seismic action; therefore rehabilitation is often needed to guarantee life safety as a minimum. On the other hand buildings designed according to modern seismic concepts can resist even to strong seismic action without collapse but with a certain amount of structural and non structural damage. Therefore, since the experience of past earthquakes clarifies that even in the case of a well performing structure life safety can be compromised by the collapse of non structural components (e.g. internal partitions, masonry infill walls), the reduction of global vulnerability preventing the building from damaging can be often the case.

Conventional upgrading techniques usually include the addition of existing walls and foundations and strengthening of frames. Most of these techniques often lead to costly consequences such as heavy demolition, lengthy construction time, reconstruction, and occupant relocation. Such costly, environmentally hostile and intrusive approach associated with conventional techniques often deters building owners from retrofitting building for improved earthquake performance.

In the last two decades retrofitting by the introduction of technologies for the reduction of seismic demand has become more and more utilized. The most two popular technologies of this kind of seismic retrofitting strategies are base isolation and dissipative braces, as shown in Figure 4.1

Base isolation is a mechanism that provides earthquake resistance to the new structure or existing building. The base isolation system decouple the building from the horizontal ground motion induced by earthquake, and offer a very stiff vertical components to the base level of the superstructure in connection to substructure (foundation). It shifts the fundamental lateral period, Ta, dissipates the energy in damping, and reduces the amount of the lateral forces that transferred to the inter-story drift, and the floor acceleration, as shown in Figure 4.3.Base isolation is the main application but it usually requires considerable space around the building.

Providing reliable mechanisms for dissipation of the destructive earthquake energy is key for the safety of structures against intense earthquakes. Inelastic deformations can limit the forces in members and provide hysteretic energy dissipation to the system. The concept of designing some sacrificial members, dissipating the seismic energy, while preserving the integrity of other main components is known as the structural fuse concept. The use of dissipative braces can be viewed as a method to increase dissipation and therefore to reduce seismic demand,as shown in Figure 4.3. The use of dissipative bracings would create an increase in initial stiffness without a strong increment in maximum shear at the base, and would give a strong increase in dissipation capacity.

Figure 4.1 retrofitting existing building with base isolation

Figure 4.2 retrofitting existing building with dissipative braces

The greater complexity derives from the non linear behaviour of the

dissipative devices and therefore of the final retrofitted structure. Despite that, during the last years, many design procedure has been published and, between those, the most useful for practical use seem to be those that are based on the capacity spectrum method. In fact with this approach non linear dynamic analyses can be skipped in favor of static non linear analyses that are simpler to be managed. Otherwise, also within those procedures, many have a theoretical approach that can be difficulty associated with a widespread professional use. In fact, frequently, the characteristics of an existing building (e.g. non regular distribution of masses and stiffness, presence of a soft story) can compromise the effectiveness of procedures that impose a predefined loading pattern during pushover analyses. As discussed in Bergami & Nuti (2013), the design of dissipative devices has two main goals: improve dissipation and regularize strength end stiffness distribution (this can be done adopting adequate criteria to distribute the braces along the elevation and inside the plan of the building).

In this section, this design procedure to determine the characteristics of dissipative braces B to retrofit an existing building S is discussed, applied and verified: the retrofitted structure S+B would guarantee life safety avoiding collapse and damage of structural and non structural elements. The procedure is based on displacement response control and on the use of the well known non linear static analysis: pushover. The presented procedure is applied on case studies using a widely diffuse and convenient mechanical type of dissipative brace: the buckling restrained brace (BRB). However the procedure can be easily used with any type of dissipative brace whose characteristics are expressed in terms of elastic stiffness and plastic excursion.

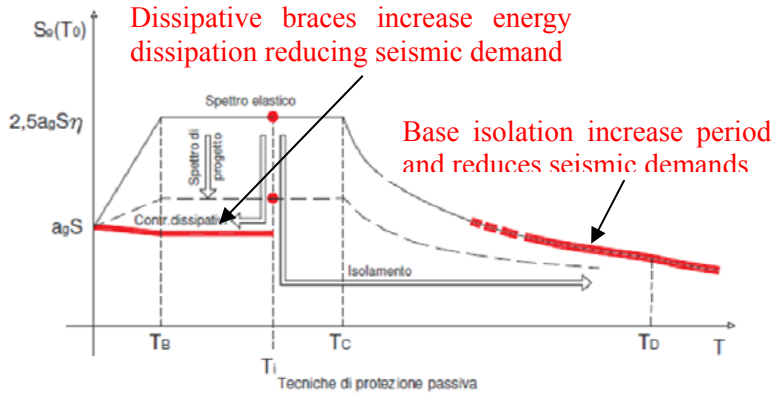

Figure 4.3 The mechanism of the base isolation and dissipative braces

4.2 The Buckling Restrained Brace (BRB)

4.2.1 BRB configuration

Research on BRBs was first carried out by Yoshino et al. (1971). Since 2000, interest and use of BRBs has been growing rapidly. At this time, there are dozens of different types and configurations of BRBs, but the most often used is the Unbonded Brace concept. This concept is the original type of BRB, which was developed and produced in Japan during the 1980's: BRBs consist of a steel core element, endowed with a special coating to reduce friction, encased in a concrete filled steel tube preventing steel core buckling in compression. Axial forces are absorbed by the core only that is free to lengthen and shorten dissipating energy by yielding both in tension and compression. As any metallic damper the behavior of a BRB depends on its geometry and mechanical characteristics, as shown in Figure 4.4.

BRBs provide stable hysteretic energy dissipation with a cyclic response very similar to steel constitutive law. The steel core can be realized in various ways according to market availability. The dissipative device can constitute a whole brace element or more frequently, especially in case of particularly small range of displacements and high stiffness, they can assume the configuration of short elements connected in series to an "elastic" brace.

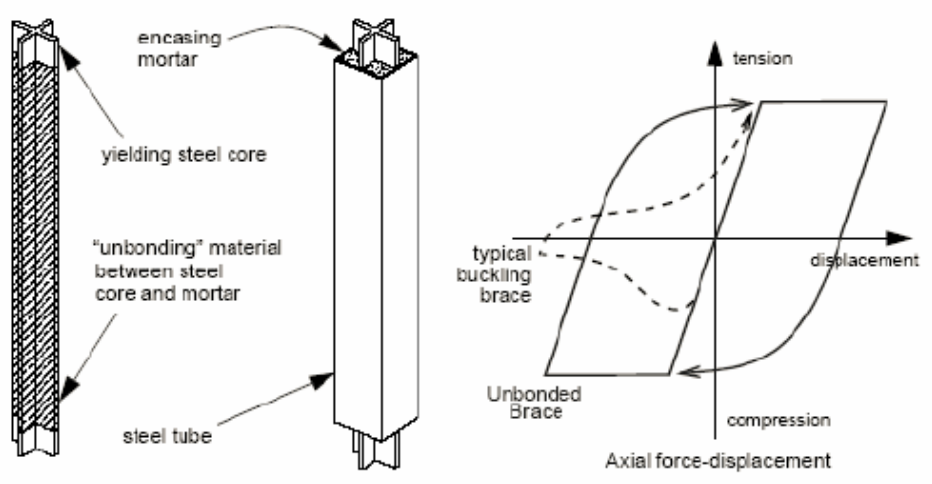

Figure 4.4 Schematic mechanism of the BRB

4.2.2 Dissipative bracings positioning: structural effects

The common configuration of the braces is shown in Figure 4.5. and the connection of brace to steel structure and R.C.strcuture are shown in Figure 4.6 and Figure 4.7, respectively.

The insertion of dissipative braces into the structural frame involves significant effects that can be grouped in two categories: effects on structural response and effects on the architecture of the building. Concerning the former the braces increase both stiffness and strength and consequently, as usually happens, both modal shapes and the capacity curve of the structure are modified indeed. Moreover, for a given top displacement, they improve dissipation and therefore modify the demand. In this respect stiffness increase could render less efficient, or even useless, the increase of dissipation. Therefore a careful mix of stiffness and dissipation is requested: this subject is discussed in the following.

Furthermore the bracing system has to be compatible with the architecture of the building: therefore spatial distribution of the braces descents from a compromise between the optimization of the dissipative system and the functionality of the building (the designer has to find a balance between a functional position of the devices and an appropriate distribution of strength and stiffness).

Although braces distribution should be analyzed case by case some general considerations can be made: braces should reduce or eliminate eventual translation-rotation coupling effects, induce constant interstorey

drifts, exclude soft storey behavior and maximize damping for a given top displacement.

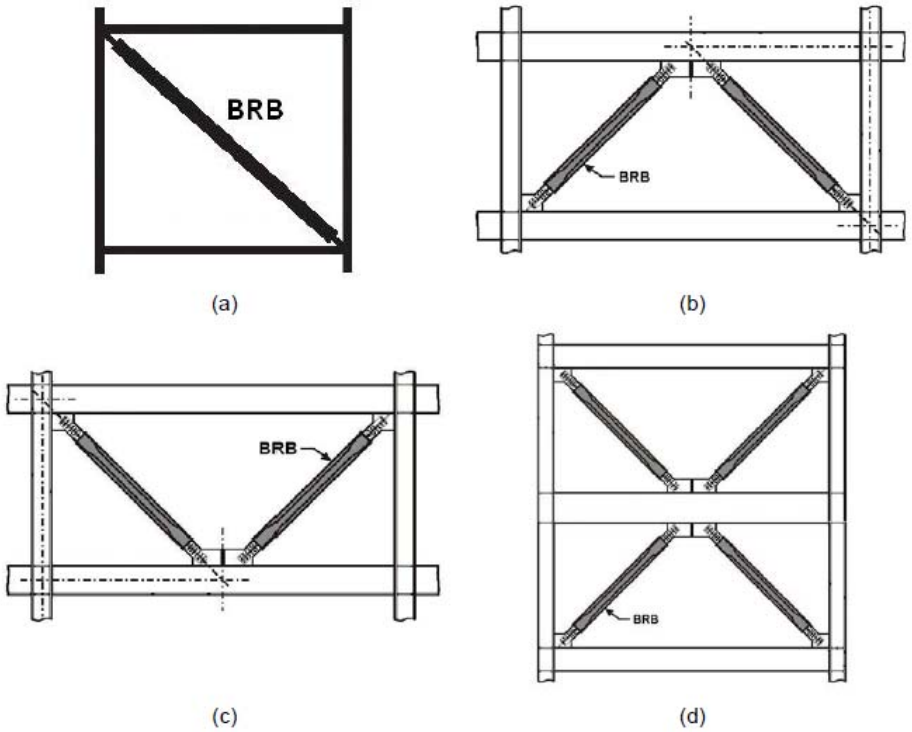

Figure 4.5 Examples of BRB bracing configurations, a) Diagonal bracing, b) Chevron bracing, c) V bracing, d) X bracing (Tremblay et.at,2004)

Figure 4.6 Connection to steel structure

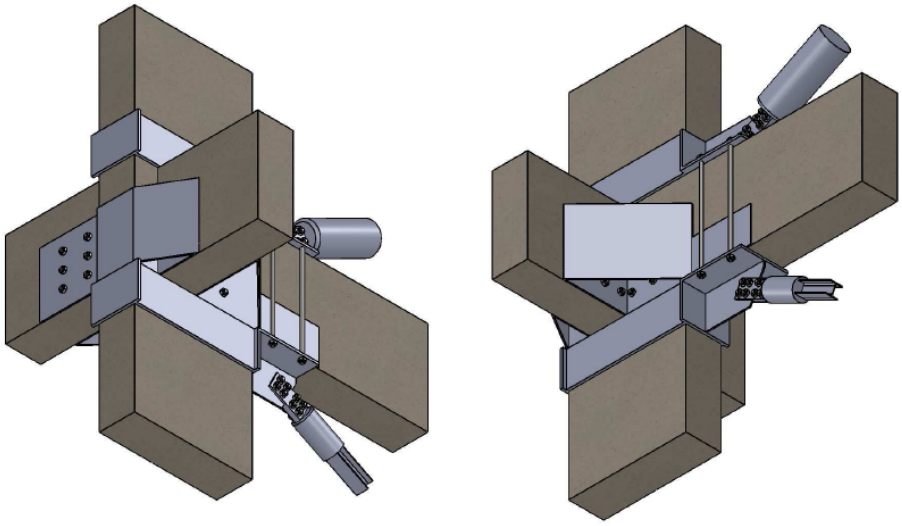

Figure 4.7 Connection to R.C. structure

4.3 State of the art of design methods

No one of the existing codes, with the partial exception of FEMA, defines design criteria for dissipative bracing systems: FEMA 274 (1997) and FEMA 356 (2000) highlight the variability of design methods accordingly to the different types of existing dissipative devices. In fact dissipative devices can be grouped into two major categories: devices with displacement dependent behaviour (yielding metallic and friction dampers) and devices with velocity dependent behaviour (visco-elastic solids or viscous fluid). Alternatively existing design methods for dissipative braces may be distinguished according to the scope of the design process: optimization of global response parameters such as the dissipated energy, or limiting maximum displacement (performance base design). In the following some representative procedure are briefly described.

Filiatrault and Cherry (1988-1990) defined a design criteria for dissipative braces, based on non linear time history analyses, that aimed at minimizing the difference between seismic input energy and dissipated energy; the existing structure is supposed to remain elastic.

Ciampi et al. (1991-1995) determine a bracing system in order to minimize a cumulative structural damage index (e.g. kinematic ductility or cumulative ductility). The structure is represented by an equivalent elasto-plastic SDOF with one equivalent dissipative brace.

More recently procedures based on the displacement based design have

been developed such as those of Vulcano et al. (1993-2010), Kim & Choi (2004) and Ponzo et al. (2010).
In Vulcano et al. the authors suggest a distribution of the braces finalized to maintain strength and stiffness distribution of the original structure and consequently, as the authors suggest, guarantee that modal shapes don't change after the insertion of the braces.
Kim & Choi assumed all the required additional damping as supplied by the braces whose distribution, and therefore strength and stiffness distribution too, is not discussed.
In Ponzo et al. the characteristics of the bracing systems are determined imposing the equivalence between the energy stored, in case of seismic event, in an equivalent elastic single degree of freedom system (the original structure) and in the elasto-plastic system (the dissipative bracing system); results are verified using the N2 method proposed by Fajfar (1999) and Fajfar P. & Gaspersic P. (2000).
Both procedures of Ponzo et al. and Kim & Choi are calibrated on the achievement of a target performance point (e.g. the target top displacement) without any consideration of other parameters.
The three latter cited displacements based design procedures (Vulcano et al., Kim & Choi, Ponzo et al.) work for design of new buildings, usually conceived regular in plan and elevation and whose seismic response can be controlled by few parameters. However, for the following reasons, these don't seem sufficiently manageable for interventions on existing buildings.
Infact Vulcano et al. assume that the structure has not to change its modal shapes: therefore irregular structures will remain such. Instead, Kim & Choi and similarly Ponzo et al., base their evaluation on global parameters, as top displacement, and do not care of significant other ones as interstorey drift, usually relevant for retrofitting design.
It is a matter of fact that existing buildings are usually irregular and characterized by a low plastic limit; the use of dissipative bracings should both regularize the structure and increase dissipation. This way seismic demand is reduced and the evaluation of the seismic response is more reliable with respect to the original irregular structure: this is especially necessary for pushover based methods which make use of nonlinear static procedures.
The methodology presented in the present paper is based on the Capacity Spectrum Method, which take in explicit consideration the energy dissipated by the analyzed structure, and therefore it is suitable for

structures with additional dampers. If compared with the one proposed by Kim & Choi (2004), it is more flexible since the contribution to dissipation of the structure S and braces B are kept distinct and the structure S can be non linear as well. In this new approach the computation of the energy dissipated by the devices is evaluated referring to the hysteretic cycle performed by each device of each braced level while, the dissipation offered by the original structure, is computed in a global matter based on pushover curve.
Furthermore, as well as top displacement, also the interstorey drift, a good indicator of irregularity, is kept under control. Finally a criterion is given to dimension BRBs at each story.

4.4 Review of the design procedure of dissipative braces for seismic upgrading structures (Bergami & Nuti, 2013)

4.4.1 Relevant parameters for design of retrofitting with BRBs

Considering a braced structure, as in Figure 4.8, being its capacity curve represented by the curve S+B of Figure 4.9, one can assume that this latter is the sum of the capacity curves of the structure (S) and of the bracing system (B): therefore the latter can be obtained subtracting S from S+B. This assumption, if the bracing system isn't extremely resistant (e.g. the yielding point of S+B isn't too much higher than the yielding point of S), is relatively accurate for design purposes: the increase of axial forces in the structure doesn't change too much the structural behaviour of S that can be approximately considered as a constant during the design process. In Figure 4.9 the capacity curve S is approximated as elasto plastic as well as the capacity curve B: therefore the curve S+B is trilinear.
In a design process the seismic action can be expressed in term of response spectrum and therefore, for a given capacity curve S+B, one can obtain the structural response in term of displacement being known the equivalent viscous damping ν_{eq} associated to each point of the curve S+B.

It is well known that the force-displacement behaviour of BRBs can be modelled by a simple bilinear law characterized by the elastic axial stiffness $K'_{b,j}$, the yield strength $F'_{b,j}$ and the hardening ratio $\beta_{b,j}$, as confirmed by numerous experimental studies (Robinsons et al. (1976),

Whittaker et al. (1991), Sakurai et al. (1992), Sakurai et al. (1992), Hanson et al. (2001), Kim et al. (2004), Black et al. (2004)) and as suggested by SEAOC/AISC (2005).

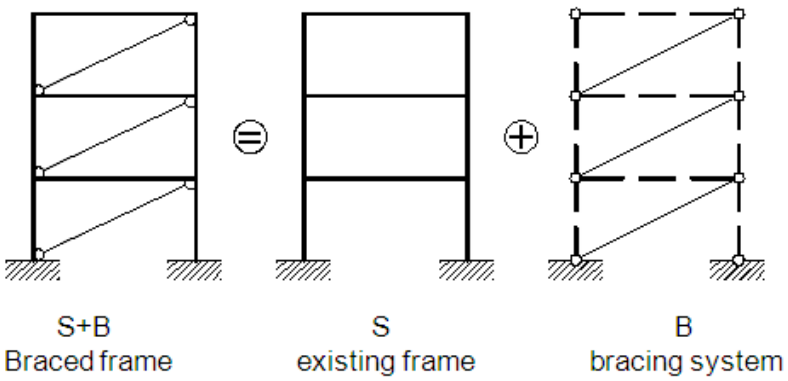

Figure 4.8 Scheme of the braced structure (S+B) as sum of the existing structure (S) and the bracing system (B)

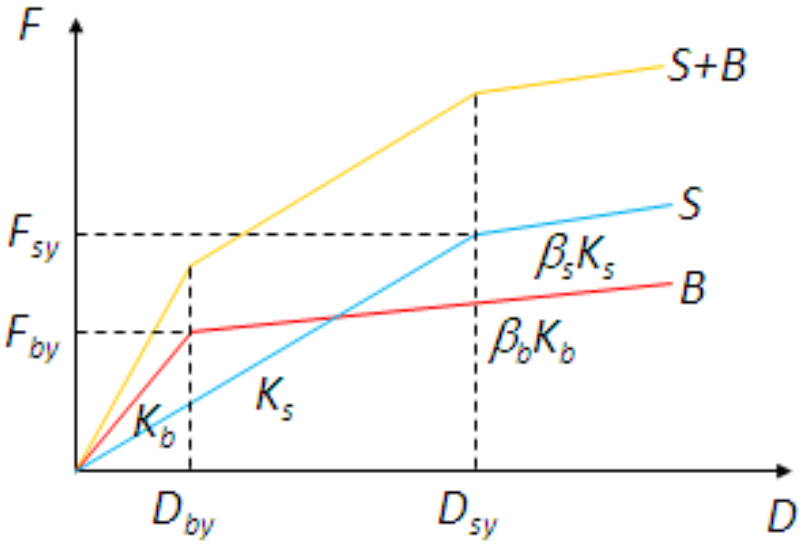

Figure 4.9 Interaction between the structure (S) and the bracing system (B) expressed in terms of horizontal components of the force-displacement relationship

The parameters of the bracings depends on the geometry of the frame and on the characteristics of the device. Parameters $K'_{b,j}$, $F'_{b,j}$, $D'_{b,j}$ and $\beta_{b,j}$ depend on mechanical properties of the selected devices while the

length lb and the inclination θ_b (Figure 4.10) of each brace can be determined referring to both geometric characteristics of the structure and braces distribution.

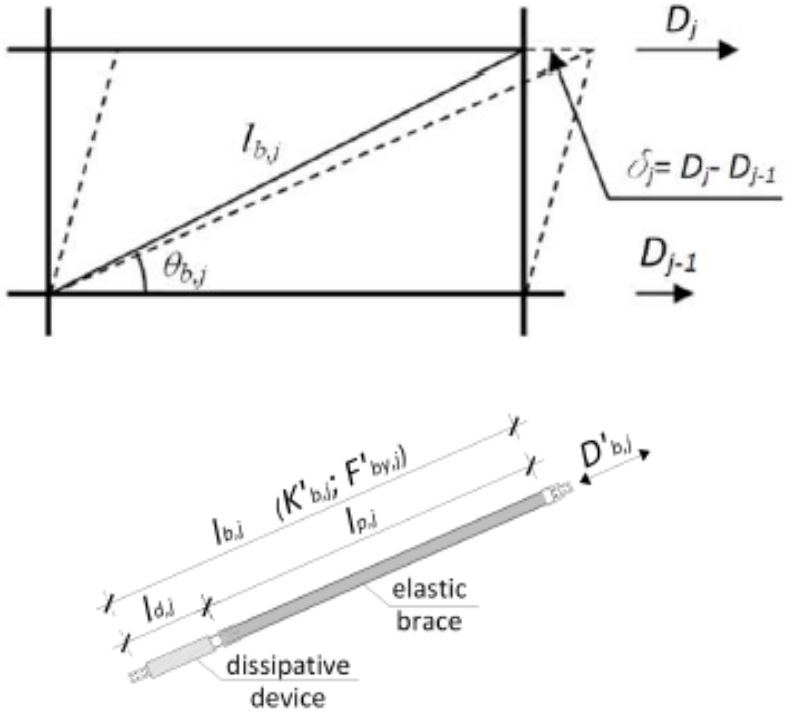

Figure 4.10 Deformed shape of a generic single part of the braced frame

Being K_b, F_{by}, D_{by} the horizontal components of stiffness, yield strength and displacement at yield of the bracing system B respectively, they can be expressed as follow:

$$K_b = K'_b \cos^2 \theta_b \tag{4.1}$$

$$F_{by} = F'_{by} \cos \theta_b \tag{4.2}$$

$$D_{by} = D'_{by} / \cos \theta_b \tag{4.3}$$

Therefore the scope of the design is the definition of the following variables:

1. the plano-altimetric configuration of the bracing system that influences

device sizing as it modifies the braced frame deformed configuration both in the linear range as well as beyond the plastic limit;
2. the axial stiffness $K'_{b,j}$ of each brace and consequently the stiffness K'_b of the entire bracing system B (K'_b directly affects the elastic stiffness of the braced structure);
3. the yielding limit of the bracing system (D'_{by}, F'_{by} in terms of axial components or D_{by}, F_{by} in terms of horizontal components) that is the point beyond which the system B becomes dissipative. It thus influences both resistance and energy dissipation capacity of the braced structure. In Figure 4.9 a representation of the cited parameters is given referring, for simplicity, to a bilinear relationship of the horizontal components of load and displacement for both S and B;
4. the hardening ratio β_b of the bracing system that affects both resistance and dissipative capacity of the braced structure.
We can proceed in different manners to determine the stiffness and strength of the braces, to be added to the floors, to reduce maximum response to the intended value in terms of displacements (total and interstorey) and base shear.
It is evident that if the dissipative system yields before the structure itself ($D_{by}<D_{sy}$) the efficiency of the intervention will increase, therefore this should and will be a basic assumption.
Moreover the designer, once defined the desired performance for the structure in terms of top displacement, can decide to avoid or admit plastic deformations of the existing structural elements.
With reference to Figure 4.9 three ranges of displacement can be identified on the capacity curve.
The first segment corresponds to a displacement range below the point of first yielding of the bracing system ($D<D_{by}$): in this range both the structure and the braces are elastic and therefore total damping of S+B coincides with the inherent damping ν_I offered by the original structure ($\nu_{tot}=\nu_I$). It is a matter of fact that, in case one uses very stiff braces, total damping could be even smaller than the original inherent damping due to the large increase of elastic energy.
Entering in the second branch, beyond first yielding of B, the structure S is still elastic ($D_{by}<D\leqslant D_{sy}$) and the bracing system dissipate energy: therefore total damping is the sum of the inherent plus the one due to braces dissipation ($\nu_{tot}=\nu_I+\nu_{eq,B}$). This latter displacement range can be assumed as acceptable at least for frequent earthquakes.

Finally, if it is accepted that also the structure yields (D >Dsy), total damping of S+B is the sum of the inherent damping and the damping offered by both the bracing system and the structure itself ($\nu_{tot} = \nu_I + \nu_{eq,B} + \nu_{eq,S}$). This latter situation is often the case: many existing structures have been designed to resist to vertical loads only or, at most, to very small horizontal forces. In general yielding of S can be accepted for rare earthquakes and excluded for frequent earthquakes in order to limit damage.
It is now useful to express each limit state of interest in terms of displacement D^*. The same D_i^* can be obtained adopting different retrofitting combinations of stiffness, strength and consequently dissipation.
The first parameter to be determined is the stiffness of the braces (additional stiffness).
Different criteria to distribute the additional stiffness are proposed in scientific literature: constant at each story, proportional to story shear, proportional to interstorey drifts of the original structure. In this work the latter is assumed and therefore, given the interstorey drift δ_j, the stiffness $K'_{b,j}$ corresponding to each storey of the bracing system is:

$$K'_{b,j} = K_{global} c_{b,j} \tag{4.4}$$

where:

$$c_{bj} = \frac{\delta_j}{\max_j \{\delta_j\}} \tag{4.5}$$

Each brace is a composite element realized coupling an elastic element (usually a steel profile) with a dissipative device in series. The latter will determines the desired yielding force whereas the former will be designed to assure the desired stiffness of the series.

4.4.2 Evaluation of the equivalent viscous damping

As mentioned in the previous section, a specific energy dissipated by the structure and the braces corresponds to each deformation reached by the structure, be it with or without dissipative braces; the dissipated energy can be expressed in terms of equivalent viscous damping.
Referring to the formula proposed by A.K. Chopra (2001), the equivalent

viscous damping of the structure $\nu_{eq,s}$ at the generic displacement D can be expressed as follows:

$$\nu_{eq,S} = \frac{1}{4\pi}\frac{E_{D,S}}{E_{S,S}} \tag{4.6}$$

All the parameters of the Eq. (4.6) can be easily determined from the capacity curve: $E_{D,S}$ is the energy dissipated in a single cycle of amplitude D and $E_{S,S}$ is the elastic strain energy corresponding to the displacement D. Referring to an equivalent bilinear capacity curve (it can be determined from the capacity curve using one of the methods available in literature) terms of Eq. (4.6), considering an ideal elasto-plastic hysteretic cycle, can be determined as follow:

$$E_{D,S}^{bilinear} = 4\left(F_{sy}D - D_{sy}F_s\left(D\right)\right) \tag{4.7}$$

$$E_{S,S} = \frac{1}{2}DF_s\left(D\right) \tag{4.8}$$

with:

D	the displacement reached from the structure
$F_s\left(D\right)$	the force corresponding to D (the force is the base shear)
D_{sy}	displacement at yielding
F_{sy}	the yielding force (base shear at yielding)

It is well known that the hysteretic cycle of a real structure differs from the ideal cycle, therefore this difference can be taken into account adopting a corrective coefficient χ_S for the structure and χ_B for the braces (χ =1 for the ideal elasto-plastic behaviour). Therefore:

$$E_{D,S} = \chi_S E_{D,S}^{bilinear} \tag{4.9}$$

$$E_{D,B} = \chi_B E_{D,B}^{bilinear} \tag{4.10}$$

with $E_{D,B}^{bilinear}$ the energy dissipated by the ideal hysteretic cycle of the dissipative brace.

For the applications discussed in this paper the parameter χ_S has been determined referring to the provisions of ATC40 (ATC, 1996). For the braces the assumption of $\chi_B \approx 1$ has been considered reasonable: In fact, according to AISC/SEAOC–Recommended Provisions for Buckling-Restrained Braced Frames (2005), the force-displacement relationship of a BRB can be idealized as a bilinear curve. However different values can be adopted, if the case, with no difference in the procedure. Authors have assumed a bilinear curve characterized by a yielding force equal to the yielding traction force (the maximum compressive strength of BRBs is slightly larger than the maximum tensile strength due to the confining effect of the external tube): the hysteretic cycle obtained is elasto-plastic but precautionary smaller than the real one. Than the evaluation of the equivalent viscous damping of the braced structure $\nu_{eq,S+B}$, to be added to the inherent damping ν_I (usually ν_I =5% for r.c. structures and ν_I =2% for steel ones), can be obtained using the following expression:

$$\nu_{eq,S+B} = \frac{1}{4\pi}\frac{E_{D,S+B}}{E_{S,S+B}} = \frac{1}{4\pi}\left[\frac{\chi_S E_{D,S}^{bilinear}}{E_{S,S+B}} + \frac{\chi_B \sum_j E_{D,B,j}^{bilinear}}{E_{S,S+B}}\right] \tag{4.11}$$

$$\nu_{eq,S} = \chi_S \frac{1}{4\pi}\frac{E_{D,S}^{bilinear}}{E_{S,S+B}}; \nu_{eq,B} = \chi_B \frac{1}{4\pi}\frac{\sum_j E_{D,B,j}^{bilinear}}{E_{S,S+B}} \tag{4.12}$$

where $E_{D,B,j}^{bilinear}$ is the energy dissipated by the dissipative braces placed at level *j*.

Eq. (4.11) can be generalized assuming that $E_{D,B,j}^{bilinear} = \sum_i E_{D,B,i}^{bilinear}$ with $E_{D,B,i}^{bilinear}$ the energy dissipated by the *i* braces placed at level *j*.

Note that $\nu_{eq,S}$ and $\nu_{eq,B}$ are obtained dividing the dissipated energy, determined from the capacity curve of S or B respectively, by the elastic strain energy of the braced structure, determined from the curve of S+B.

4.4.3 Proposed design procedure

In this section, we discussed the main aspect of the evaluation of seismic

response of a structure with BRBs; in this paragraph the proposed procedure is detailed.
The procedure is based on the capacity spectrum method: the target is expressed in terms of displacement. Iteration are required since the addition of braces modifies structural response and the capacity curve has to be updated as long as the characteristics of the new braces are defined. Moreover, the energy dissipated by the braces is considered additional to the dissipative capacity of the structure, computed on the capacity curve of the original one.
Structural response is obtained reducing the design spectrum on the base of the damping of the braced structure ν_{tot}.

$$\nu_{tot} = \nu_I + \nu_{eq,S+B} \tag{4.13}$$

In a displacement based design perspective the performance desired is selected at first as the displacement (target displacement) corresponding to a selected limit state for a given seismic action. Than the required total effective damping needed to make the maximum displacement not larger than the target one is determined. The additional damping, due to bracing, is estimated as the difference between total damping and hysteretic damping of the structure without braces. The characteristics of the braces to guarantee the required additional damping are finally determined. The procedure is iterative but it converges in few iterations: the main steps follow.

1. Define the seismic action: the seismic action is defined in terms of elastic response acceleration spectrum (T-Sa).

2. Select the target displacement: the target displacement is selected (for example the top displacement *Dt**) according to the performance desired (limit state).

3. Define the capacity curve: the capacity curve of the braced structure S+B, in terms of top displacement and base shear (D_t-V_b), is determined via IMPA. In the IMPA procedure, the lateral load distribution is proportional to the modal shape, it is important to underline that the modal shape is influenced by the bracing system and consequently, each iteration the load profile has to be updated to the modal shape of the

current braced structure.

4. Define the equivalent bilinear capacity curve: the capacity curve is approximated by a simpler bilinear curve D_t-F_{s+b} that is completely defined by the yielding point ($D_{s+b,y}$, $F_{s+b,y}$) and the hardening ratio β_{s+b} (at the first iteration the parameters correspond to $D_{s,y}$, $F_{s,y}$, β_s of the existing building).

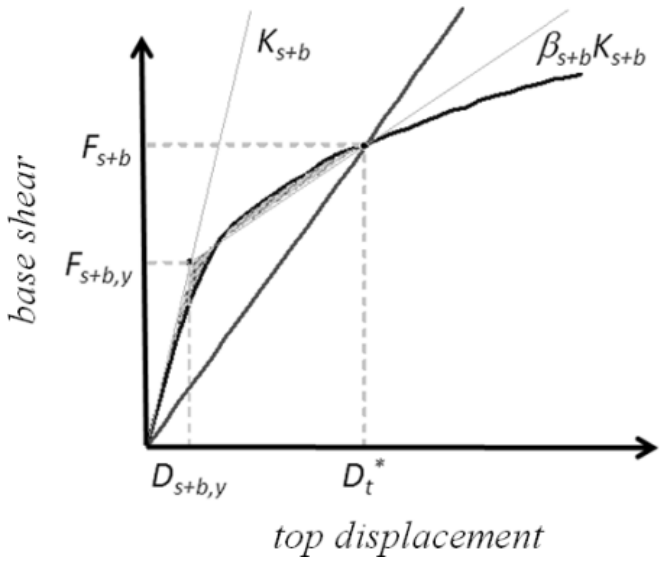

Figure 4.11 Evaluation of the equivalent bilinear capacity curve

5. Define equivalent single degree of freedom: MDOF system is converted in a SDOF system by transforming the capacity curve into the capacity spectrum (S_{dt}-S_{ab})

$$S_{dt} = \frac{D_t}{\Gamma \phi_t}; S_a = \frac{F_{S+B}}{\Gamma \cdot L} \tag{4.14}$$

where Γ is the participation factor of the modal shape ϕ ($\Gamma = (\phi^T MI)/(\phi^T M\phi)$) and $L = \phi^T MI$.

The modal characteristics of the braced structure may change at every iteration due to new brace characteristics. Therefore Γ, ϕ and L have to be updated with the current configuration.

6. Evaluate the required equivalent viscous damping: the equivalent viscous damping $\nu^*_{eq,S+B}$ of the braced structure to meet the displacement of the equivalent SDOF system and the target spectral displacement $S^*_{dt} = D^*_t / (\Gamma \phi^T)$ is determined.
According to the Capacity Spectrum Method the demand spectrum is obtained reducing the 5% damping response spectrum by multiplying for the damping correction factor h that is function of ν_{tot}.

$$\eta = \sqrt{\frac{10}{5 + \nu_{tot} \cdot 100}} = \frac{S_{\nu_{eff}}}{S_{5\%}} \tag{4.15}$$

From Eq. (4.15) one obtain the damping needed to reduce displacement up to the target S^*_{dt}.

$$\nu^*_{tot} = 0.1 \left(\frac{S_{5\%}}{S^*_{dt}} \right)^2 - 0.05 \tag{4.16}$$

7. Evaluate the equivalent viscous damping contribution due to the naked structure: the contribute to damping of the structure $\nu^*_{eq,S}(D^*_t)$ can be determined from Eq. (4.12) being D^*_t the top displacement corresponding to $E^{bilinear}_{D,S}$ and $E_{S,S+B}$ that are the energy dissipated by S and the elastic strain energy of S+B ($E^{bilinear}_{D,S}$ and $E_{S,S+B}$ are determined from the capacity curve of S and S+B respectively).

8. Evaluate the additional equivalent viscous damping contribution due to braces: given ν^*_{tot} from Eq. (4.16) the equivalent viscous damping needed to be supplied by the braces $\nu^*_{eq,B}(D^*_t)$ is evaluated from Eq. (4.11) and Eq. (4.13) as follows:

$$\nu^*_{eq,B}(D^*_t) = \nu^*_{tot}(D^*_t) - \nu^*_{eq,S}(D^*_t) - \nu_I \tag{4.17}$$

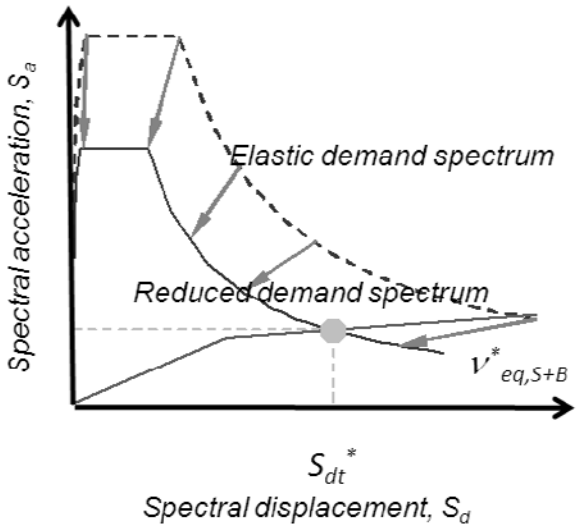

Figure 4.12 Evaluation of the equivalent viscous damping needed to achieve the target performance point

9. Dimensioning of the braces: once the required equivalent viscous damping has been evaluated from Eq. (4.17), axial stiffness and yielding strength required to achieve the desired additional damping can be determined with the same procedure previously adopted for the structure (step 7).

The energy dissipated by the braces inserted at each *j*th level can be expressed as:

$$E_{D,B}^{bilinear} = \sum_{j=1}^{n} 4\left(F_{by}^{'}\delta_{j}^{'} - \delta_{y,j}^{'}F_{b,j}^{'}(\delta_{j}^{'})\right) \tag{4.18}$$

being $\delta_j^{'}$ the component of the interstory drift δ_j at *j*th of the *n* floors along the axe of the brace ($\delta_{y,j}^{'}$ is the axial displacement corresponding to yielding of the device).

The axial displacement of the damping brace at the *j*th-floor $\delta_{b,j}^{'}$ can be determined from its inclination angle $\theta_{b,j}$ and interstorey drift $\delta_j = D_j - D_{j-1}$: therefore $\delta_{b,j}^{'} = \delta_j \cos\theta_{b,j}$.

The dissipative brace is usually constituted by a dissipative device (e.g.

the BRB) assembled in series with an extension element (e.g. realized with a steel profile) in order to connect the opposite corners of a frame.

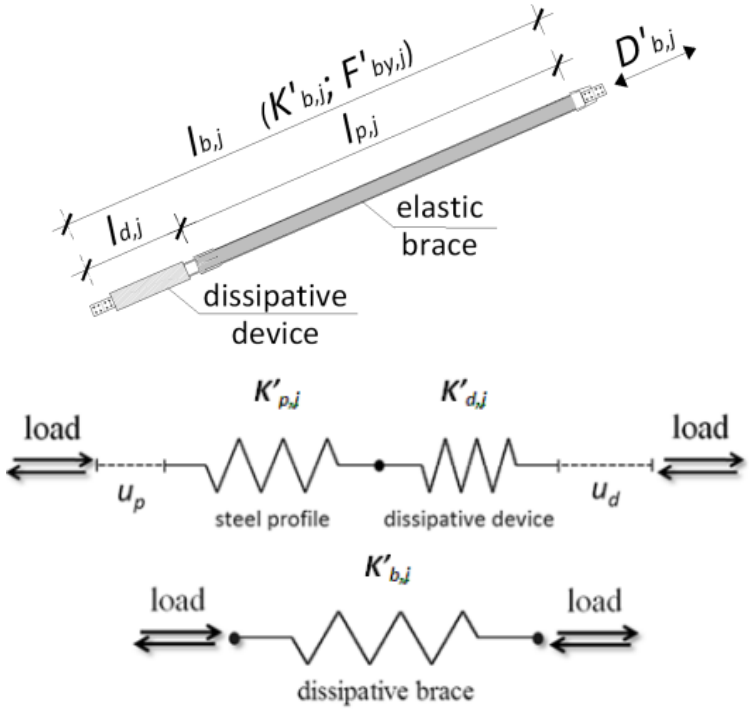

Figure 4.13 Dissipative device "j" assembled in series with an extension element (e.g. a steel profile): equivalent model of springs in series ($K'_{d,j}$; $K'_{p,j}$) and equivalent single spring model ($K'_{b,j}$)

Therefore, being $K'_{b,j}$ and $K'_{p,j}$ the equivalent stiffness of the spring series in the elastic and plastic range respectively, $a = K_{p,j}'/K_{d,j}'$ the ratio between elastic stiffness of the steel profile and of the device and $\beta_{d,j}$ the ratio between stiffness after and before yielding of the dissipative device, the following expression can be derived:

$$K'_{b,j} = \frac{K'_{d,j}}{\frac{1}{\alpha_j}+1}; \quad K'_{by,j} = \frac{\beta_{d,j} K'_{d,j}}{\frac{\beta_{d,j}}{\alpha_j}+1}; \alpha_j = \frac{K'_{p,j}}{K'_{d,j}} \tag{4.19}$$

Therefore:

$$F_{b,j}^{'} = F_{by,j}^{'} + (\delta_j^{'} - \delta_{y,j}^{'}) \frac{\beta_{d,j} K_{d,j}^{'}}{\frac{\beta_{d,j}}{\alpha_j} + 1} \tag{4.20}$$

$$\delta_{y,j}^{'} = \frac{F_{by,j}^{'}}{K_{b,j}^{'}} = \frac{F_{by,j}^{'}}{K_{d,j}^{'}} (\frac{1}{\alpha_j} + 1) \tag{4.21}$$

Consequently, if there is one brace per direction and per floor, substituting Eq. (4.21) into Eq. (4.18), $v^*_{eq,B}(D_t^*)$ can be expressed in the following way:

$$v^*_{eq,B}(D_t^*) = \chi_B \frac{2}{\pi} \frac{\sum_{j=1}^{n} \left\{ F_{by,j}^{'} \delta_j^{'} - \delta_{y,j}^{'} \cdot \left[F_{by,j}^{'} + (\delta_j^{'} - \delta_{y,j}^{'}) \frac{\beta_{d,j} K_{d,j}^{'}}{\frac{\beta_{d,j}}{\alpha_j} + 1} \right] \right\}}{F_{S+B}(D_t^*) \cdot D_{S+B}^*} \tag{4.22}$$

$\delta_j^{'}$ are determined from the pushover analysis for the top displacement D_t and $\delta_{y,j}^{'}$, that is the yielding displacement of devices, can be reasonable assumed as $\delta_{y,j}^{'} \le \delta_j^{'} / 4$.

$F_{y,j}^{'}$ is, for each direction, the yielding force of the floor brace: once $\delta_{y,j}^{'}$ has been defined $F_{y,j}^{'}$ is consequently determined Eq. (4.21).

Thus, remembering Eq. (4.4) and according to (4.19), $K_{d,j}^{'}$ can be expressed as follows:

$$K_{d,j}^{'} = K_{global} \cdot c_{b,j} \cdot (\frac{1}{\alpha_j} + 1) \tag{4.23}$$

Therefore substituting Eq. (4.23) into Eq. (4.22), K_{global} can be determined as follows:

$$K_{global} = \frac{\pi \cdot v^*_{eq,B}(D_t^*) \cdot F_{S+B}(D_t^*) \cdot D^*_{S+B}}{2 \cdot \chi_B \cdot C_1} \tag{4.24}$$

with:

$$C_1 = \sum_{j=1}^{n} c_{b,j} \left\{ \delta'_{y,j} \cdot \delta'_j - \delta'_{y,j} \left[\delta'_{y,j} + (\delta'_j - \delta'_{y,j}) \frac{\beta_{d,j}(\frac{1}{\alpha_j} + 1)}{\frac{\beta_{d,j}}{\alpha_j} + 1} \right] \right\} \tag{4.25}$$

A value of $\alpha_j > 3$ is usual in applications, therefore $K'_{b,j} > 3/4 K'_{d,j}$, while the steel profile must be stronger (neither yielding nor buckling) than the device: for a given interstorey drift the larger is α_j the larger are device displacements and hysteretic cycles.
At this point all terms of Eq. (4.24) are known so, from Eq. (4.23) and Eq. (4.19) , the floor brace stiffnesses $K'_{b,j}$ can be defined (the yielding force $F'_{by,j}$ can be directly derived since the stiffness $K'_{b,j}$ and the yielding displacement $\delta'_{y,j}$ have been defined).
Though in this work the procedure is discussed referring to Eq. (4.22) it is important to underline that, in a general case, one can have m different braces for each level j. In fact, at the same level, each brace i can be characterized by its specific properties as a consequence, for example, of the geometry of the bays of the structural frame. Consequently Eq. (4.22) can be generalized as follows.

$$v^*_{eq,B}(D_t^*) = \frac{2}{\pi} \frac{\sum_{j=1}^{n} \sum_{i=1}^{m} \chi_{B,i} \left\{ F'_{by,j,i} \delta'_j - \delta'_{y,j,i} \cdot \left[F'_{by,j,i} + (\delta'_j - \delta'_{y,j,i}) \frac{\beta_{d,j,i} K'_{d,j,i}}{\frac{\beta_{d,j,i}}{\alpha_{j,i}} + 1} \right] \right\}}{F_{S+B}(D_t^*) \cdot D^*_{S+B}} \tag{4.26}$$

A simplified approach of this step is presented as in the following: this

simplified procedure is useful to get a first dimension of the bracing system.
Assuming that the dissipative device is an elasto-plastic truss element with cross section $A_{d,j}$ and yielding strength $F'_{dy,j}$ ($F'_{by,j}= F'_{dy,j}$), the following expression can be derived:

$$F'_{by,j} = f_{dy,j} A_{d,j} = f_{dy,j} \frac{K'_{d,j} \cdot l_{d,j}}{E_{d,j}} \tag{4.27}$$

$$A_{d,j} = K'_{b,j} (\frac{1}{\alpha_j} + 1) \frac{l_{d,j}}{E_{d,j}} = \frac{K'_{d,j} l_{d,j}}{E_{d,j}} \tag{4.28}$$

$$\delta'_{y,j} = \frac{F'_{by,j}}{K'_{d,j}} (\frac{1}{\alpha_j} + 1) = \frac{f_{dy,j} \cdot l_{d,j}}{E_{d,j}} (\frac{1}{\alpha_j} + 1) \tag{4.29}$$

$$K'_{b,j} = \frac{K'_{d,j}}{\frac{1}{\alpha_j} + 1}; K'_{d,j} = \frac{E_{d,j} \cdot A_{d,j}}{l_{d,j}} \tag{4.30}$$

Therefore Eq.(4.26) can be expressed as the following Eq. (4.31):

$$v^*_{eq,B}(D^*_t) = \chi_B \frac{2}{\pi} \frac{\sum_{j=1}^{n} \left\{ \frac{f_{dy,j} K'_{b,j} l_{d,j} \delta'_j}{E_{d,j}} - \delta'_{y,j} \left[\frac{f_{dy,j} K'_{b,j} l_{d,j}}{E_{d,j}} + (\delta'_j - \delta'_{y,j}) \frac{\beta_{d,j} K'_{b,j}}{\frac{\beta_{d,j}}{\alpha_j} + 1} \right] \right\}}{F_{S,S+B}(D^*_t) \cdot D^*_{S,S+B}} \tag{4.31}$$

where $f_{dy,j}$, $E_{d,j}$ and $l_{d,j}$ are respectively the yielding stress, the elastic modulus and the length of the device. Consequently the coefficient C_1 of Eq. (4.25) can be expressed as follows (this expression of C_1 is named C^*_1):

$$C_1^* = \sum_{j=1}^{n} c_{b,j} \left\{ f_{dy,j} \frac{l_{d,j}}{E_{d,j}} \delta_j' - \delta_{y,j}' \left[f_{dy,j} \frac{l_{d,j}}{E_{d,j}} + (\delta_j' - \delta_{y,j}') \frac{\beta_{d,j}}{\frac{\beta_{d,j}}{\alpha_j} + 1} \right] \right\} \tag{4.32}$$

Moreover with a further simplification the dissipative braces can be considered as a one piece devices all realized with the same material (the device is directly connected with both the corners of the frame; f_{dy}, β_d and $E_d$are known as the material has been selected and $l_{d,j}$ is known from the geometry of the structure), thus Eq. (4.32) can be further simplified as follows (this simplified expressions of C^*_1 is named $C^*_{1,S}$):

$$C_{1,S}^* = \sum_{j=1}^{n} c_{b,j} \left\{ f_{dy} \frac{l_{d,j}}{E_d} \delta_j' - f_{dy} \frac{l_{d,j}}{E_d} \left[f_{dy} \frac{l_{d,j}}{E_d} + (\delta_j' - f_{dy} \frac{l_{d,j}}{E_d}) \beta_d \right] \right\} \tag{4.33}$$

Since as commercial devices are characterized by a narrow range of lengths (usually: $1000\ mm < l_d < 1400\ mm$) an approximate evaluation of l_d (e.g. $l_d = 1200\ mm$) can be made without influence results.
Therefore, remembering Eq. (4.27)-(4.28) and similarly to the standard procedure, $K'_{b,j}$ and $F'_{by,j}$ can be immediately determined.
This simplified expression can be useful for predimensioning the bracing system.

10. Check convergence: one must repeat steps from 3 to 9 until the performance point of the braced structure converges to the target displacement with adequate accuracy.

4.5 Application to steel concentric braced frames (CBF)

Recent studies and experimental courses have pointed out that the seismic capacity of steel concentric braced frames (CBF) is limited by diagonal yielding while buckling of compressed diagonals can be tolerated if they remain in the elastic range. The contribution of compressed diagonals is

disregarded in design, though it can affect seismic response, reducing the period of vibration of the structure, while increasing the absorbed energy.
The retrofit procedure previously presented has been specialized also to the case of CBFs, and is presented in this paragraph. The structural elements: beams and columns usually act as pendulum, hinged at their ends, though this assumption can be removed without any modification to the presented procedure.
The procedure allows designing a dissipative bracing system that can guarantee the upgrade of the existing CBF avoiding yielding in tension of the existing diagonals, or even, in some cases, to prevent compressed original diagonal from elastic buckling. In the latter case the pushover analysis can be easily performed using a software for structural analysis in fact, this typologies of structures (CBF) after the retrofitting should remain linear elastic even under seismic action (in some cases, as a rare seismic event, a limited plastic excursion of the diagonals could be accepted to guarantee to survive the event) and therefore the nonlinearity can be concentrated only in the dissipative devices. In case one accept elastic buckling of the compressed original braces, one should consider the nonlinear elastic behavior of these elements, unless it is proved that their contribution to total stiffness is negligible, and disregarded in the analysis.
The specialized procedure can be summarized by modifying steps 2 and 3 as follows:
2. Select the target displacement: the target displacement is selected (for example the top displacement D_t*) according to the performance desired (limit state). Usually, working with steel buildings, deformation limits are relevant for the dimensioning. For CBF (concentric braced frame) the target can be selected as the inter story drift that corresponds to the stability limit of the existing braces in compression. When this latter is too small to be considered than one should accept elastic buckling and displacement corresponding to yielding in tension of the existing diagonals should be the maximum admissible state at least for life safety. Larger target displacement is usually of small practical interest.

3. Define the capacity curve: Given the target CBF displacement, the analysis can be reduced to the evaluation of the top displacement that corresponds to the achievement yielding in tensile original bracings or at most, the prevention of buckling in compressed original braces. This latter seems an excessive request as buckling in the elastic range has small

consequences on structural damage and should usually be accepted. However if one prevent buckling than the capacity curve of the existing CBF (that is the S of the procedure) will be linear elastic, otherwise it will be non linear elastic due to compressed buckled braces. When their contribution to structural stiffness is negligible, less than 15%, they can certainly be disregarded.

If we disregard compressed diagonals or assume the stability limit of compressed diagonals as performance point, we shall design an additional bracing system that yields well before the performance point (reduction of the interstorey drift to the critical deformation that corresponds to diagonal yielding or buckling: ultimate limit state that corresponds to the ultimate top displacement *Du*). The retrofitted system S+B would be elasto-plastic with a post yielding hardening (elastic before reaching $D_{b+s,y}$ and hardening in $D_{b,y}$-D_u). The CBF (S) is in its elastic range (Figure 4.14), and the structure yields when the dissipative braces yields $D_{b,y}=D_{b+s,y}$.

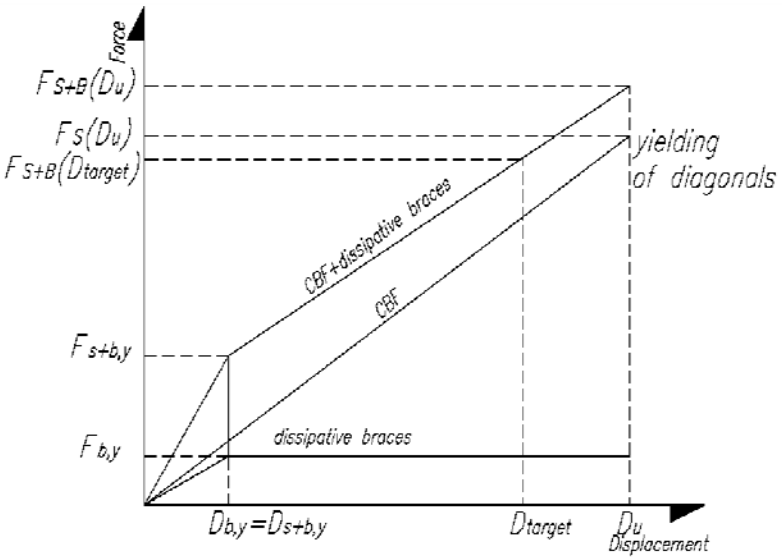

a) original compressed braces neglected

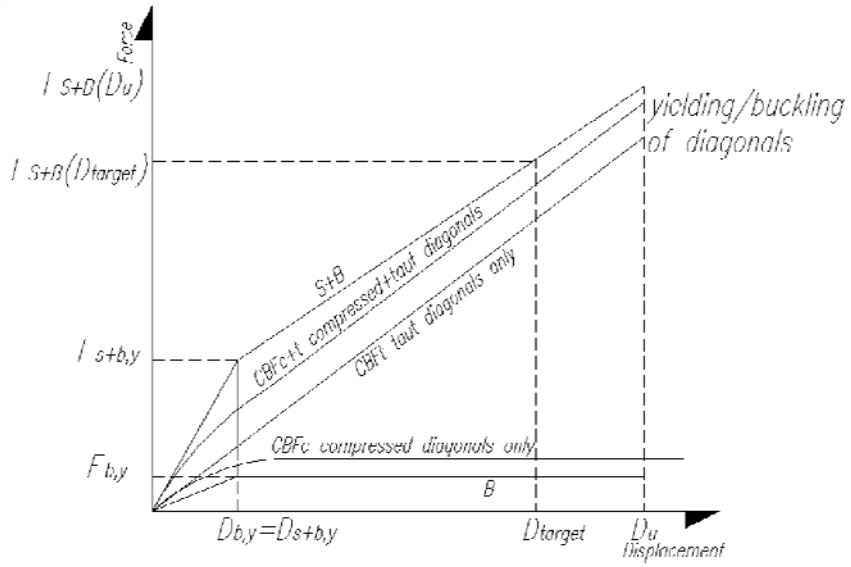

b) original compressed braces considered. B is the bracing systems (the BRBs) and S is the existing structure (CBF=CBFc+CBFt)

Figure 4.14 Force-Deformation of the existing structure (CBF) and of the retrofitted structure (CBF+dissipative braces). Dtarget is the target of the retrofitting design: diagonals must remain elastic and $D_{target}<D_u$.

In case we admit elastic buckling in compressed original braces and we cannot disregard their contribution to structural stiffness, than the pushover curve of the original structure: S will be non linear elastic, we shall add the elastic plastic curve of the new braces to the original curve. In this case one should note that for the same displacement, the original structure has a larger response with respect to the case of disregarded compressed diagonal, and the equivalent damping is smaller adding the same BRB due to the larger elastic energy at the denominator.

During the design phase it is important to evaluate if, inside the range of displacement that allow to dissipate enough energy to obtain the performance target required, the existing diagonals remain elastic (e.g. according to code requirements). If this condition is verified the dissipative braces will be inserted inside the structure without modifying the CBF configuration. In the opposite case the designer can decide, for example, to remove the existing diagonals and realize a completely new system of diagonals with the dissipative braces.

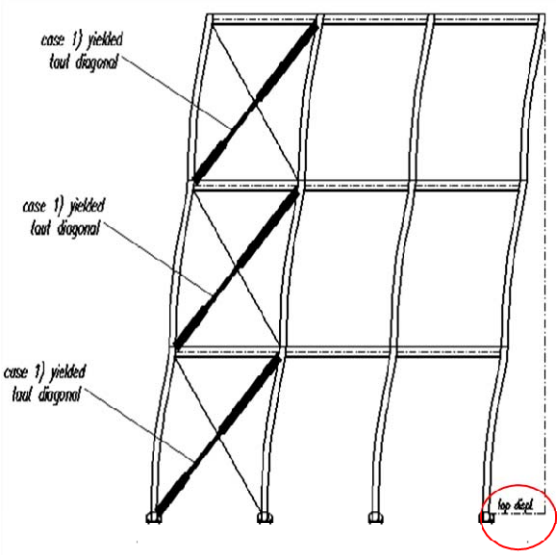

a) Yielding of taut brace we do not care about compressed ones (usually already buckled)

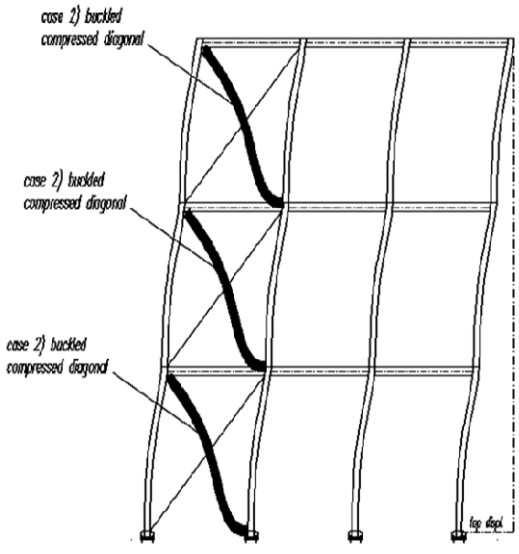

b) Buckling before yielding of taut brace (usual)
Figure 4.15 existing structure (CBF) under seismic action

The deformed shape before and after retrofitting are illustrated in Figure 4.15 and Figure 4.16

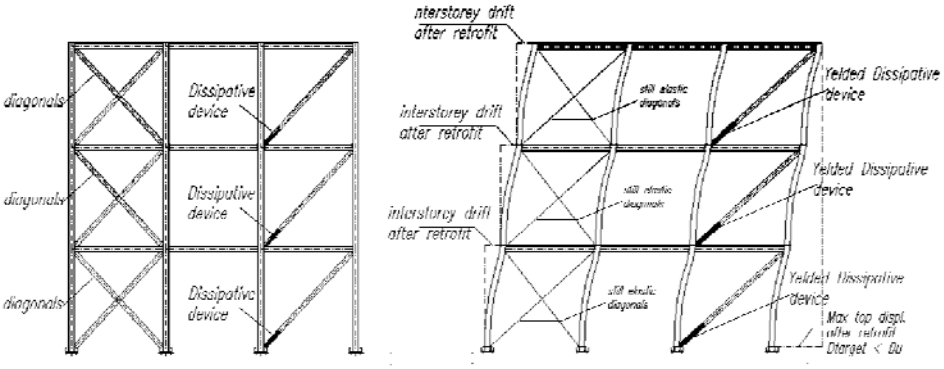

Figure 4.16 Retrofitted structure (CBF+dissipative braces) before and during seismic action. The diagonals are still elastic and the dissipative braces are yielded D_{top} after retrotting is limited in order to obtain the retrofitting of the structure: $D_{top}=D_{target}>D_u$

5. Case study

5.1 Introduction

In this and following chapters, the seismic response predicted by NSPs, capacity curve developed by IMPA and the design procedure of dissipative braces presented in previous chapters will be applied to an existing building.

In this chapter, an existing hospital, which shows a strong irregularity in plan and vertical, is sleeted as case study. The building detected as case study is an existing nine stories RC framed building, it is a strategic building, situated in a seismic area of Italy, which has been designed and built in the 1970s without seismic details. it is not due to negligence during the design phase, but to a total absence of regulations to define general principles and standards of safety in regard to structural performance require against seismic actions, as the project building detected dates back to early periods of 1970.

An extensive and hard study on the paper design documents, laboratory test of the current state of the members and site survey in 2009 were conducted to estimate the mechanical properties of the concrete and steel reinforcement in the existing RC building.

The geometric, material and mass properties of the case study analyzed are presented in the first part of the chapter.

The seismic action definition according to Italian Technical Code NTC 2008 (NTC2008) is described in the second part.

The modeling features assumed during the performed studies and the nonlinear properties of the buildings are described in the third part.

5.2 Regular structure

5.2.1 Building description

The nine-story (9-story) benchmark structure is 45.73 m by 45.73 m in plan, and 37.19 m in elevation as shown in Figure 5.1. The bays are 9.15 m on center, in both directions, with five bays each in the north-south (N-S) and east-west (E-W) directions. The building's lateral load-resisting system is comprised of steel perimeter moment-resisting frames (MRFs) with simple framing on the furthest south E-W frame. The interior bays of the structure contain simple framing with composite floors.

The columns are 345 MPa steel. The columns of the MRF are wide-flange. The levels of the 9-story building are numbered with respect to the ground level. The ninth level is the roof. The building has a basement level denoted B-1. Typical floor-to-floor heights (for analysis purposes measured from center-of-beam to center-of-beam) are 3.96 m. The floor to-floor height of the basement level is 3.65 m and for the first floor is 5.49 m. More details about the building can be referenced to Ohtori etc. (2000).

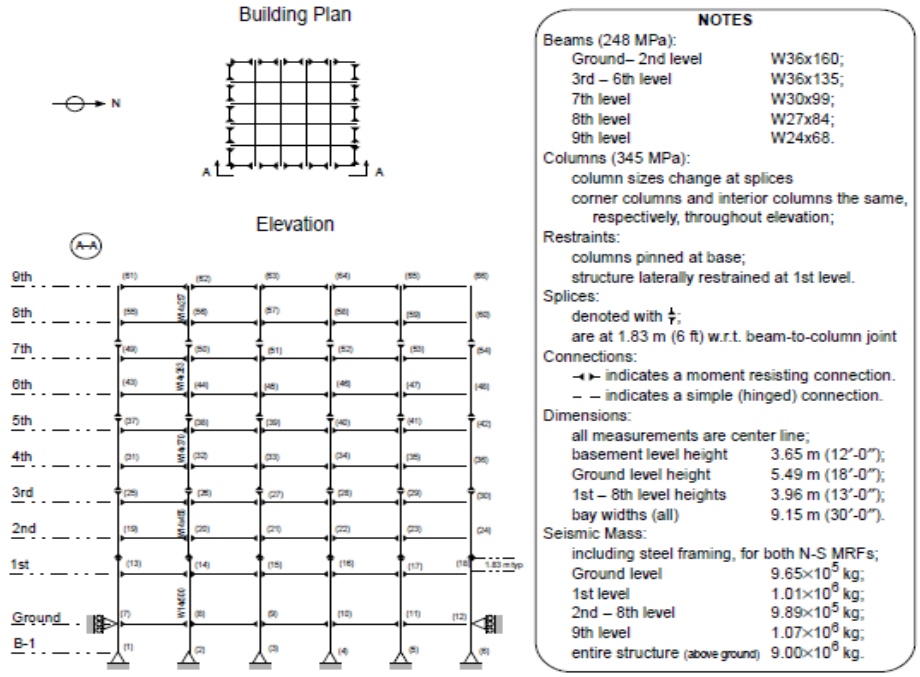

Figure 5.1 Nine-storey building (adapted from Ohtori etc. (2000)).

5.2.2 Seismic action

For this building, a set of 20 ground motion records were assembled representing probabilities of exceedance of 2%, 10% and 50% in 50 years (Somerville et al. 1997). This set of ground motions enables testing of the NSPs under the most conditions from elastic stage to plastic stage. Their response spectrums are shown from Figure 5.1 to Figure 5.3.

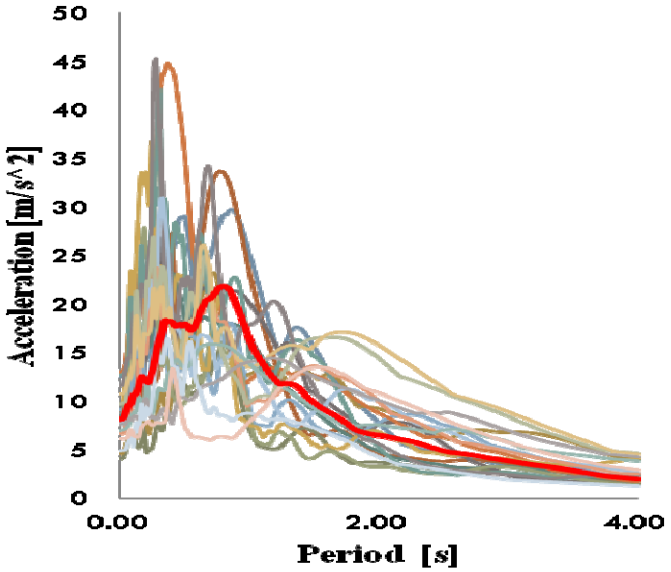

Figure 5.2 Response spectrum of 2/50 set of records

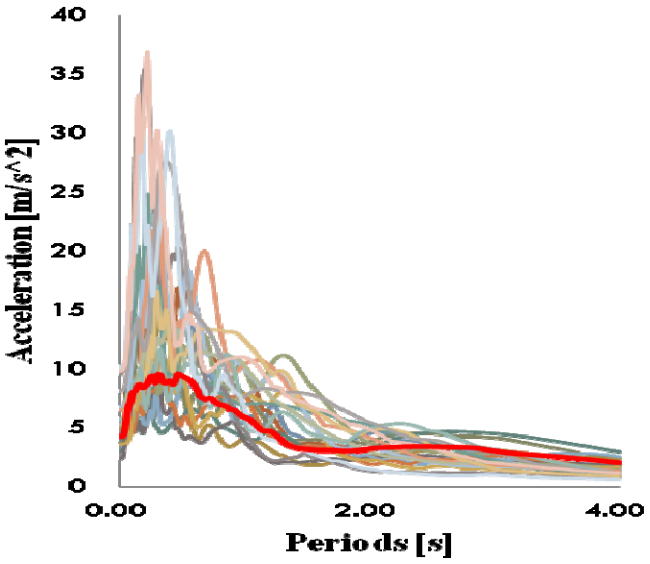

Figure 5.3 Response spectrum of 10/50 set of records

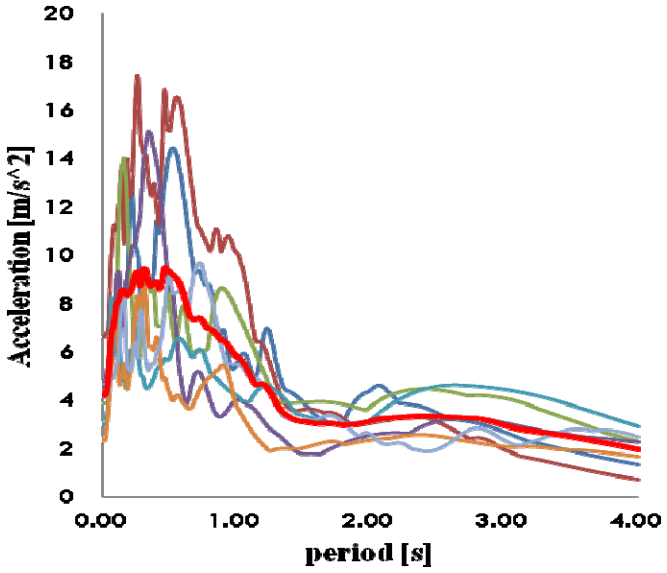

Figure 5.4 Response spectrum of 50/50 set of records

5.2.3 Structural modeling

A two-dimensional (2D) finite element model was built in SAP2000 software, as shown in Figure 5.5: beam and column elements are modeled as frame elements with lumped nonlinearity by defining plastic hinges at the critical sections (extremities of beams and columns). A coupled axial force and biaxial bending moment hinges (P-M2-M3 hinge) are assigned to columns whereas moment hinges (M3 hinge) are assigned to beams. Nonlinear shell elements are used to simulate walls. The foundations, which beyond the current study, are modeled with joints constraints.

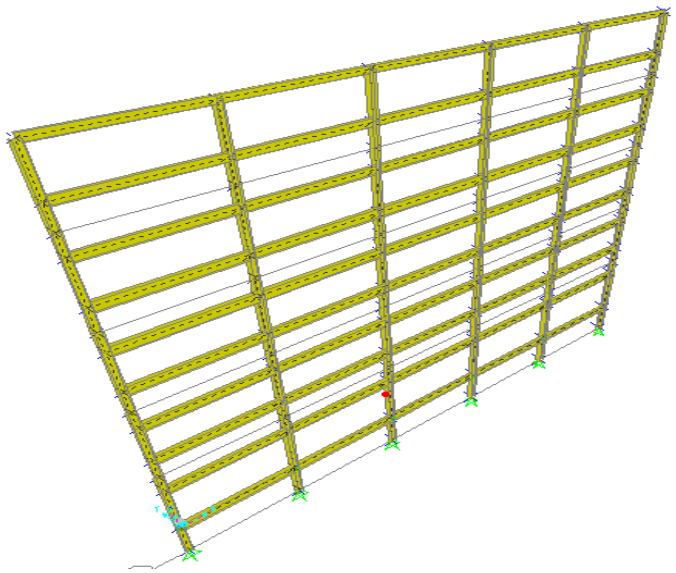

Figure 5.5 2D finite element model in SAP2000

5.3 Irregular structure

5.3.1 Building description

1. Geometry

The nine stories RC existing framed building located in the seismic area of Italy, consists of a ground floor, eight-storey elevation and a roof terrace and it is therefore structurally composed of ten decks. The plan and elevation layout of the existing building are shown in Figure 5.6 and Figure 5.7, respectively.

From a structural point of view, the plan is an irregular polygon where the resistant elements are distributed unevenly: the concentration on the left side of shear walls and the one way orientation of the beams cause a strong irregularity.

It is observed from Figure 5.6, the beams are characterize by one way orientation (along the longitudinal direction), lack of beams along the transverse direction except the beams at the edges of the building. These structural arrangements are outdated, strictly unacceptable today by the earthquake regulations since it involves a lack of connection to the columns along the transverse direction and consequently a significant difference in the structural frame behavior along two orthogonal directions.

From Figure 5.8, it is observed that the floor 5 differs greatly from all others not only for the balcony and the corresponding cantilevered roof, which is located on the floor 6, but also for the different beam type: intradossate beam are used for floor 5, extradossate beams are used for other floors.

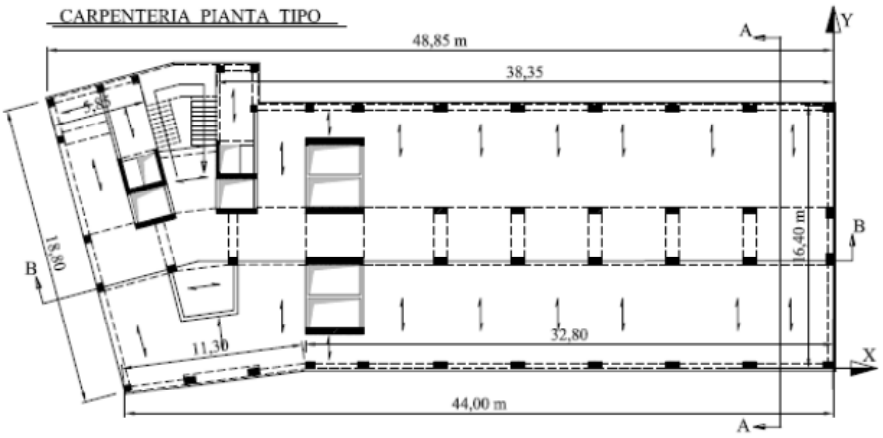

Figure 5.6 Plan layout of the existing building

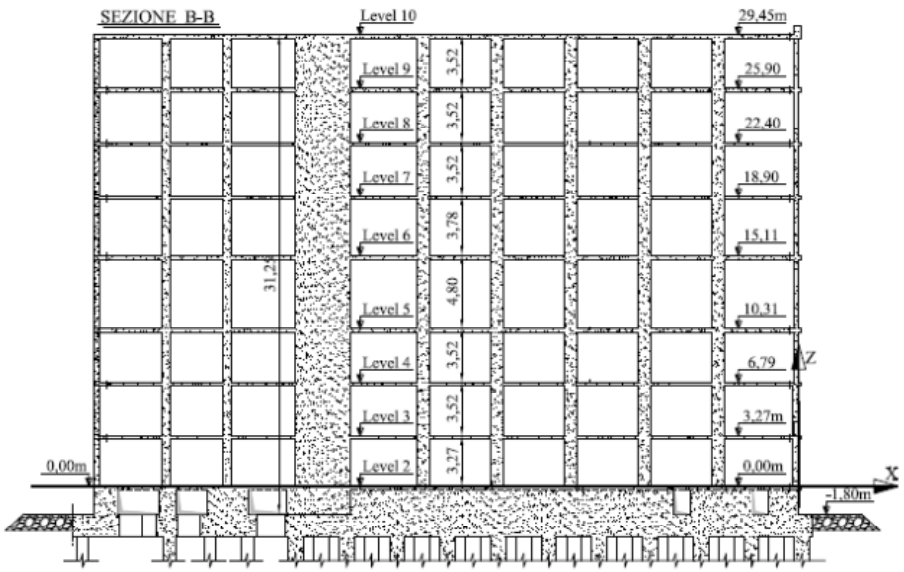

Figure 5.7 Elevation layout of the existing building

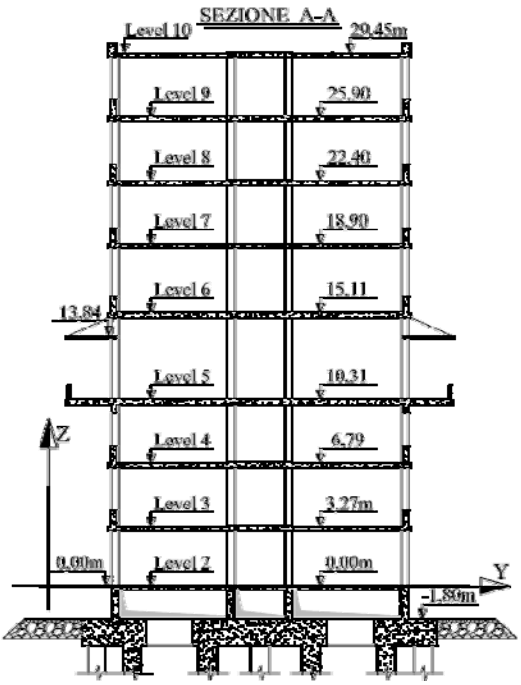

Figure 5.8 Section A-A

Another significant difference of floor 5 is its maximum height: The ground floor is 3.08m high, 3.27m for the floor 2, 3.52 m for the floor 3, 4,7,8,9, 4.80m for the floor 5 and 3.78m for the floor 6, as shown in Figure 5.7.

2. Materials and sections

With regard to the availability of historical documentation of this project, it is for graphic architectural character and only the distribution of the reinforcement in the horizontal elements, no graphical illustration of reinforcement in the vertical columns and walls.

An extensive and hard study on the paper design documents and site survey in 2009 were conducted to estimate the mechanical properties of the concrete and steel reinforcement in the existing RC building, as shown in Figure 5.9.

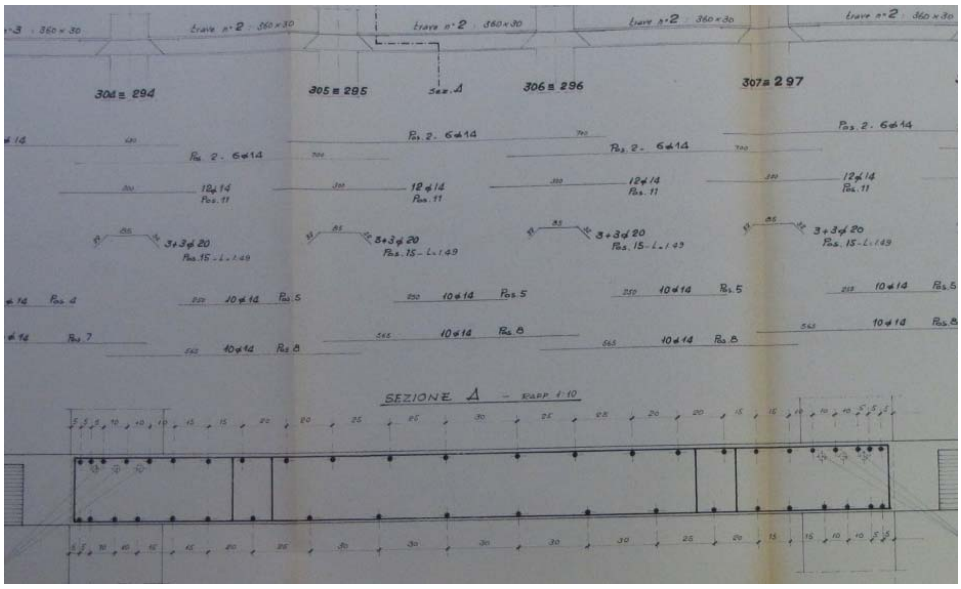

Figure 5.9 Graphic documentation type for the project

The material properties of the concrete and steel reinforcements are listed in Table 5.1 and

Table 5.2. Excerpt of sections of beams and reinforcement for specific beams are listed in Table 5.3.

Table 5.1 Concrete properties

Material Properties: Concrete - Ref N.T.C. 2008			
R_{ck}	25	[MPa]	The cube cocnrete compression strength from 1970's project
$f_{ck,is}$	***10,1***	[MPa]	The cylinder concrete compression strength from the site survey in 2009
γ_c	1	[-]	Partial factor for concrete
α_{cc}	1	[-]	The coefficient taking account of long term effects on the compressive strength
f_{cd}	10,10	[MPa]	Design value of concrete compressive strength
f_{ctm}	1,40	[MPa]	Mean value of axial tensile strength of concrete
f_{ctd}	0,98	[MPa]	Design value of concrete tensile strength
ε_{c1}	0,0020	[-]	Compressive strain in the concrete at the peak stress f_{cy}
ε_{cu}	0,0035	[-]	Ultimate compressive strain in the concrete
E_{cm}	26286	[MPa]	Secant modulus of elasticity of concrete
ν	0,30	[-]	Poisson's ratio
G	10110	[MPa]	Shear modulus

Table 5.2 Steel properties

Material Properties : Steel "FeB38K" - Ref NTC 2008			
f_{ym}	395,8	[MPa]	Mean yield strength of reinforcement in site survey
γ_s	1	[-]	Partial factor for steel
E_s	200000	[MPa]	Elastic modulus
f_{tnom}	480	[MPa]	Characteristic nominal strength
f_{yd}	395,8	[MPa]	Design yield strength of reinforcement
f_{tnom}/f_{yk}	1,2	[-]	The ratio of tensile strength to the yield stress
ε_{syk}	0,0020	[-]	Strain of reinforcement steel at yield strength
ε_{syd}	0,0198	[-]	Claculation value for the strain of reinforcement steel at yield strength
ε_{uk}	0,075	[-]	Ultimate strain
ε_{ud}	0,0675	[-]	Claculation value for ultimate strain
f_{ud}	480,0	[MPa]	Calculation value for the ultimate strength of steel

Table 5.3 Excerpt of variability of the sections and reinforcements beams at various levels

Hinge Reinforcement				*Numbering Beams*								
section	upper	middle	lower	*Level2*	*Level3*	*Level4*	*Level5*	*Level6*	*Level7*	*Level8*	*Level9*	*Level10*
[BxH]	[n° - diameter]											
34x114	2ϕ12	2ϕ10	2ϕ12	1	23	23	2	22	15	15	15	0
34x114	4ϕ12	2ϕ10	2ϕ12	0	1	1	0	1	1	1	1	0
40x30	2+2 ϕ12		2ϕ12	0	3	3	3	3	3	3	3	3
40x30	2+2 ϕ12		2+4ϕ12	1	1	1	1	1	1	1	1	1
40x30	4ϕ12		4ϕ12	0	1	1	1	1	1	1	0	1
40x30	3ϕ12		3ϕ12	0	0	0	1	1	0	0	0	0
20x80	2ϕ12		2ϕ12	2	2	2	2	2	2	2	2	0
20x80	2+2 ϕ12		2ϕ12	2	2	2	2	2	2	2	2	0
20x80	2ϕ10		2ϕ10	2	2	2	2	2	2	2	2	0
20x80	2ϕ8		2ϕ10	2	2	2	2	2	2	2	2	0
20x80	2ϕ8+1ϕ12		2ϕ12	1	1	1	1	1	1	1	0	1
60x24	4 ϕ12		4ϕ12	0	1	1	0	0	0	0	0	0
60x30	4ϕ12		4ϕ12	0	0	0	2	1	0	0	0	0
40x24	3ϕ12		3ϕ12	0	0	0	0	0	1	1	1	1
80x24	4ϕ12		4ϕ12	0	1	1	0	0	1	1	1	1
80x24	4ϕ16+2ϕ14		6ϕ16	0	0	0	0	0	0	0	1	1
80x24	4ϕ16+4ϕ14		6ϕ17	0	0	0	0	0	0	0	2	2
20x24	2ϕ12		2ϕ12	0	4	4	0	0	4	4	2	0
20x24	2ϕ12+2ϕ14		2ϕ12+2ϕ14	0	0	0	0	0	0	0	2	0
20x30	2ϕ12		2ϕ12	0	0	0	4	4	0	0	0	0
80x30	7ϕ12		4ϕ14	0	1	1	0	0	0	1	1	0
80x30	4ϕ12		4ϕ14	0	1	1	0	0	0	1	1	0
80x30	9ϕ12		3ϕ14	0	5	5	0	0	0	5	5	0

3. Loads and masses

As will be shown below, SAP200 was used for modeling the finite element model, which allows defining the linearly distributed loads on the beams and automatically assign the corresponding masses to the node converging to it. To determine therefore the distributed load on the beams were initially evaluated.
Since the purpose of this study is to evaluate the inelastic deformations of the structure before collapse through modal pushover analysis, the permanent and variable, variable load and their combination are defined for the structure according to the definition of the ultimate limit state (ULS) in accordance with the Regulations in NTC'08, as shown in Table 5.4.

Table 5.4 Mass distribution for the structure

Total mass for each floor				
Floor	**Δh**	**Z**	**Mx=My**	**Joz**
	[m]	[m]	[Ton]	[Tonm^2]
2	1,8	0	1307	311527
3	3,27	3,27	1248	291520
4	3,52	6,79	1248	291136
5	3,52	10,31	1870	440379
6	4,8	15,11	1729	397243
7	3,78	18,89	1247	289538
8	3,52	22,41	1240	288160
9	3,52	25,93	1271	297896
10	3,52	29,45	1051	228104

5.3.2 Seismic action

In this study, the seismic is defined by the horizontal acceleration spectrum and artificial earthquake records. The horizontal seismic action is described by two orthogonal components assumed as being independent and represented by the same response spectrum, and the vertical component of the seismic action is ignored.
The action varies in relation to the seismicity of the zone where building is located. A factor of 5% it is conventionally assumed as structural damping. Seismic action is defined in Italy for all country sites at a net of about 5 by 5 km, at different return periods. For each site spectrum four different mean return periods are given since the Italian Code highlights

four limit states, related to different probability levels of occurrence of the seismic event. The life safety (SLV) limit state is related to a disservice that can cause human loss, which is consistent with the goal of this work. The return period T_R of the earthquake actions is given by:

$$T_R = -\frac{V_R}{\ln(1-P_{VR})} \tag{5.1}$$

$$V_R = V_N C_N \tag{5.2}$$

where V_R is the reference design life and P_{VR} probability of exceedance of the seismic action, expressed as a function of the limit state, V_N the nominal life, and C_N the importance coefficient.

From the site survey, the soil foundation can be classified as type B, according to the classification implemented in the NTC'08. For the horizontal components of the seismic action, the elastic response spectrum $S_e(T)$ is defined by the following expressions

$$\begin{aligned}
0 \le T < T_B: &\quad S_e(\mathrm{T}) = a_g \cdot S \cdot [1 + \frac{T}{T_B}(\eta \cdot 2.5 - 1)] \\
T_B \le T < T_C: &\quad S_e(\mathrm{T}) = a_g \cdot S \cdot \eta \cdot 2.5 \\
T_C \le T < T_D: &\quad S_e(\mathrm{T}) = a_g \cdot S \cdot \eta \cdot 2.5 \cdot [\frac{T}{T_C}] \\
T_D \le T \le 4s: &\quad S_e(\mathrm{T}) = a_g \cdot S \cdot \eta \cdot 2.5 \cdot [\frac{T_C T_D}{T^2}]
\end{aligned} \tag{5.3}$$

where T is the vibration period of a linear single-degree-of-freedom system; a_g is the design ground acceleration on type A ground; T_B and T_C are the lower and upper limit of the period of the constant spectral acceleration branch, respectively; T_D is the value defining the beginning of the constant displacement response range of the spectrum; S is the soil factor; η is the damping correction factor. The values of the parameters employed for defining the spectrum of the horizontal acceleration are listed in Table 5.5.

According to the elastic response spectrum previous described, a set of 7 natural time histories are defined using the software Rexel, they are named by TH1~TH7. In Figure 5.10 the elastic response spectrums defined by NTC'08 is shown with the response spectrum of each time history record.

The mean and standard deviation of the natural records' response spectrums can be calculated by the following equations:

$$\sigma(T_i) = \sqrt{\frac{1}{N}\sum_{j=1}^{N}(S_{aj}(T_i) - \overline{S_a}(T_i))^2} \tag{5.4}$$

$$\overline{S_a}(T_i) = \frac{1}{N}\sum_{j=1}^{N} S_{aj}(T_i) \tag{5.5}$$

where $\sigma(T_i)$ represents the standard devisation of the response spectrums of the natutral records in correspondence of the period T_i, $S_{aj}(T_i)$ is the pseudo-acceleration of the jth spectrum, $\overline{S_a}(T_i)$ is the mean pseudo-acceleration, N is the number of the natural records.
For each period T_i, assume the normal distribution for response spectrums of the natutral records, the mean response spectrum of 7 natural records $\overline{S_a}(T_i)$ plus and minus one standard deviation (σ) in correspondence of the period T_i to achive a 68% confidence interval, as shown in Figure 5.10.

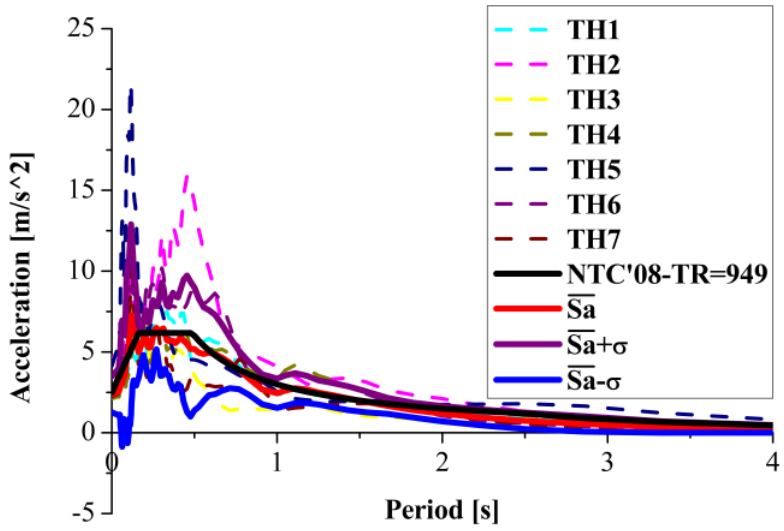

Figure 5.10 Response spectra of the code-compliant set of Time Histories (TH): TH1..TH7 are the selected ground motion records, NTC'08 is the response spectra according to Italian technical code for a returning period of T_R=949 years, Sa is the average response spectra from the set and $Sa \pm \sigma$ is the range of variation according to standard deviation

The compatibility of the response spectrum of one natural record with the reference elastic spectrum obtained from NTC is shown Figure 5.11 and its accelerogram is shown in Figure 5.12.

Table 5.5 the parameters defining the elastic spectrum

	parameter	value	unit
Independent parameters	V_N	50	year
	C_U	2	-
	V_R	100	year
	T_R	949	year
	ag	0,25	g
Dependent parameters	S	1,19	-
	η	1,00	-
	TB	0,16	s
	TC	0,48	s
	TD	2,45	s

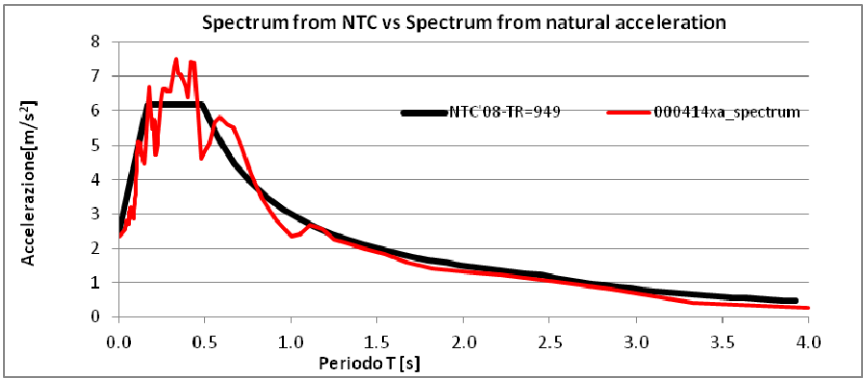

Figure 5.11 Code- compliant and earthquake acceleration horizontal response spectra

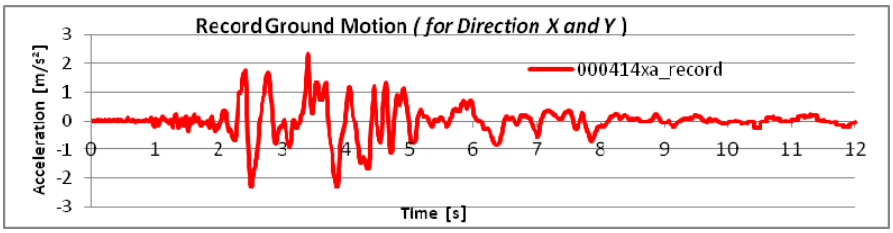

Figure 5.12 Natural accelerogram associated with SLV Tr = 949 years

5.3.3 Structural modeling

A three-dimensional finite element model was built in SAP2000 software, as shown in Figure 5.13~Figure 5.17: beam and column elements are modeled as frame elements with lumped nonlinearity by defining plastic

hinges at the critical sections (extremities of beams and columns). A coupled axial force and biaxial bending moment hinges (P-M2-M3 hinge) are assigned to columns whereas moment hinges (M3 hinge) are assigned to beams. Nonlinear shell elements are used to simulate walls. The foundations, which beyond the current study, are modeled with joints constraints.

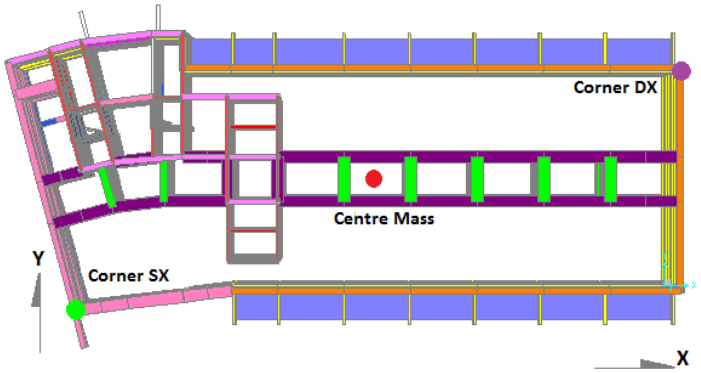

Figure 5.13 Transverse sections of the building.

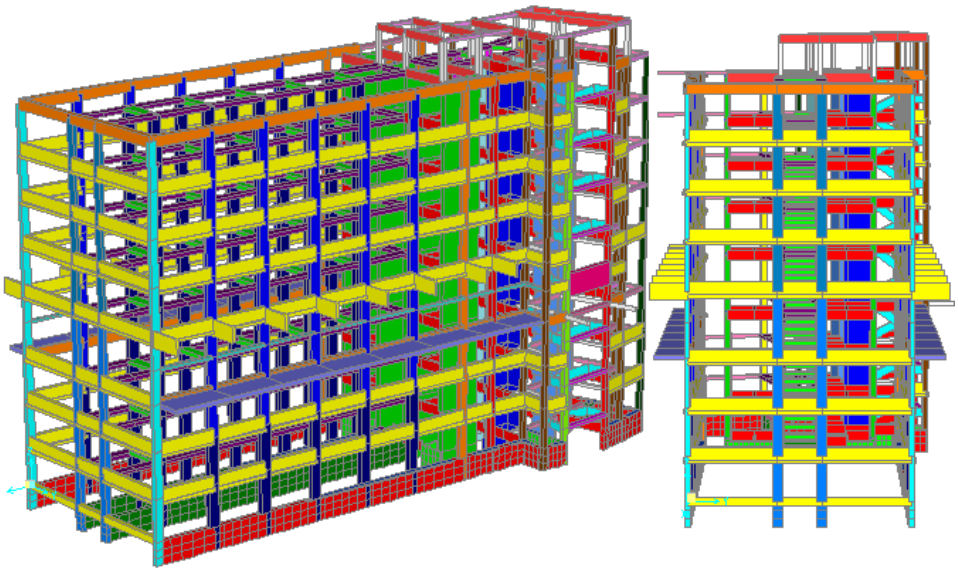

Figure 5.14 Longitudinal sections of the building

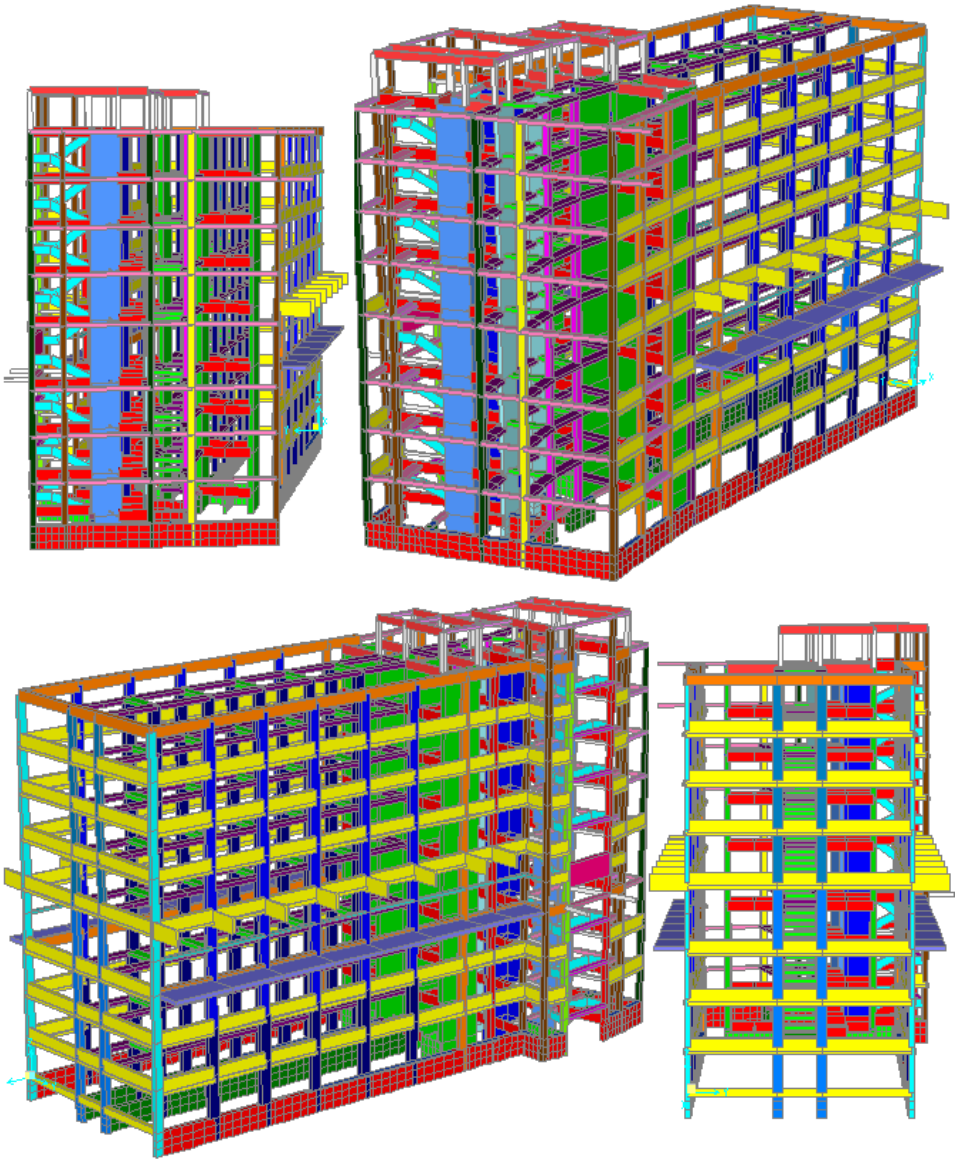

Figure 5.15 oblique views

The real structure is made up of elements that have non-negligible size sections whose axes do not always converge in the nodal points. An example of axes of the elements not converged at a single point is when the beams are present difference in thickness or is a variation of the column section in elevation. In this regard, it was decided not to use rigid connections, and such misalignment type have been simplified by

adopting a criterion of definition of the structural axes not deviate too much from the actual position with respect to a reference system global and relative displacement between the same elements.

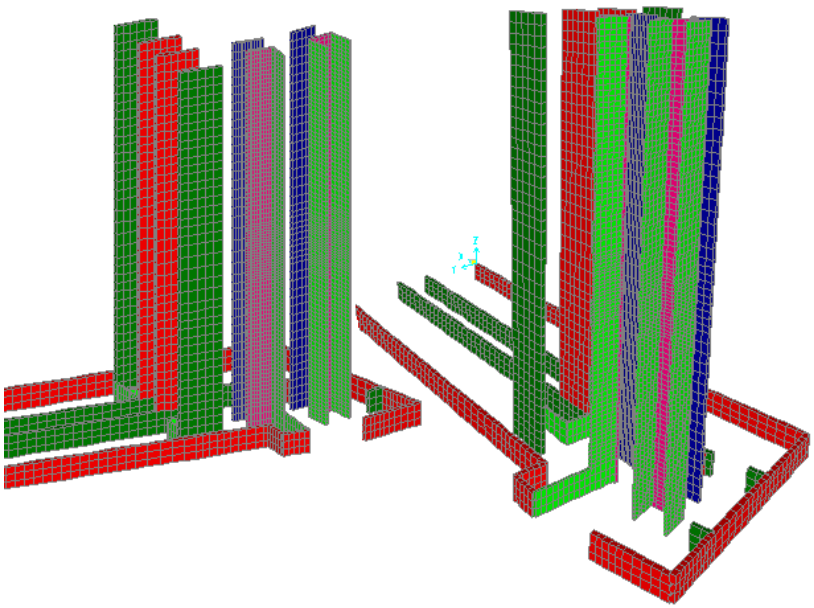

Figure 5.16 simulation of shell wall

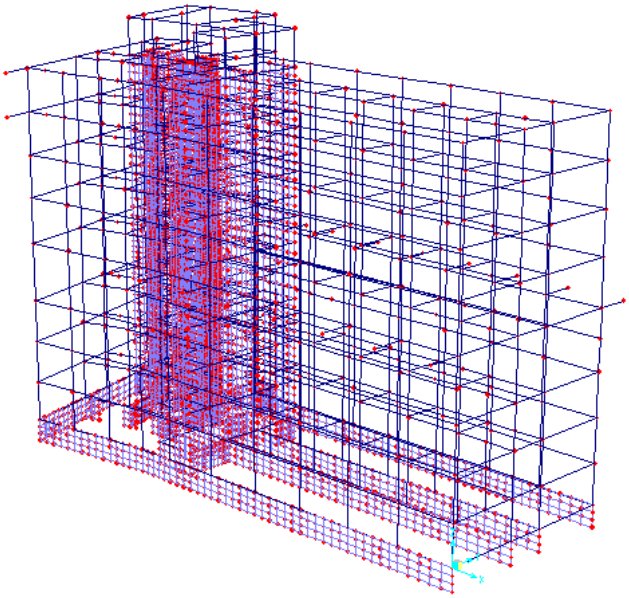

Figure 5.17 oblique view

6. Seismic assessment with common nonlinear static analysis

6.1 Introduction

It is well known that the most accurate method of seismic demand prediction and performance evaluation of structures is nonlinear time history analysis. However, this analysis is very time consuming, which is a relevant drawback especial in design phase. During the last decade, the Nonlinear Static Pushover analysis has been proposed among the structural engineering society as an alternative mean of analysis. The purpose of the pushover analysis is to assess the structural performance by estimating the strength and deformation capacities using static, nonlinear analysis and comparing these capacities with the demands at the corresponding performance levels.

Nonlinear Static Procedures (NSPs) are deemed to be very practical tools to assess the nonlinear seismic response of structures. Seismic design codes, like theATC-40, FEMA440 and Eurocode 8, have recommended the use of this technology.

Several scientific studies were developed demonstrating the good performance of some NSPs on the seismic assessment of relatively simple structures such as regular buildings capable of being analyzed by planar frames and bridges.

However, irregularity conditions in existing buildings can go far beyond the code definition of plan (and vertical) irregularity and, in any case, it is very likely that vertical and plan irregularities are combined. Few studies focused on the extension of NSPs to the case of 3D irregular structures, lack of application of NSPs to real irregular structure limits the employment of NSPs to assess actual existing structures. In addition, these few studies were typically concentrated on the application and verification of a single nonlinear static procedure only, rather than providing a comparative evaluation of the different available methodologies describing their relative accuracy and limitations.

Therefore, this section is aimed at checking whether the commonly used procedures can be successful even in the case of very complex irregularity conditions: Capacity Spectrum Method (CSM) adopted in ATC-40, Displacement Coefficient Method integrated into FEMA356, and N2

method presented in Eurocode 8 and modal pushover analysis (MPA).
To this purpose, the existing hospital building presented in previous chapter, which presents both vertical and plan irregularities, is selected as case study. Comparison of the results obtained with nonlinear dynamic analysis, which is taken as "exact" results, enables the evaluation of the accuracy of the different NSPs. NSP performance is evaluated by comparing the seismic response estimation of the analyzed buildings in terms of roof displacement and inter-storey drifts. Then the influences of lateral load patterns on the capacity curve and the distribution of seismic response along the height of the structure are discussed.

6.2 Regular structure

6.2.1 Modal analysis

The modal mass participation and modal shapes for the first three modes are shown in Figure 6.1 and Figure 6.2, respectively. It is clear that the first three modes take about 97% of the total mass, so it is sufficient to consider their contributions to the total seismic response.

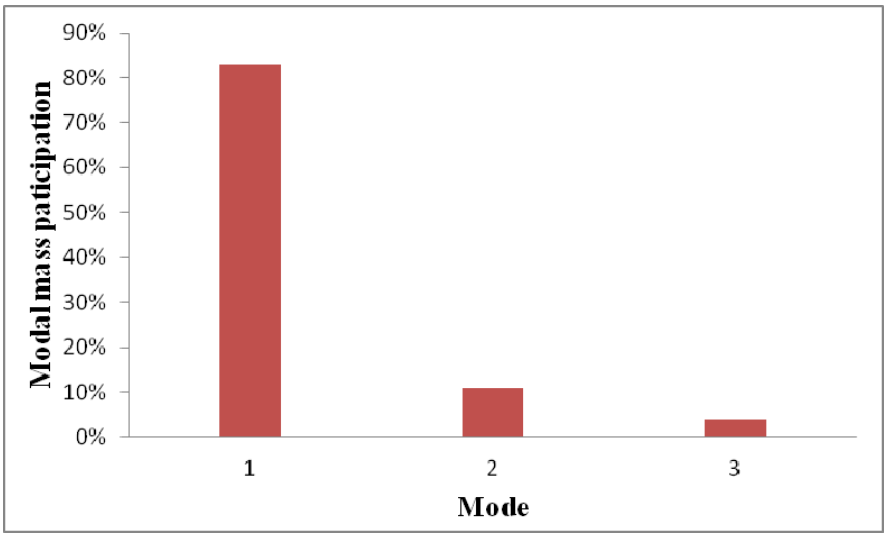

Figure 6.1 Modal mass participation for the first three modes

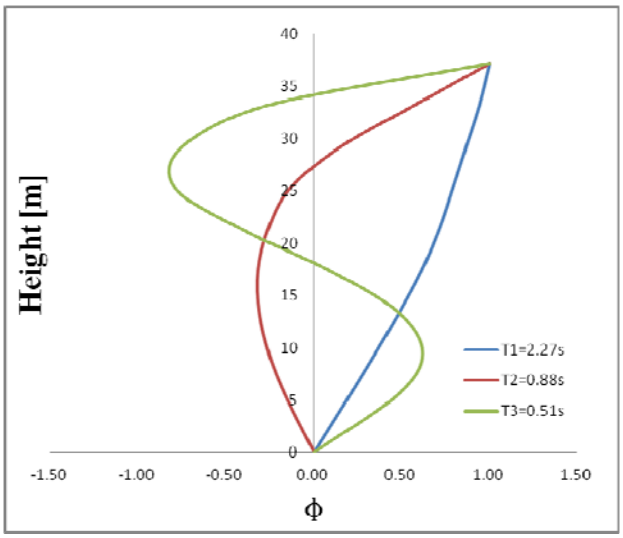

Figure 6.2 Modal shapes for the first three modes

6.2.2 Target displacement

1. Capacity spectrum method (CSM)

The mean elastic response spectra of the set of records is taken as the demand spectrum. It is observed that the structure enters in the nonlinear state for the first mode.

When structure enters nonlinear plastic stage, and the spectral reduction factor depends on the effective viscous damping of equivalent Single Degree of Freedom (SDF) system ξ_n , and the corresponding damping, which takes into account the energy dissipation capacity of the structure as examined, is defined blow:

$$\xi_n = \xi_0 + k\frac{1}{4\pi}\frac{E_{Dn}}{E_{S0n}} = \xi_0 + k\xi_{eqn} \tag{6.1}$$

The effective damping ratio for the first modes is 27%. The performance point is obtained via CSM, as shown in

Once the P.P. obtained from the capacity spectra, which is in terms of the spectral acceleration (S_{an}) and spectral displacement (S_{dn}), can be converted to P.P. in the capacity curve, which is in terms of the roof displacement (Ur) and base shear V corresponding to Ur:

$$U_{rn} = \Gamma_n S_{dn}\phi_{rn} \tag{6.2}$$

The P.Ps obtained from capacity curve are shown in Figure 6.4 .

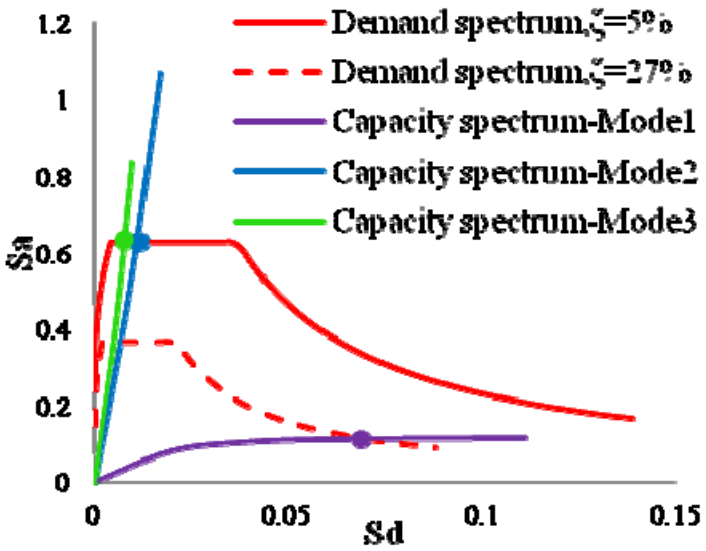

Figure 6.3 P.P. is determined via CSM from original and reduced demand spectrum for the first mode.

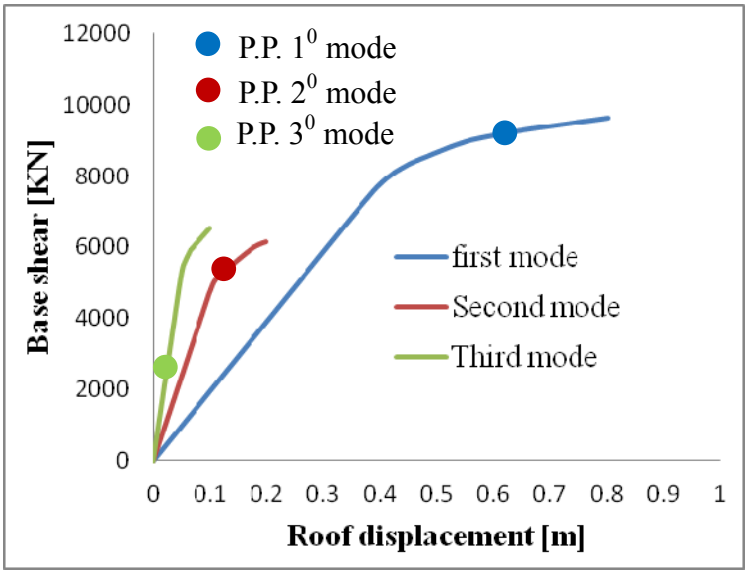

Figure 6.4 P.P. in terms of spectral acceleration and spectral displacement can be converted to P.P. in terms of the roof displacement (Ur) and base shear Vbn corresponding to Ur from the pushover capacity curve through Eq.(6.2)

2. Displacement Coefficient Method (DCM)

In this procedure proposed in FEMA 356, the nonlinear MDF system's

displacement is obtained from the linear elastic demand spectrum, using certain coefficients which are based on empirical equations derived by calibration against a large number of dynamic analyses, as shown in Table 6.1.

Table 6.1 P.P. obtained from DCM

C_0	C_1	C_2	C_3	S_a [m]	T_e [s]	d_t [m]	V_d [KN]
1.27	1.02	1.1	1	0.49	2.34	0.851	9725

3. N2

For medium and long period structure, the target displacement of the inelastic system is equal to that of an elastic structure, as shown in Figure 6.5.

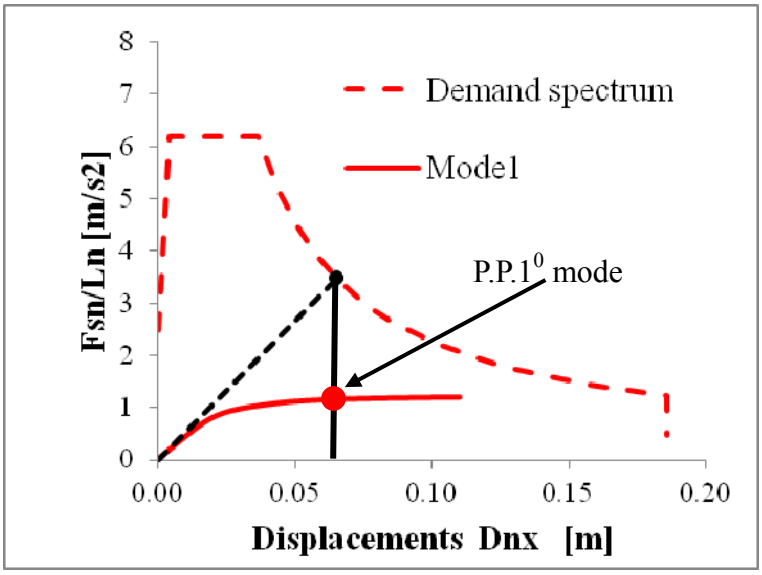

Figure 6.5 P.P. is determined via N2

6.2.3 Floor displacement and interstorey drifts

The comparison of the different NSPs and the nonlinear dynamic results in terms of lateral displacement and interstory drifts profiles are presented in this section. The time-history median results are taken as exact results.

The lateral displacement and interstorey drifts profiles for the control points are plotted from Figure 6.6 to Figure 6.8.

For the structure under minor earthquakes, the structure remains elastic

stage, all NSPs could provide a good estimate for the floor displacements, but underestimate of the interstorey drifts for the upper floors; MPA could improve the estimate for the interstorey drifts for the upper floors, as shown in Figure 6.6.

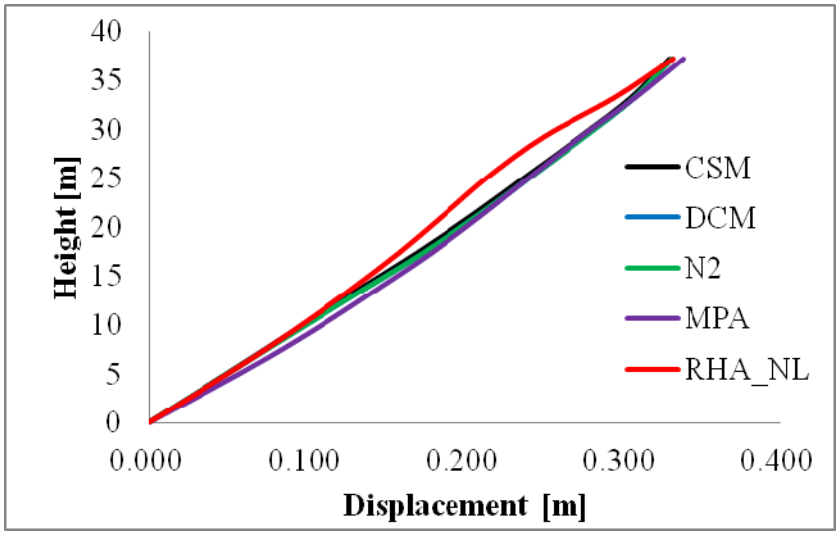

a) Roof displacement

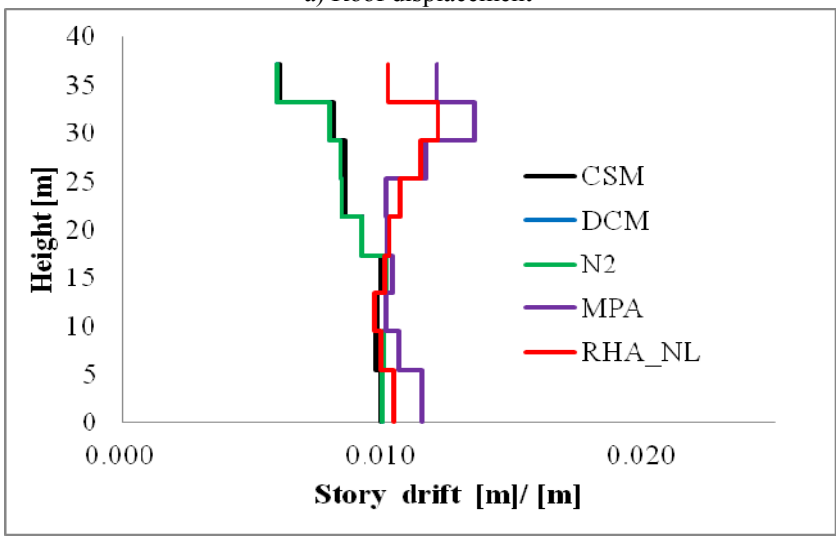

b) Interstorey drifts

Figure 6.6 Peak response of 50/50 set of records

For the structure under major earthquakes, the structure enters plastic stage, CSM and MPA could provide a good estimate for the floor

displacements, DCM and N2 would overestimate the floor displacements, especially for the upper floors. NSPs would underestimate the interstorey drifts for the upper floors, but overestimate for the middle floors. This phenomenon is more evident when the PGA of records increases. Among these NSPs, MPA perform best by improving the prediction of interstorey drifts for the upper floors, as shown in Figure 6.7 and Figure 6.8.

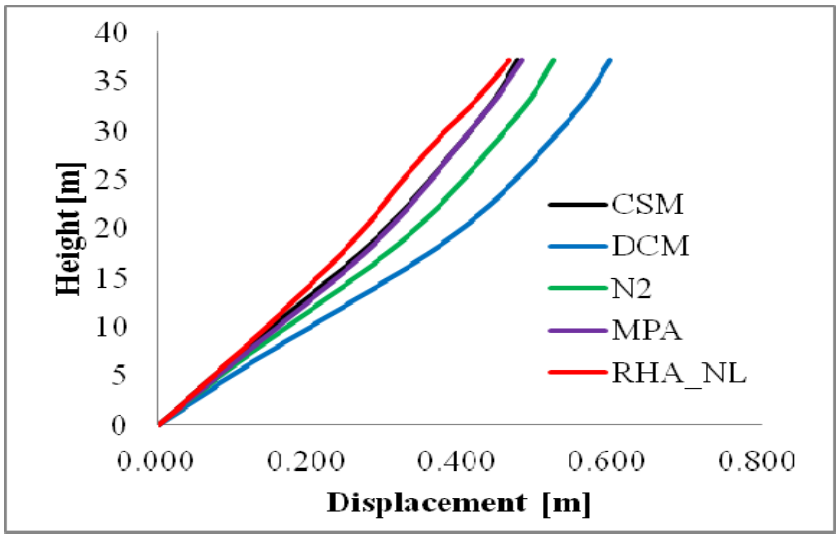

a) Roof displacement

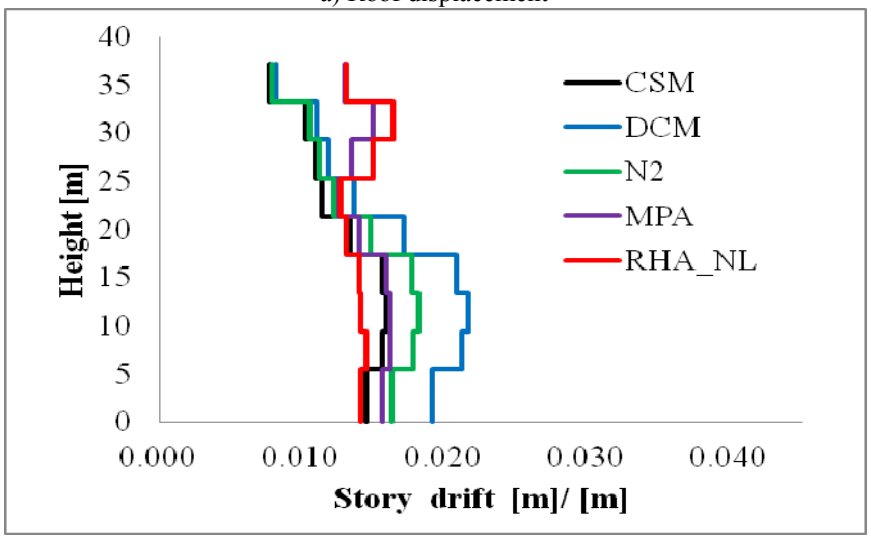

b) Interstorey drifts

Figure 6.7 Peak response of 10/50 set of records

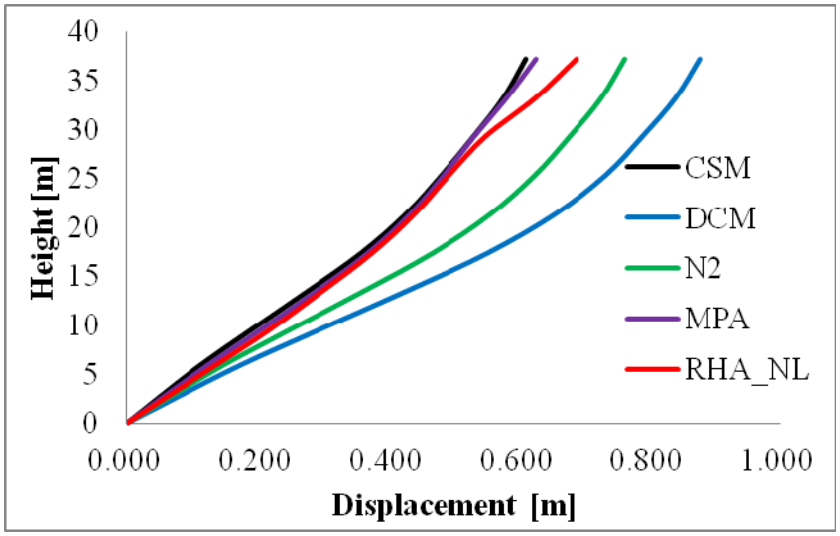

a) Roof displacement

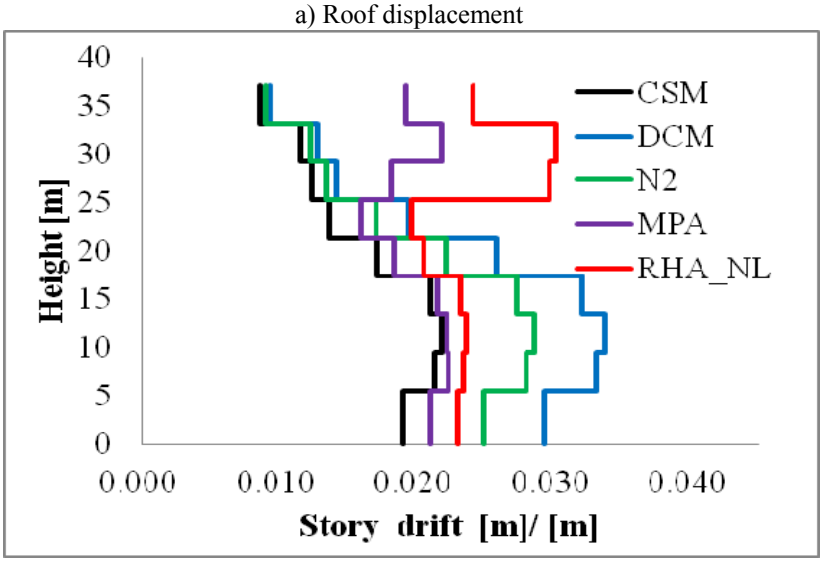

b) Interstorey drifts

Figure 6.8 Peak response of 2/50 set of records

6.2.4 Effects of lateral loads

The accuracy of NSP is strongly related to the load pattern used in performing pushover analyses, which influences both the capacity curve and the distribution of seismic response along the height of the structure. In this section, the influence of lateral load patterns on the seismic response in terms of floor displacement and interstorey drifts is discussed.

Five lateral load patterns defined in section 2.4 are selected to conduct the nonlinear pushover analysis and CSM is selected to obtain the target displacement. The normalized lateral load distributions of 10/50 and 2/50 set of records are plotted in Figure 6.9 and Figure 6.11. It can be observed that different lateral load patterns lead to the quite different lateral load distribution.

The lateral displacement and interstorey drifts profiles of 2/50 and 10/50 set of records are plotted from Figure 6.10 and Figure 6.12. It is observed the SRSS distribution and the MPA procedure are able to reproduce the pattern of storey drift distribution. In the lower storeys uniform distribution predict a storey drift much larger than the dynamic one, but greatly underestimate for the upper floors. The standard NSPs would underestimate the storey drifts for upper floors, and the MPA would improve the estimate for the upper floors. In the pushover analysis, different lateral load distribution should be considered to estimate the seismic response of structure.

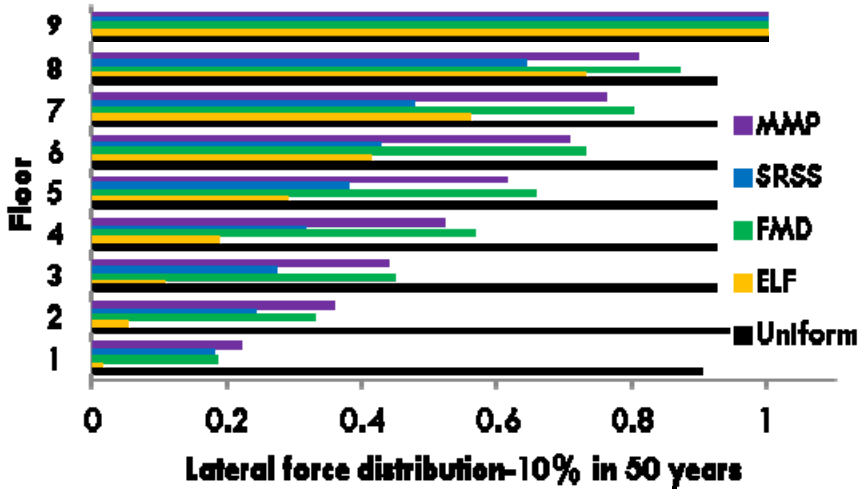

Figure 6.9 Normalized lateral load distributions of 10/50 set of records

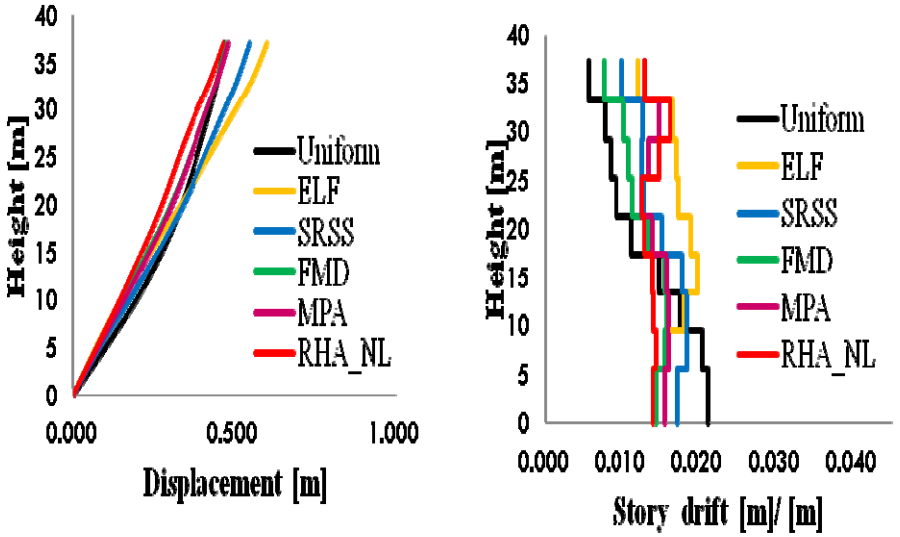

Figure 6.10 Peak response of 10/50 set of records a) floor displacements profile, b) storey-drifts profile

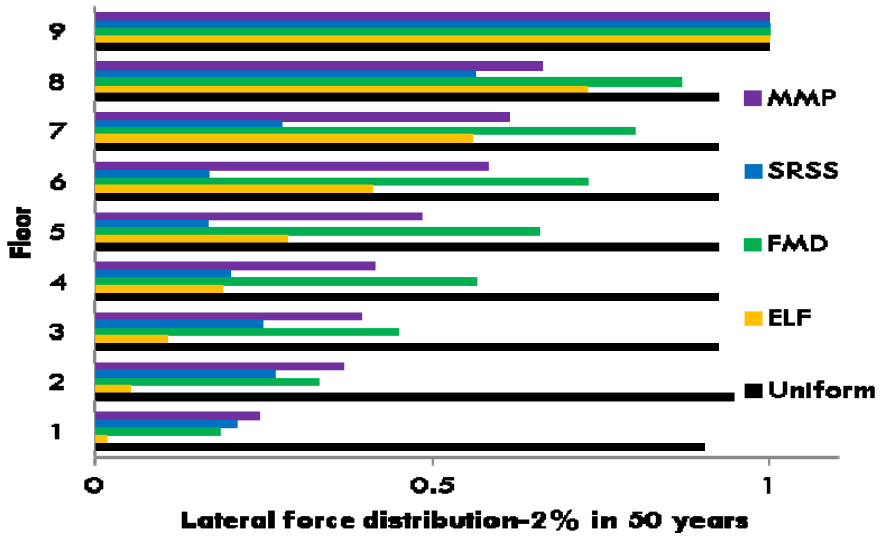

Figure 6.11 Normalized lateral load distributions of 2/50 set of records

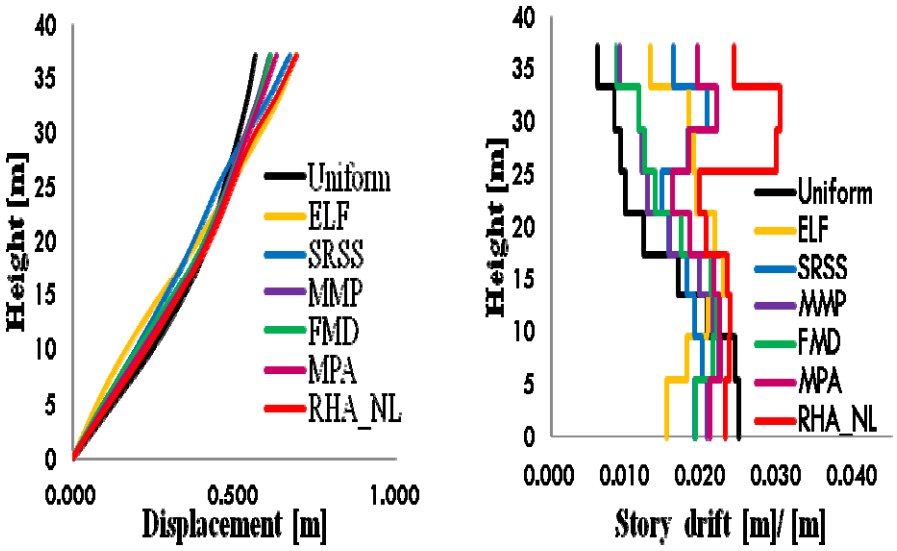

Figure 6.12 Peak response of 2/50 set of records a) floor displacements profile, b) storey-drifts profile

6.3 Irregular structure

6.3.1 Modal Analysis

Modal analysis is employed to identify the dynamic behavior of the existing structure and investigate the relevance of higher modes. The participating translational masses along X direction (MT_X), along Y direction (MT_Y) and rotational mass with respect to the vertical direction Z (MR_Z) of the first ten modes are listed in Table 6.2 and plotted in Figure 6.13.

It can be found that the existing building shows a strong flexible behavior. The first and The first and fourth modes have about 74% of participation mass along Y direction; direction; along X direction the third and ninth mode has about 76% of participation participation mass. One also can observe that the first mode is substantially translation substantially translation along Y direction, but also presents a significant rotation; the rotation; the third mode is characterized, neglecting the small amount of mass mass participation associated with the rotation, by a so-called pure translation along translation along direction X, as shown in

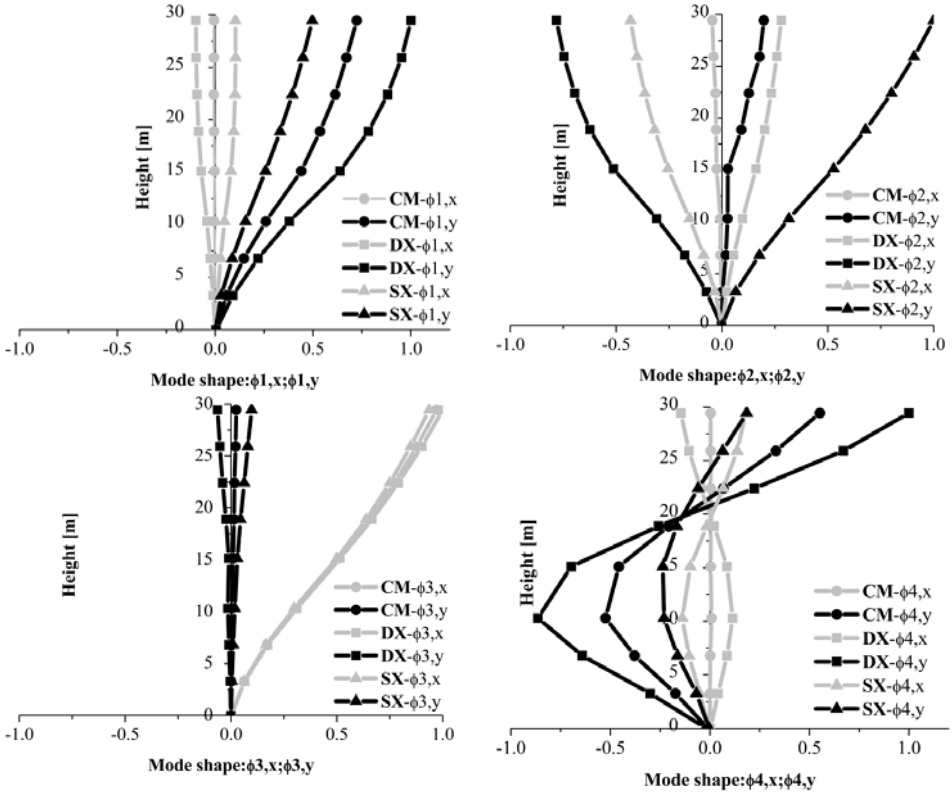

Figure 6.14.

Table 6.2 modal periods and participating mass

Mode	T(s)	MT_X (%)	MT_Y (%)	MR_Z (%)	∑MT_X (%)	∑MT_Y (%)	∑MR_Z (%)
1	1,76	0,0087	63,8	28,2	0,009	64	28
2	1,27	0,20	3,57	29,93	0,2	67	58
3	0,94	65,56	0,03	6,82	66	67	65
4	0,55	0,00	10,11	4,04	66	78	69
5	0,37	0,01	1,30	6,56	66	79	76
6	0,35	0,00	0,01	0,04	66	79	76
7	0,32	0,01	3,68	1,66	66	83	77
8	0,30	0,00	0,00	0,00	66	83	77
9	0,28	10,00	0,00	0,82	76	83	78
10	0,21	2,76	0,17	0,52	79	83	79

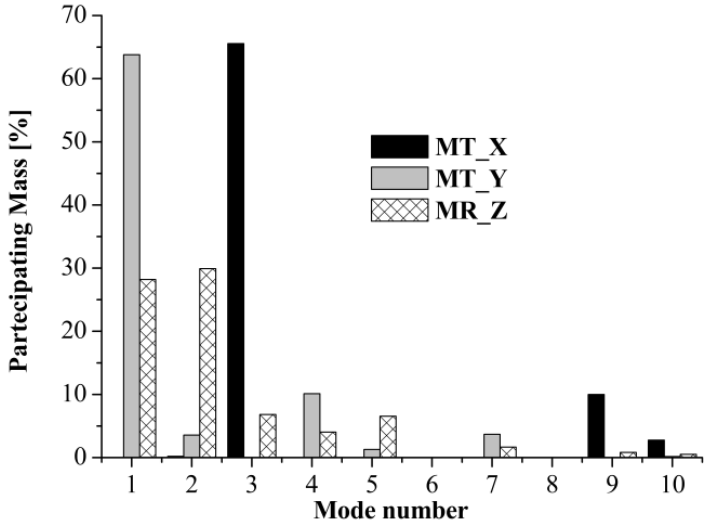

Figure 6.13 Modal mass participation

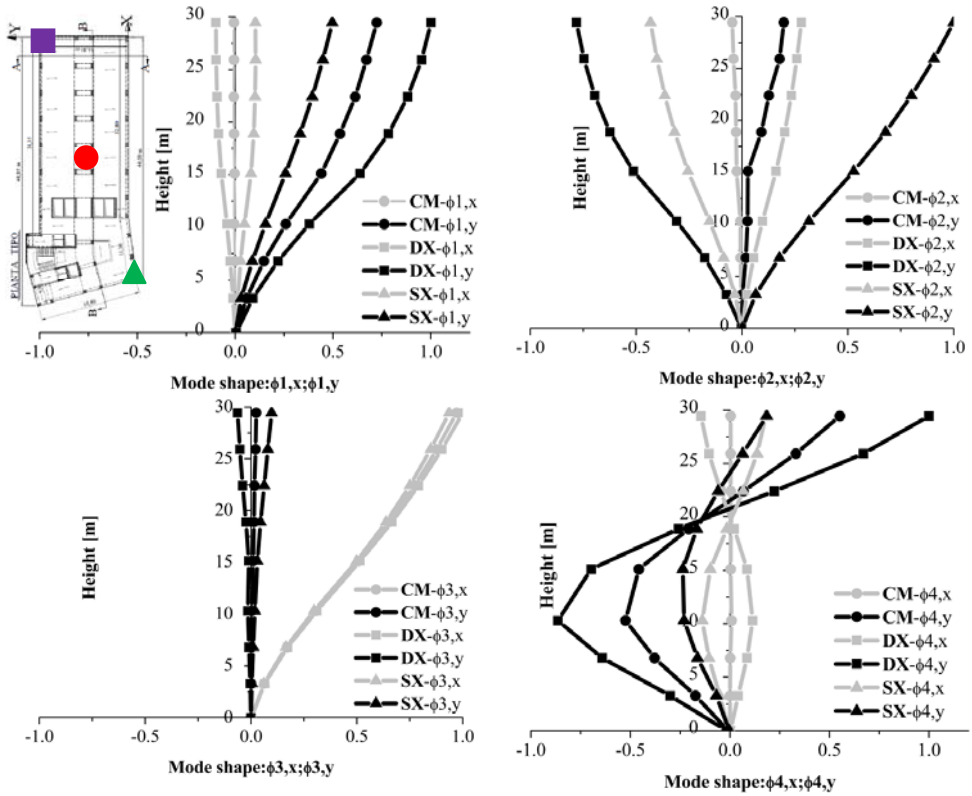

Figure 6.14 Modal shape configurations considering different control nodes: CM, DX, SX a) ϕ1,b) ϕ2, c) ϕ3, d) ϕ4

In this study, the center of mass (CM) and two corners (SX, DX) are taken as control points, as shown in Figure 5.13: the displacements associated to these three control points for the first four modes are shown in Fig 8. It can be found that the structure exhibits a behavior with decoupled translational and rotational along X direction, where there are strongly couple along Y direction especially in the right side of the building. This peculiarity is an indicator of lack of structural regularity in plan. The right side of the building is more deformable of the opposite side as a result of lack of vertical elements in this area.

6.3.2 Nonlinear response history analysis

Nonlinear response history analysis (RHA_NL) is the most rigorous procedure to compute seismic demands in terms of displacement and inter story-drifts, such analyses were conducted with respect to suites of seven different groups of earthquake natural records scaled linearly for the code-compliant limit states both for X and Y directions, and their results are taken as the "exact"results to estimate the accuracy of the static nonlinear analysis. As an example, the history response in roof of the building subjected to the earthquake record which is illuminate in Figure 5.11 is shown in Figure 6.15 and Figure 6.16, respectively. The peak value of the displacements and inter story-drifts obtained from RHA_NL for the seven earthquakes are plot in Figure 6.17 and Figure 6.18, respectively. The figures show that the responses of the corners do not deviate from the response of CM in X direction, while great deviation in Y direction. It is an indication of the irregularity in Y direction for the structure.

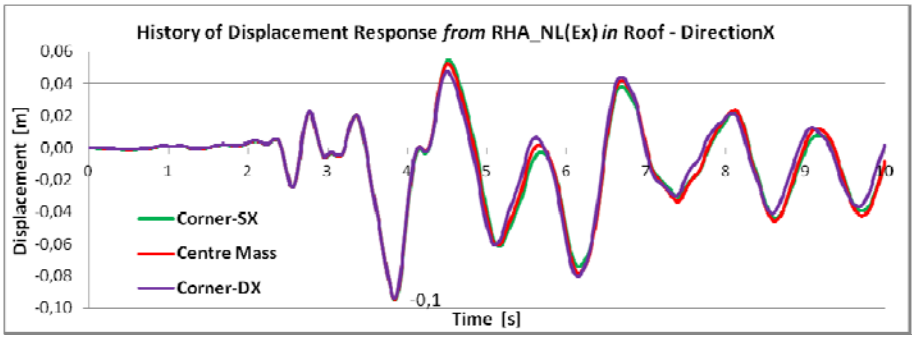

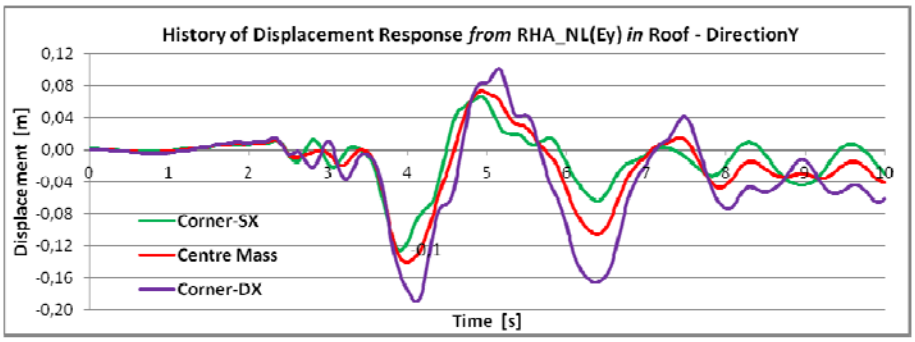

Figure 6.15 Nonlinear response history of displacement for control points in roof

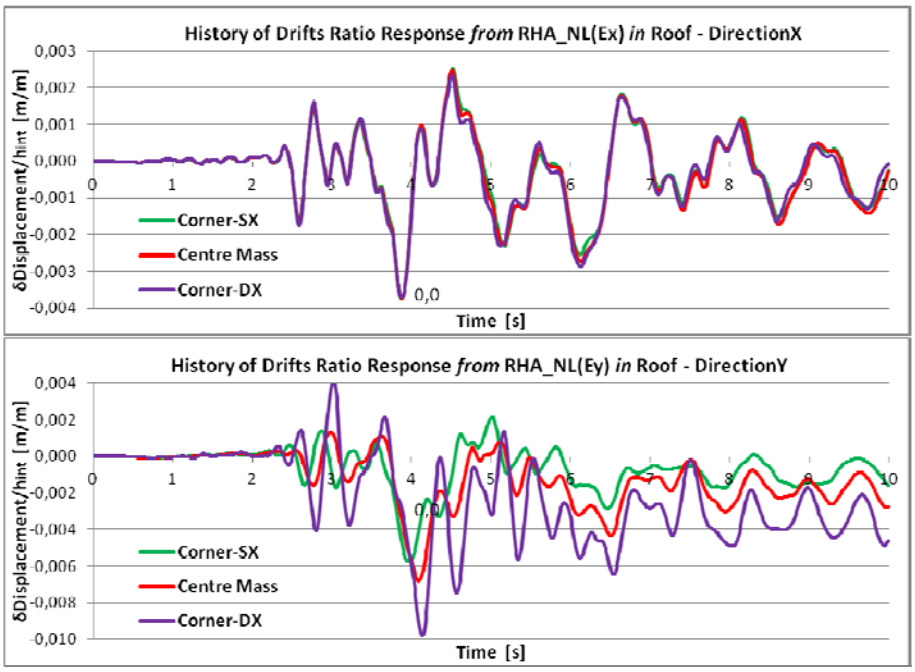

Figure 6.16 Nonlinear response history of storey-rift for control points in roof

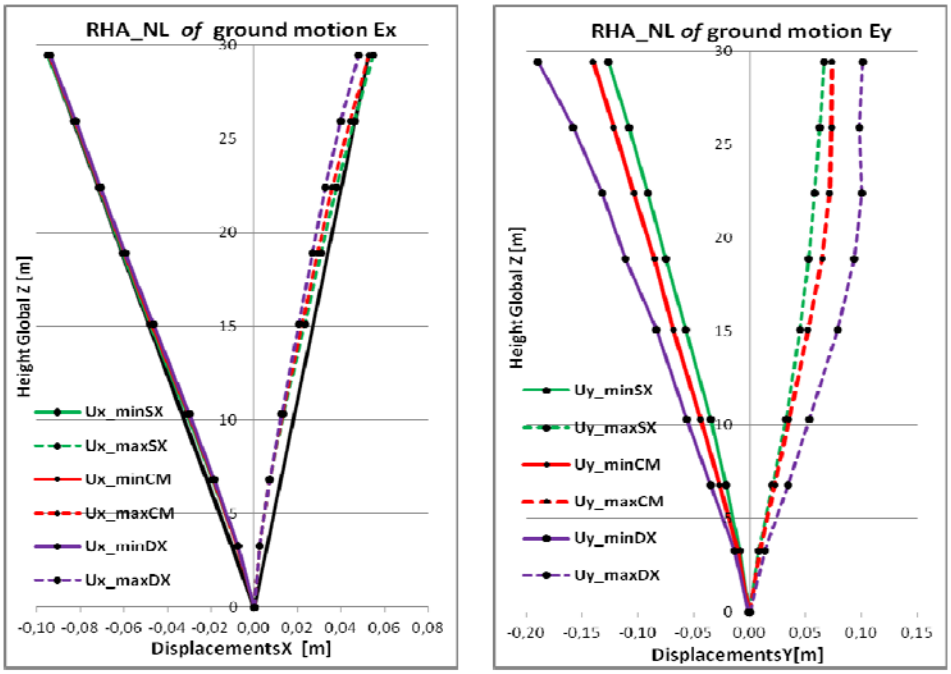

Figure 6.17 Maximum and minimum floor displacements from RHA_NL

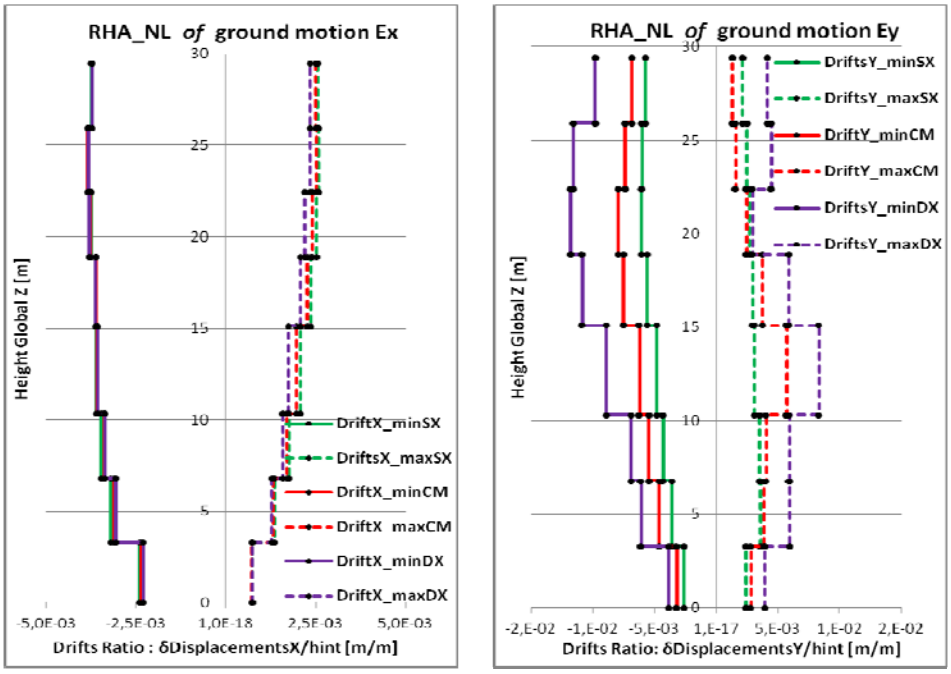

Figure 6.18 maximum and minimum storeydrifts from RHA_NL

6.3.3 Target displacement

1. Capacity spectrum method (CSM)

From Table 6.2 and Figure 6.13, it is clear that for X direction the dominant mode is the third one, while for Y direction the first mode. Figure 6.19 shows the performance point (P.P.) obtained from capacity spectra. CSM is used to search the P.P. of predominate mode inelastic SDF system. The elastic response spectra defined by NTC2008 is taken as the demand spectrum. It is observed that along X direction, the third mode of the structure exhibits its inelastic behavior. Along Y direction, the structure enters in the nonlinear state for the first mode.

Table 6.3 list the equivalent SDF systems' parameters for the first and third modes and the effective damping ratios for the third and first modes are 27% and 23%, respectively.

Table 6.3 SDF Parameters: Equivalent Elasto-Viscous system

SDF Parameters:	1st mode	3rd mode	unit
Elastic stiffness	13,09	46,27	$[rad/sec]^2$
Elastic period T_e	**1,76**	**0,94**	[s]
the acceleration at the yield point of the structure. a_y	0,33	0,95	$[m/s^2]$
the displacement at the yield point of the structure. d_y	0,025	0,021	[m]
Ultimate acceleration a_c	0,520	1,181	$[m/s^2]$
Ultimate displacement. d_c	**0,114**	**0,072**	[m]
Post-Elastic stiffness	2,155	4,426	$[rad/sec]^2$
Hardening factor α	0,16	0,10	[-]
Equivalent period T_{eq}	**2,95**	**1,55**	[s]
Equivalent damping ξ_{eq}	26,2	33,2	[%]
modification factor $k(\xi_{eq})$	0,670	0,650	[-]
Total damping . $\xi_n = \xi_0 + k\xi_{eq}$	**22,5**	**26,6**	[%]

Table 6.4 P.P. obtained from capacity spectra and capacity curve

Direction	Mode	Γ_n	Performance Point (P.P.)			
			Capacity spectra		Capacity curve	
			S_{dn}	S_{an}	Ur [m]	V [KN]
X	1	1.44	0.060	0.111	0.087	9610
Y	3	1.22	0.011	0.050	0.104	3787

Once the P.P. obtained from the capacity spectra, which is in terms of the spectral acceleration (S_{an}) and spectral displacement (S_{dn}), can be converted to P.P. in the capacity curve, which is in terms of the roof

displacement (Ur) and base shear V corresponding to Ur through Eq.(6.2). The P.Ps obtained from capacity curve are shown in Fig 7and Fig 9, their values are listed in Table 6.4.

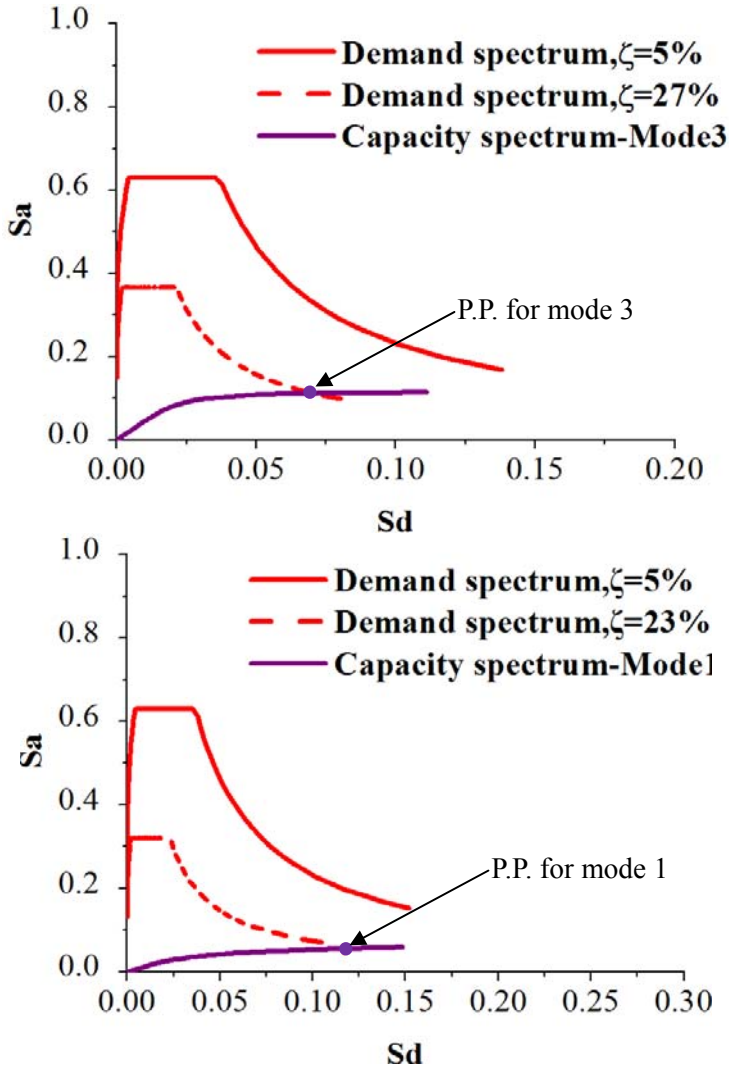

Figure 6.19 P.P. for the CM is determined via CSM from original and reduced demand spectrum for the first mode. a) Capacity spectra along X direction, b) Capacity spectra along Y direction.

2. Displacement Coefficient Method (DCM)

In this procedure proposed in FEMA 356, the nonlinear MDF system's displacement is obtained from the linear elastic demand spectrum, using

certain coefficients which are based on empirical equations derived by calibration against a large number of dynamic analyses, as shown in Table 6.5.

Table 6.5 P.P. obtained from DCM

	C_0	C_1	C_2	C_3	S_a [m]	T_e [s]	d_t [m]	V_d [KN]
X direction	1.44	1.02	1.1	1	0.26	0.97	0.092	9497
Y direction	1.22	1.00	1.1	1	0.13	1.90	0.157	4258

3. N2

For medium and long period structure, the target displacement of the inelastic system is equal to that of an elastic structure, as shown in Fig 8.

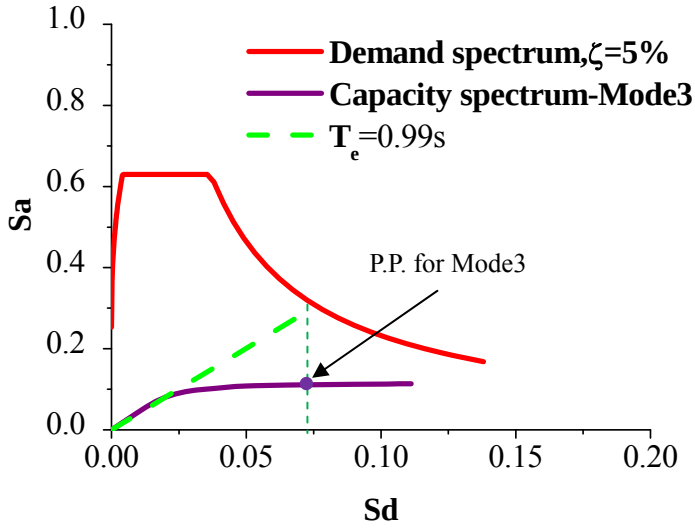

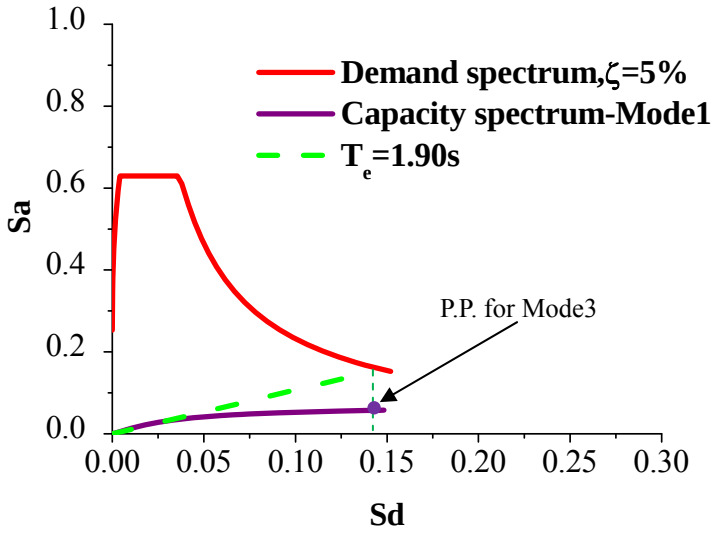

Figure 6.20 P.P. for the CM is determined via N2, a) along X direction, b) along Y direction

4. Modal pushover analysis (MPA)

From Figure 6.13, it is clear that for X direction the dominant mode is the third one, while for Y direction the first mode. MPA takes into account minor contribution of high modes to determine the total response of the structure. For X direction, the third, ninth and tenth modes exhibit more than 79% of participation mass, while for Y direction, the first, fourth and seventh modes exhibit more than 83% of the participation mass, these modes will be considered in the MPA.

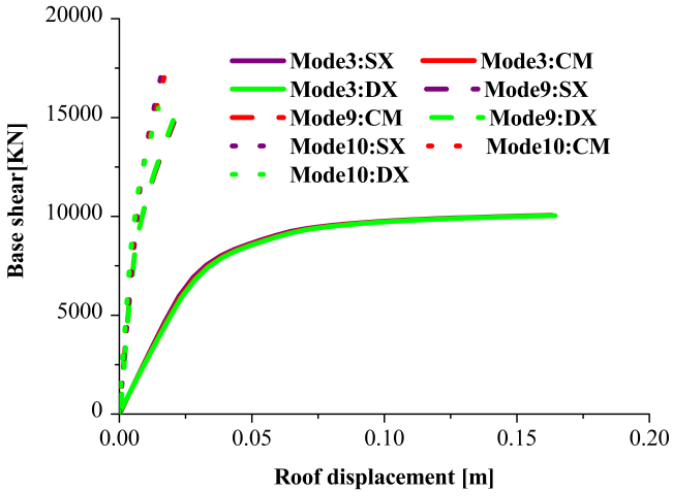

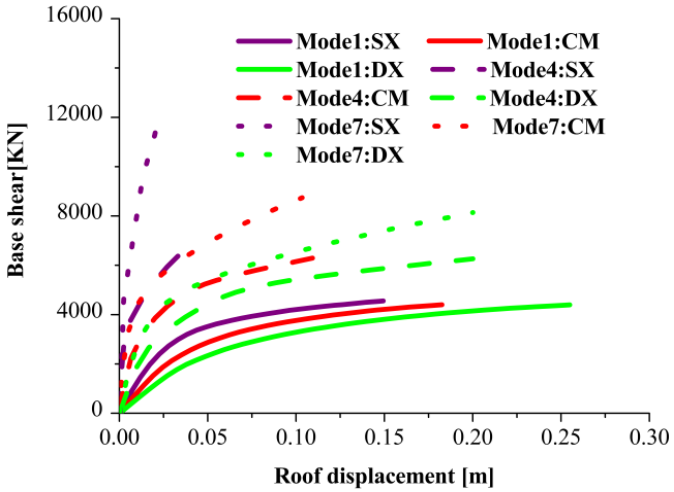

Figure 6.21 Pushover curves obtained with different load distributions (Mode1…Mode n) and considering different control joints. a) Pushover curves along X direction, b) Pushover curves along Y direction

Figure 6.21 shows pushover curves for the structure subjected to lateral forces proportional to the primary modes along X and Y directions, respectively. The comparison of the pushover curves between X and Y directions confirms, as already expected, the behavior of pure translation along X direction (pushover curves for different control nodes superimpose in this direction), while demonstrating a behavior with decoupled translational and rotational along Y direction (pushover curves for different control nodes deviate at the start).

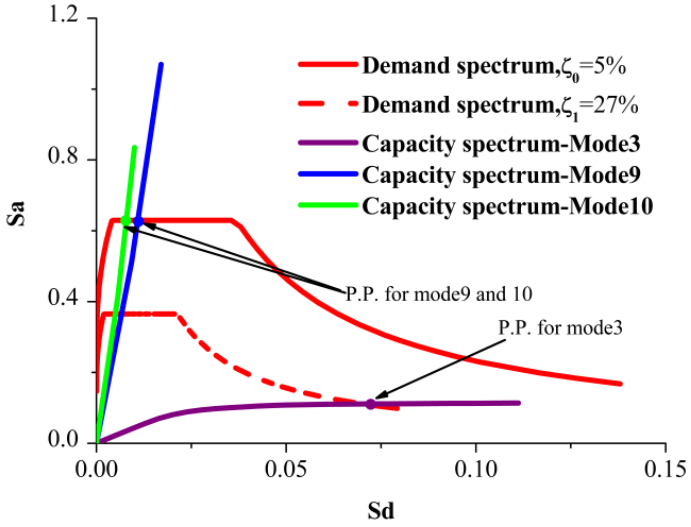

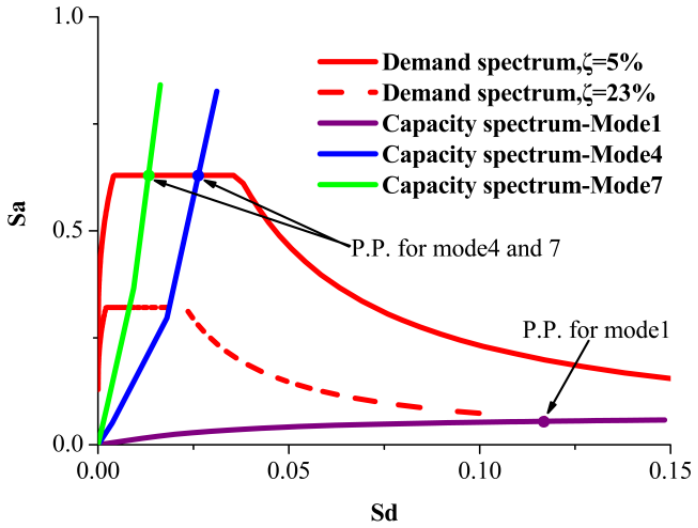

Figure 6.22 P.P. for the CM is determined via CSM from original and reduced demand spectrum for the predominate modes. a) Capacity spectra along X direction, b) Capacity spectra along Y direction.

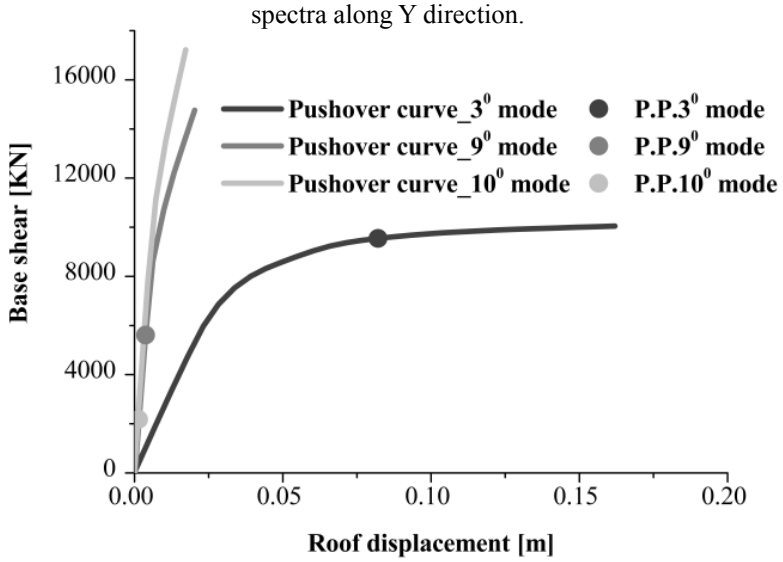

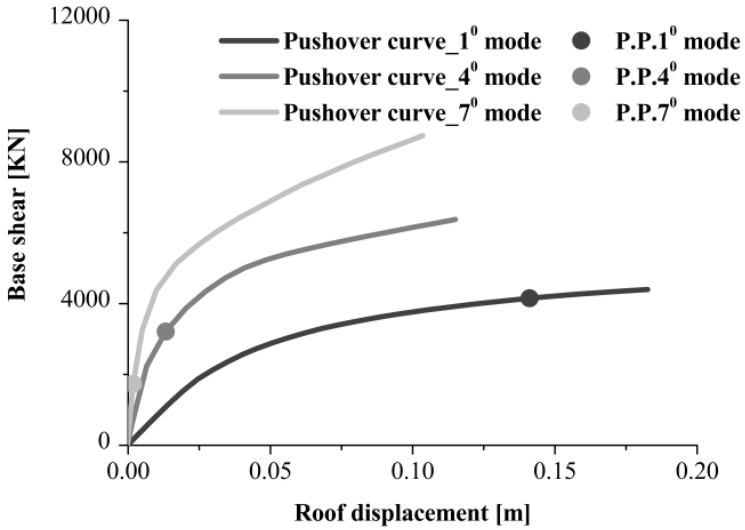

Figure 6.23 P.P. in terms of spectral acceleration and spectral displacement can be converted to P.P. in terms of the roof displacement (*Ur*) and base shear V_{bn} corresponding to *Ur* from the pushover capacity curve through Eq.10 a) P.P. along X direction, b) P.P. along X direction,

Figure 6.22 shows the performance point (P.P.) obtained from capacity spectra. CSM is used to search the P.P. of the ith mode inelastic SDF system. The elastic response spectra defined by NTC'08 is taken as the demand spectrum. It is observed that along X direction, the third mode of the structure exhibits its inelastic behavior and the remaining modes are still in almost linear elastic state. Along Y direction, the structure enters in the nonlinear state for the first mode, and linear elastic state for fourth and seventh mode.

Once the P.P. obtained from the capacity spectra, which is in terms of the spectral acceleration (S_{an}) and spectral displacement (S_{dn}), can be converted to P.P. in the capacity curve, which is in terms of the roof displacement (U_r) and base shear V_{bn} corresponding to U_{rn} from the pushover database through Eq.(6.2). The P.Ps obtained from capacity spectrum and capacity curve are shown in Figure 6.22and Figure 6.23, their values are listed in Table 6.6.

Table 6.6 P.P. obtained from capacity spectra and capacity curve

Direction	Mode	Γ_n	Performance Point (P.P.)			
			Capacity spectra		Capacity curve	
			S_{dn}	S_{an}	Ur [m]	V [KN]
X	3	1.44	0.067	0.111	0.096	9734
	9	0.36	0.011	0.667	0.004	5614
	10	0.11	0.009	0.613	0.001	2181
	SRSS					
Y	1	1.22	0.055	0.116	0.141	4151
	4	0.27	0.033	0.754	0.009	2567
	7	0.20	0.015	0.693	0.003	2114
	SRSS					

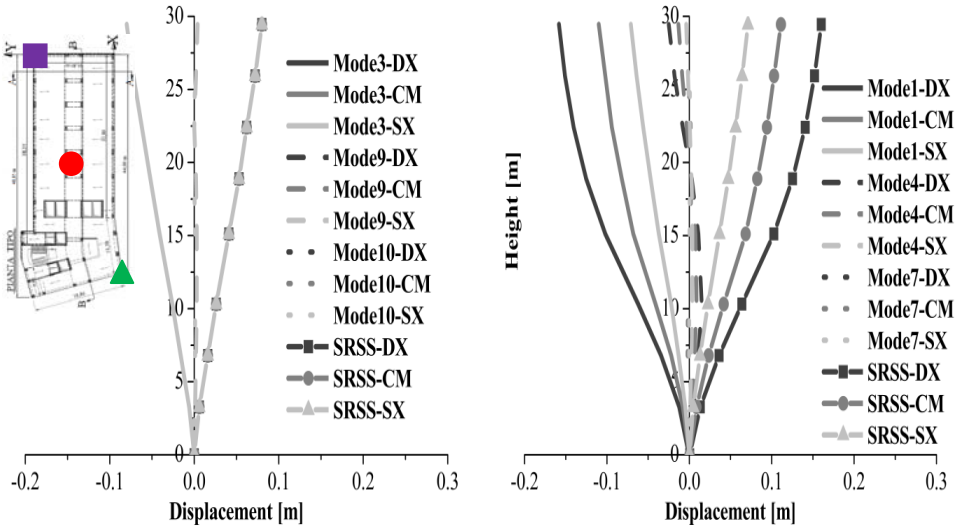

Figure 6.24 Floor displacements from the predominate modal pushover analysis and their combination through SRSS for SX, CM and SX, a) X direction for mode 3,9,10 and their combination, b) Y direction for mode 1,4,7 and their combination

From Figure 6.24, in accordance with expectations, it's evident the behavior with pure translation along X direction: all control points in the plan structure undergo the same displacements and the fundamental mode contributes 90% to the total response, while the higher modes, characterized by a small percentage of mass participation, exhibit an almost negligible contribution. Instead, along Y direction, the behavior with translation and rotation strong coupled: the displacement vector of the three control points in plan does not superimpose, but rather it

highlights that the right side of the building is less flexible than the left side, and the effect of the higher modes cannot be neglected.

6.3.4 Floor displacement and interstorey drifts

The comparison of the different NSPs and the nonlinear dynamic results in terms of lateral displacement and interstory drifts profiles are presented in this section. The time-history median results are taken as exact results.
The lateral displacement and interstorey drifts profiles for the control points along X direction are plotted from Figure 6.25 to Figure 6.27. As expected, the symmetric direction of the building, different NSPs lead to quite similar results, and results are very close to the results of nonlinear dynamic analysis. The structure exhibits pure translation along X direction, the higher modes exhibit an almost negligible contribution to the total response. MPA provide a better estimate for story drift, especially for the upper floors. It also shows that vertical irregularity does not affect significantly the ability of conventional pushover analysis to correlate well results from inelastic dynamic analysis.

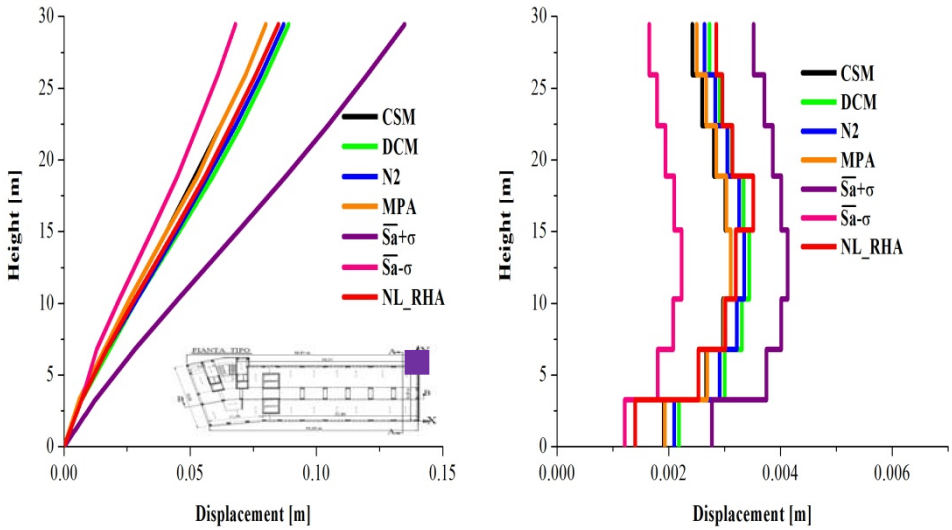

Figure 6.25 Peak response for SX along X direction, a) floor displacements profile, b) storey-drifts profile

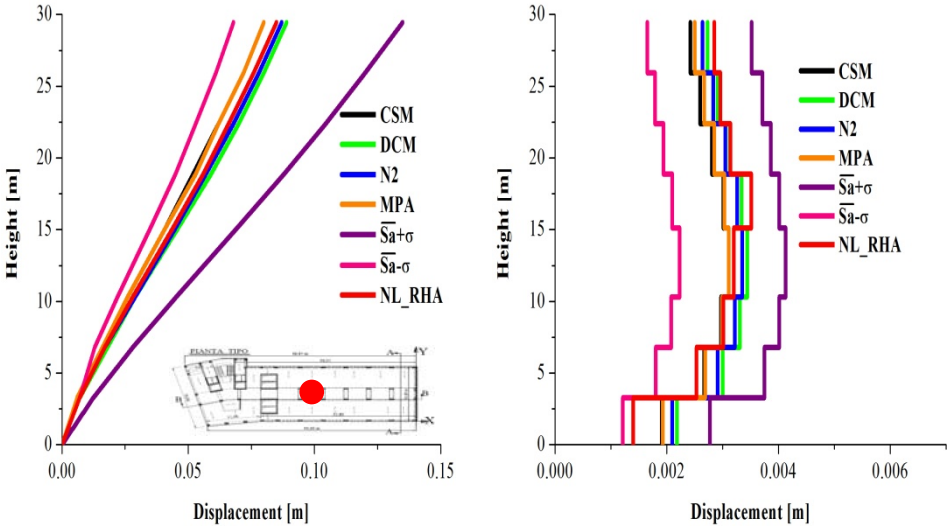

Figure 6.26 Peak response for CM along X direction, a) floor displacements profile, b) storey-drifts profile

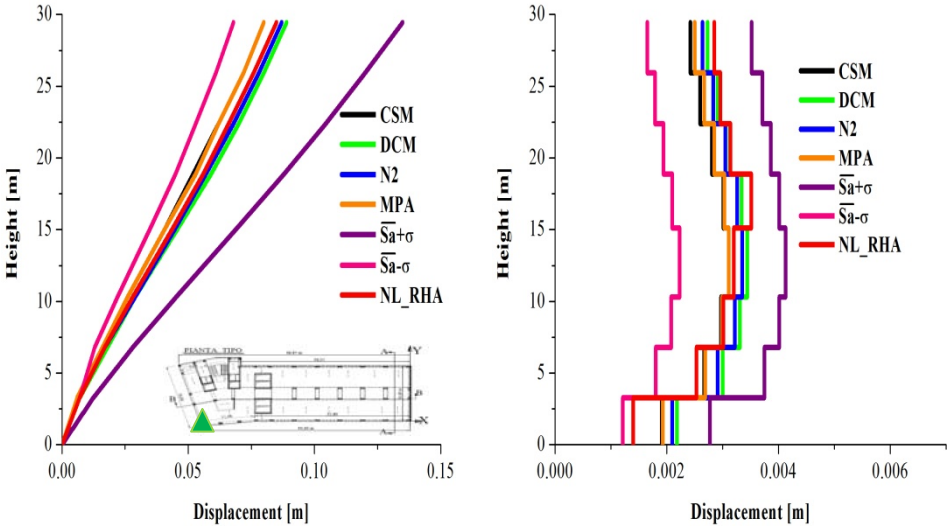

Figure 6.27 Peak response for DX along X direction, a) floor displacements profile, b) storey-drifts profile

For the Y direction, the asymmetric direction of the building, the lateral displacement and interstorey drifts profiles for the control points are shown from Figure 6.28 to Figure 6.30. Accurate prediction of the target displacement at the center of mass (CM) is a primary issue for application of pushover analysis to regular structures and it is a pre-requisite for any

further extension of pushover analysis to irregular structures. It is observed that CSM would provide a good estimate for the floor displacement; DCM and N2 methods would overestimate the floor displacements. For the interstorey drifts, CSM leads to accurate prediction for the low and middle floors, and underestimate for upper floors. DCM and N2 method lead to slightly underestimate for the upper floors and largely overestimate for middle floors. Along Y direction, the overlap of the floor displacements in the MPA procedure indicates that first ‘‘mode’’ alone is adequate for estimating floor displacements. For center of mass (CM), MPA provides a better estimate in story drifts for upper floors. However, MPA greatly underestimate the story drifts for rigid side (SX) and overestimate the story drifts for the lower floors for flexible side (DX). It appears to be that MPA can satisfy its fundamental purpose of an accurate prediction for the inelastic response of the irregular structure, and can identify the sensitivity of irregular structure through the simplified procedure.

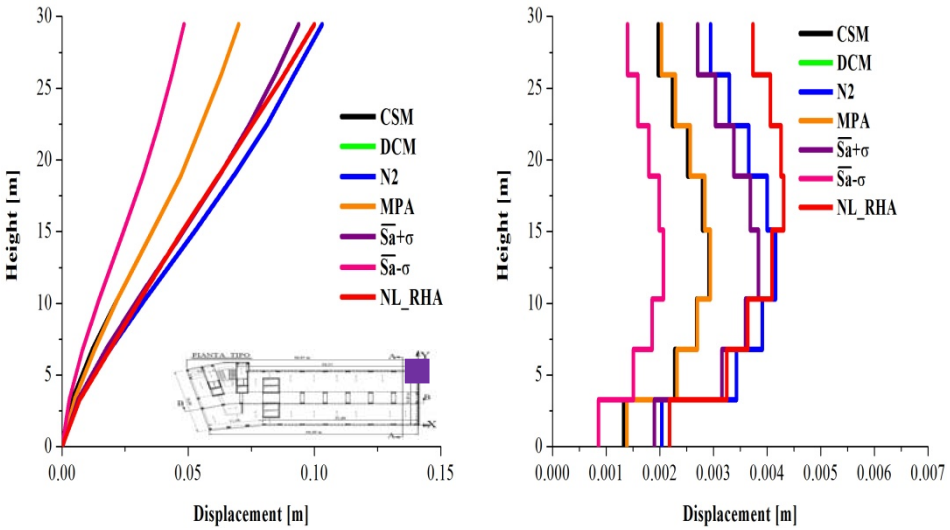

Figure 6.28 Peak response for SX along Y direction, a) floor displacements profile, b) storey-drifts profile

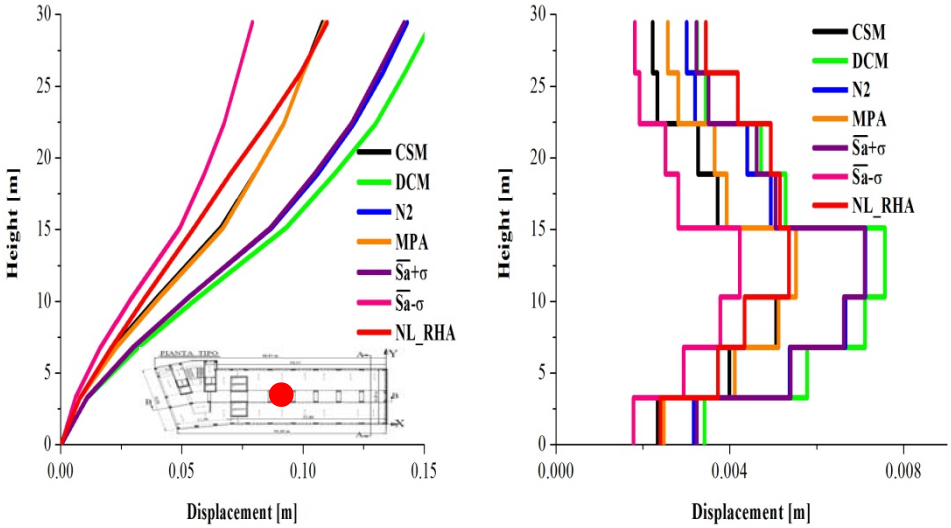

Figure 6.29 Peak response for CM along Y direction, a) floor displacements profile, b) storey-drifts profile

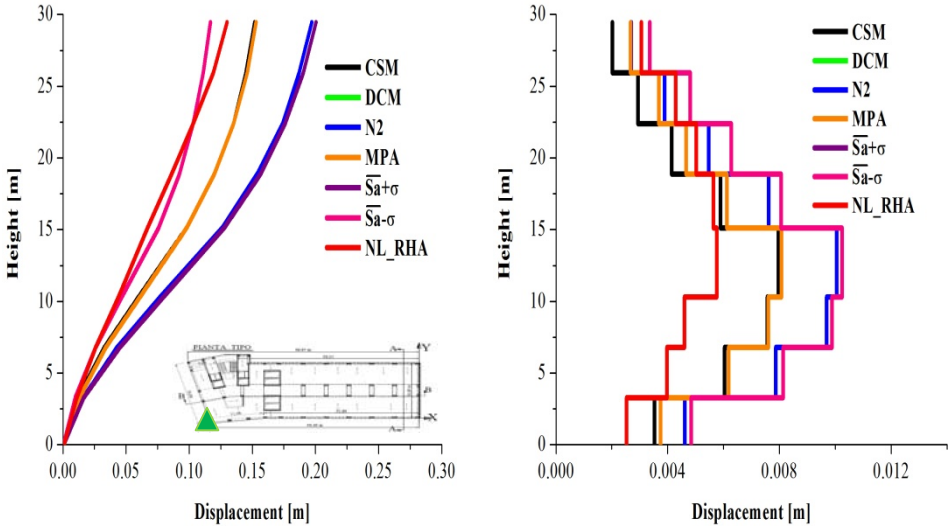

Figure 6.30 Peak response for DX along Y direction, a) floor displacements profile, b) storey-drifts profile

As already underlined, the key problem that undermines suitability of conventional pushover analysis in the presence of plan irregularity is plan variation of maximum top lateral displacements. Due to floor rotations, during excitation maximum top lateral displacement are attained at different times along the building plan, so that, even under the assumption

of rigid floor slabs, their envelope is nonlinear. For rigid side (SX), the NSPs largely underestimate the ineterstorey drifts; for flexible side (DX), the NSPs would well predict for the upper floors but largely underestimate for low and middle floors. As a consequence, conventional pushover analysis is unsuitable for translation and rotation strongly coupled direction of irregular structure, because these NSPs cannot fully evaluate amplification of displacements at corners of building with respect to mass center by dynamic amplification of static eccentricity due to onset of torsional inertia moments

6.3.5 Effects of lateral load patterns

The accuracy of NSP is strongly related to the load pattern used in performing pushover analyses, which influences both the capacity curve and the distribution of seismic response along the height of the structure. In this section, the influence of lateral load patterns on the seismic response in terms of floor displacement and interstorey drifts is discussed, and its influence on capacity curve will be discussed in the next section.
Five lateral load patterns defined in section 2.4 are selected to conduct the nonlinear pushover analysis and CSM is selected to obtain the target displacement. The normalized lateral load distributions for both directions are plotted in Figure 6.31.

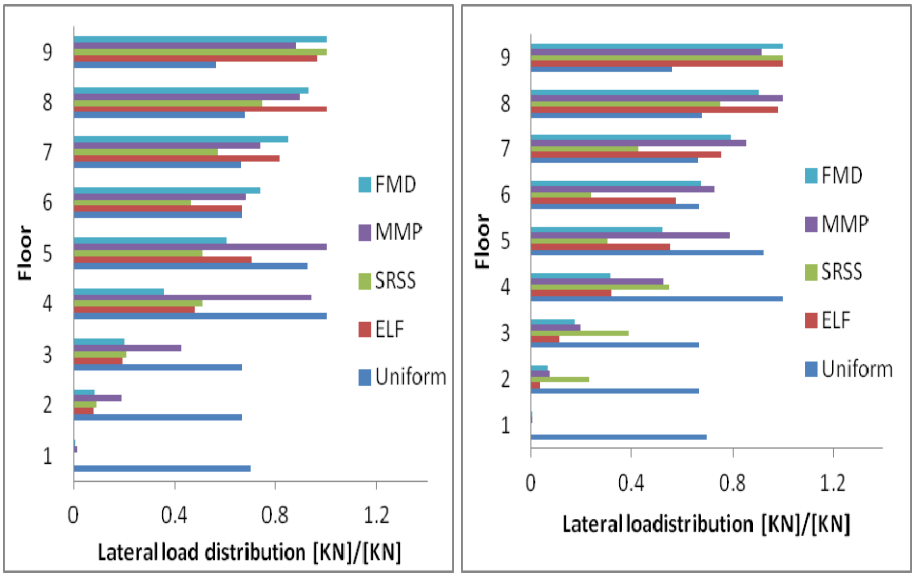

Figure 6.31 Normalized lateral load distributions, a) X direction, b) Y direction

The lateral displacement and interstorey drifts profiles for the control points along X direction are plotted from Figure 6.32 to Figure 6.34. The results for three control points obtained from different lateral patterns are almost the same as a result of pure translation along this direction. The uniform pattern load distribution would over estimate the interstorey drifts for the low and middle floors, and all patterns would underestimate interstorey drifts for upper floors.

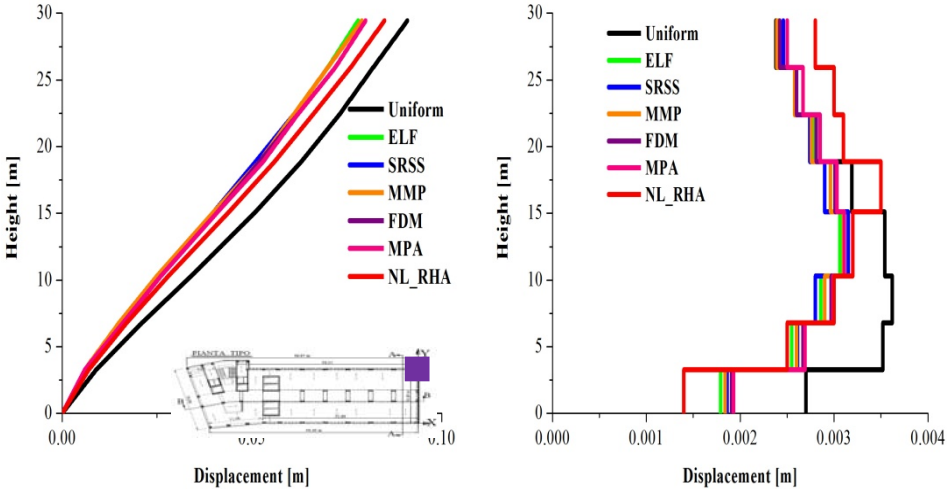

Figure 6.32 Peak response for SX along X direction, a) floor displacements profile, b) storey-drifts profile

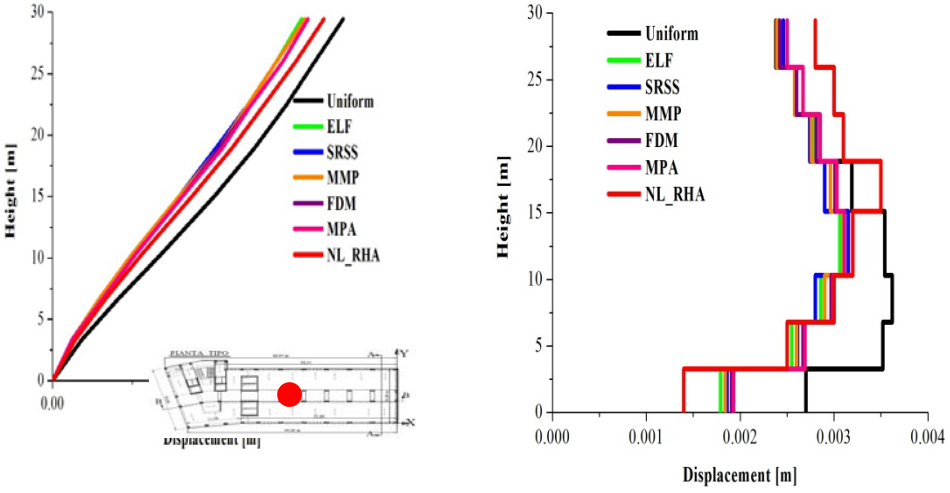

Figure 6.33 Peak response for CM along X direction, a) floor displacements profile, b) storey-drifts profile

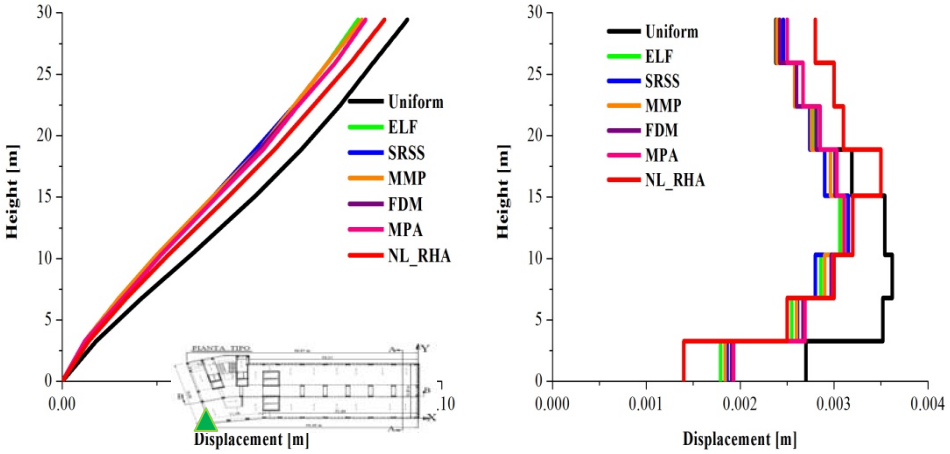

Figure 6.34 Peak response for DX along X direction, a) floor displacements profile, b) storey-drifts profile

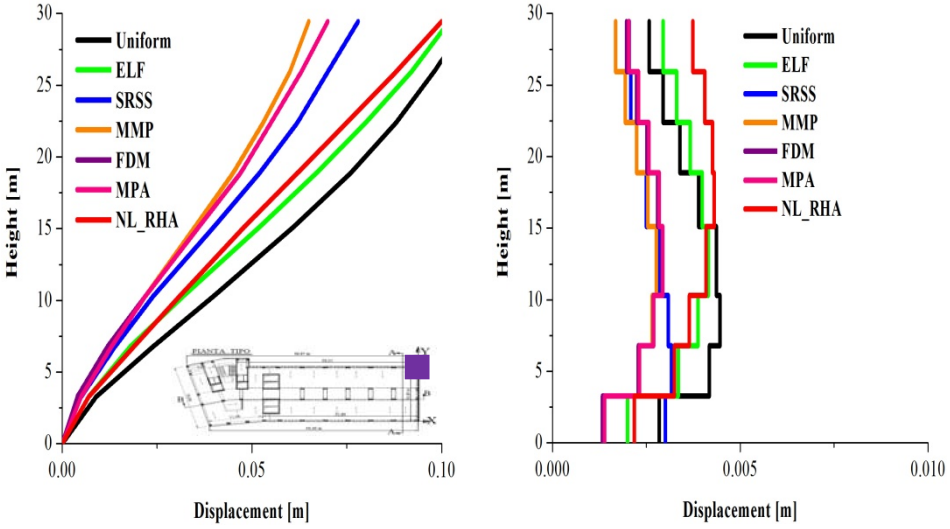

Figure 6.35 Peak response for SX along Y direction, a) floor displacements profile, b) storey-drifts profile

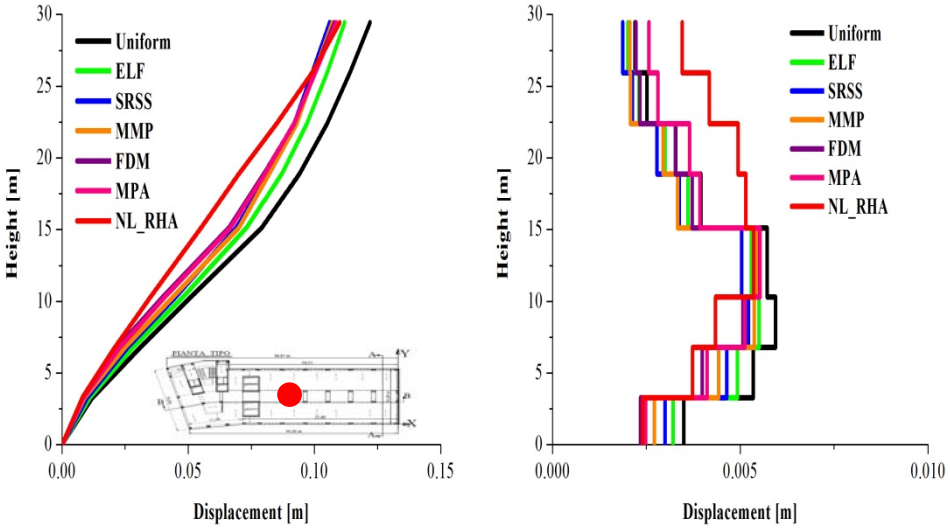

Figure 6.36 Peak response for CM along Y direction, a) floor displacements profile, b) storey-drifts profile

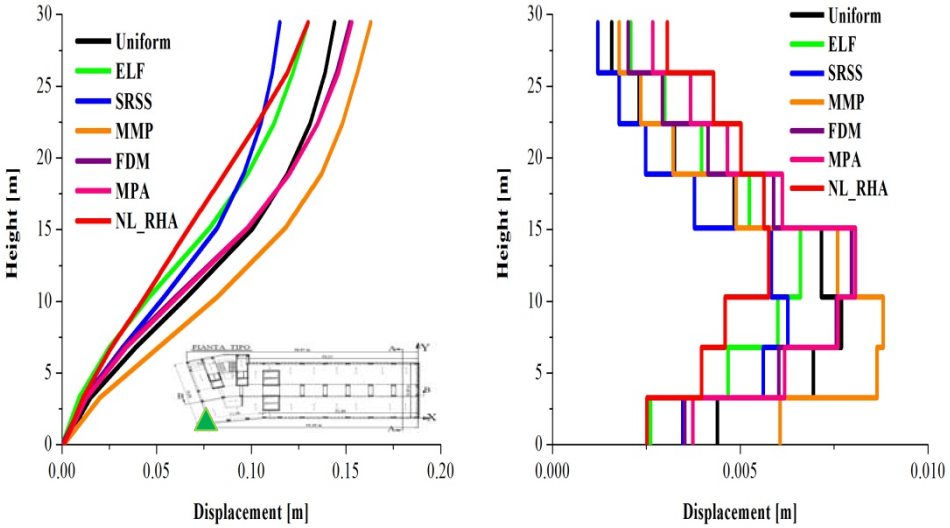

Figure 6.37 Peak response for DX along Y direction, a) floor displacements profile, b) storey-drifts profile

The lateral displacement and interstorey drifts profiles for the control points along Y direction are plotted from Figure 6.35 to Figure 6.37. The results for three control points obtained from different lateral patterns are quite different as a result of translation and rotation strongly coupled along this direction. For the center of mass (CM), NSPs would

underestimate the interstorey drifts for upper floors. For the flexible side (DX), the MMP pattern largely underestimates interstorey drifts for whole floors, especially the upper floors. The ELF and uniform pattern would well estimate for low and middle floors but underestimate for upper floors. For the rigid side (SX), the NSPs would underestimate for upper floors, but overestimate for middle floors.

6.3.6 Capacity curve

In this section, the influence of lateral load patterns on the capacity curves is discussed. The capacities curves obtained by different load patterns are plotted in Fig 23. The capacity curve obtained from Incremental dynamic analysis (IDA) is included as reference, which is considered to be the most exact method to predict the capacity of structures (Vamvatsikos and Cornell, 2002). The capacity curve by IDA is in terms of maximum base shear Vs maximum roof displacement. Along the X direction, superimpose of the capacity curves obtained from different load patterns except uniform. Along Y direction, it is clear in all cases that the response of the buildings is sensitive to the shape of the lateral load distribution. This is particularly true when moving into inelastic phase. The NSPs cannot catch up the increasing of base shear in the inelastic phase.

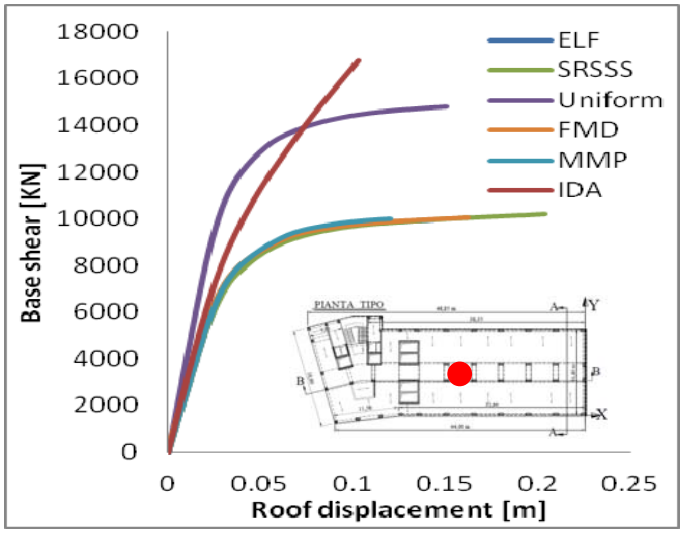

a) along X direction

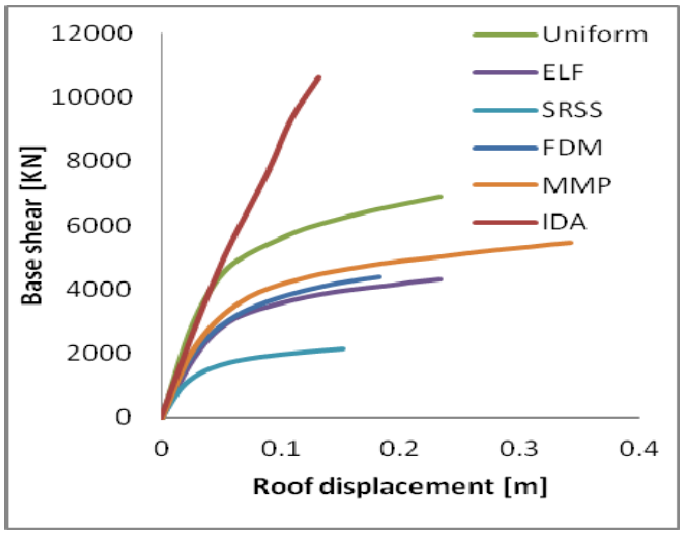

b) along Y direction

Figure 6.38 Capacity curves for center of mass (CM)

6.4 Conclusion

Given the increasing use of nonlinear static pushover analysis in engineering practice, the aim of the present section is to evaluate the accuracy of current used NSPs to irregular structures: CSM integrated into ATC-40, DCM included in FEMA356 and N2 method adopted by Eurocode 8.

These three commonly used NSPs were applied to real existing plan and vertical irregular RC building, which shows pure translation along longitudinal direction and translation and rotation strongly coupled along transverse direction. The seismic response in terms of floor displacement and interstorey drifts were compared with the time-history nonlinear dynamic analysis. On the whole, predictions of floor displacement and interstory drifts by selected NSPs are close to values from inelastic dynamic analysis along longitudinal direction. Along the transverse direction, for center of mass(CM), selected NSPs would underestimate the interstory drifts for upper floors; for rigid side (SX), largely underestimate the ineterstorey drifts; for flexible side (DX), the NSPs would well predict for the upper floors but largely underestimate for the low and middle floors.

The accuracy of NSP is strongly related to the load pattern used in performing pushover analyses, which influences both the capacity curve and the distribution of seismic response along the height of the structure.

Along the transverse direction, the response of the buildings is sensitive to the shape of the lateral load distribution. The NSPs cannot catch up the increasing of base shear in the inelastic phase.
As a consequence, conventional pushover analysis is unsuitable for translation and rotation strongly coupled direction, because these NSPs cannot fully evaluate tornioanl effects.

7. Application IMPA to existing building

7.1 Introduction

In chapter 3, a non linear static procedure for the evaluation of the seismic capacity of buildings sensitive to higher modes is proposed. This procedure, named Incremental Modal Pushover Analysis (IMPA), is proposed as alternative to the non linear incremental dynamic analysis (IDA).

It is well known that the IDA implies the execution of many non linear response histories and therefore it requires a complex and computationally heavy activity: non linear dynamic analysis (NL_RHA) requires the preliminary definition of a set of time histories and, after the execution of the analysis, a not immediate and univocal interpretation of results. In fact the IDA curve, which represents the non linear response of the structure to each one of the time history selected and scaled, may be realized according to different approaches: maximum displacement and maximum base shear, maximum displacement and corresponding base shear, or maximum base shear and corresponding displacement etc. According to this, and considering that the non linear dynamic analyses are difficult to be performed, a simpler approach as IMPA may constitute a valid alternative especially for professional use.

The IMPA is based on performing the well known modal pushover MPA (Chopra and Goel, 2002) but it is finalized to obtain a capacity curve (the capacity curve is commonly obtained with a standard pushover analysis) considering also the effect of higher modes: this approach widen the range of applicability of the non linear static analysis including irregular and high rise buildings.

In IMPA the MPA is used to estimate the seismic demand and capacity of structures over the entire range of structural response: the demand curve (the response spectrum) is scaled from lower to higher intensity values starting from the definition of a design response spectrum. According to MPA and using the capacity spectrum method (CSM) a multimodal performance point (P.P.mm) can be defined for each intensity: the multimodal capacity curve (MCC) is the conjunction of all the multimodal performance points obtained.

This approach is now applying it to an existing irregular mid rise building presented in chapter 5 to check its accuracy. On this case study many

analyses have been performed (standard pushover, MPA, NL_RHA) and the relevance of the control joint selected has been discussed. In fact, according to suggestion of many international codes and scientific publications, control joints should be selected on top of the building in the mass center: this suggestion can't be considered as prescriptive because the real configuration of the building must be considered and consequently the "best" choice is not univocally definable. The analysis herein presented on this building, which is characterized by a long rectangular planar shape, highlighted that along the longitudinal direction (along this direction there is pure translation) the higher modes exhibit an almost negligible contribution to the total response. Whereas, along the transverse direction, translation and rotation are strongly coupled and therefore the effect of higher modes cannot be neglected. In this latter case the selection of the position of the control joint is relevant: selecting the mass center, MPA if compared with NL_RHA can provide a good estimate for the roof displacement and underestimate inter story-drift for upper floors; however, referring to the corners as control joint, the error of MPA is more significant and therefore it can't be considered reliable for the estimation of drifts at the extremities of the building (where torsion implies a non negligible translation).

7.2 Regular structure

IMPA is first applied to regular structure described in section 5.
For each intensity level, mutiply the response spectrum by Scale Factor (SF), then determine the corresponding P.P.mm for the modal MDOF system, in terms of roof displacement and corresponding base shear as shown in Figure 7.1, to form the Multimodal Capacity Curve (MCC). By rule of SRSS of the individual modal responses, both for roof displacements and base shear are determined and then all those pairs, each relative to corresponding SF, form the IMPA curve by the writers as shown in Figure 7.2.
It is worthy to note that in the NL_RHA, the maximum base shear is asynchronous with the maximum roof displacement. The response of the existing building subjected to El Centro (1940) ground motion is shown in Figure 7.4. The El Centro (1940) ground motion is shown in Figure 7.3. The base shear corresponding to the maximum roof displacement is much less than maximum base shear: the base shear corresponding to the maximum roof displacement is 4437 KN but the maximum base shear

-12092 KN. Similarly, the roof displacement corresponding to the maximum base shear is much less than maximum roof displacement: the roof displacement corresponding to the maximum base shear is 0.36m but the maximum roof displacement 0.47m. In the IDA procedure, the mean of maximum base shear and maximum roof displacement to an ensemble of earthquake excitations are used to form the capacity curve.

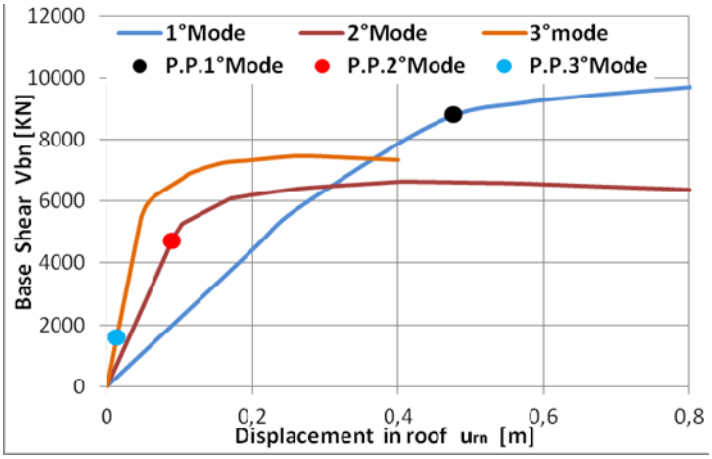

Figure 7.1 P.P. for the first three modes

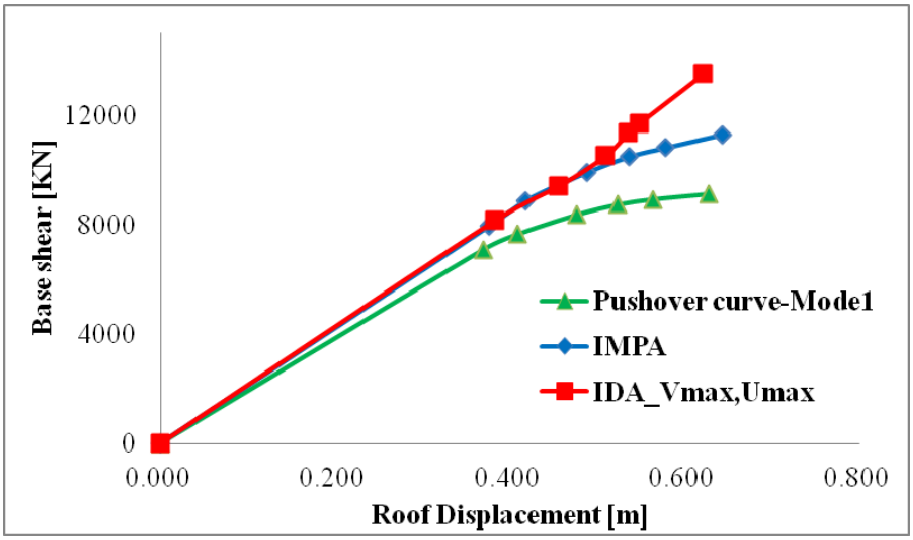

Figure 7.2 capacity curves obtained from different methods: the standard pushover analysis (for the predominate mode), IMPA method and IDA method

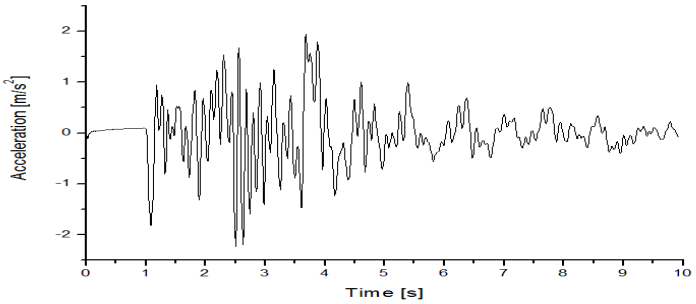

Figure 7.3 El Centro (1940) ground motion

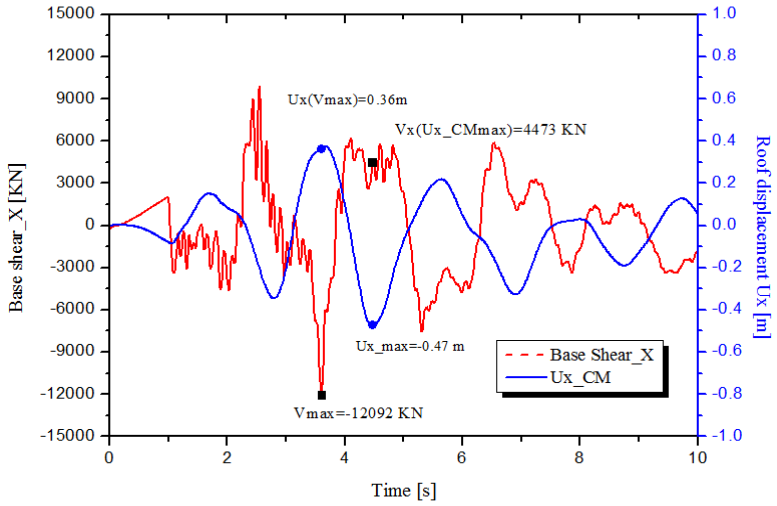

Figure 7.4 the maximum base shear is asynchronous with the maximum roof displacement in the NL_RHA of El Centro, the maximum roof displacement and maximum base shear is obtained to form the IDA curve

The P.P. obtained from the single mode pushover curve and IMPA together with IDA are shown in Figure 7.2. It is clear that IMPA curve including the contribution of higher modes to the base shear make the capacity curve from IMPA stiffer, and more close to the IDA curve, the IMPA curve and IDA curve superimpose before the structure enters plastic stage, but big errors in the inelastic phase.

The effectiveness of IMPA is sensitive to the PGA (the distance between IMPA and IDA increase with PGA). Both IMPA and IDA curves show a hardening behavior, IDA results stiffer in the plastic range, while the pushover curve is mostly elasto-plastic.

7.3 Existing irregular building

For each intensity level, mutiply the response spectrum by SF, then determine the corresponding P.P.mm for the modal MDOF system, in terms of roof displacement and corresponding base shear, to form the Multimodal Capacity Curve (MCC). By rule of SRSS of the individual modal responses, both for roof displacements and base shear are determined and then all those pairs, each relative to corresponding SF, form the MCC by the writers as shown in Figure 7.5.

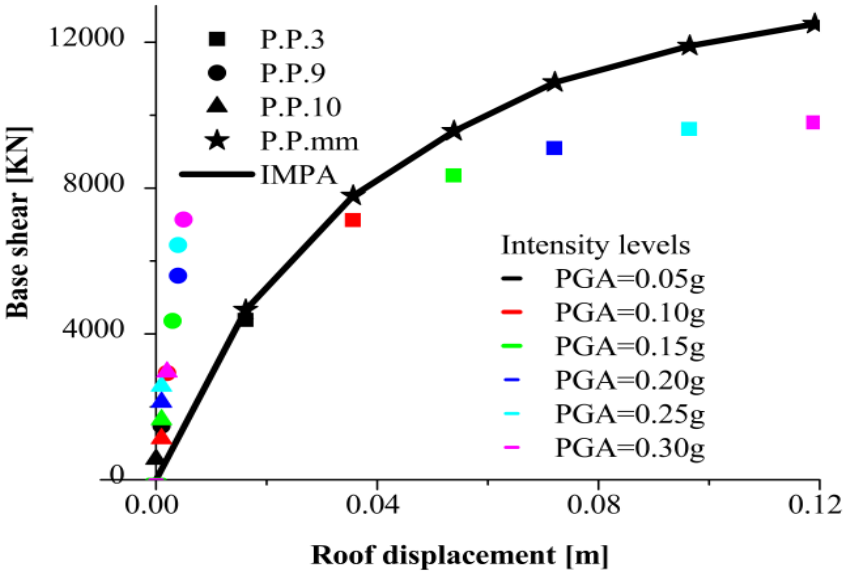

a) MCC for X direction

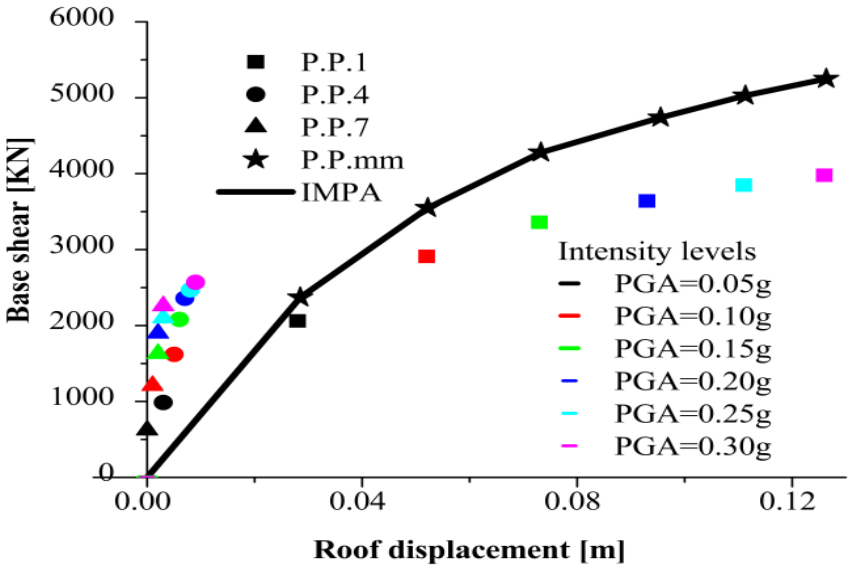

b) MCC for Y direction

Figure 7.5 Construction MCC from the IMPA procedure. The P.P.mm is obtained by applying SRSS rule with the P.P. obtained from single mode pushover (Mode1..Mode n) and for each intensity level, repeat this procedure for a range of intensity levels (the response spectrum is scaled from lower to higher intensity levels and the MCC can be obtained

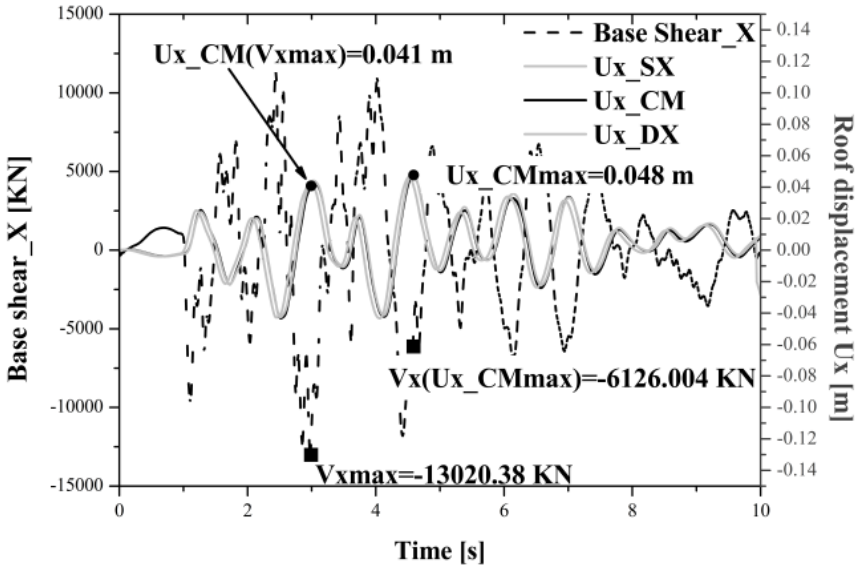

a) the roof displacement for three control points and base shear along X direction,

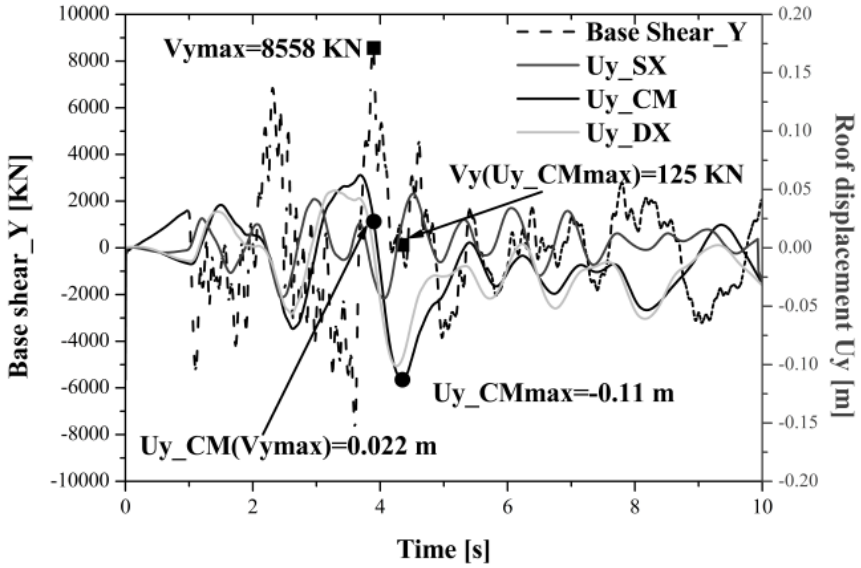

b) the roof displacement for three control points and base shear along Y direction

Figure 7.6 the maximum base shear is asynchronous with the maximum roof displacement in the NL_RHA of TH1, the maximum roof displacement for the CM and maximum base shear is obtained to form the IDA curve

It is obviously that in the NL_RHA, the maximum base shear is asynchronous with the maximum roof displacement. The response of the existing building subjected to one single ground motion (TH1) is shown in Figure 7.6. The base shear corresponding to the maximum roof displacement is much less than maximum base shear: the base shear corresponding to the maximum roof displacement is 6126 KN but the maximum base shear 13202 KN along the X direction; the base shear corresponding to the maximum roof displacement is 125 KN but the maximum base shear 8558 KN along the Y direction. Similarly, the roof displacement corresponding to the maximum base shear is much less than maximum roof displacement: the roof displacement corresponding to the maximum base shear is 0.041m but the maximum roof displacement 0.048m along the X direction; the roof displacement corresponding to the maximum base shear is 0.022m but the maximum roof displacement 0.11m along the Y direction. In the IDA procedure, the mean of maximum base shear and maximum roof displacement to an ensemble of earthquake excitations are used to form the capacity curve.

The P.P. obtained from the single mode pushover curve and IMPA together with IDA are shown in Figure 7.7 to Figure 7.9. From the

projection onto the PGA-roof displacement plane, the superimpose the single mode pushover curve on the IMPA curve indicate that IMPA will not increase the roof displacements. From the projection onto the PGA-base shear plane, it is clear that IMPA curve including the contribution of higher modes to the base shear is more close to the IDA curve, but big errors in the inelastic phase. From the base shear-roof displacement plane, compared to standard pushover curve, the increase of base shear in the IMPA make the capacity curve from IMPA more stiff, and more close to the IDA curve.

The effectiveness of IMPA is sensitive to the PGA (the distance between IMPA and IDA increase with PGA). Both IMPA and IDA curves show a hardening behavior, IDA results stiffer in the plastic range, while the pushover curve is mostly elasto-plastic. For the X direction, the capacity curves for different control points are almost the same, it is also another indication that the pure translation along this direction. When PGA is 0.2g, the P.Ps. obtained from standard pushover curve, IMPA and IDA are (0.072m, 9100KN), (0.072m, 10900KN) and (0.062m, 12600KN), respectively. Compared to IDA, standard pushover underestimate base shear with an error of 28%, the IMPA underestimate base shear with an error of 13%.

For Y direction, the underestimation of base shear for the inelastic phase is more evident. When PGA is 0.2g, for the CM, the P.Ps. obtained from standard pushover curve, IMPA and IDA are (0.093m, 3634KN), (0.096m, 4740KN) and (0.091m, 7770KN), respectively. Compared to IDA, standard pushover underestimate base shear with an error of 53%, the IMPA underestimate base shear with an error of 39%.

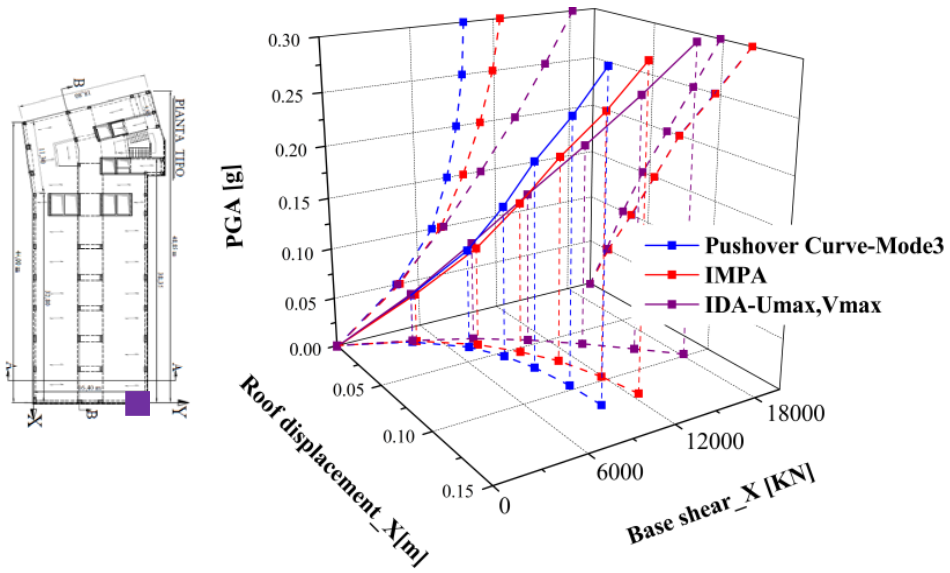

a) capacity curves along X direction.

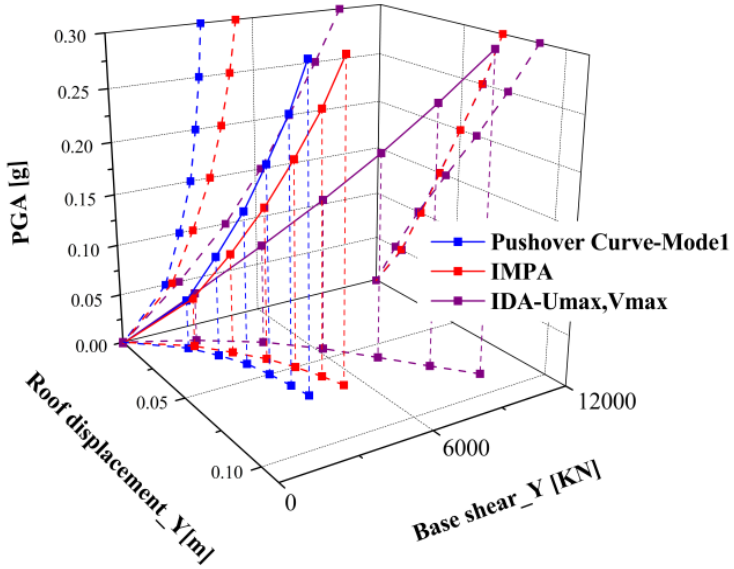

b) capacity curves along Y direction.

Figure 7.7 capacity curves obtained from different methods: the standard pushover analysis (for the predominate mode), IMPA method and IDA method for the left edge of building (SX)

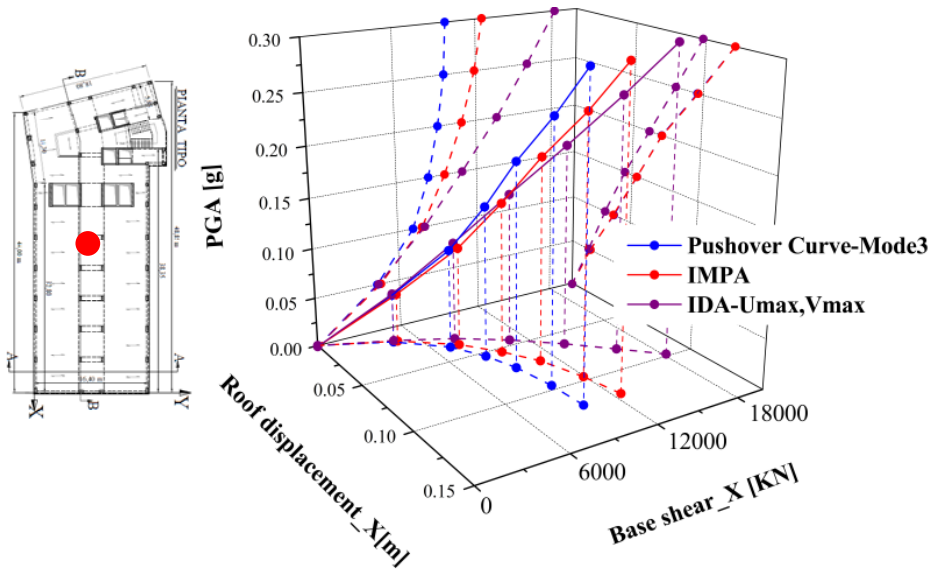

a) capacity curves along X direction,

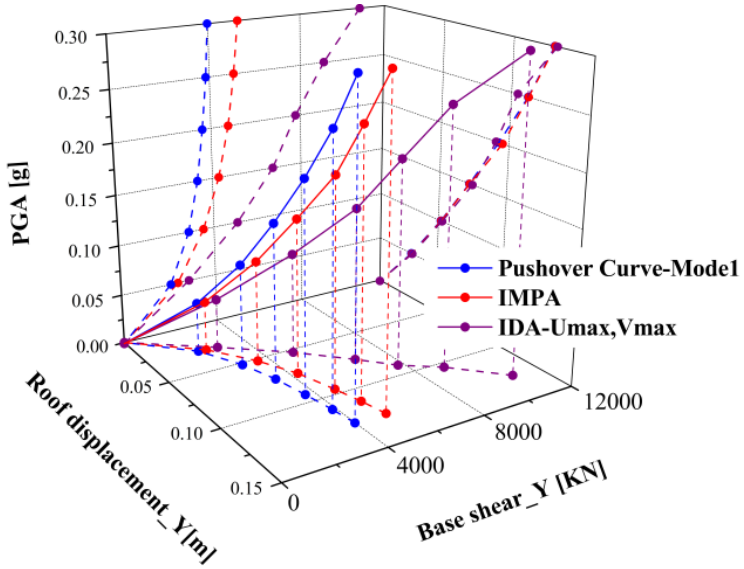

b) capacity curves along Y direction.

Figure 7.8 capacity curves obtained from different methods: the standard pushover analysis (for the predominate mode), IMPA method and IDA method for the center of building (CM).

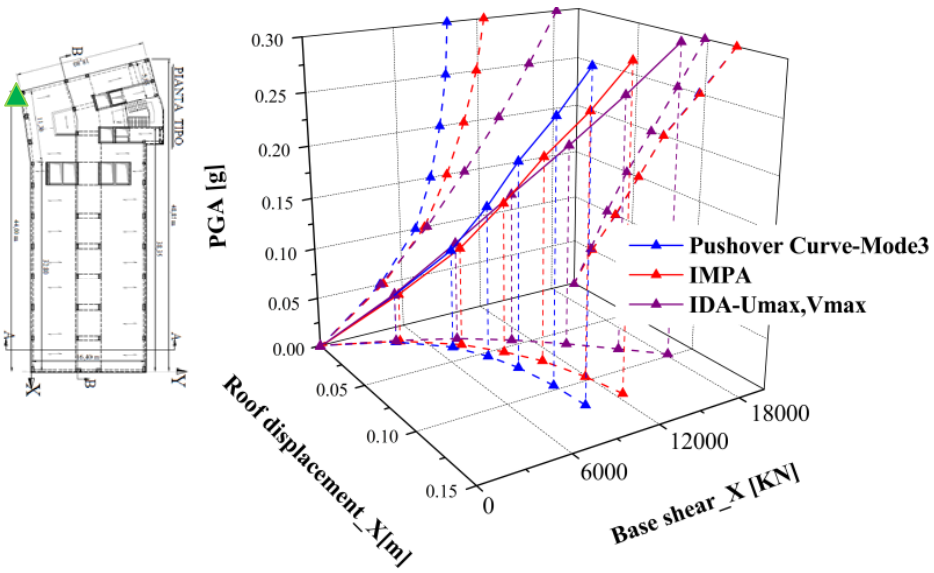

a) capacity curves along X direction

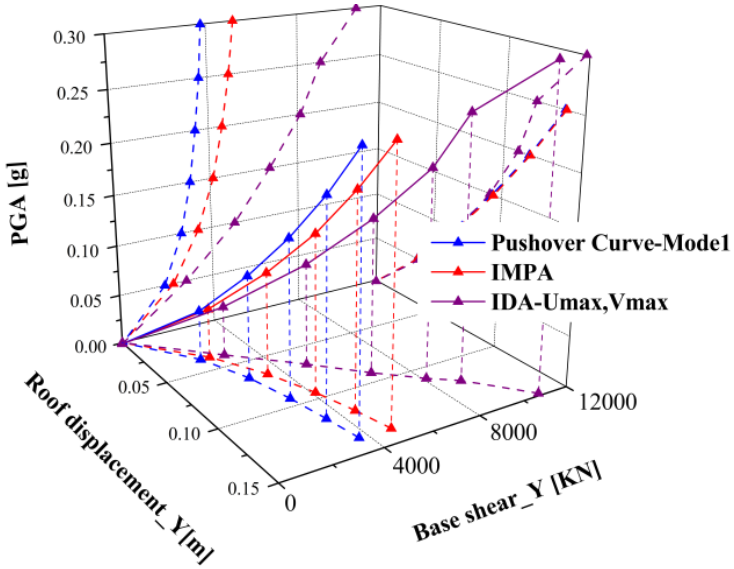

b) capacity curves along Y direction.

Figure 7.9 capacity curves obtained from different methods: the standard pushover analysis (for the predominate mode), IMPA method and IDA method for the right edge of building (DX)

When PGA is 0.2g, for the rigid side (DX), the P.Ps. obtained from standard pushover curve, IMPA and IDA are (0.050m, 3400KN), (0.050m,

4550KN) and (0.059m, 7610KN), respectively. Compared to IDA, standard pushover underestimate base shear with an error of 55%, the IMPA underestimate base shear with an error of 40%; for the flexible side (SX), the P.Ps. are (0.117m, 3440KN), (0.118m, 4590KN) and (0.110m, 8140KN), respectively. Compared to IDA, standard pushover underestimate base shear with an error of 58%, the IMPA underestimate base shear with an error of 44%.The static pushover cannot fully catch up the torsional effect on base shear for the irregular structure, so there are bigger errors for the corners in the inelastic phase.

7.4 Conclusion

Comparing results in terms of base shear-top displacement between IDA, standard pushover and IMPA, the effectiveness of IMPA has been demonstrated: the multimodal capacity curve obtained with IMPA results closer to IDA curve. The effectiveness of IMPA is sensitive to the PGA (the distance between IMPA and IDA increases with PGA). Both IMPA and IDA curves show a hardening behavior, IDA results stiffer in the plastic range, while the pushover curve is mostly elasto-plastic. Therefore, for the pure translation direction, standard pushover underestimate base shear with an error of 28%, the IMPA underestimate base shear with an error of 13%. Static pushover cannot fully catch up the torsional effect on base shear for the irregular structure, so there are bigger errors for the corners in the inelastic phase for the standard pushover analysis and IMPA. IMPA curve is closer to the IDA curve, and IMPA is suggested to predict the capacity curve for the structure during the design phase.
According to this the procedure can be consider a valid tool for professional use for the estimation of the capacity of structures and therefore for the definition of the capacity curve including the effect of higher significant modes.

8. Application of the design procedure to the irregular structure

8.1 Introduction

A displacement-based procedure to design dissipative braces for the seismic protection of buildings is proposed by Bergami & Nuti (2013). The procedure is based on the displacement using the capacity spectrum method; no dynamic non linear analyses are needed. Two performance objectives have been considered: protect the structure against structural damage or collapse and avoid non-structural damage as well as excessive base shear. The compliance is obtained dimensioning dissipative braces to limit global displacements and interstorey drifts. The design of dissipative devices has two main goals: improve dissipation and regularize strength and stiffness distribution (this can be done adopting an adequate criterion to distribute the braces along the elevation and inside the plan of the building).

During the design procedure, Nonlinear Static Procedure (NSP) is adopted to evaluate the seismic response of the existing and retrofitted structure. Few studies focused on the extension of NSPs to the case of braced irregular structures, therefore the second aim of this section to check the whether the commonly used NSPs can be used to evaluate the seismic response for the braced structure. Moreover, in case of medium rise building (quite widespread in Italy), it is a matter of fact that the relevance of higher modes depends not only on their level of irregularity but it is also related to the quite high number of stories. The necessity of using a multi modal pushover (Goel & Chopra, 2004) instead of the standard single mode pushover procedure has been investigated performing multimodal pushover and non linear dynamic analysis on both the existing and retrofitted building.

To these purposes, the design procedure of dissipative braces is applied to an existing irregular structure, which presents both vertical and plan irregularities, to protect the structure against structural damage during given seismic event. Comparison of the results obtained with nonlinear dynamic analysis, which is taken as “exact” results, enables the evaluation of the accuracy of the different NSPs on the braced structure to check the effectiveness of the design procedure.

8.2 Design procedure

As a strategic building, which means the function of the building should be maintained during the earthquake, so the performance objective is to reduce displacement and limit the interstorey drift to 5‰ at whichever level in order to avoid damage on both r.c. elements and masonry panels.
First the nonlinear dynamic analyses for both directions are carried out, as shown in Figure 8.1. One can easily find that the superimpose of structural inter-story drifts of three control points along X direction indicate pure translation along this direction, and structural inter-story drifts can satisfy the performance objective ; however, owing to the torsional effect, the deviation of structural inter-story drifts of three control points lead to the inter-story drifts of rigid side (SX) can satisfy performance objective but center of mass (CM) and flexible side (DX) beyond the performance objective. Consequently, only retrofitting with dissipative braces for the transverse direction (Y direction) is conducted in this paper.

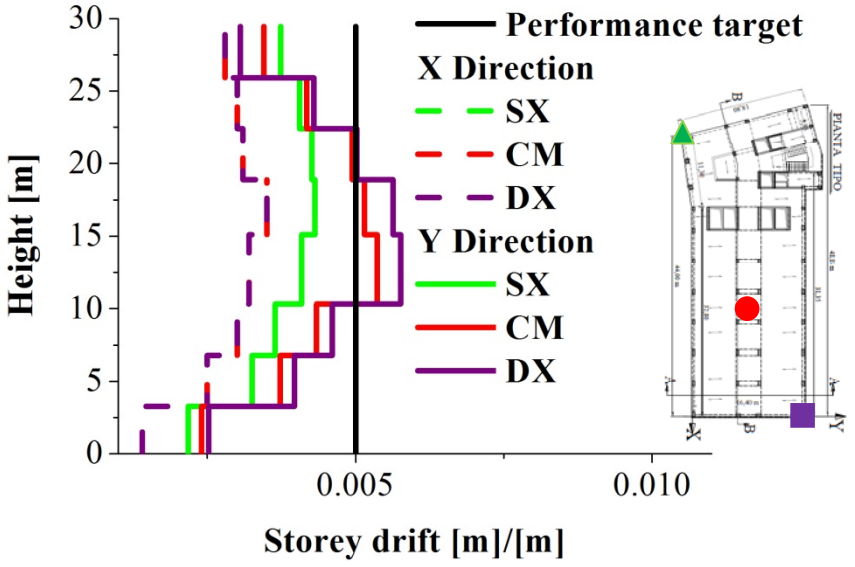

Figure 8.1 Structural interstorey drifts by nonlinear dynamic analysis.

Accurate prediction of the target displacement at the center of mass (CM) is a primary issue for application of pushover analysis to regular structures and it is a pre-requisite for any further extension of pushover

analysis to irregular structures. In the design procedure, CM will be taken as the control point to conduct pushover analysis, and the capacity curve has been derived considering a loading profile proportional to the first mode shape. The Performance Point (P.P.) of the existing structure in terms of base shear and top displacement is V_S =4027 kN and $D_{t,S}$=126 mm. the capacity curves and P.P. after each iteration are plotted in Figure 8.2. Interstorey drifts profiles along height after each iteration are plotted in Figure 8.3. Convergence to the desired values has been obtained with four iterations and the final result (performance point, iter 4) is the base shear V_{S+B}=4995 kN, with a 19% increase with respect to the original building, and the top displacement $D_{t,S+B}$=102 mm (practically coincident with the target, see Figure 8.2).

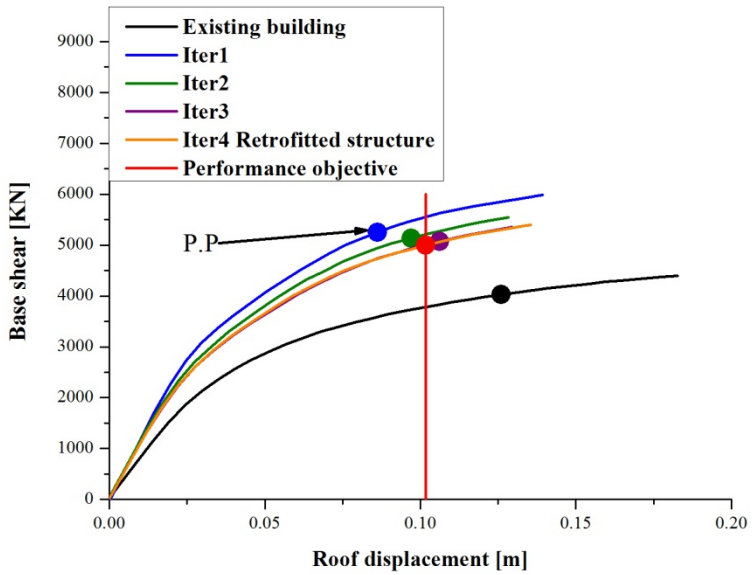

Figure 8.2 Design procedure of dissipative braces: capacity curve and P.P.

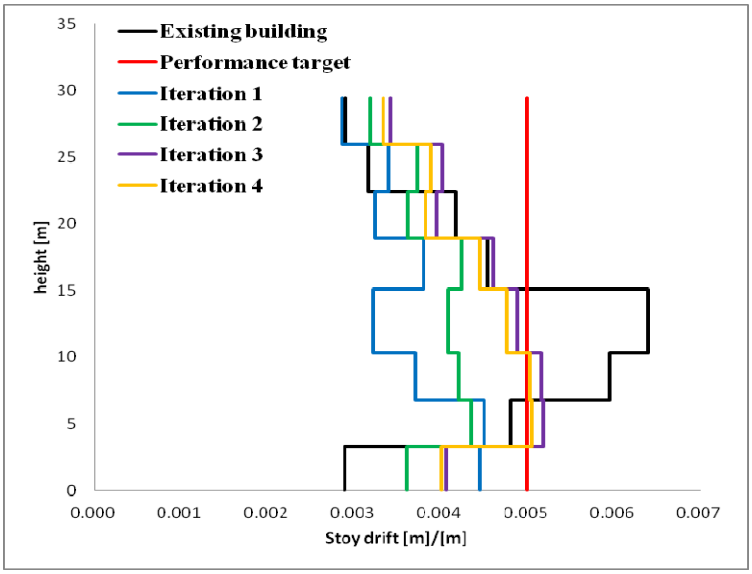

Figure 8.3 Design procedure of dissipative braces: interstorey drifts profiles

The distribution of dissipative braces for the existing building is shown in Figure 8.4 and Figure 8.5. From the plan layout, one can observed that the braces are concentrated on the flexible side to increase stiffness, thus make the structure more regular. From the elevation layout, no braces located on the top and first floor, where the interstorey drifts largely less than performance objective. The braces are concentrated on the 3~7th floors, where interstorey drifts are larger than other floors. This arrangement is to exclude the soft floors. The arrangement of braces would improve the irregularity of the structure.

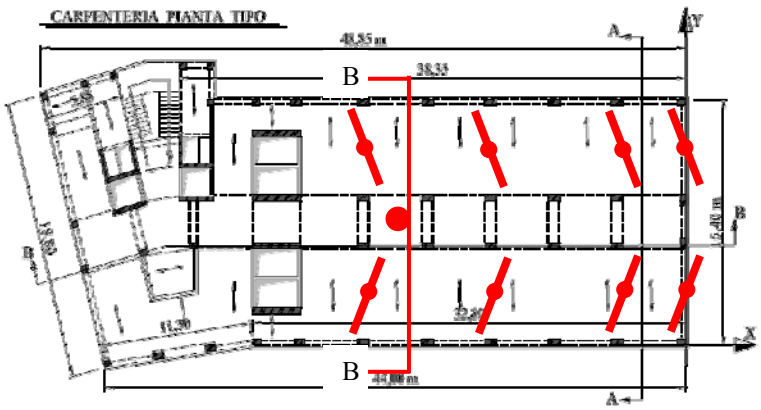

Figure 8.4 Distribution of the dissipative braces: Plan layout

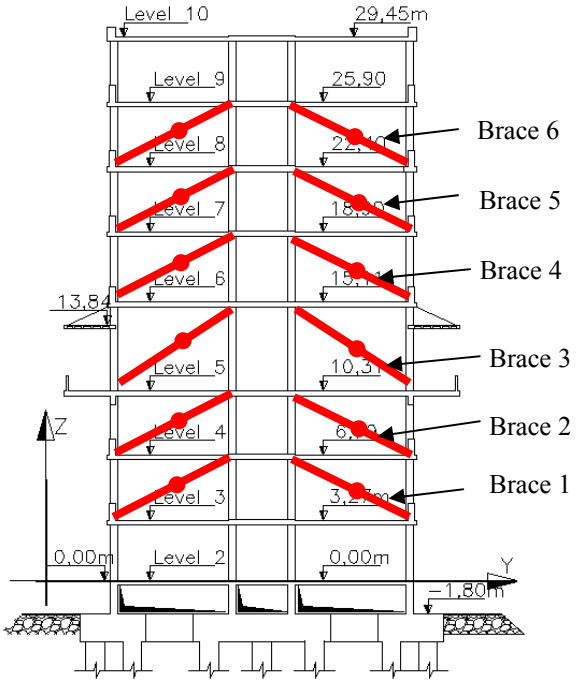

Figure 8.5 Distribution of the dissipative braces: Elevation layout (B-B section)

The parameters of material and geometry of dissipative braces are listed in Table 8.1, they are the length of brace (L), elasticity modulus (E), yield stress (Qy), the yield force (Fy) and the area (A).

Table 8.1 Parameters of dissipative braces for each floor

Floor	H	L	E	Qy	Fy	A
	[m]	[m]	[pa]	[Pa]	[N]	[m^2]
8	3.52	7.304	2.1E+11	2.35E+08	8.46E+05	1.48E-03
7	3.52	7.304	2.1E+11	2.35E+08	8.46E+05	1.95E-03
6	3.52	7.304	2.1E+11	2.35E+08	8.46E+05	1.92E-03
5	3.78	7.433	2.1E+11	2.35E+08	8.46E+05	2.36E-03
4	4.8	8.000	2.1E+11	2.35E+08	8.46E+05	2.12E-03
3	3.52	7.304	2.1E+11	2.35E+08	8.46E+05	2.43E-03
2	3.52	7.304	2.1E+11	2.35E+08	8.46E+05	2.20E-03

Variation of the total equivalent viscous damping with the spectral displacement for the existing and retrofitted building is shown in Fig 10. The damping difference between the existing and retrofitted building at

the P.P.is the contribution to dissipation offered by the dissipative system: $\nu_{eq,\mathrm{B}} = 8\%$ ($\nu_{eq,\mathrm{S+B}} = 19\%$ for the retrofitting building, and $\nu_{eq,S} = 11\%$ for the existing building).

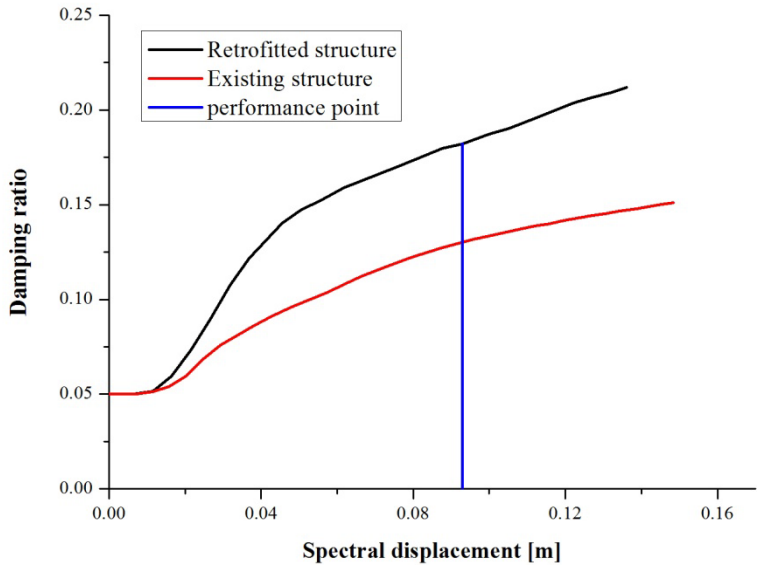

Figure 8.6 Variation of the total equivalent viscous damping with the spectral displacement Sd. At the p.p., $V_{eq,S+B}$=19% for the retrofitted structure and $V_{eq,S}$ =11% for the existing building.

8.3 Evaluation of NSPs for seismic response of retrofitted structure

In the design procedure, the capacity curve and interstorey drifts are predicted by "standard" monomodal pushover where the structure is subjected to monotonically increasing lateral forces, with an invariant spatial distribution (fundamental mode based), until collapse displacement is reached. This fundamental mode based force distribution doesn't account for higher mode contribution, which can be relevant, and therefore this limits the applicability of this approach to cases where the fundamental mode is dominant. Anyway it has to be highlighted that braces, if well designed, regularize the structure that can become strongly fundamental mode dependent.

In this section, both the existing structure and the retrofitted structure have been studied using the MPA in order to evaluate the effectiveness of the "standard" procedure and therefore the advantages on using the

monomodal pushover for such a building: in this case the effectiveness of the procedure has been confirmed and, comparing results from monomodal and multimodal pushover applied on the retrofitted structure, the use of multimodal pushover can be considered not substantial for the design process applied on this typology of building.

8.3.1 Modal analysis

Modal analysis is employed to identify the dynamic behavior of the existing and braced structure to investigate the relevance of higher modes. The periods of vibration , the participating translational masses along X direction (MT_X), along Y direction (MT_Y) and rotational mass with respect to the vertical direction Z (MR_Z) of the first ten modes are listed in Table 8.2 and Figure 8.7.

Table 8.2 Modal periods and participating mass for existing and retrofitted structures

Mode	Existing structure				Retrofitted structure			
	T (s)	MT_X (%)	MT_Y (%)	MR_Z (%)	T (s)	MT_X (%)	MT_Y (%)	MR_Z (%)
1	1.76	0	64	28	1.03	1	45	54
2	1.27	0	4	30	0.94	65	1	10
3	0.94	66	0	7	0.64	0	29	0
4	0.55	0	10	4	0.35	0	0	0
5	0.37	0	1	7	0.30	0	0	0
6	0.35	0	0	0	0.29	0	10	12
7	0.32	0	4	2	0.28	10	0	2
8	0.30	0	0	0	0.25	0	1	0
9	0.28	10	0	1	0.21	3	0	0
10	0.21	3	0	1	0.19	0	1	3

For the retrofitted structure, owing to the stiffness introduced by the braces along Y diecrion, the fundamental period along Y direction is reduced; the fundamental period along X direction is the same as the existing one. For the Y direction, it can be found that the retrofitted building shows a strong flexible behavior. The first three modes (first, fourth and sixth mode) have about 84% of participation mass along Y direction, which means it is sufficient to consider the contribution of these three modes to the total seismic response.
Figure 8.8 shows the first four modal shapes considering the three control

points. As the existing structure, one also can observe that the first mode is translation and rotation coupled along Y direction; the third mode is characterized by a pure translation along direction X.

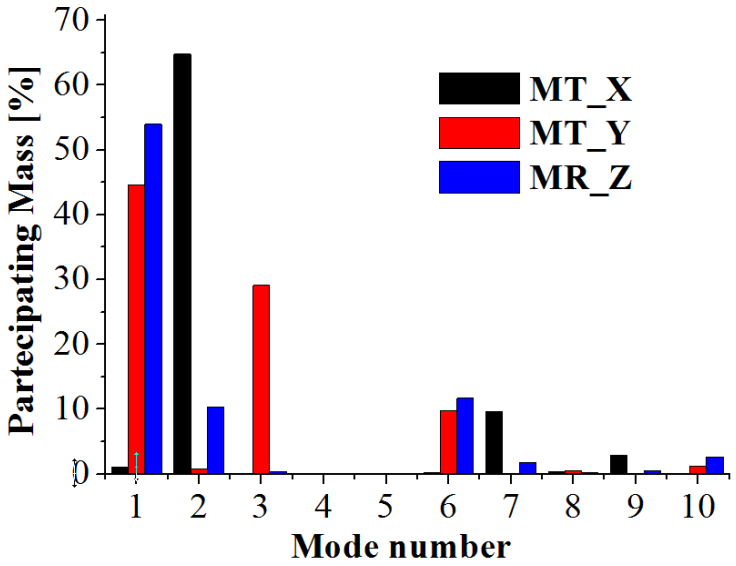

Figure 8.7 Modal mass participation for retrofitted structure

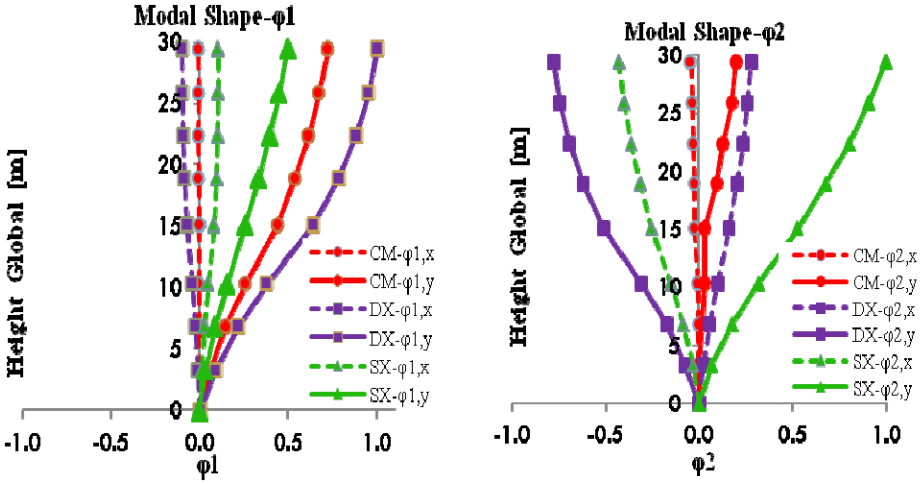

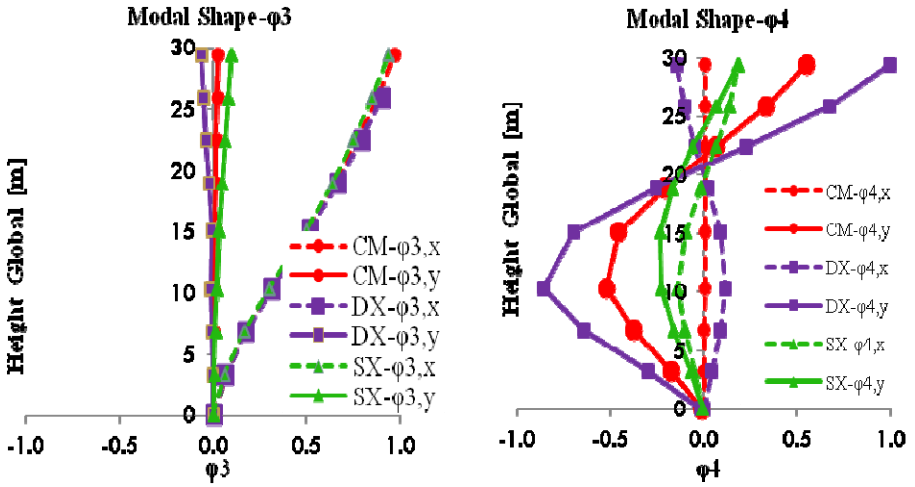

Figure 8.8 Modal shape configurations considering different control nodes: CM, DX, SX a) ϕ1,b) ϕ2, c) ϕ3, d) ϕ4

8.3.2 Target displacement

1. Capacity spectrum method (CSM)

From Table 8.2, it is clear that for the retrofitted structure, along Y direction the dominant mode is the first one. Figure 8.9 shows the performance point (P.P.) obtained from capacity spectra. CSM is used to search the P.P. of predominate mode inelastic SDF system. The elastic response spectra defined by NTC2008 is taken as the demand spectrum. It is observed along Y direction, the structure enters in the nonlinear state for the first mode. For the existing building, along Y direction the dominant mode is the first one.

When structure enters nonlinear plastic stage, and the spectral reduction factor depends on the effective viscous damping of equivalent Single Degree of Freedom (SDF) system , and the corresponding damping, which takes into account the energy dissipation capacity of the structure as examined, is defined by Eq. (6.1). The equivalent SDF systems' parameters for the first and third modes and the effective damping ratio for the first mode is 19% for the retrofitted structure.

Once the P.P. obtained from the capacity spectra, which is in terms of the spectral acceleration (S_{an}) and spectral displacement (S_{dn}), can be converted to P.P. in the capacity curve, which is in terms of the roof displacement (U_r) and base shear V_b corresponding to Ur through

Eq.(6.2).

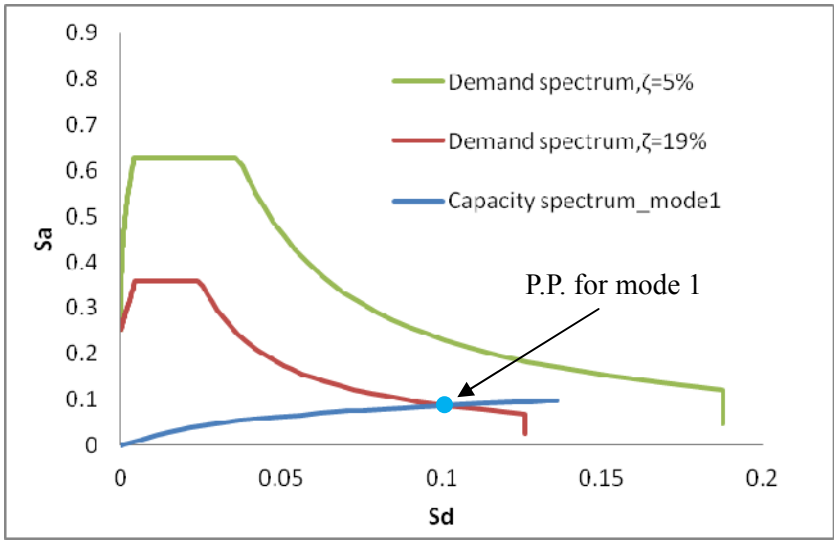

Figure 8.9 P.P. for the CM is determined via CSM from original and reduced demand spectrum for the first mode Capacity spectra along Y direction

2. Displacement Coefficient Method (DCM)

In this procedure, the nonlinear MDF system's displacement is obtained from the linear elastic demand spectrum, using certain coefficients which are based on empirical equations derived by calibration against a large number of dynamic analyses, as shown in Figure 8.9 and Table 8.3.

Table 8.3 P.P. obtained from DCM

	C_0	C_1	C_2	C_3	S_a [m]	T_e [s]	d_t [m]	V_d [KN]
Retrofitted building	1.02	1.0	1.1	1	0.16	1.70	0.124	5327

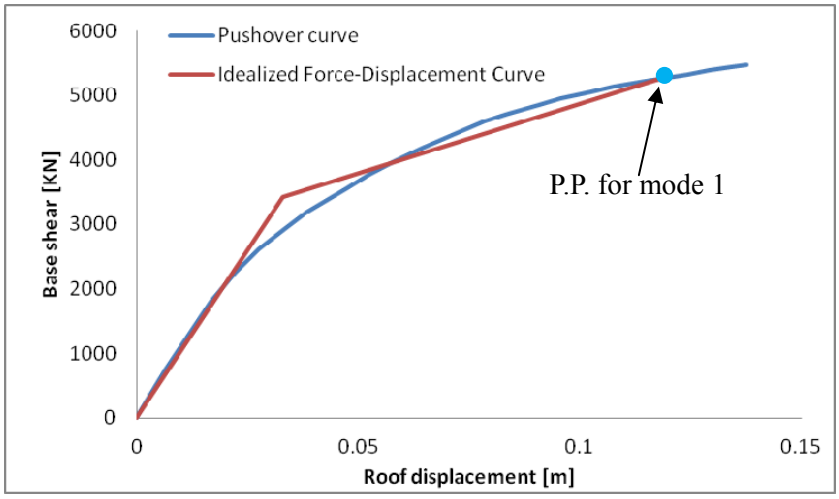

Figure 8.10 P.P. for the CM is determined via DCM

3. N2

For medium and long period structure, the target displacement of the inelastic system is equal to that of an elastic structure, as shown in Fig 13 c), Fig 14 c).

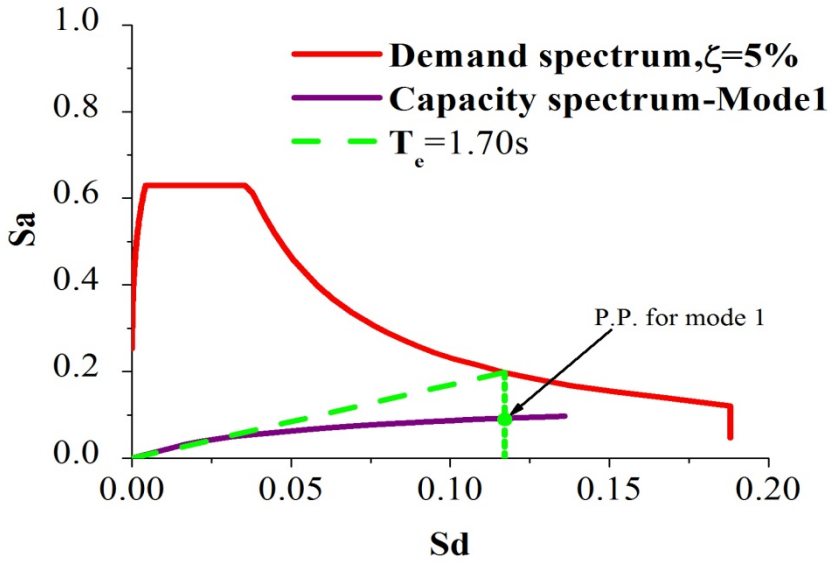

Figure 8.11 P.P. for the CM is determined via N2

4. Modal pushover analysis (MPA)

MPA is an extension of conventional pushover analysis to include contribution of higher `modes. In the MPA procedure, the CSM is adopted to determine the P.P. for the single mode.

From Table 8.2, the first three modes (first, fourth and sixth mode) have about 84% of participation mass along Y direction, which means it is sufficient to consider the contribution of these three modes to the total seismic response. Their pushover curves are plotted in Figure 8.12.

The P.P. for the first three significant modes of retrofitted buildings from the capacity spectrum are plotted in Figure 8.13, their values are listed in Table 8.4. Determine the total response MPA by combining the peak `modal' responses using appropriate modal combination rule, e.g., SRSS.

The P.Ps. obtained from the capacity curve by different methods are shown in Figure 8.14. For the retrofitted building, the target displacements obtained are almost the same, which is also an indication of the improved regularity of the retrofitted structure.

Table 8.4 P.P. obtained from capacity spectra and capacity curve

Retrofitted building					
Mode	Γ_n	Capacity spectra		Capacity curve	
		S_{dn}	S_{an}	Ur [m]	V [KN]
1	1.04	0.099	0.087	0.103	5036
3	0.71	0.084	0.078	0.060	4500
6	0.29	0.017	0.566	0.005	2244
SRSS				0.119	7116

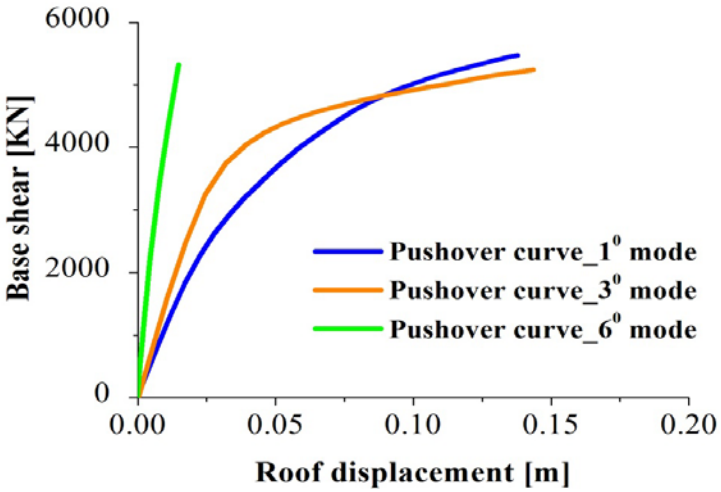

Figure 8.12 Pushover curves for the first significant three modes

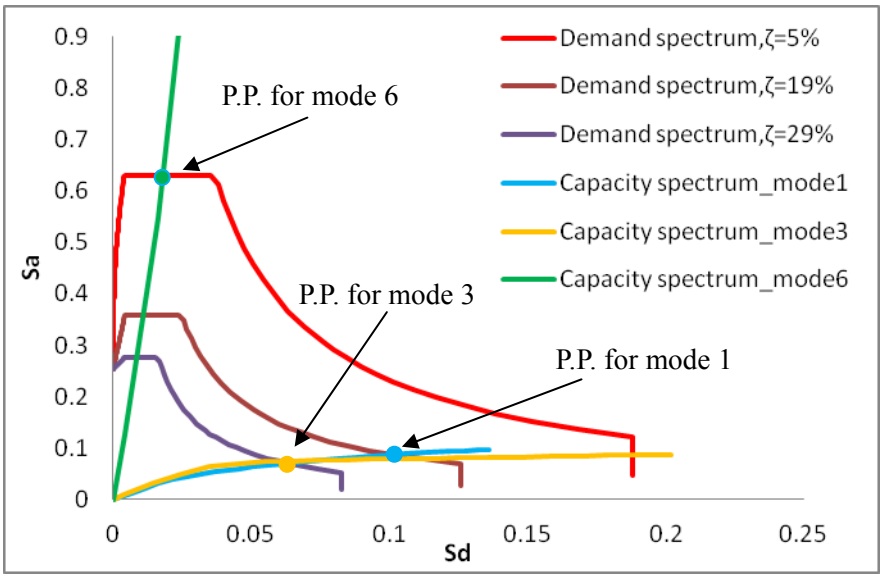

Figure 8.13 P.P. for the CM is determined via CSM from original and reduced demand spectrum for the predominate modes along Y direction

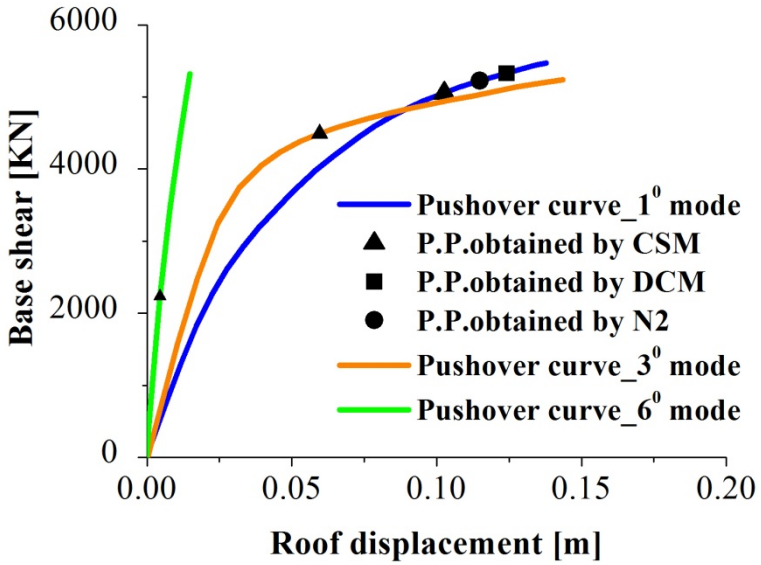

Figure 8.14 P.P. obtained from different NSPs

When the structure reaches its performance point (P.P.), the deformations of braces are plotted in Figure 8.15. It can be observed that all braces

enter their plastic phase to dissipate energy.

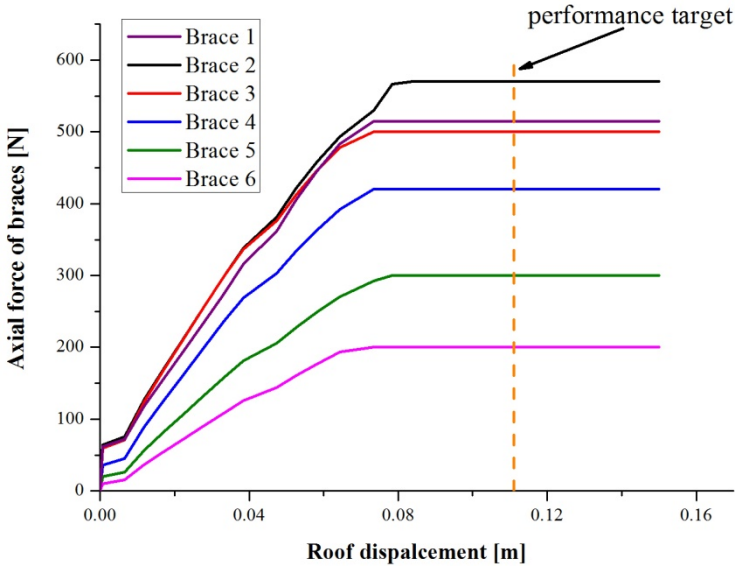

Figure 8.15 Deformation of braces

8.3.3 Floor displacements and interstorey drifts

The comparison of the different NSPs and the nonlinear dynamic results in terms of lateral displacement and interstory drifts profiles for the existing and retrofitted building are presented in this section. The time-history median results are taken as exact results.

The lateral displacement and interstorey drifts profiles for the existing building along Y direction are plotted in Fig 15 a) and c). One can observed that CSM would provide a good estimate for the floor displacement; DCM and N2 methods would overestimate the floor displacements; the contributions of higher `modes' of MPA and IMPA procedures to floor displacements are not significant. For the interstorey drifts, CSM leads to accurate prediction for the low and middle floors, and underestimate for upper floors; DCM and N2 method lead to slightly underestimate for the upper floors and largely overestimate for middle floors; MPA would improve the estimate for the upper floors.

The lateral displacement and interstorey drifts profiles for the existing building along Y direction are plotted in Fig 15 b) and d). Compared to existing building, the storey drift demands predicted by NSPs are able to follow the nonlinear dynamic results. The braced structure is strongly

characterized by dominate first mode and consequently the contributions of higher modes of MPA in the response of BRBF buildings are generally not significant, so the first ‘mode’ alone may be adequate.

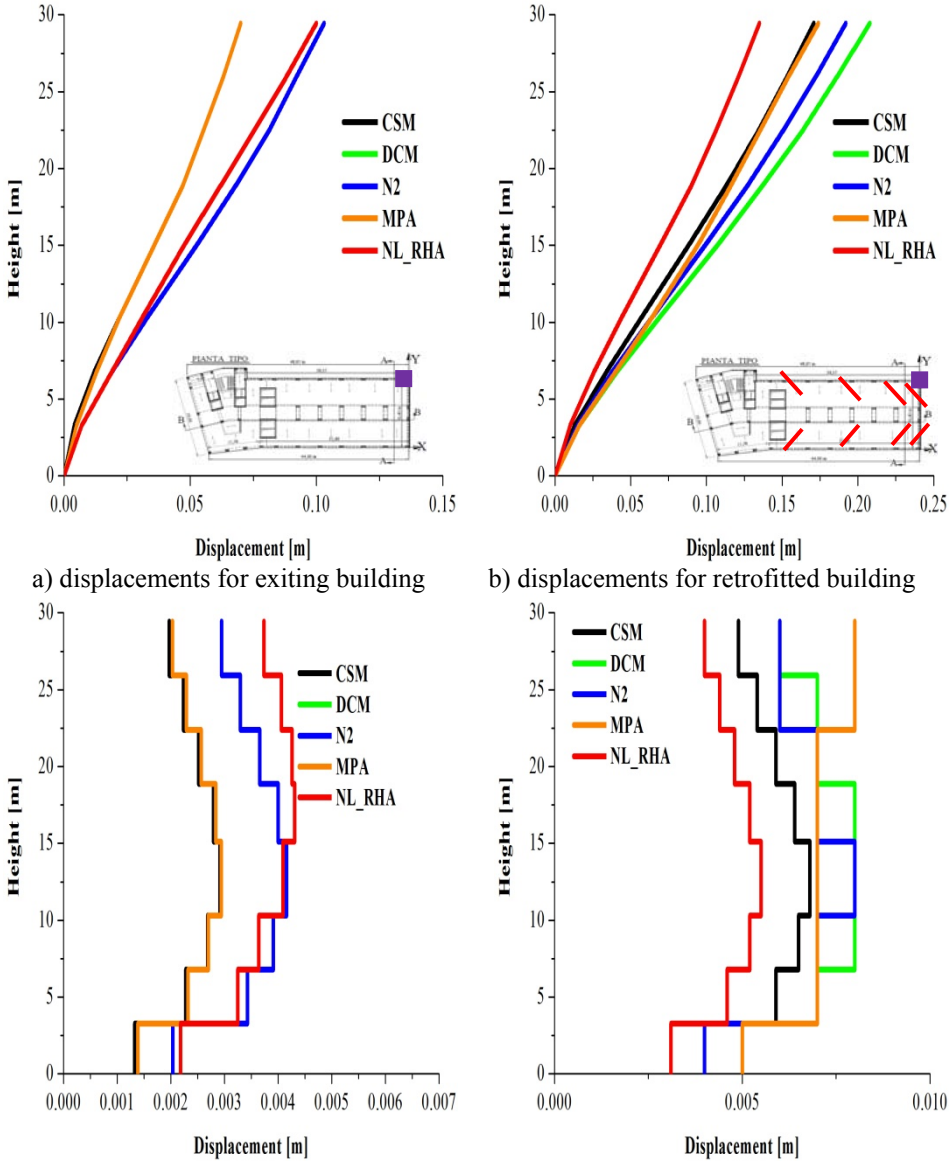

a) displacements for exiting building b) displacements for retrofitted building

c) interstorey drifts for exiting building d) interstorey drifts for retrofitted building

Figure 8.16 Peak response for SX along Y direction

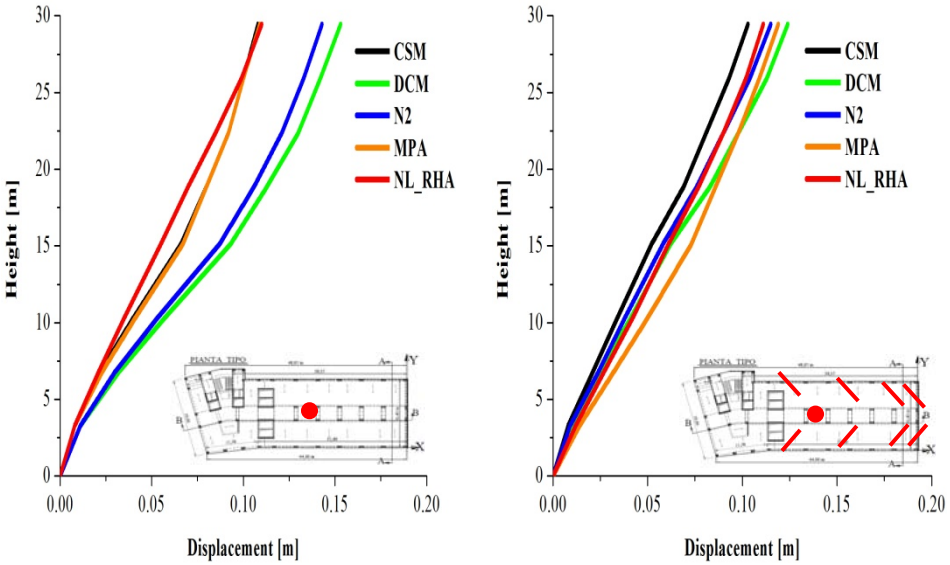

a) displacements for exiting building b) displacements for retrofitted building

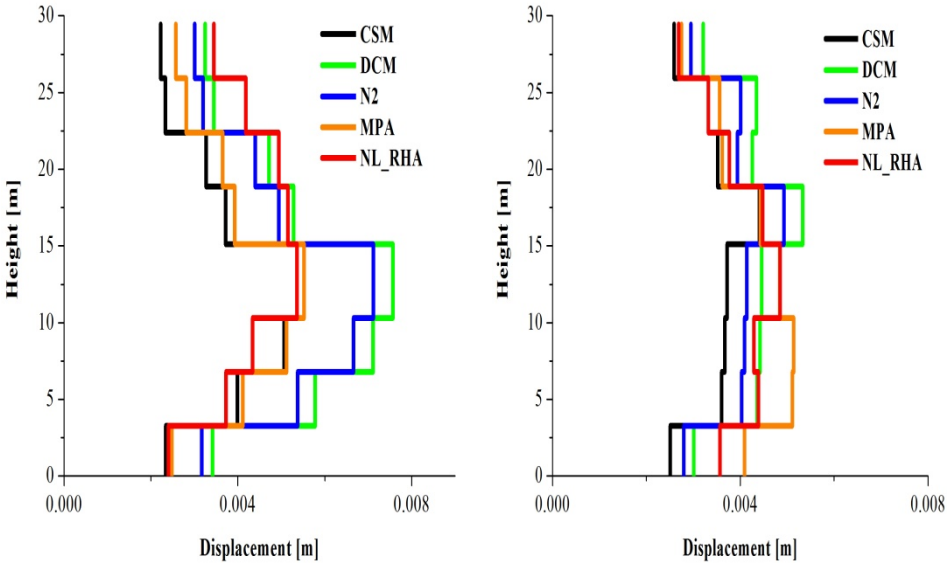

c) interstorey drifts for exiting building d) interstorey drifts for retrofitted building

Figure 8.17 Peak response for CM along Y direction

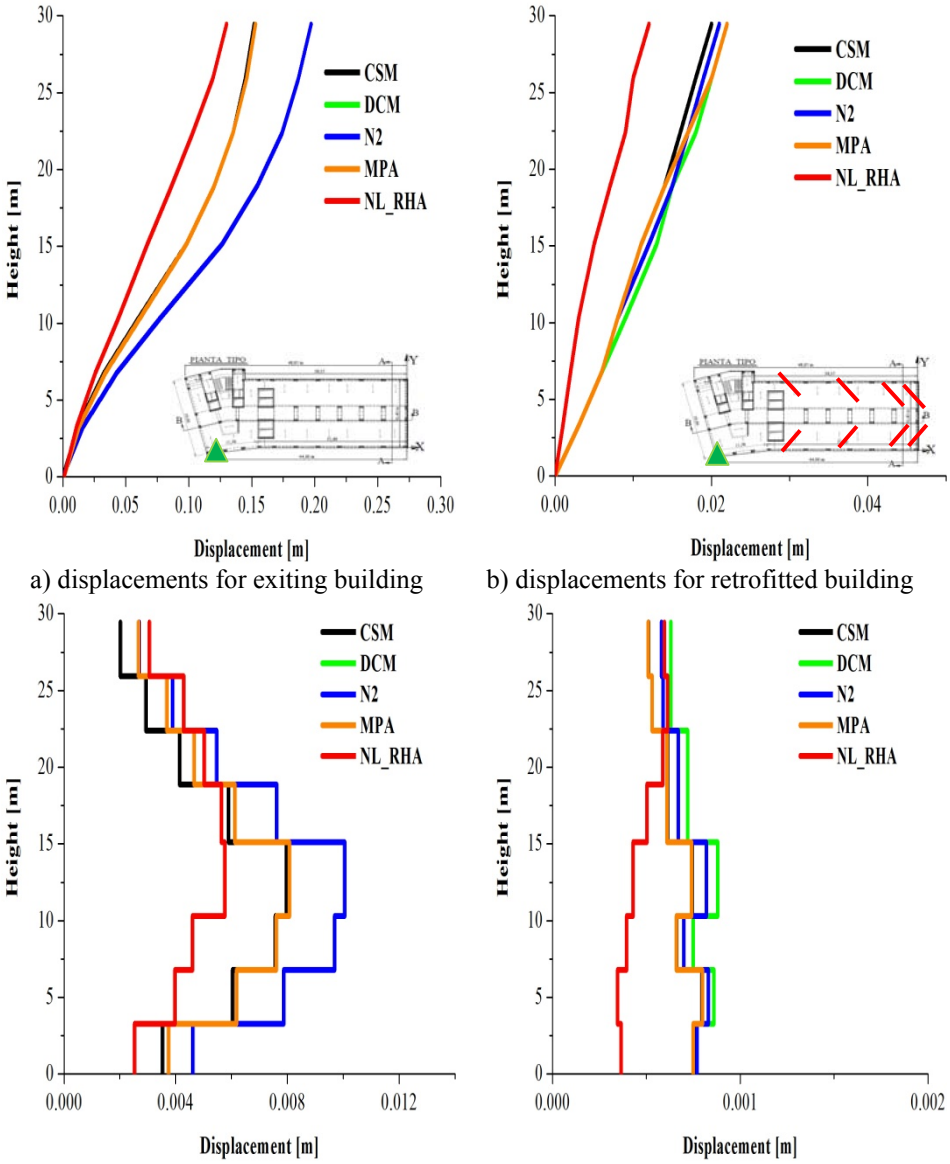

a) displacements for exiting building b) displacements for retrofitted building

c) interstorey drifts for exiting building d) interstorey drifts for retrofitted building

Figure 8.18 Peak response for DX along Y direction

8.3.4 Effects of lateral load patterns

The accuracy of NSP is strongly related to the load pattern used in performing pushover analyses, which influences both the capacity curve

and the distribution of seismic response along the height of the structure. In this section, the influence of lateral load patterns on the seismic response in terms of floor displacement and interstorey drifts is discussed, and its influence on capacity curve will be discussed in the next section.
Five lateral load patterns are selected to conduct the nonlinear pushover analysis and CSM is selected to obtain the target displacement: 1) uniform pattern-lateral load proportional to story masses at each story level; 2) Equivalent Lateral Force (ELF)- a lateral load distributed across the height of the building; 3) Fundamental Modal Distribution(FMD)-lateral load proportional proportional to the shape of the fundamental mode; 4) Multi-Modal Profile (MMP)- The lateral forces are determined for each independent mode and then combined using an appropriate combination rule such as SRSS . The normalized lateral load distributions for both directions are plotted in Figure 8.19.

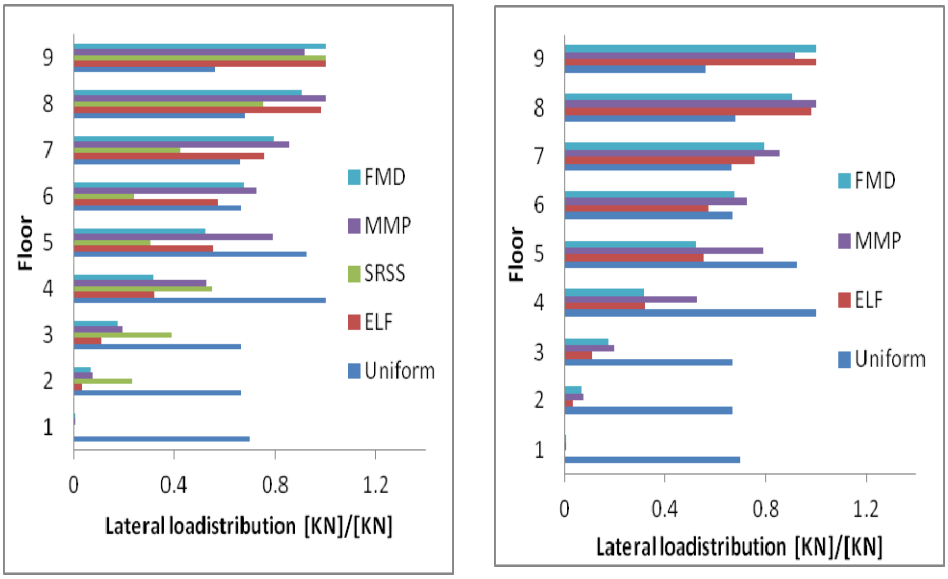

a) existing building b) retrofitted building

Figure 8.19 normalized lateral load distributions

The lateral interstorey drifts profile for the CM is plotted from Figure 8.20. One can observed that uniform patterns would underestimate interstorey drifts for upper floors, other pattern would provide a good estimate for the interstorey drifts due to the improved regularity by braces

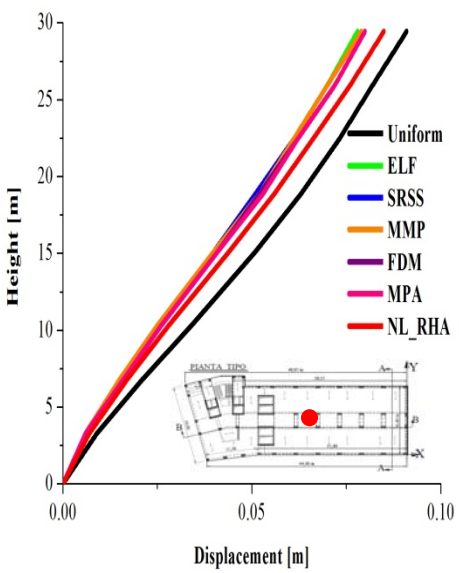

a) displacements for exiting building

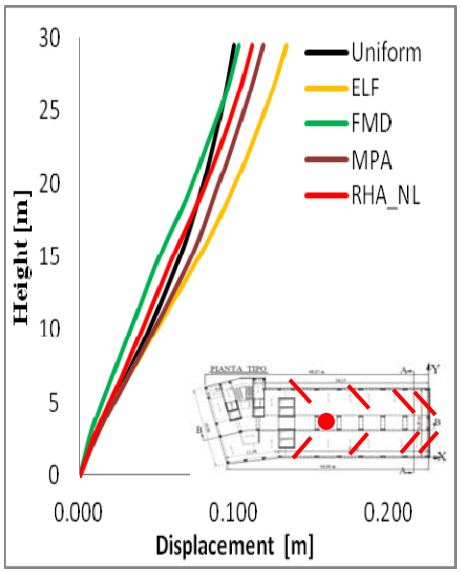

b) displacements for retrofitted building

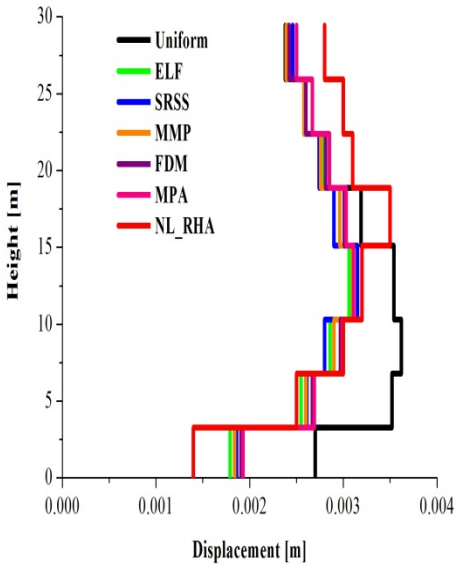

c) interstorey drifts for exiting building

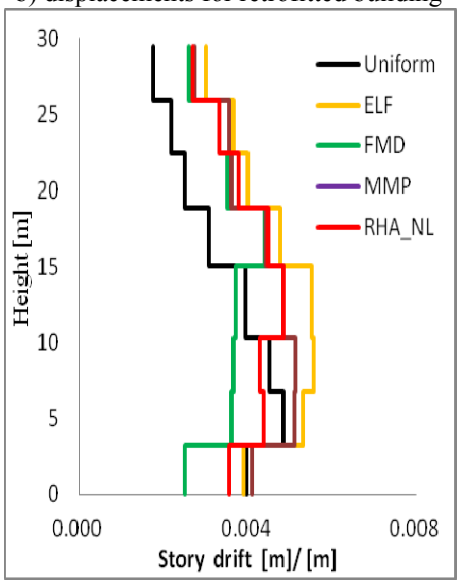

d) interstorey drifts for retrofitted building

Figure 8.20 Effects of lateral load patterns

8.4 Energy dissipation by BRBs

The mechanism of BRBs is through material yield to absorb earthquake induced energy as well as increase effective damping. From Figure 8.21, it is clear that all braces enter the plastic stage; the braces perform well to

dissipate energy.

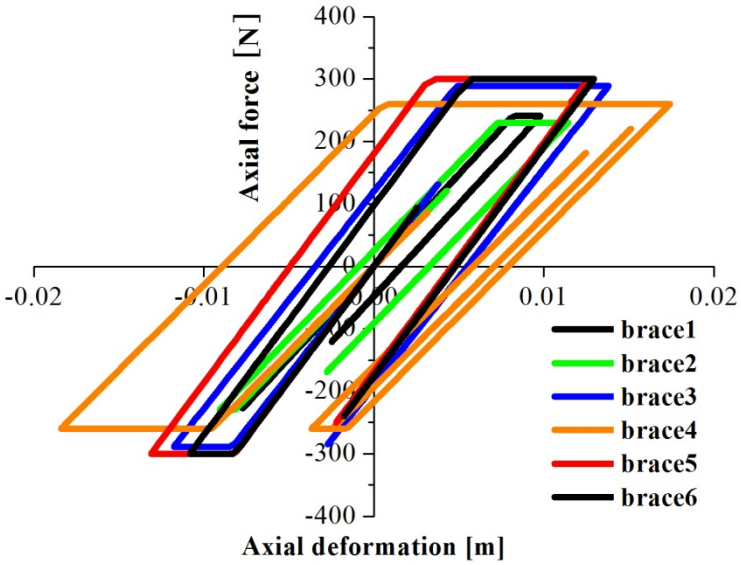

Figure 8.21 Force–displacement curves of BRBs

8.5 Capacity curves

In this section, the influence of lateral load patterns on the capacity curves is discussed. The capacities curves obtained by different load patterns are plotted in Fig 17. The capacity curve obtained from Incremental dynamic analysis (IDA) is included as reference, which is considered to be the most exact method to predict the capacity of structures (Vamvatsikos and Cornell, 2002). The capacity curve by IDA is in terms of maximum base shear Vs maximum roof displacement.

It is clear in all cases that the response of the buildings is sensitive to the shape of the lateral load distribution. This is particularly true when moving into inelastic phase. The NSPs cannot catch up the increasing of base shear in the inelastic phase.

One advantage of use of dissipative braces is to obtain the needed global energy dissipation with a limited increase of base shear (reducing the yielding force of the dissipative system) and thus reducing the need of foundation strengthening. Compared the base shear at the P.P. between the existing (Vb=3878 KN)and retrofitted building (Vb=5036 KN), a light increase in t base shear, is obtained, but with a substantial reduction in displacement with respect to the original structure.

.

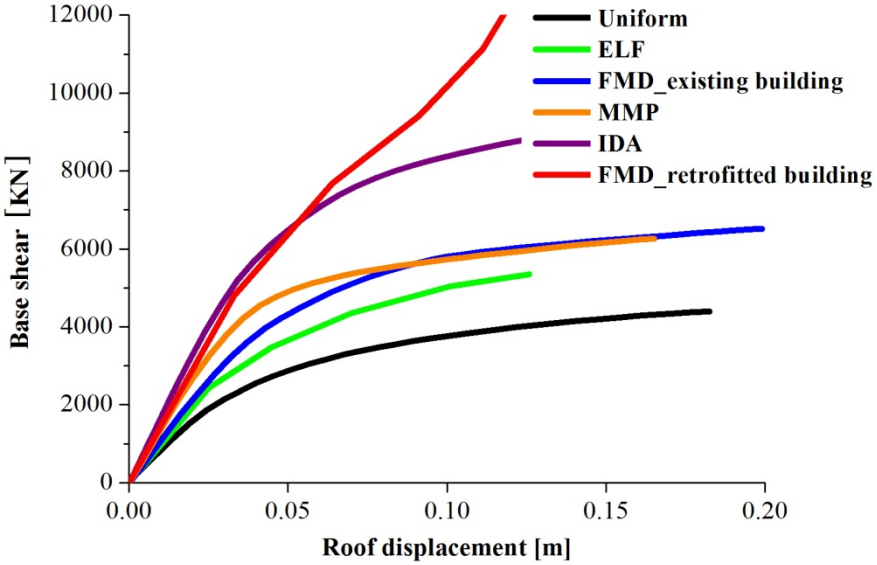

Figure 8.22 Capacity curves for CM

8.6 Application IMPA to retrofitted building

In this part, IMPA will be applied to retrofitted structure in the previous section: for each intensity level, mutiply the response spectrum by SF, then determine the corresponding P.P.mm for the modal MDOF system, in terms of roof displacement and corresponding base shear, by rule of SRSS of the individual modal responses, both for roof displacements and base shear are determined and then all those pairs, each relative to conresponding SF, form the MCC, as shown in Figure 8.23.

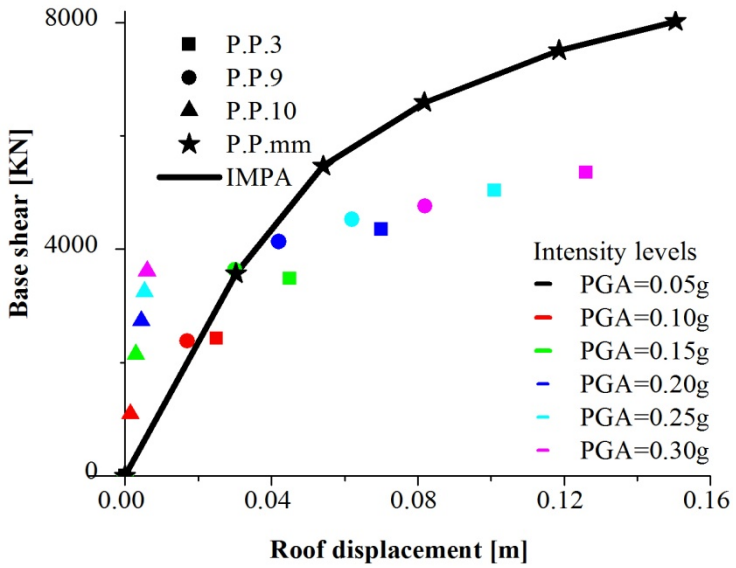

Figure 8.23 Construction MCC from the IMPA procedure. The P.P.mm is obtained by applying SRSS rule with the P.P. obtained from single mode pushover (Mode1..Mode n) and for each intensity level, repeat this procedure for a range of intensity levels (the response spectrum is scaled from lower to higher intensity levels and MCC can be obtained

The response of the retrofitted building subjected to one single ground motion (TH1) is shown in Figure 8.24. It is obviously that in the NL_RHA, the maximum base shear is asynchronous with the maximum roof displacement. The base shear corresponding to the maximum roof displacement is -4237 KN but the maximum base shear 10786 KN along the Y direction. Similarly, the roof displacement corresponding to the maximum base shear is much less than maximum roof displacement: the roof displacement corresponding to the maximum base shear is 0.015m but the maximum roof displacement 0.111m along the Y direction. In the IDA procedure, the mean of maximum base shear and maximum roof displacement to an ensemble of earthquake excitations are used to form the capacity curve.

The deviations of roof displacement of the control points (SX, CM and DX) are much less than the existing building. It can be an indication that the insert of BRBs make the structure more regular along the transverse direction.

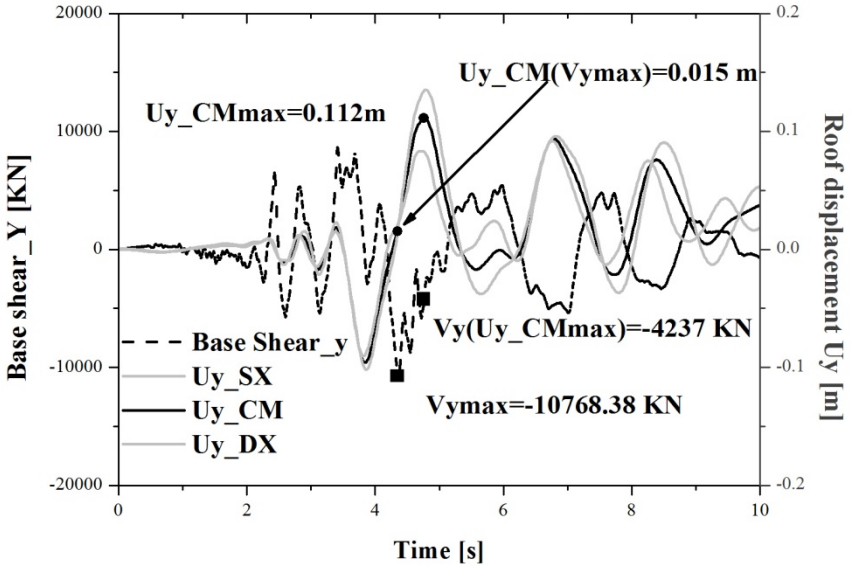

Figure 8.24 the maximum base shear is asynchronous with the maximum roof displacement in the NL_RHA of TH1, the maximum roof displacement for the CM and maximum base shear is obtained to form the IDA curve

The P.P. obtained from the single mode pushover curve and IMPA together with IDA are shown in Figure 8.25 to Figure 8.27. From the projection onto the PGA-roof displacement plane, the superimpose the single mode pushover curve on the IMPA curve indicate that IMPA will not increase the roof displacements. From the projection onto the PGA-base shear plane, it is clear that IMPA curve including the contribution of higher modes to the base shear is more close to the IDA curve, but big errors in the inelastic phase. From the base shear-roof displacement plane, compared to standard pushover curve, the increase of base shear in the IMPA make the capacity curve from IMPA more stiff, and more close to the IDA curve.

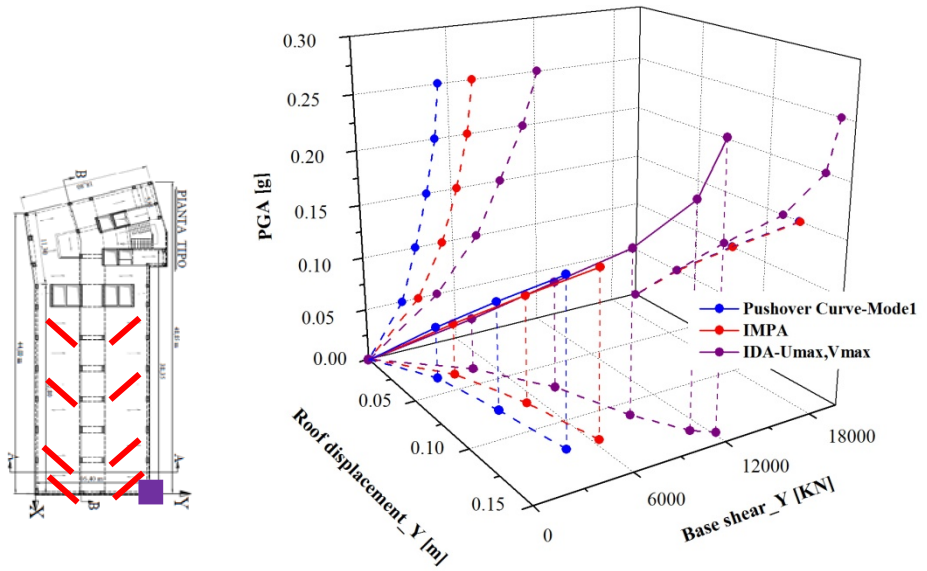

Figure 8.25 capacity curves obtained from different methods: the standard pushover analysis (for the predominate mode), IMPA method and IDA method for the left edge of building (SX)

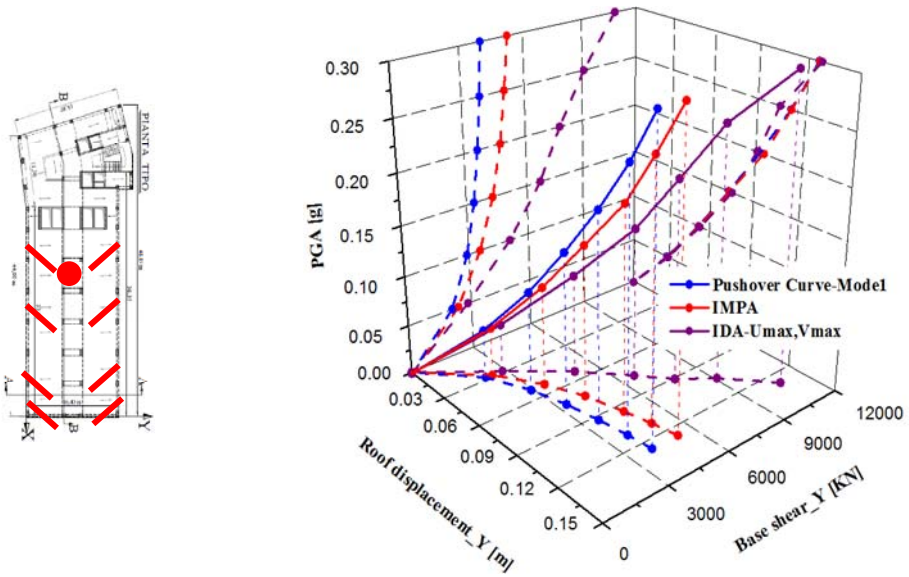

Figure 8.26 capacity curves obtained from different methods: the standard pushover analysis (for the predominate mode), IMPA method and IDA method for the center of building (CM)

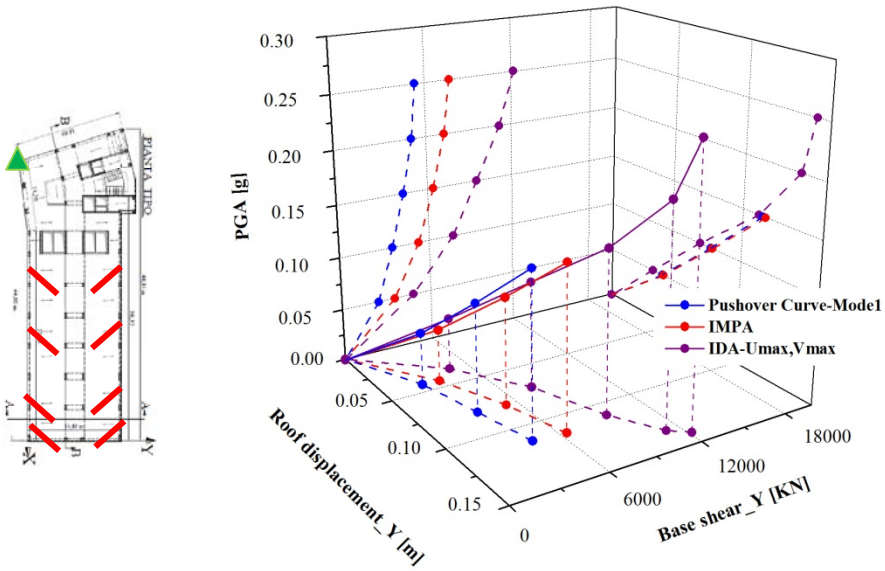

Figure 8.27 capacity curves obtained from different methods: the standard pushover analysis (for the predominate mode), IMPA method and IDA method for the right edge of building (DX)

The effectiveness of IMPA is sensitive to the PGA (the distance between IMPA and IDA increase with PGA). Both IMPA and IDA curves show a hardening behavior, IDA results stiffer in the plastic range, while the pushover curve is mostly elasto-plastic. For Y direction, the underestimation of base shear for the inelastic phase is more evident. When PGA is 0.2g, for the CM, the P.Ps. obtained from standard pushover curve, IMPA and IDA are (0.101m, 5036KN), (0.119m, 7227KN) and (0.112m, 11134KN), respectively. Compared to IDA, standard pushover underestimate base shear with an error of 55%, the IMPA underestimate base shear with an error of 35%.

from Figure 8.25 and Figure 8.27, compared to IDA, standard pushover and the IMPA would underestimate base shear with bigger errors. The static pushover cannot fully catch up the torsional effect on base shear for the irregular structure, so there are bigger errors for the corners in the inelastic phase.

8.7 Application to steel concentric braced frames (CBF)

In this section, a 3-story, 3-bay steel frame is selected to introduce the design procedure to CBF. The bays are 7 m, and floor-to-floor heights are 4m. Diagonal braces are inserted in the side bay. The Geometry of the original structure is shown in Figure 8.28. The columns and beams are 414 MPa steel wideflange sections. W27x114 and W24x94 are selected for column and beam, respectively. W8x13 is used for diagonal braces.

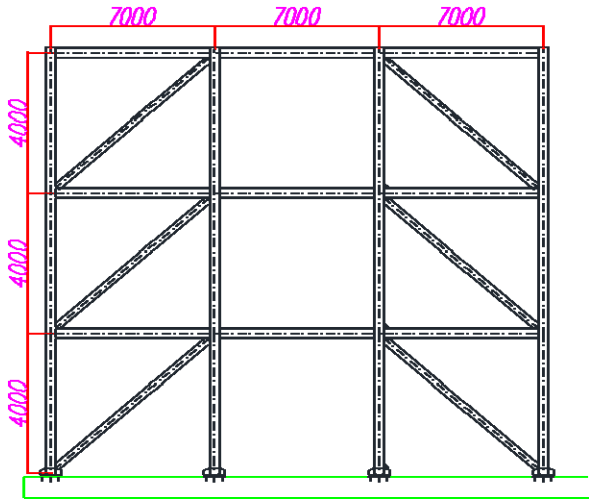

Figure 8.28 Geometry of the original structure

The 2D model is built in Opensees, and the NonlinearColumnBeam element is selected to simulate the column and beam. The initial imperfection of the diagonal braces is considered by dividing the diagonal braces into two elements, and their distances of their connection points to the centre line equal to 1 ‰ of the brace length, as shown in Figure 8.29.

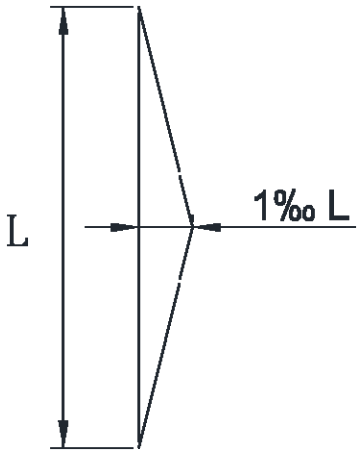

Figure 8.29 Simulation of the initial imperfection of diagonal braces

The structure has been analyzed referring to a seismic action characterized by a response spectrum given by NTC2008 defined in section 5. The performance points of the existing structures in terms of base shear and top displacement are 252KN and 109 mm. Then, the performance objective is to reduce maximum displacements in order to avoid damage in steel elements. For the design seismic event the target displacement mentioned has been selected adopting the following parameters: for the bare structure about 5‰ of total height ($D_{t,Sbare,targ}$=64 mm).

According to the proposed approach, pushover analyses have been carried out to define the capacity curves and to evaluate the structural response of both existing and braced frames. First mode proportional load profiles have been applied.

The capacity spectrum method is used to search the performance points obtained for the original and retrofitted structure, as shown in Figure 8.30 and Figure 8.31. It is clear that the performance points of the retrofitted structures in terms of base shear and top displacement are 219 KN and 62 mm, which satisfies the performance target. The properties of the designed BRBs are listed in Table 8.5. The axial force-displacement curve for the BRBs is plotted in Figure 8.32.

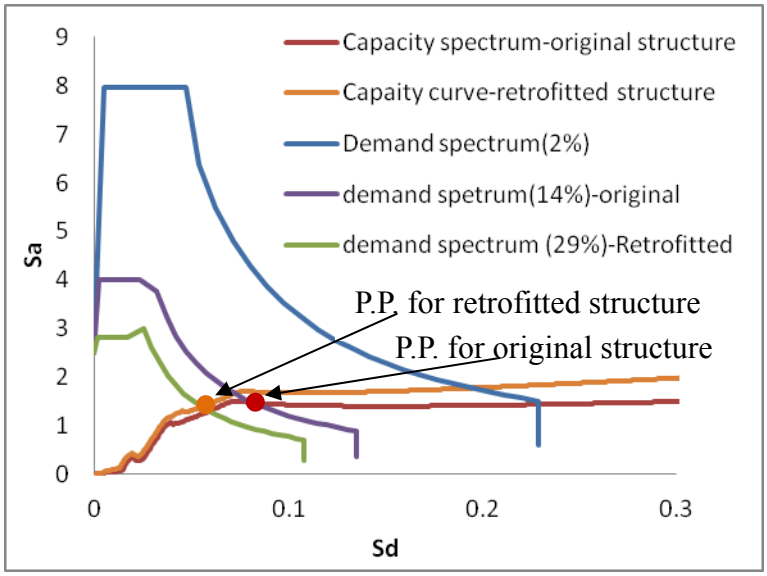

Figure 8.30 P.P. is determined via CSM from original and reduced demand spectrum for the first mode Capacity spectra

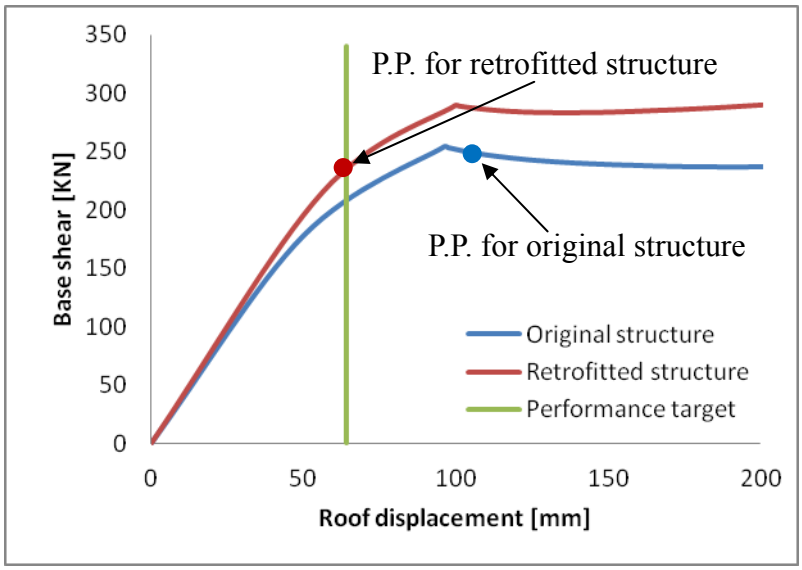

Figure 8.31 P.P. for the CM is determined from original and reduced demand spectrum for the first mode pushover curve

Table 8.5 Parameters of BRBs

Parameters	Description	Value
Fy (KN)	Yielding force	93

Dy (mm)	Yielding displacement	2.2
A (mm^2)	Area	1910

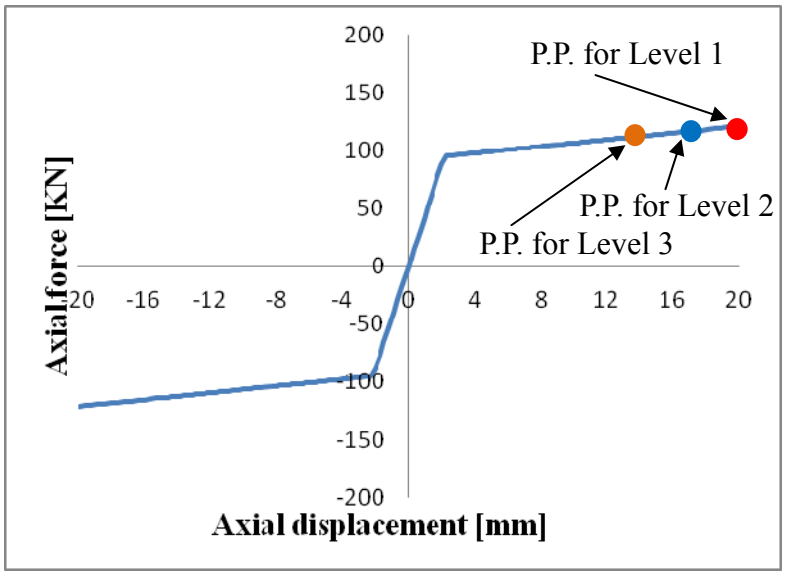

Figure 8.32 the axial force-displacement curve for BRBs

When the structure reaches the displacement limit (64 mm), the P.P.s for the BRBs are shown in Figure 8.32. It is observed that all BRBs for different floors enter plasticity stage. The plastic deformation of BRBs would dissipate energy, so the effective damping ratio for the retrofitted structure is 29%, however 14% for the original structure. Geometry of the retrofitted structure is shown in Figure 8.33.

The P.P. for the diagonal braces are shown in Figure 8.34 and Figure 8.35. From the picture, the diagonal braces in the left bay are in tension, the diagonal braces in the first and second floor enter plastic stage, it is good for the energy dissipation; the diagonal braces in the right bay are in compression, they will be buckled, even collapse for the first floor if no BRBs retrofitted.

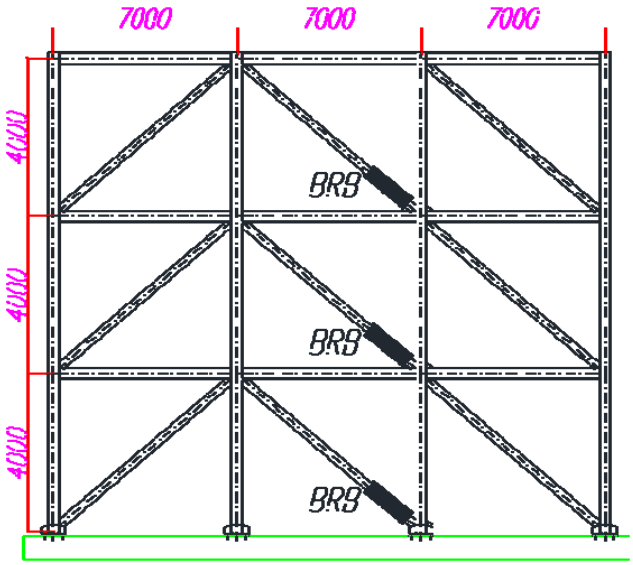

Figure 8.33 Geometry of the retrofitted structure

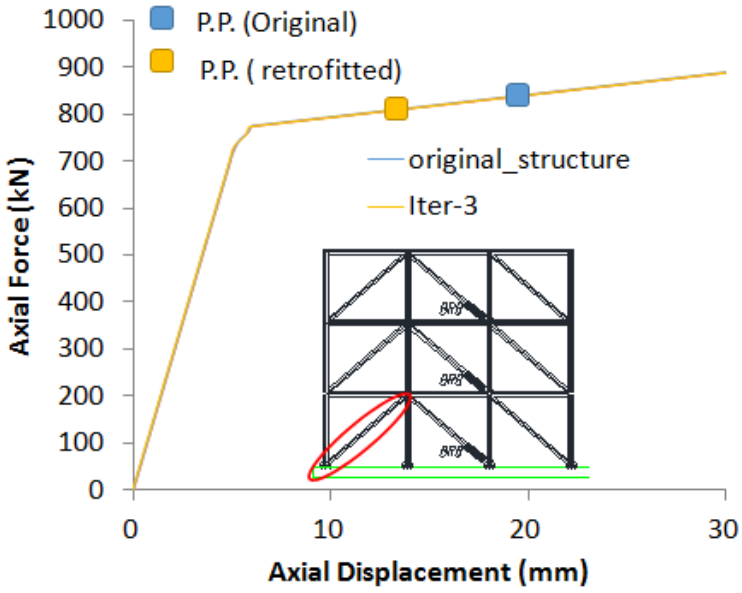

a) floor 1

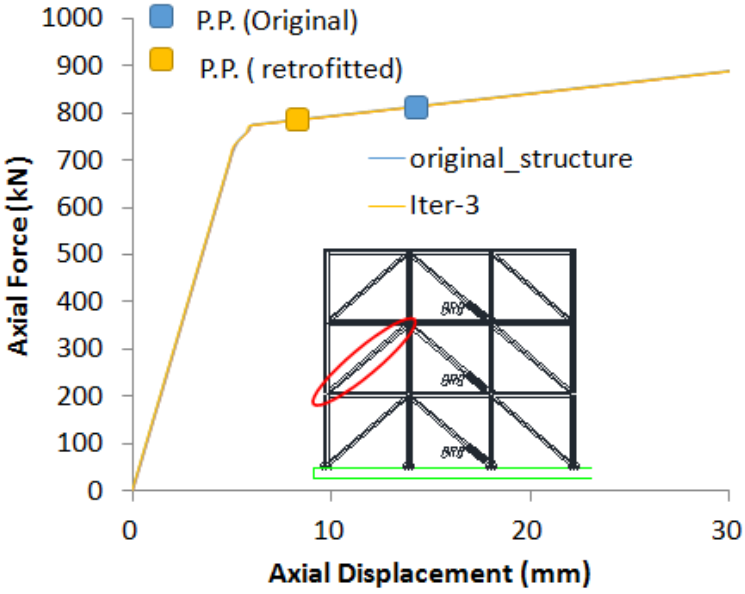

b) floor 2

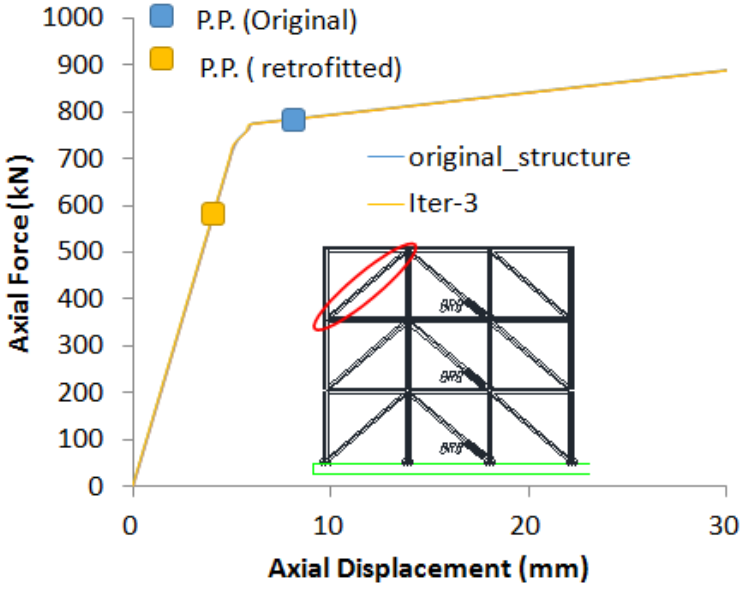

c) floor 3

Figure 8.34 P.P. for diagonal braces in tension

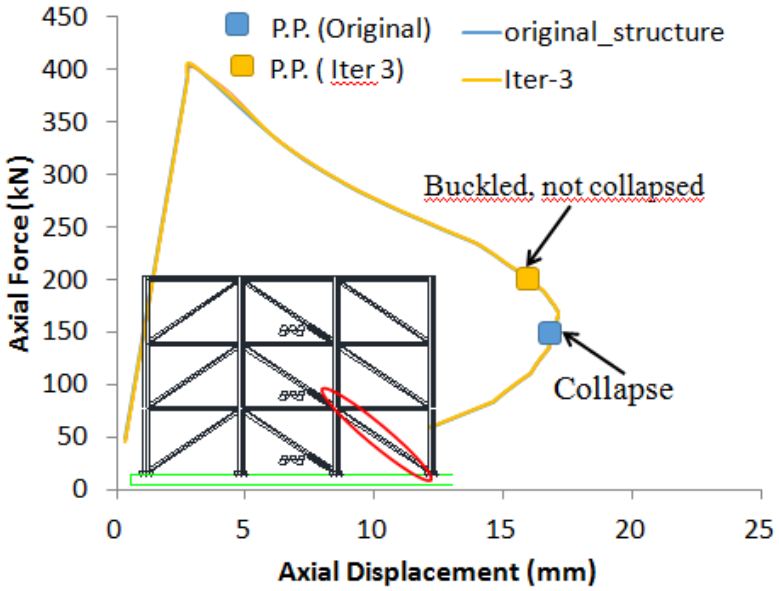

a) floor 1

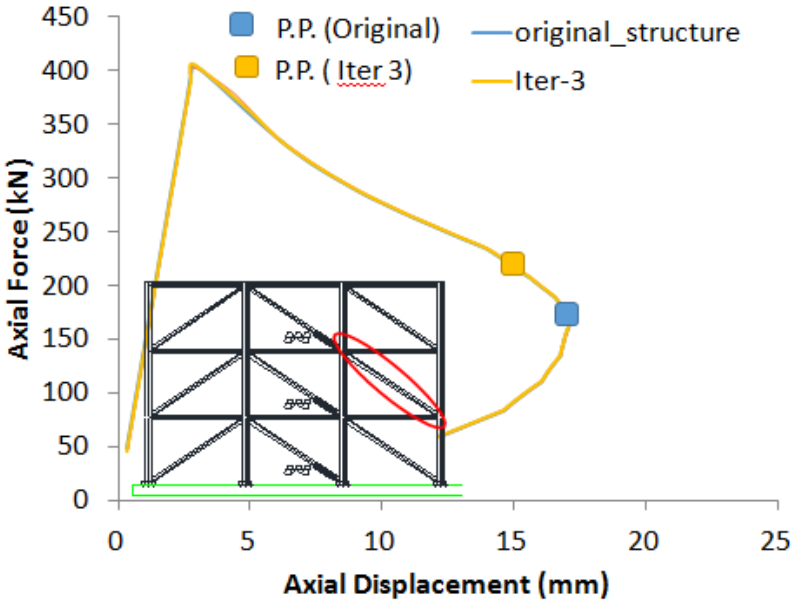

b) floor 2

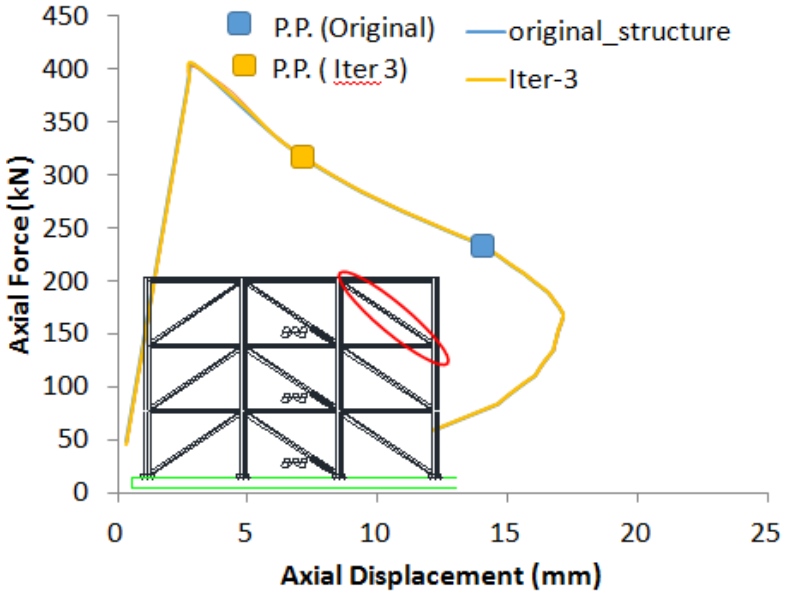

c) floor 3

Figure 8.35 P.P. for diagonal braces in compression

8.8 Conclusion

In present section, a displacement-based procedure to design dissipative bracings for the seismic protection of frame structures proposed by Bergami & Nuti (2013) is applied to a medium rise existing r.c. building, which presents both vertical and plan irregularities. The target displacement has been determined in order to limit both interstory drifts and ductility demand on existing structural elements. Afterwards, the evaluation of commonly Nonlinear Static Procedures (NSPs) for seismic response of the existing and retrofitted structure is presented to check the suitability of the use of NSP in the design procedure: the use of conversional NSPs to be not suitable for the case of irregular building but, once this building is retrofitted, and therefore regularized, with a bracing system, the use of NSPs for seismic response of the braced structure is effective. Moreover, from this comparison, has been observed that, in terms of drifts and displacements, the multimodal pushover can be considered not relevant for the design procedure for dissipative braces proposed by Bergami and Nuti (2012) if it is applied on structures such as the one analyzed (midrise r.c. frame building).

9. Retrofitting the existing building with alternative passive energy dissipation devices

9.1 Introduction

Recent strong earthquakes in China since 2008 resulted in severe damage in school buildings and cause lost of students' lives. For instance, about 60% school buildings collapsed or severely damaged in Wenchuan earthquake in 2008, a magnitude of MW 8.0, and about 70% in Yushu earthquake in 2010, a magnitude of MW 7.1. After the Wenchuan Earthquake, a new Chinese seismic design code (CMC, 2011) was issued in order to update protection categories and seismic intensities. The protection categories of buildings are classified into four categories: moderate protection (MP), standard protection (SP), emphasized protection (EP), and particular protection (PP). Protection categories, for school buildings, have been increased from SP buildings to not lower than EP buildings. With this new approach for SP buildings, seismic forces and structural details must be designed referring to design intensity, whereas, for the EP buildings, seismic forces must be calculated commensurate with the design intensity while structural details must be checked according to an intensity of one degree higher than design one, for the PP buildings, seismic forces and structural details must be checked one degree higher than the design intensity. On the other hand, the seismic intensities of many cities in China have been increased by half degree or more, for instance, the seismic intensity in Doujiangyan increased from 7, with Peak Ground Acceleration (PGA) of 0.1g, to 8 with PGA of 0.2g. Therefore, lots of school buildings are not complied with new seismic code requirements and thus need to be retrofitted. The government started a nationwide mission in 2009, aiming at checking and upgrading the seismic capacity of school buildings through inspection and retrofit activities.

If compared to traditional retrofitting practice (i.e., strengthen damaged members and joints with reinforced concrete or steel jacketing, increasing the cross section of the members) and seismic isolation, the use of passive energy dissipation devices result easier for installation and it does not require demolition of decorations and undamaged members. Passive energy dissipation devices, which have most commonly been used for seismic protection of structures, include Buckling Restrained Brace

(BRB), Viscous Dampers (VD), Viscoelastic Dampers (VED), and Metallic Dampers (MD), etc.

Although damper technologies are specified in new version seismic design code (GB50011) (CMC, 2011), only general information is given, no guidelines for the design. To facilitate the adoption and implementation of passive energy devices, the development of suitable design methods is necessary. The aim of the work is to evaluate feasibility of force-based and displacement-based approaches, and investigate the effectiveness of different passive energy devices. In the following, after a brief description of the state of the art of the dissipative energy devices and two design methods, the mathematical models for the different dampers are presented. Then, these two design methods are applied to retrofit a school building located in shanghai, the comparisons of the two design methods and the seismic behavior of the retrofitting structure with different passive energy dissipation devices are discussed.

9.2 Design methods of passive energy dissipation devices

A large number of passive control systems or passive energy dissipation (PED) devices have been developed and installed in structures for performance enhancement under earthquake loads. In North America, PED devices have been implemented in approximately 103 buildings and many bridges, either for retrofit or for new construction (Soong and Spencer Jr., 2002).

9.2.1 Mathematical Models

1. Viscous dampers

Experimental testing Seleemah and Constantinou (1997) has shown that a suitable mathematical model for describing the behavior of viscous fluid dampers is given by the following nonlinear force-velocity relation.

$$F_d = C|v|^a \cdot sign(v) \tag{9.1}$$

Where F_d is the damping force of a single viscous damper, C is the damping factor, v is the velocity of the viscous damper and its exponential parameter a determines the relationship between force and velocity. It should be evident that when $a = 1$, Eq. (9.1) expresses the relationship of linear viscous dampers.

It is assumed that the displacement and the velocity of dampers are expressed in Eqs. (9.2) and (9.3).

$$d = A\sin wt \tag{9.2}$$

$$v = \dot{d} = Aw\cos wt \tag{9.3}$$

Thus,

$$F_d = C|v|^a \cdot sign(v) = C|Aw\cos wt|^a \cdot sign(Aw\cos wt) \tag{9.4}$$

Keeping the same displacement (A = *60 mm*) and force (F_{di} = *516 kN*), the force–displacement curves at a = *0.2* and a = *1.0* are given in Figure 9.1 . It can be seen that the shape of the curve at a = *0.2* is closer to a rectangle while the shape of the curve at a = *1.0* to an ellipse. Apparently, more energy dissipation area will be achieved when a is taken a smaller value. In order to achieve a certain amount of force using a smaller a, a larger C has to be chosen at the same time. The value C, however, is a parameter correlating to the stiffness of dampers. An excessively high damper stiffness would potentially create difficulty in designing the structural elements connecting with the dampers. Thus, selecting the appropriate a and C values deserve special attention in the design stage.

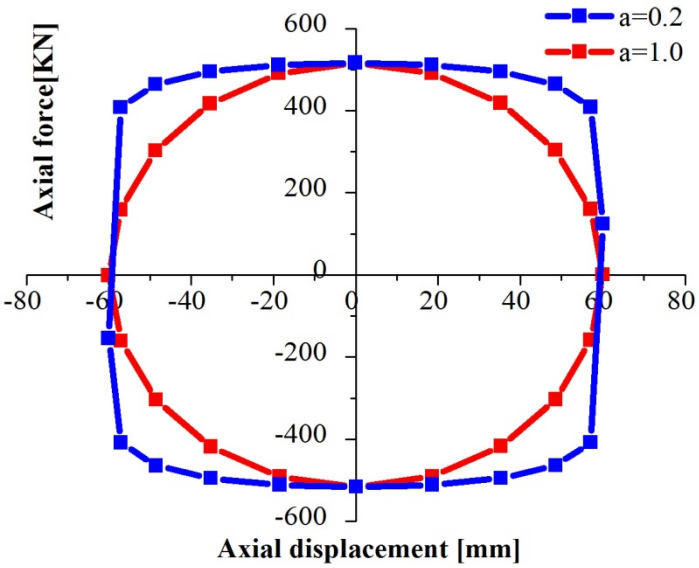

Figure 9.1 Force-displacement curves of viscous damper under various a

2. Viscoelastic dampers

Viscoelastic dampers generally consist of solid elastomeric pads bonded to steel plates. The steel plates are attached to the structure within chevron or diagonal bracing. As one end of the damper displaces with respect to the other, the viscoelastic material is sheared resulting in the development of heat which is dissipated to the environment. By their very nature, viscoelastic solids exhibit both elasticity and viscosity.

Experimental testings (e.g., Bergman and Hanson 1993; Lobo et al. 1993; and Chang et al. 1995) have shown that, under certain conditions, the behavior of viscoelastic dampers can be modeled using the Kelvin model of viscoelasticity. The force–displacement curves of viscoelastic damper is shown in Figure 9.2.

$$F_d = \mathrm{K}u + Cv \tag{9.5}$$

Where K is storage stiffness of the damper, and C is the damping coefficient.

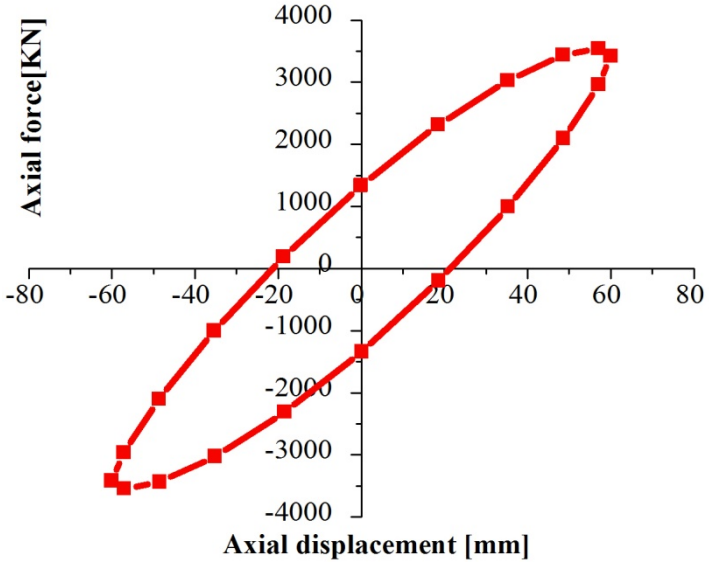

Figure 9.2 Force-displacement curves of viscoelastic damper

3. Metallic dampers

Two major types of metallic dampers are buckling-restrained brace (BRB) dampers and added damping and stiffness (ADAS) dampers.

During the initial elastic response of the BRB damper, the device provides

stiffness only. As the BRB damper yields, the stiffness reduces and energy dissipation occurs due to inelastic hysteretic response. The hysteretic behavior of a BRB damper can be represented by various mathematical models that describe yielding behavior of metals. One example is the Bouc–Wen model (Wen, 1976), which is described by Black et al. (2004) and compared with experimental test data therein.

$$F_d = \beta \mathrm{K} u(t) + (1\text{-}\beta)\ \mathrm{K} u_y Z(t) \tag{9.6}$$

Where β is ratio of post stiffness, K is the initial stiffness, u_y is the yield displacement and $Z(t)$ is the evolutionary variable.

$$u_y Z(t) + \gamma \left| \dot{u}(t) \right| Z(t) \left| Z(t) \right|^{\delta-1} + \eta \dot{u}(t) \left| Z(t) \right|^{\delta} - \dot{u}(t) = 0 \tag{9.7}$$

Where γ , η and dimensionless parameters that define the shape of the hysteresis loop.

The hysteretic behavior of an ADAS damper is similar to that of a BRB damper and can be represented by various mathematical models that describe yielding behavior of metals. As for the BRB dampers, the dissipated energy in an ADAS damper is the result of inelastic material behavior and thus the ADAS damper will be damaged after an earthquake and may need to be replaced.

For prcatical design, an idealized bilinear model may be sufficient to capture the global response characteristics of a BRB or ADAS damper, as shown in Figure 9.3.

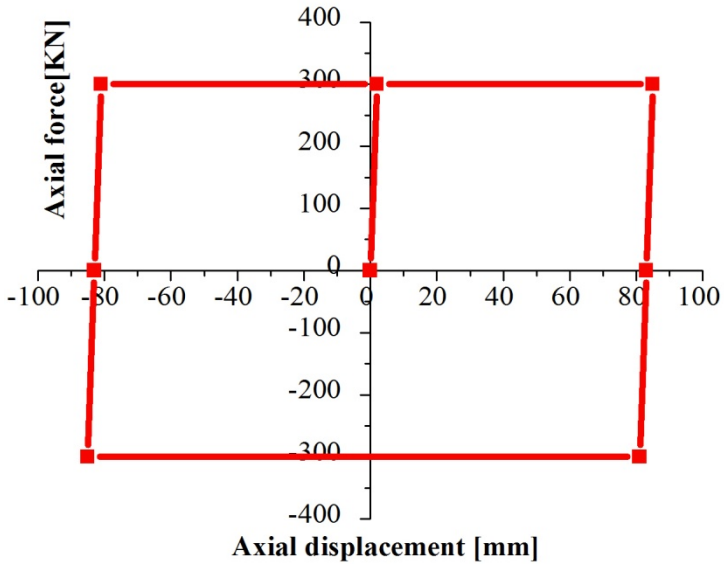

Figure 9.3 Force-displacement curves of metallic damper

9.2.2 Design method for the passive energy devices

The application and development of PED devices have led to a number of publications that present detailed discussions on the principles of operation and mathematical modeling of such devices, analysis of structures incorporating such devices, and applications of the devices to various structural systems.

Aguirre (1997) proposed an iterative design method based on linear static analysis. This force-based method rely on a force reduction factor, does not directly address the inelastic nature of the structure during the earthquake and the resulting displacement is then checked at the end of the design process to satisfy serviceability criteria. Energy-based seismic design method utilizes hysteretic energy as the main design parameter. Riddell and Garcia(2001) developed a procedure for the hysteretic energy demand spectrum. Leelataviwat.et al. (2002) proposed a seismic design method based on energy balance and Kim and Choi (2004) extended the energy balance concept to develop a simplified seismic design procedure for steel frames with BRBs.

More recently displacement based design procedures have been developed, such as FEMA-274 (1997) coefficient method, ATC-40 (1996)

capacity-spectrum method and the direct displacement-based design method by Lin, Tsai, Hwang, and Chang (2003). Kim and Choi (2004) proposed the procedure focused on the achievement of a target performance point (e.g. the target top displacement or the maximum story drift): no references to other relevant parameters are made. The displacement-based design method is easy to be applied and, consequently, suitable for practical applications; moreover it permits explicit check of the achievements.
Among these methods, a direct displacement-based design procedure of dissipative bracing proposed by A. V. Bergami and C. Nuti (2013) use the capacity spectrum method to determine the target displacement and no dynamic non linear analyses are needed. Zhou and Lu (2012) proposed a practical force based design procedure for reinforced concrete (RC) structures with viscous dampers.

1. Displacement based approach

A displacement-based procedure to design dissipative bracing for the seismic protection of structures is proposed by A. V. Bergami and C. Nuti (2013), described in section 4 The procedure is based on the capacity spectrum method: the target is expressed in terms of displacement. Iteration is required since the addition of braces modifies structural response and the capacity curve has to be updated as long as the characteristics of the new braces are defined. Moreover, the energy dissipated by the braces is considered additional to the dissipative capacity of the structure, computed on the capacity curve of the original one.
In this displacement based design procedure, the performance desired is selected at first as the displacement (target displacement) corresponding to a selected limit state for a given seismic action. Then the required total effective damping needed to make the maximum displacement not larger than the target one is determined. The additional damping, due to bracing, is estimated as the difference between total damping and hysteretic damping of the structure without braces. The characteristics of the braces to guarantee the required additional damping are finally determined. The procedure is iterative but it converges in few iterations.

2. Force based approach

A practical design method for reinforced concrete structures with viscous dampers is proposed by Zhou and Lu (2012). The proposed design process is divided into two stages. In the preliminary stage of designing viscous dampers in a structure, the following tasks needed to be done: (1) determine the number of viscous dampers, (2) choose the parameters of viscous dampers, and (3) configure the layout of viscous dampers:

1). Determine the number of viscous dampers:

$$n = F_d / F_{di} \tag{9.8}$$

$$F_d = 0.3F \tag{9.9}$$

Where F_d is the force providing by viscous dampers in each story, F is the story shearing force , F_{di} is damping force of a single viscous damper.

In general, it is not desirable for a damper to reach its capacity either too early under a minor earthquake or too later under a major earthquake. It is thus assumed here that a damper reaches its capacity under a moderate earthquake. So F is the story shear force under moderate earthquake.

2). Choose the parameters of viscous dampers

$$F_{di} = C \cdot |v|^a \cdot sign(v) \tag{9.10}$$

where C is the damping factor, v represents the velocity of the viscous damper and its exponential parameter a determines the relationship between force and velocity.

3). Configure the layout of viscous dampers

The main concept to keep in mind when determining the configuration of the viscous dampers in a building is to place them in those stories where inter-story drifts are relatively large.

In the second stage of design, engineers should check the structural deformations, the additional damping ratio, and the dampers' connection to other structural elements in order to ensure the workability of the damper systems.

9.3 Case study

9.3.1 Building description

The case study located in Shanghai, is a ten-storey school building built in the 1996 according to the provisions of Chinese 1989 code for seismic design (CMC,1989). According to this building code, protection category of the structure was classified to be SP, now is EP or PP. The plan measures approximately 39.6m×14.2m. The inter story heights for the stories are 3.9m for the first floor and 3.4m for the others, respectively. The total height of the structure is 34.5m. The structural system is RC frame-shear wall hybrid structure. Views of plan and of section of the original structure are depicted in Figure 9.4 and Figure 9.5, respectively.
The cross sections are 400×500 mm for columns, 250×630mm for the beams in the longitudinal direction and to 250×510 mm in the transverse direction. The thickness of the slab at each level is 100 mm. Class of all the concrete is C30 that correspond to a cubic compressive strength of 14.3 MPa.

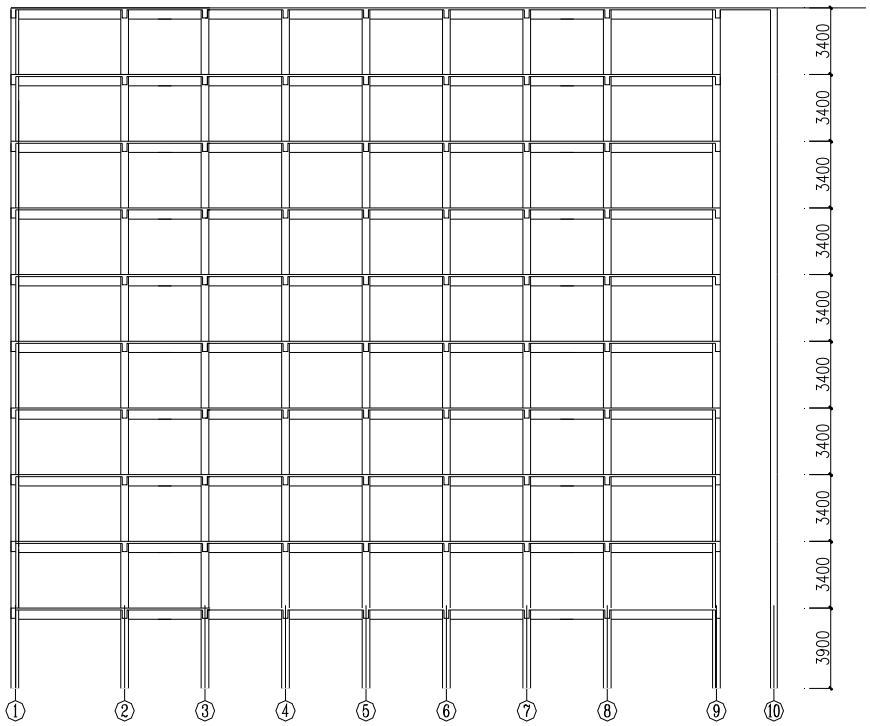

Figure 9.4 Elevations of the existing structure

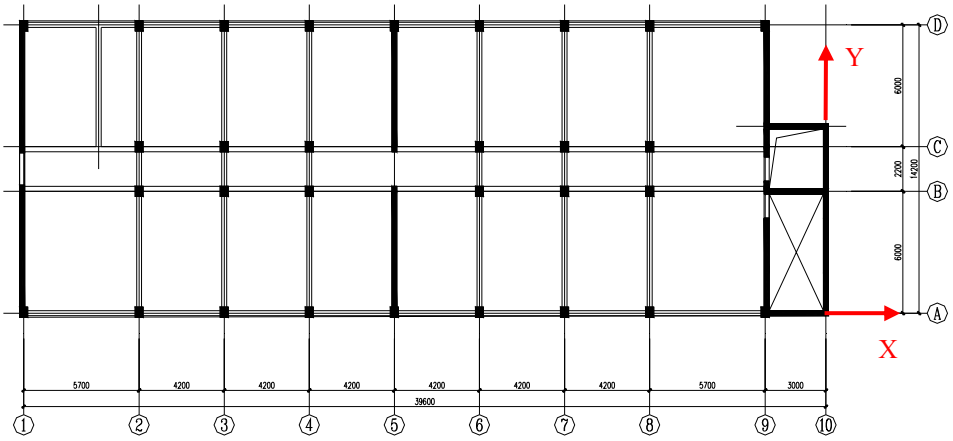

Figure 9.5 Plan view of the existing structure

9.3.2 Seismic actions

According to Code for seismic design of buildings (J10284-2013), two artificial accelerogram and five natural ground motions are necessary for time history analysis: two artificial accelerogram (SHW1~SHW2), 1999 kocaeli earthquake ground motion record (SHW3), 1999 Hector Mine earthquake ground motion (SHW4), 2002 Denali earthquake ground motion (SHW5), and two 1999 Chichi earthquake ground motions (SHW6, SHW7) are recommended in the code. The PGA is scaled down to 0.07 g, 0.20 g, 0.4 g to commensurate with the PGA under minor, moderate, and major earthquakes of intensity 8.

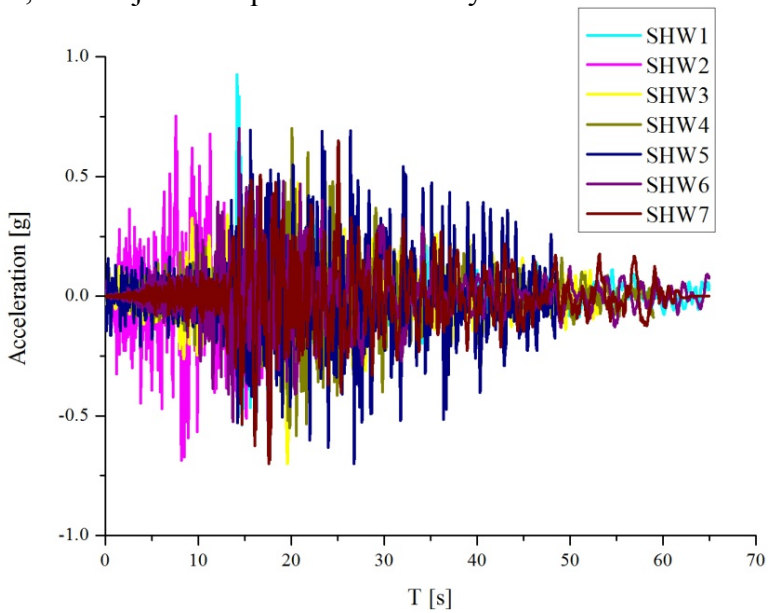

Figure 9.6 Time history of the ground motions

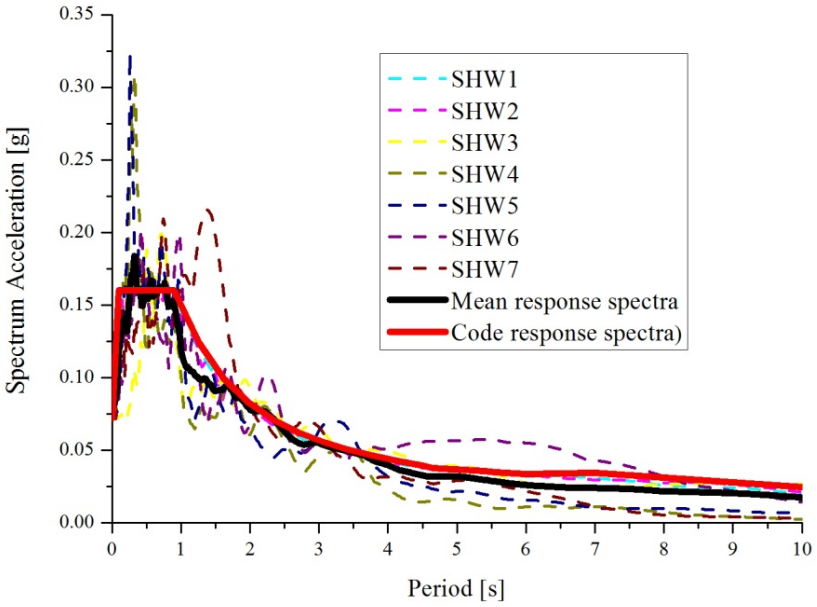

Figure 9.7 Response spectrum curves under different earthquake waves

The time history and response spectra are shown in Figure 9.6 and Figure 9.7, respectively. The response spectra in the seismic code (J10284-2013) is shown in Figure 9.7, the seismic coefficient under intensity 8 of shanghai is 0.08 and the site characteristic period is 0.95s.

9.4 Definition of the performance objective for the existing building

9.4.1 Performance objective

According to Code for Seismic Design of Buildings (GB50011, 2011), the main performance objectives for buildings are to ensure structures immediate occupancy without damage under minor earthquakes, operational with repairable damage under moderate earthquakes, and functional without severe collapse under major earthquakes. These objectives are fulfilled by checking forces and elastic displacements under minor earthquakes, and by checking elastoplastic displacements under major earthquakes, which is so called ‘‘two stages’’. The requirement for the moderate earthquake level is only satisfied by the design of structural details. The inter-story drift objectives of the RC structures under different earthquakes are listed in Table 9.1(CMC, 2010, Lu, 2008). For

the existing frame-shear wall hybrid structure, inter story drift limits are 1/800 and 1/100 under minor and major earthquakes, respectively.
According to the inspection report of the subjective building, the structural details are designed with the design intensity. However, according to the new version of seismic design code (GB50011, 2011), its protection category was increased from SP to EP or PP. the protection category for the existing building is defined conservatively as PP, which means the seismic force will be calculated one degree higher than design intensity.

Table 9.1 Interstorey drift limit

	Minor earthquake	Moderate earthquake	Major earthquake
Frame structure	1/550	1/250	1/50
Hybrid structure	1/800	1/400	1/100
Shear Wall structure	1/1000	1/500	1/120

9.4.2 Seismic evaluation for the existing building

An analytical model is built in Sap2000, as shown in Figure 9.8: beam and column elements are modeled as frame elements with lumped nonlinearity by defining plastic hinges at the critical sections (extremities of beams and columns). A coupled axial force and biaxial bending moment hinges (P-M2-M3 hinge) are assigned to columns whereas moment hinges (M3 hinge) are assigned to beams. Nonlinear shell elements are used to simulate walls. The foundations, which beyond the current study, are modeled with joints constraints. Later the link elements will be used to simulate the braces and dampers. The first six periods of the existing structure are listed in Table 9.2.

Table 9.2 First six periods of the structure

Mode	Period(s)	Mode shape
1	1.16	X translation
2	0.49	Y translation
3	0.40	Torsion
4	0.32	X translation
5	0.15	Y translation
6	0.15	Torsion

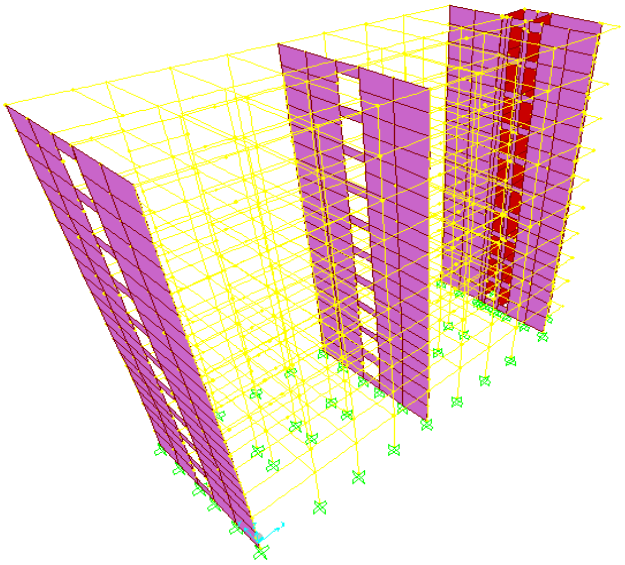

Figure 9.8 Analytical mode of the school building

The ground motions (SHW1-SHW7) are adopted to study the dynamic response of the existing building, and the PGAs in the time history analysis are scaled to 0.07g and 0.4g to accommodate the minor and major earthquake of seismic intensity 8, respectively. The median value of the drift ratios obtained from time history analysis together with performance objective for both directions are shown in Figure 9.9 and Figure 9.10. One can easily find that the inter-story drifts in X direction beyond the performance objective, and those in Y direction can satisfied the objective, so additional dissipative devices are only required to control the structural response in X direction.

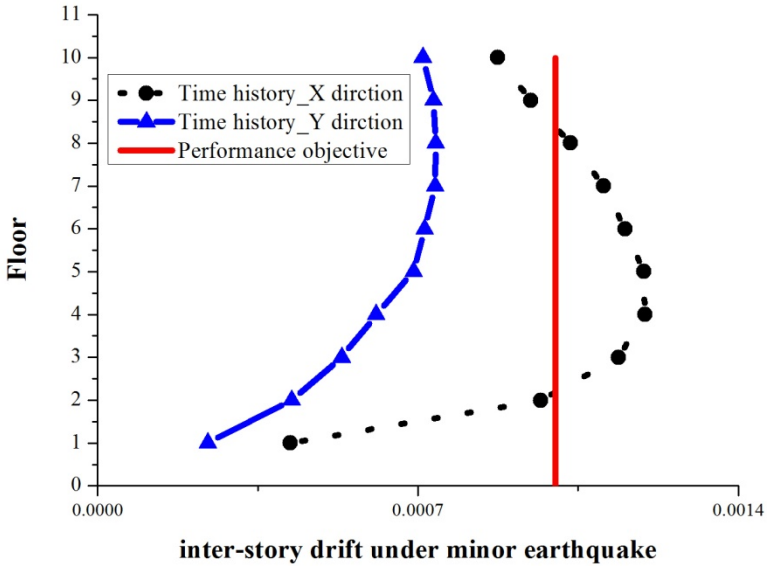

Figure 9.9 Inter-story drift under minor earthquake

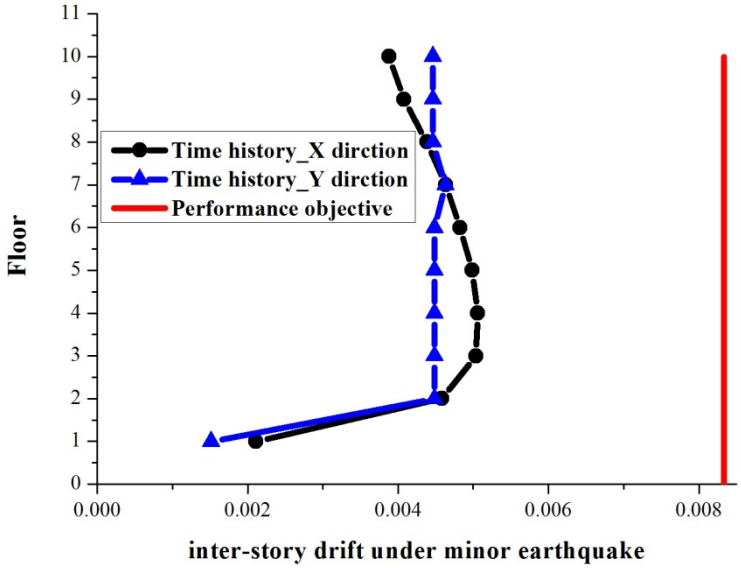

Figure 9.10 inter-story drift under major earthquake

9.5 Retrofitting the building with different dissipative devices

9.5.1 Retrofitting the building with BRBs

In recent years, BRBs have become relatively popular among the several typologies of dissipative devices. Within this context, the existing building was retrofitted with BRBs through displacement based and force based approaches. The structural performance of the different versions of retrofitted buildings was estimated by subjecting each one to a set of seven ground motions representative of the design earthquake to evaluate the effectiveness of the two design methods.
For the purpose of investigating the seismic responses of the structure retrofitted by viscous dampers, metallic dampers and viscoelastic dampers, the building added with the different dampers, through force based approach, are analyzed respectively on the premise that different dampers have the approximately equal maximum damping force under moderate earthquake.

1. Displacement based approach

For the subject building, the BRBs are adopted to improve its seismic performance under minor earthquake with a PGA=0.07g. According to proposed procedure, modal pushover analyses have been carried out to evaluate the structural response for longitudinal directions.
The performance point of the existing structures, in terms of roof displacement and base shear, is 0.061m and 5843 KN, and corresponding maximum inter-story drift is 0.21% in the 4th level. The performance objective is to reduce maximum inter-story drifts in order to avoid damage on the RC elements and reduce damage on the non-ductile elements under minor earthquake. For the seismic event, the target top displacement corresponding with the achievement of the inter-story drift has been updated at each iteration because the intervention of braces will change the stiffness of the whole structure and the drift distribution, in the last iteration the target displacement was 0.031m. The capacity curves determined performing the design procedure is shown in Figure 9.11 and Figure 9.12. The procedure converged at second iteration; afterwards a final refinement of all BRBs has been executed. The performance point in

terms of top displacement and base shear for the retrofitted building are 0.031 m and 8223 KN, and the corresponding maximum inter-story drift is 0.11% in the 4th level. The locations of the braces are shown in Figure 9.14and Figure 9.15. The parameters of the BRBs are listed in Table 4.

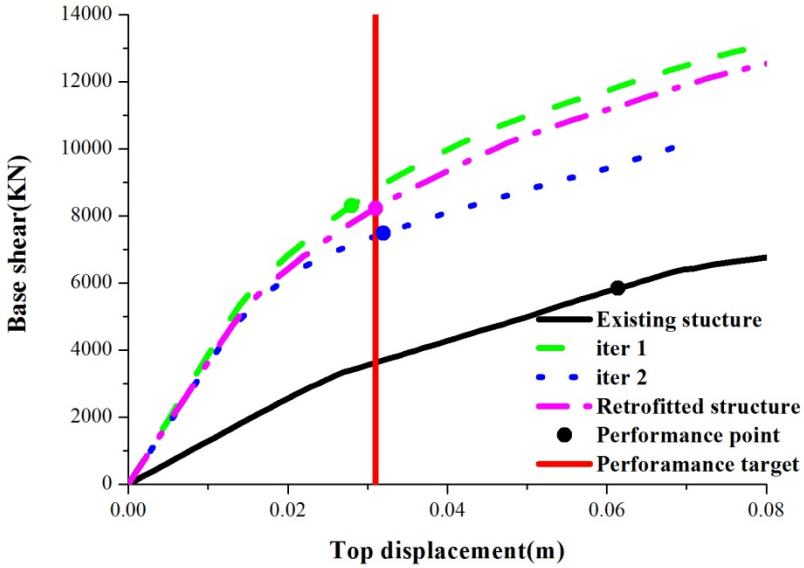

Figure 9.11 Deign procedure for BRBs: performance points

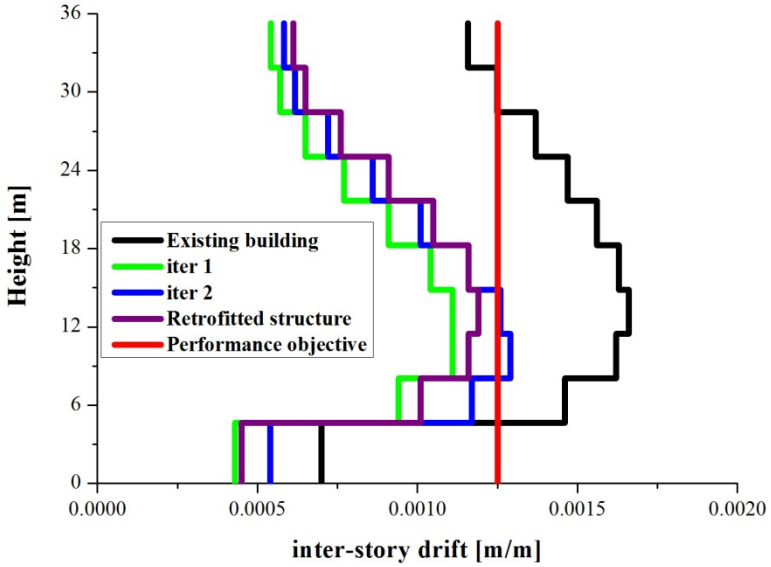

Figure 9.12 Deign procedure for BRBs: Interstorey drifts

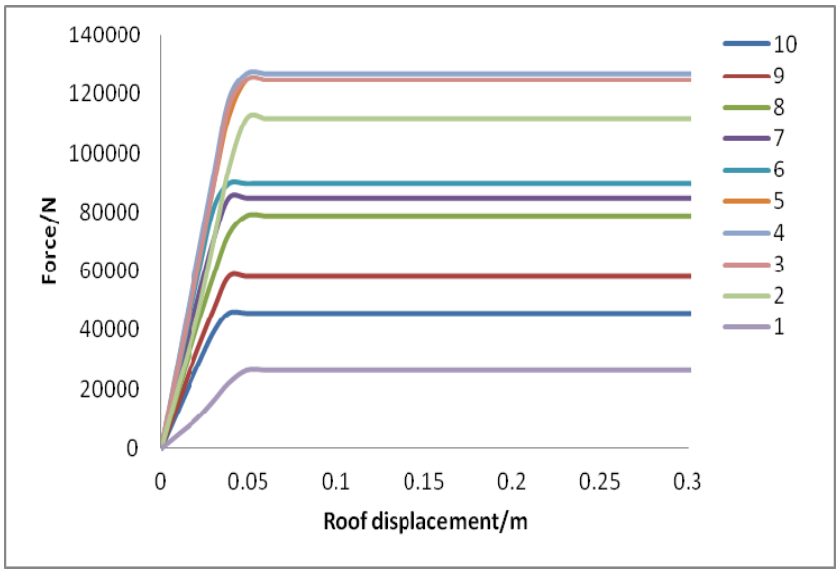

Figure 9.13 Optimization of BRBs

2. Force based approach

The structural properties of the existing building under seismic intensity 8 are shown in Table 3. As introduced in Section 2.3.2, the preliminary design damping forces are taken as 30% of the shear forces of stories. Those forces for the target building are also listed in Table 9.3, and design and distribution of expected damping forces of the building are conducted. Sixteen of the same braces were employed in each story in X direction.

Table 9.3 Shear forces and story drifts of time history analysis

Floor	Height (m)	Story mass (t)	Shear force (KN)	Expect damping force [KN]	Inter-story drift
10	3.45	559	3530	1060	0.0007
9	3.4	727	7746	2324	0.0015
8	3.4	727	11570	3470	0.0016
7	3.4	727	14928	4478	0.0017
6	3.4	727	17780	4534	0. 0016
5	3.4	727	20094	6028	0.0016
4	3.4	750	21912	6574	0.0015
3	3.4	750	23185	6946	0.0014
2	3.4	750	23864	7160	0.0012

1	4.65	801	24160	7248	0.0012

Note: The shear forces and story drift are obtained under moderate and minor earthquake, respectively.

Table 9.4 the parameters of the BRBs designed by two different approaches

Floor	Brace Length(m)	Displacement based approach			Force based approach		
		Area (m^2)	Ki (N/m)	Fy (N)	Area (m^2)	Ki (N/m)	Fy (N)
10	5.435	3.74E-02	9.03E+07	8.27E+04	4.14E-02	2.0E+08	2.00E+05
9	5.404	8.66E-02	2.09E+08	1.90E+05	8.28E-02	4.0E+08	4.00E+05
8	5.404	1.01E-01	2.43E+08	2.22E+05	1.24E-01	6.00E+08	6.00E+5
7	5.404	1.06E-01	2.56E+08	2.33E+06	1.24E-01	6.00E+08	6.00E+5
6	5.404	1.06E-01	2.56E+08	2.33E+06	1.66E-01	8.00E+08	8.00E+5
5	5.404	1.02E-01	2.47E+08	2.25E+06	1.66E-01	8.00E+08	8.00E+5
4	5.404	1.16E-01	2.80E+08	2.56E+06	1.66E-01	8.00E+08	8.00E+5
3	5.404	1.08E-01	2.60E+08	2.35E+06	2.48E-01	6.00E+08	6.00E+5
2	5.404	8.12E-02	1.96E+08	1.78E+06	2.48E-01	6.00E+08	6.00E+5
1	6.266	7.50E-02	1.81E+08	1.91E+05	2.48E-01	6.00E+08	6.00E+5

The parameters of the BRBs designed by two approaches are listed in Table 9.4. From this table, it can be observed that the use of BRBs designed by force based approach exceed greatly another version. In the displacement base approach, the BRBs would installed more in the soft stories, this distribution would improve the building more vertical irregularity; in the force based approach, the BRBs would installed more in the lower stories, whose shear forces are larger than other floors, this distribution would make the lower floors more stiff.

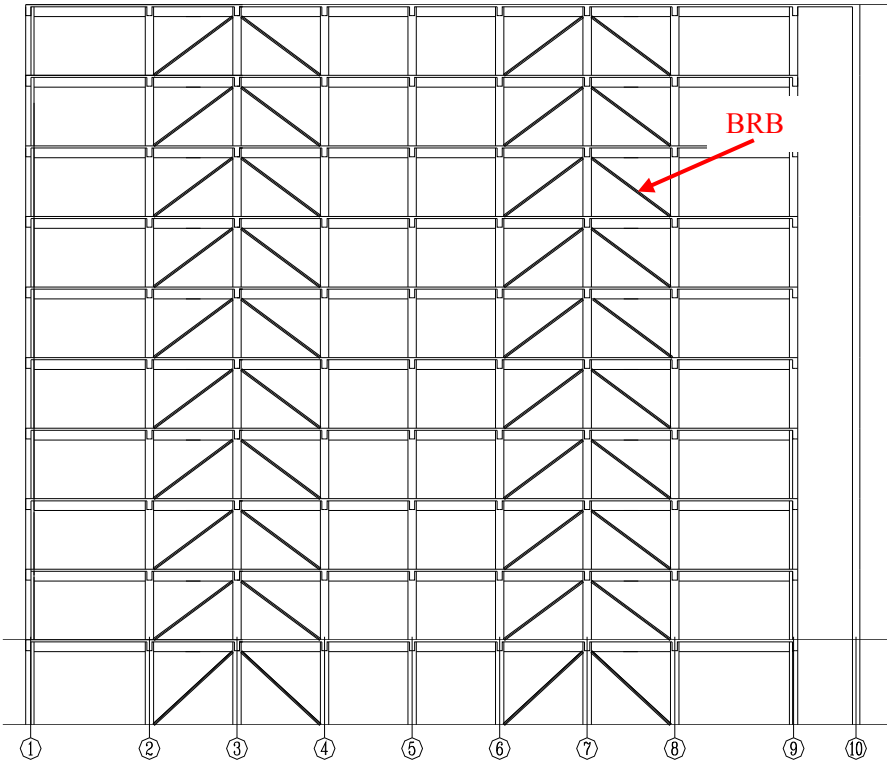

Figure 9.14 Elevation layout of the BRBs

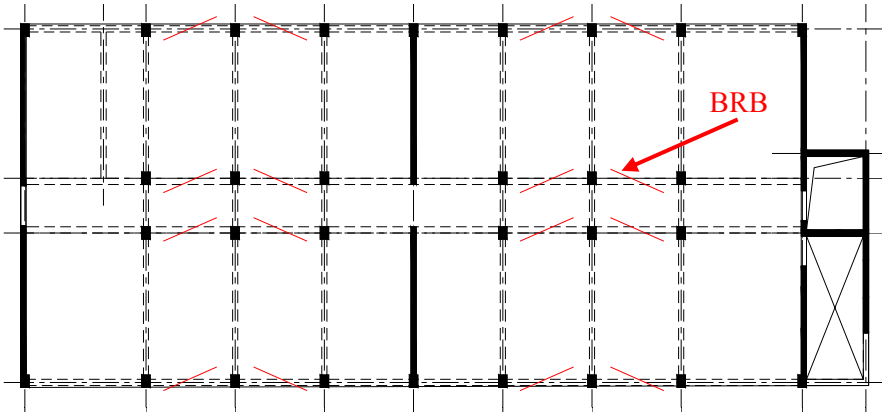

Figure 9.15 Plan layout of the BRBs

9.5.2 Retrofitting of the building with alternative solutions: ADAS, viscous and viscoelatsic dampers

Based on the simplified retrofitting design procedure introduced above, design and distribution of expected damping forces of the frames are conducted. The parameters and distribution of the added dampers is listed in Table 5. As to viscous damper, where Cd is the damping coefficient, α is the velocity exponent, and Kd is the stiffness of viscous damper that assigned to 70% of Cd according to the previous experiments. As to ADAS damper, where K is the stiffness, F is the yield strength, r is post yield stiffness ratio, exp is the yielding exponent. As to viscoelastic dampers, Kd is the storage stiffness, Cd is the damping coefficient, η is the loss factor of the viscoelastic material. Their distributions are listed in Table 9.5.

Dampers can be installed as diagonal members, as part of a chevron brace, horizontally at the top of a chevron brace, or as a toggle brace. The horizontal chevron configuration is applied here as shown in Fig 14and Fig 15. Two viscous or viscoelastic dampers are installed in parallel and supported by a steel chevron brace. Lead rubber bearings are installed at the top of the brace to keep the stability of the brace and to dissipate the energy under minor earthquake. The final plan layouts of dampers in the structure are shown in Figure 9.18 and Figure 9.19.

Table 9.5 the parameters of the dampers

Damping Force	Viscous damper(VD)			ADAS				Viscoelastic damper		
	C_d	a	K_d	K	exp	r	F	K_d	η	C_d
200	80	0.2	56	200	2	0.01	200	31	6	0.8
400	160	0.2	112	400	2	0.01	400	31	6	0.8
600	240	0.2	168	600	2	0.01	600	36	7	0.8
800	320	0.2	224	800	2	0.01	800	57	12	0.8
1000	/	/	/	1000	2	0.01	1000	/	/	/

Table 9.6 Distribution of the Added Dampers

Floor	Expect damping force	VD	ADAS	VED
10	1060	8X200	8X200	8X200
9	2324	8X400	8X400	8X400
8	3470	8X600	8X600	8X600
7	4478	8X600	8X600	8X600
6	4534	8X800	8X800	8X800
5	6028	8X800	8X800	8X800

4	6574	8X800	8X800	8X800
3	6946	16X600	8X1000	16X600
2	7160	16X600	8X1000	16X600
1	7248	16X600	8X1000	16X600

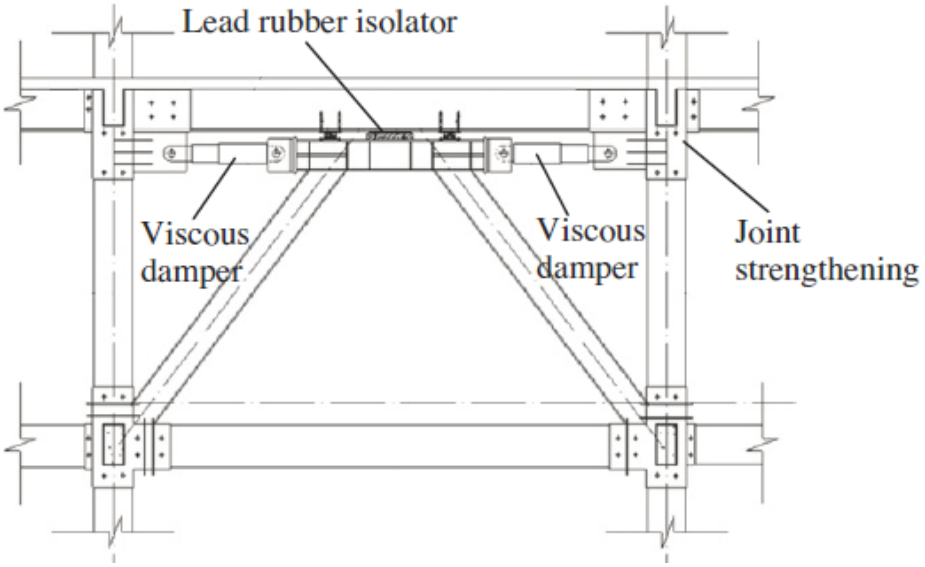

Figure 9.16 Configuration of viscous and viscoelastic dampers

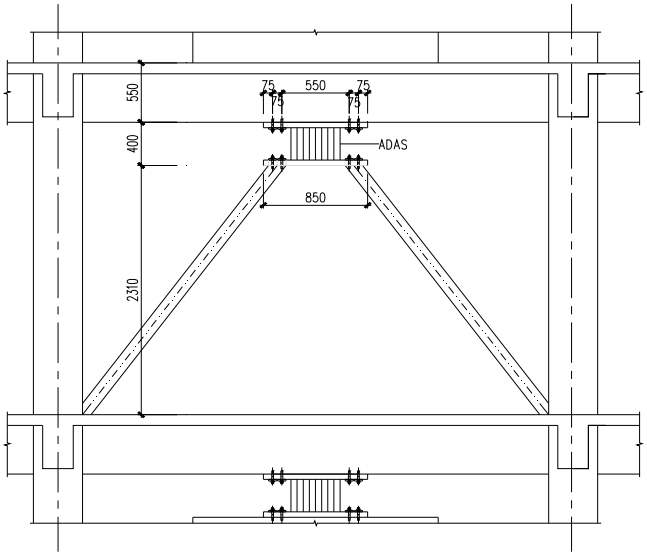

Figure 9.17 Configuration of ADAS damper

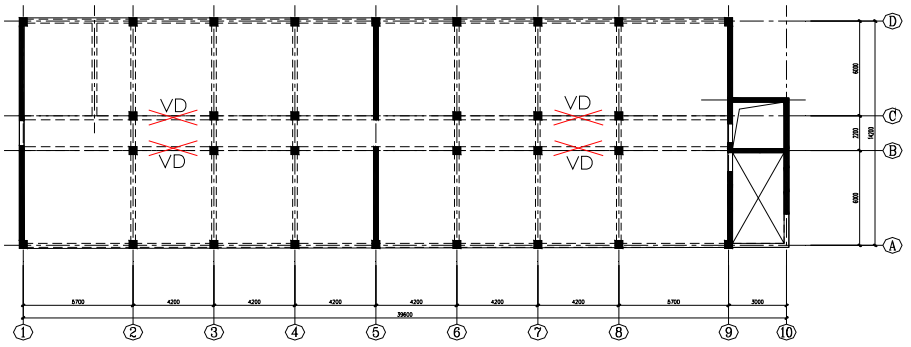

a) Story1~3

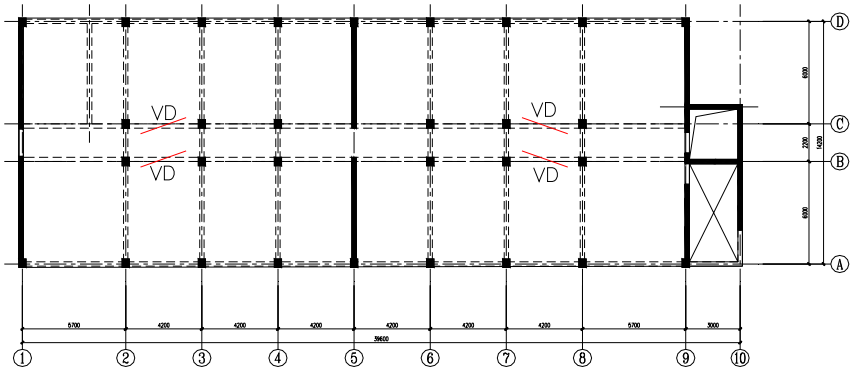

b) Story 4~10

Figure 9.18 Plan layouts of viscous or viscoelastic dampers

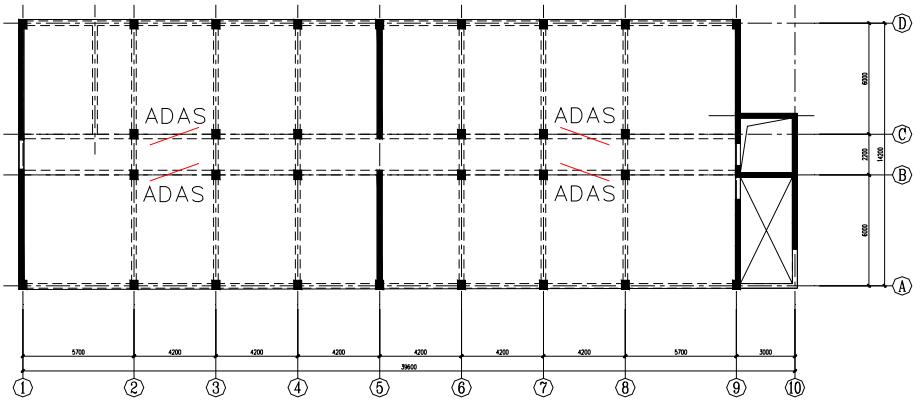

Figure 9.19 Plan layouts of ADAS dampers

9.6 Retrofitting results: comparison of the results from all configuration

The seismic response of the retrofitting building with BRBs, viscous dampers (VD), viscoelastic dampers (VED) and ADAS are performed through nonlinear response history analysis(RHA_NL) with the aforementioned accelerograms. And the seismic response of the original building without dissipation devices (ND) is taken as reference.

9.6.1 Dynamic properties

Table 9.7 list the first six periods of the structure retrofitted with different dissipation devices. If compared to the existing structure, one can easily find that the application of additional dissipative devices will add stiffness to original structure, especially the BRBs, and consequently reduce fundamental period. The additional dissipative devices are only required to control the structural response in X direction, so the periods for the mode along Y direction do not change.

Table 9.7 First six periods of the structure

Mode	ND [s]	BRBs (displacements based) [s]	BRBs (force based) [s]	VD [s]	ADAS [s]	VED [s]	Modal shape
1	1.13	0.69	0.73	0.95	0.89	1.00	X Translation
2	0.46	0.45	0.46	0.46	0.46	0.46	Y Translation
3	0.38	0.37	0.38	0.38	0.38	0.38	Torsion
4	0.31	0.22	0.22	0.26	0.25	0.29	X Translation
5	0.15	0.14	0.14	0.16	0.16	0.16	Y Translation
6	0.15	0.13	0.13	0.16	0.16	0.16	Torsion

The first two modal shapes of the existing building and retrofitted building are shown in Figure 9.21. It is observed that the modal shapes are almost the same for different cases.

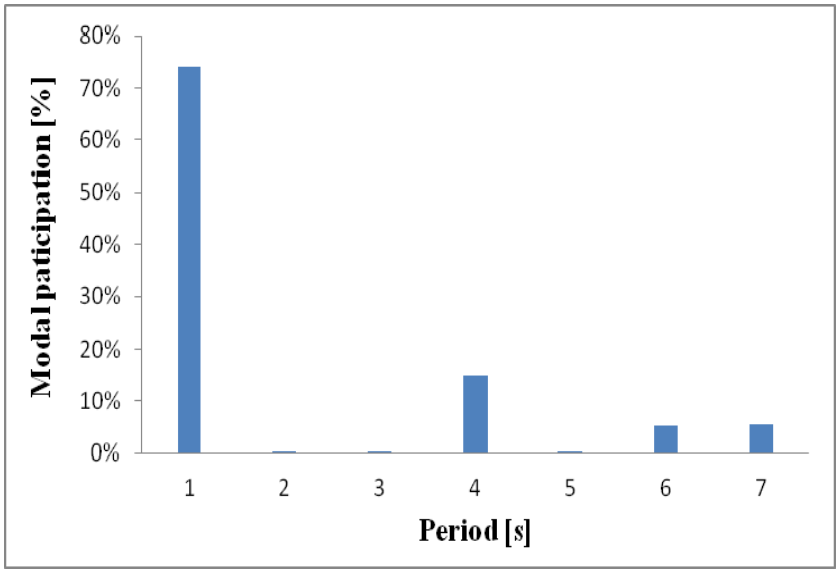

Figure 9.20 modal mass pacitipation: BRB designed through displacement base approach

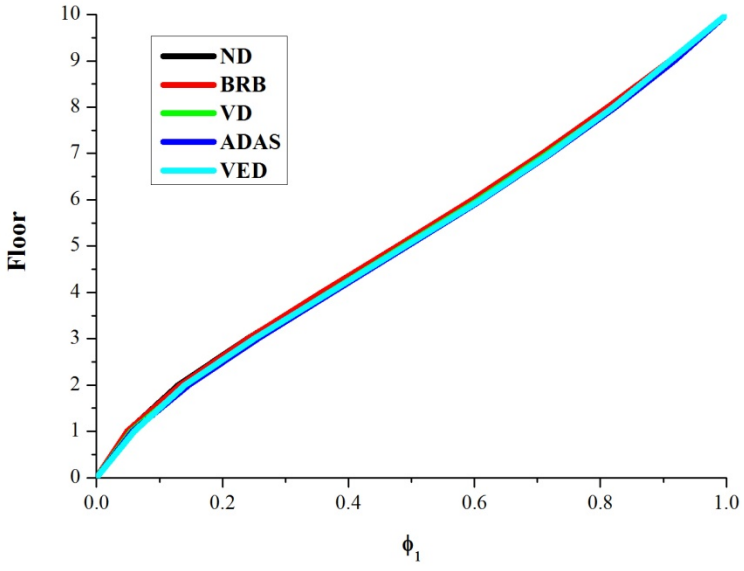

a) mode 1

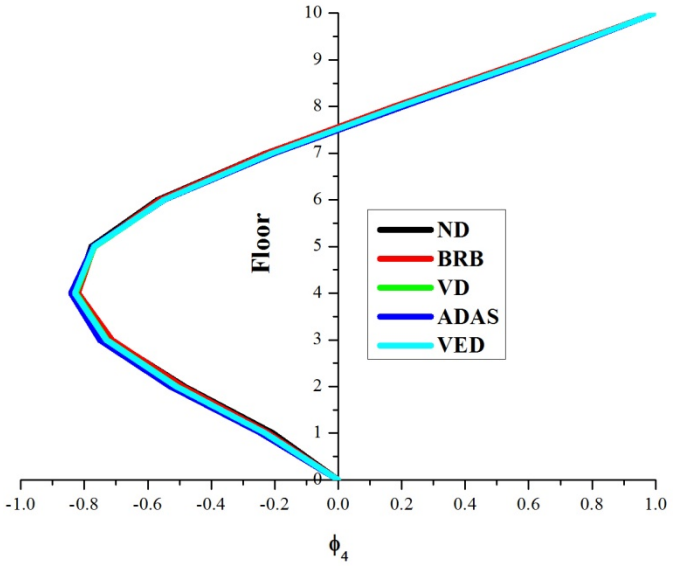

b) mode 4

Figure 9.21 modal shapes

9.6.2 Floor displacements and interstorey drifts

Figure 9.22 and Figure 9.23show the maximum roof displacement and inter-story drifts of the structure with different passive energy devices under minor or major earthquake scenarios. It can be seen that with dampers, the structural deformation curves apparently satisfy the code limitation of 1/800 for minor earthquakes and 1/100 for major earthquakes.

From these figures, it is easily seen that all three buildings of BRBs, VD, ADAS and VED have excellent structural performances and remarkable control effect compared to existing building. As expected, the retrofitting devices significantly reduce the drifts demands that the maximum story drifts are well controlled within the performance objective. In addition, it can be observed that the retrofitted building exhibit a more uniform height-wise distribution of inter-story drift, which means the retrofitting devices improve the vertical irregularity of the existing building. So, all energy dissipative devices can be appropriately designed to control seismic behavior of non-ductile concrete structures.

While dull-red lines are used in the case where the braces were sized according to a displacement based approach, green lines correspond to the force-based procedure. In general, it can be observed that the addition of

braces maximal reduces the story drifts compared to other dissipative devices. Nevertheless, in the case of the building braced according to a force based approach, the inter-story drifts demands exhibit large variations along height: sharply reduction of inter-story drifts for lower floors and slowly reduction for upper floors.

For alterative passive energy devices, the displacement control of VD is apparently superior to that of ADAS and VED under major earthquake. VD has better control effect in the story drifts under the major earthquake, while ADAS has better control effect under minor earthquake.

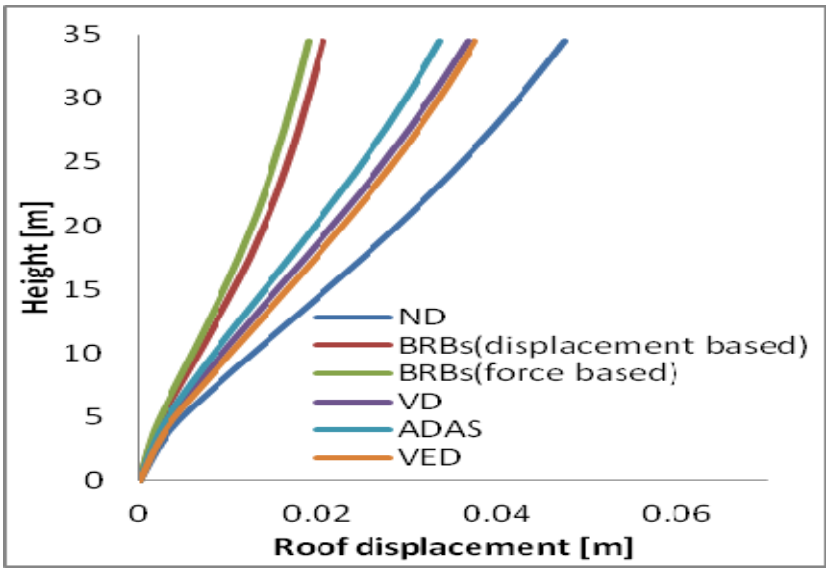

a) roof displacement

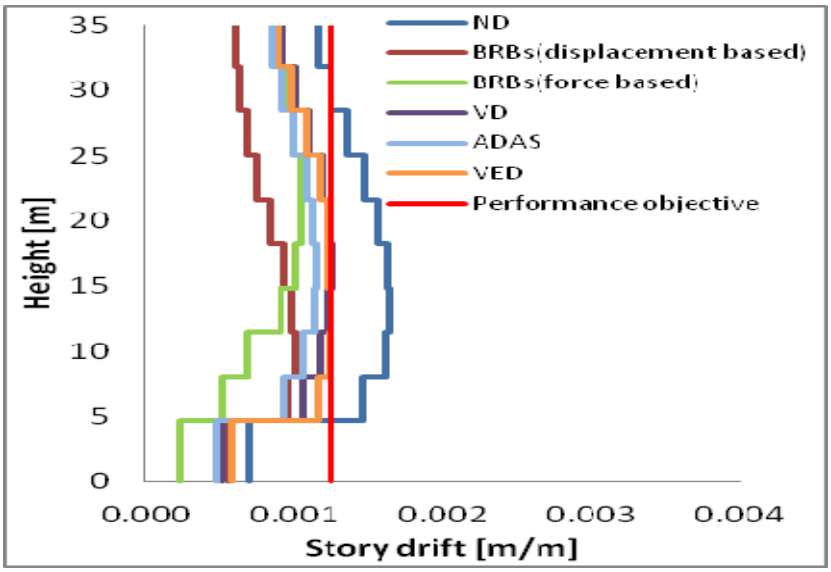

b) story drift

Figure 9.22 Seismic response of the retrofitting structure under minor earthquake

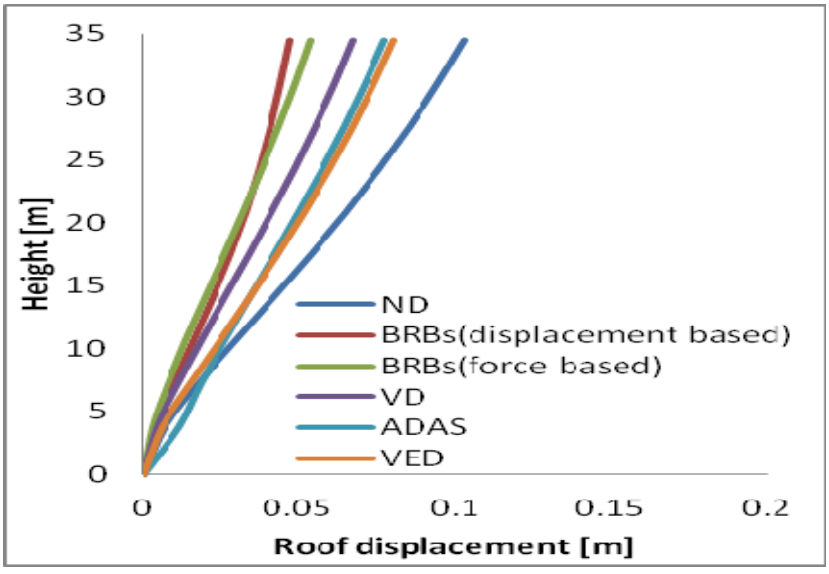

a) roof displacement

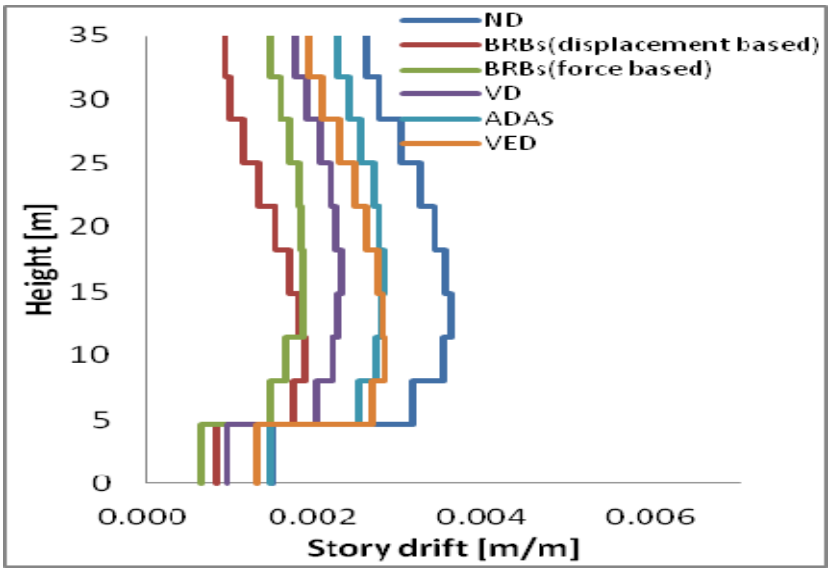

b) story drift

Figure 9.23 Seismic response of the retrofitting structure under major earthquake

9.6.3 Base shear

The first objective of retrofitting the existing building with dissipative devices is to obtain a defined target inter-storey drift, increasing both stiffness and dissipation; a second objective is the limitation of base shear increase. The maximum base shears of the existing and retrofitted buildings obtained from NL_RHA are shown in Figure 9.24. From the figure, the application of dissipative devices will increase the maximum the base shear compared to existing building. The BRBs designed according to displacement based approach would obtain the needed global energy dissipation with a limited increase of base shear (about ten percent) and thus reducing the need of foundation strengthening.

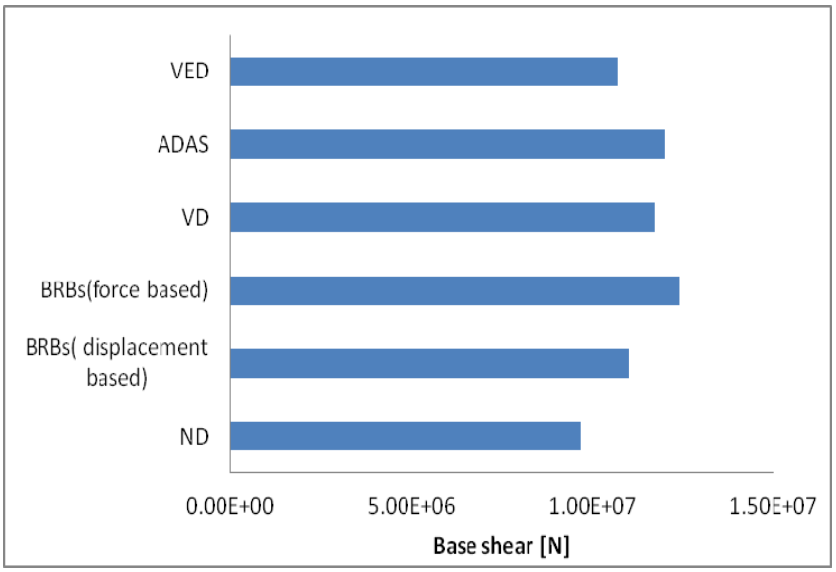

Figure 9.24 Maximum base shear

9.6.4 Energy dissipation

The mechanism of passive energy dissipation devices is through material yield to absorb earthquake induced energy as well as increase effective damping. The hysteresis loop of energy dissipation devices subjected to one given seismic action represents its capacity of energy dissipation. The larger of the hysteresis loop, more energy dissipated by the passive energy dissipation device.

Figure 9.26 and Figure 9.27 show the hysteresis loop of BRBs at the fifth floor, respectively. It is observed that the area of the BRB designed through displacement based approach is much larger than the area of hysteresis loop of BRB designed through force based approach. The displacement base approach is an explicit design procedure, during every step, the energy dissipated by the BRBs is considered to reduce the seismic demand to the floor displacement and interstorey drifts; during the force based procedure, the parameter control the design is the expecting force providing by the BRBs, the energy dissipated by BRB is not considered. As a result, the BRB is designed batter by the displacement based approach to make larger energy dissipation by BRBS.

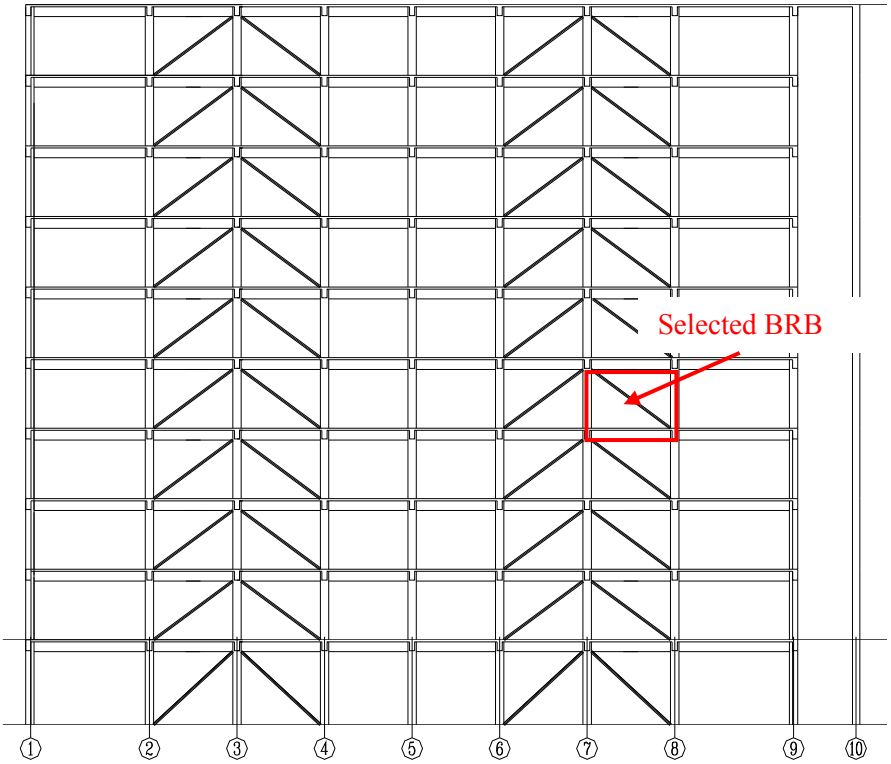

Figure 9.25 Location of the selected BRB to check the energy dissipation

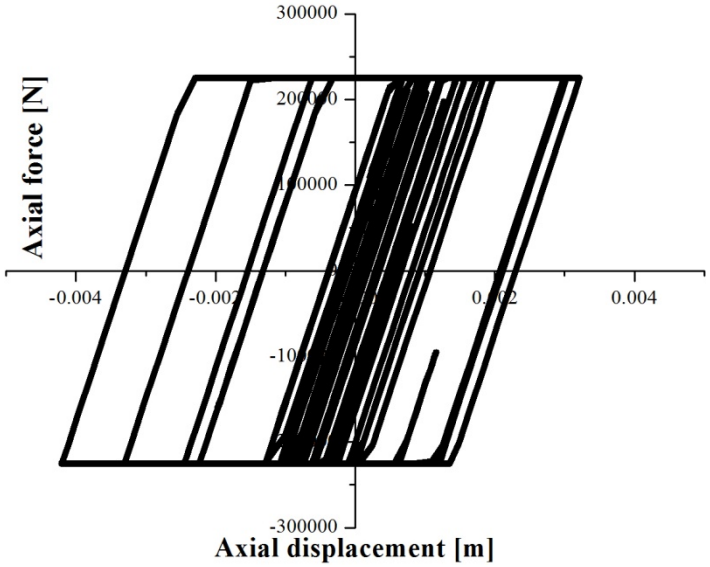

Figure 9.26 Axial foece-displacement of the BRB designed through displacement based approach

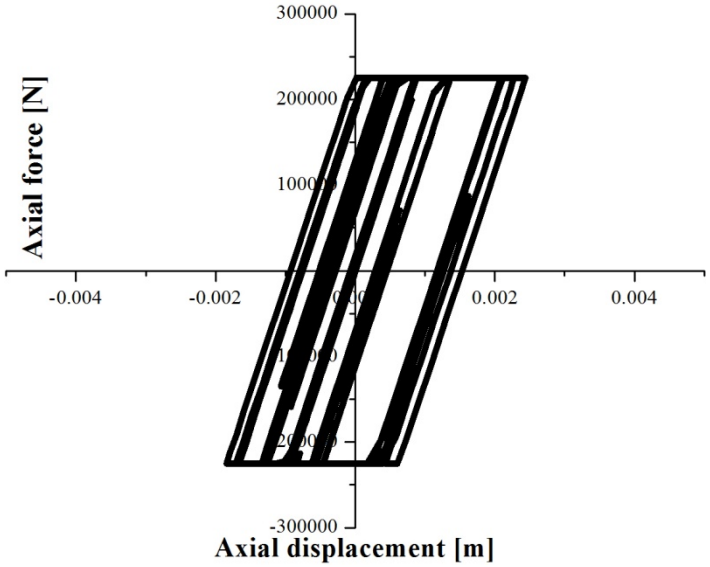

Figure 9.27 Axial force-displacement of the BRB designed through force based approach

The hysteresis loops of energy dissipation devices at the same position with BRBs through force based approach subjected to major earthquakes are shown from Figure 9.28 to Figure 9.30. It is clear that all devices enter its plasticity stage to dissipate energy through their plasticity deformation.

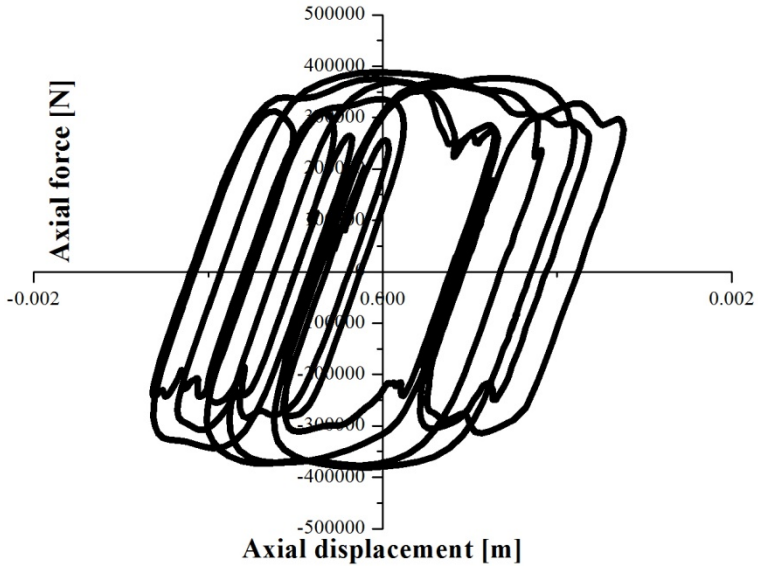

Figure 9.28 Axial force-displacement of the viscous damper designed through force based approach

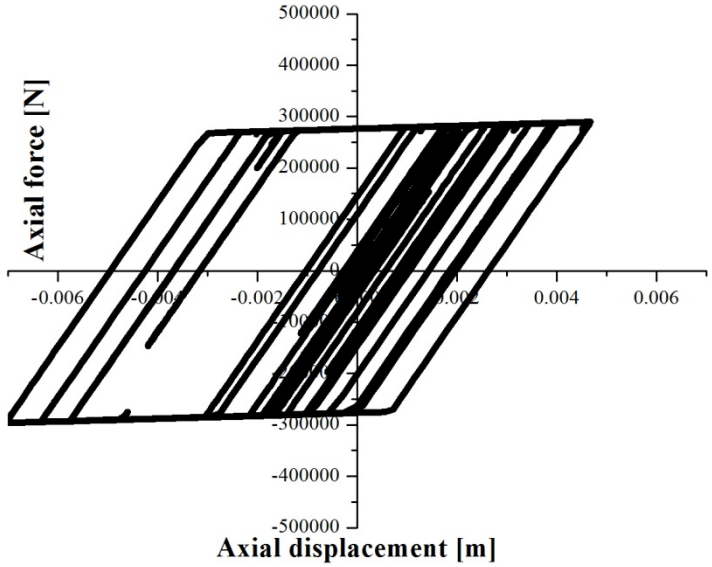

Figure 9.29 Axial force-displacement of the ADAS damper designed through force based approach

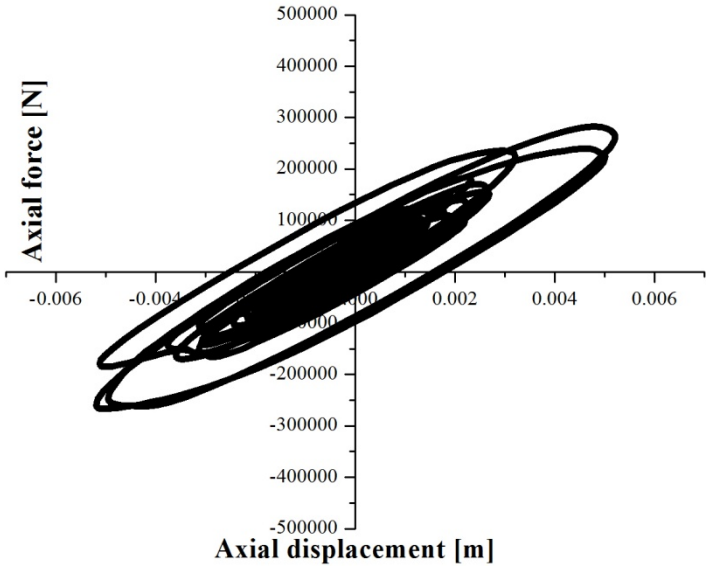

Figure 9.30 Axial force-displacement of the Viscoelastic designed through force based approach

9.6.5 Internal forces of the column

The results of Uriz and Whittaker (2001) showed that although the retrofitted structural global seismic performance was improved by dampers, the original beams, columns and foundations also need to be strengthened to ensure enough force transfer strength. Generally, a third objective is the limitation of axial force increase of the adjacent column. The application of passive energy dissipation devices will increase the internal axial force of the adjacent column as shown in Fig 21.

As expected, the building braced according to displacement based approach exhibit a limited and more uniform height-wise distribution of column axial forces, no need of column strengthening. The devices according to force based approach would sharply increase the axial force, especially the lower floors, in some cases the columns strengthen is required.

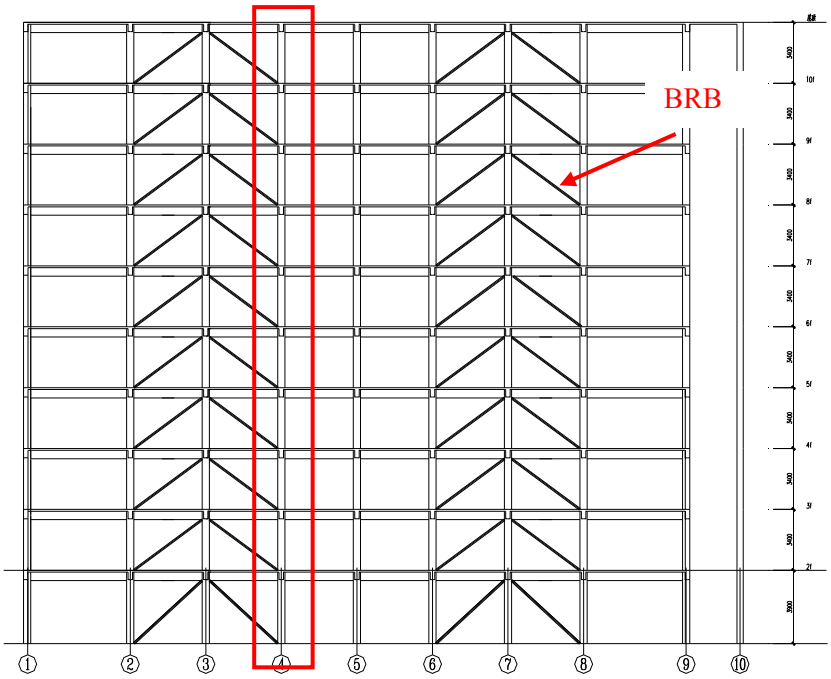

a) location of the columns to be checked

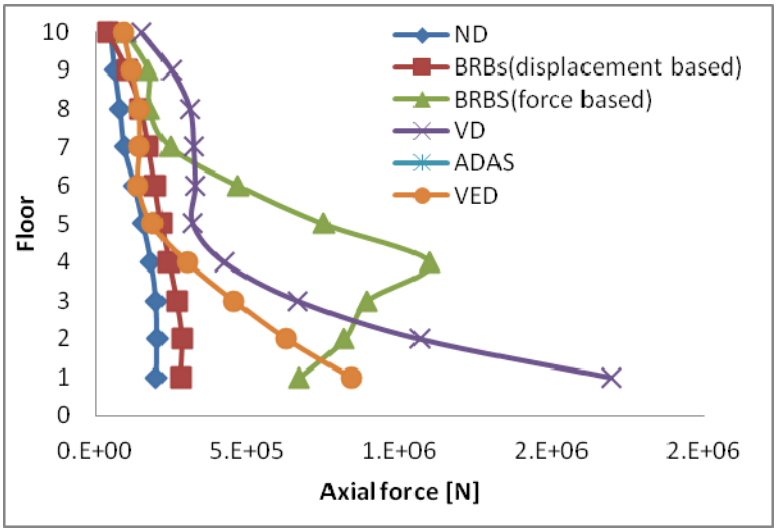

b) the axial force of columns

Figure 9.31 the internal force of the column

9.7 Conclusion

After recent strong earthquakes in china, the new Chinese seismic code issued in 2011 update protection categories for the school buildings and seismic intensity for some cities. As a result, a lot of schools need to be retrofitted to satisfy the new seismic requirements. The passive energy dissipation devices, such as the buckling restrained braces (BRBs) viscous dampers (VD), steel dampers (SD) and viscoelastic dampers (VED), are popular strategies for seismic retrofitting.

To facilitate the adoption and implementation of passive energy devices, the development of suitable design methods is necessary. The aim of the section is to evaluate feasibility of force-based and displacement-based approaches, and investigate the effectiveness of different passive energy devices. In this section, two popular design methods are applied to retrofit a school building located in shanghai, the comparisons of the two design methods and the seismic behavior of the retrofitting structure with different passive energy dissipation devices are discussed.

The displacement base approach is an explicit design procedure, during every step, the energy dissipated by the BRBs is considered to reduce the seismic demand to the floor displacement and interstorey drifts; during the force based procedure, the parameter control the design is the expecting force providing by the BRBs, the energy dissipated by BRB is not considered. As a result, the BRB is designed batter by the displacement based approach to make larger energy dissipation by BRBS: the material used in the retrofitted building through displacement approach is much less than the one through force base approach, the inter-story drifts demands through force base approach exhibit large variations along height: sharply reduction of inter-story drifts for lower floors and slowly reduction for upper floors.

The comparison on the seismic response through different energy dissipation devices show that although there are some differences in energy dissipation principle and mechanical properties, all the four types of dampers show excellent damping effect and evidently can be used to achieve the expected retrofitting objective if designed and distributed properly.

As to the retrofitted building retrofitted with viscous dampers, matallic dampers and viscoelastic dampers, the average inter-story drift can be reduced nearly one-half compared to the building without dampers. When four types of dampers are designed through force base approach, it is apparent that BRBs has better control effect of interstorey drifts,

especially under major earthqukes. The dampers can dissipate a large amount of energy and the force-displacement curves of dampers are very full. The ratio of actual damping forces to the expected damping force under moderate earthquake indicates that the initial damper parameter design is proper.

10. Conclusions and future developments

10.1 Conclusions

The main aim of the work described in this thesis is to investigate the nonlinear static procedures for analysis and retrofitting existing buildings with dissipative braces. The use of NSPs for the seismic assessment of plan regular buildings and bridges is widespread nowadays. Their good performance in such cases is widely supported by the extensive number of scientific studies described in the previous studies. The use of NSPs in the case of real existing structures has so far been studied by a limited number of authors. This fact limits the application of NSPs to assess current existing structures. In addition, these few studies were typically concentrated on the application and verification of a single nonlinear static procedure only, rather than providing a comparative evaluation of the different available methodologies describing their relative accuracy and limitations.

In order to provide a comparative evaluation of the commonly used procedures (CSM, DCM, N2 and MPA) describing their relative accuracy and limitations, a nine-story benchmark structure that can be simplified to 2D model and an existing R.C. frame, which presents both vertical and plan irregularities, are selected as case studies. The seismic response in terms of floor displacement and interstorey drifts were compared with the time-history nonlinear dynamic analysis. On the whole, predictions of floor displacement and interstory drifts by selected NSPs are close to values from inelastic dynamic analysis for the regular structure and the pure translation direction of the irregular structure. Along the translation and rotation strongly coupled direction of the irregular structure, for center of mass (CM), selected NSPs would underestimate the interstory drifts for upper floors; for rigid side (SX), largely underestimate the ineterstorey drifts; for flexible side (DX), the NSPs would well predict for the upper floors but largely underestimate for the low and middle floors. The accuracy of NSP is strongly related to the load pattern used in performing pushover analyses, which influences both the capacity curve and the distribution of seismic response along the height of the structure.

A displacement-based procedure to design dissipative bracings for the seismic protection of frame structures proposed by Bergami & Nuti (2013)

is applied to a medium rise existing r.c. building and a 3-story steel concentric braced frames (CBF). The use of conversional NSPs to be not suitable for the case of irregular building but, once this building is retrofitted, and therefore regularized, with a bracing system, the use of NSPs for seismic response of the braced structure is effective. Results obtained from the application of monomodal pushover have been compared with results from multimodal pushover for the braced struture: the effectiveness of the design procedure has been proved.

Comparing results in terms of base shear-top displacement between IDA, standard pushover and IMPA, the effectiveness of IMPA has been demonstrated: the multimodal capacity curve obtained with IMPA results closer to IDA curve. The effectiveness of IMPA is sensitive to the PGA (the distance between IMPA and IDA increases with PGA). Both IMPA and IDA curves show a hardening behavior, IDA results stiffer in the plastic range, while the pushover curve is mostly elasto-plastic. For the irregular structure, static pushover cannot fully catch up the torsional effect on base shear for the irregular structure, so there are bigger errors for the corners in the inelastic phase for the standard pushover analysis and IMPA. IMPA curve is closer to the IDA curve, and IMPA is suggested to predict the capacity curve for the structure during the design phase. IMPA can be consider a valid tool for professional use for the estimation of the capacity of structures and therefore for the definition of the capacity curve including the effect of higher significant modes.
To evaluate feasibility of force-based and displacement-based approaches and investigate the effectiveness of different passive energy devices, two popular design methods are applied to retrofit a school building located in shanghai, the comparisons of the two design methods and the seismic behavior of the retrofitting structure with different passive energy dissipation devices are discussed. The displacement base approach is an explicit design procedure, during every step, the energy dissipated by the BRBs is considered to reduce the seismic demand to the floor displacement and interstorey drifts; during the force based procedure, the parameter control the design is the expecting force providing by the BRBs, the energy dissipated by BRB is not considered. The BRBs designed through displacement based approach work better.The comparison on the seismic response through different energy dissipation devices show that although there are some differences in energy dissipation principle and

mechanical properties, all the four types of dampers show excellent damping effect and evidently can be used to achieve the expected retrofitting objective if designed and distributed properly.

10.2 Future developments

For the NSPs, the comparative studies limited to frame, it will be possible to extend these studies to other structures, for instance, the shear wall structure, the frame-shear wall structure, frame-tube structure and tube structure, etc. For the braced structure, braces yields before the structure, it will be possible to improve the pushover analysis for the braced structure considering the yielding of braces. NSPs cannot fully catch up the torsional effects, so there are bigger errors for the corners in the inelastic phase. Research is recommended to evaluate torsional effects to improve the application of NSPs on real structure.

For the design procedure of dissipative braces, a simple application to steel concentric braced frames (CBF); it will be possible to extend the application to real complex steel structure.

For the IMPA, static pushover cannot fully catch up the torsional effect on base shear for the irregular structure, so there are bigger errors for the corners in the inelastic phase. Research is recommended to investigate the evaluation of torsional effect on the base shear to improve the accuracy of IMPA on irregular structure.

For the application of passive energy dissipation devices, comparative study of different devices is evaluated on a simple structure, research is also recommended to develop a design procedure to optimize the choose of devices.

Reference

Aguirre.M, 1997. Earthquake-resistant structure: structural frame damper system –an approach to design. Proceedings of the ICE - Structures and Buildings,122(2): 165 –172.

Applied Technology Council. (1996). “Seismic evaluation and retrofit of concrete buildings”. Report ATC-40, Redwood City, California.

Ang, A.H.-S and Leon, D.De., (1997). Determination of optimal target reliabilities for design and upgrading of structures. Structural Safety; 19(1):19–103.

Bergami A.V., Nuti C. (2013). A design procedure of dissipative braces for seismic upgrating structures. Earthquakes and Structures, Vol. **4**, No. 1, 85-108.

Bergami A. V., Nuti C. (2014), “Design of dissipative braces for an existing strategic building with a pushover based procedure”, Journal of civil engineering and architecture, USA, accepted for publication.

Bracci, J. M., Kunnath, S. K. and Reinhorn, A. M.. Seismic performance and retrofit evaluation for reinforced concrete structures, J.Struct. Engng, ASCE 1997, 123 (1), 3-10.

Bobadilla, H., Chopra, A.K. and Eeri, M. (2008), "Evaluation of the MPA Procedure for Estimating Seismic Demands: RC-SMRF Buildings", Earthquake Spectra, 24(4), 827-845.

Berman JW, Brruneau M., (2009), “Cyclic testing of buckling restrained braced frame with uncostrained gusset connections”. Journal of Structural Engineering - ASCE, 135(12), 1499-1510.

Black CJ, Makris N., Aiken ID (2004), “Component testing, seismic evaluation and characterization of buckling restrained braces”. Journal of Structural Engineering - ASCE, 130(6), 880-894.

Casarotti, C. and Pinho, R. (2007), “An adaptive capacity spectrum method for assessment of bridges subjected to earthquake action”, Bulletin of Earthquake Engineering, 5(3), 377–390.

CEN （2004） “Eurocode 8: Design of structures for earthquake resistance. Part 1: general rules,seismic actions and rules for buildings,” EN 1998-1:2004 Comité Européen de Normalisation,Brussels, Belgium.

China Ministry of Construction (CMC). Code for seismic design of buildings (GB50011-20010). Beijing, China: China Architecture & Building Press; 20011.

China Ministry of Construction (CMC). Code for seismic design of

buildings (GB50011-2001). Beijing, China: China Architecture & Building Press; 2001.
China Ministry of Construction (CMC). Standard for classification of seismic protection of building constructions (GBJ11-1989). Beijing, China: China Architecture & Building Press; 2008 [in Chinese].Architecture & Building Press; 1989 [in Chinese].
Chopra, A.K. and Goel, R.K. (2002), "A modal pushover analysis procedure for estimating seismic demands for buildings", Earthquake Engineering & Structural Dynamics, 31(3), 561-582.
Chopra, A.K. and Goel, R.K. (2004), "A modal pushover analysis procedure to estimate seismic demands for unsymmetric-plan buildings", Earthquake Engineering & Structural Dynamics, 33(8), 903-927.
Chopra, A.K., Goe, R.K., and Chintanapakdee, C.,(2004). "Evaluation of a Modified MPA Procedure Assuming Higher Modes as Elastic to Estimate Seismic Demands" Earthquake Spectra, 20(3): 757-778.
Chopra, A. K., and Chintanapakdee, C., (2004). Evaluation of modal and FEMA pushover analyses: Vertically ''regular'' and irregular generic frames, Earthquake Spectra 20 (1), 255–271.
Ciampi, V., (1991). "Use of energy dissipating devices, based on yielding of steel, for earthquake protection of structures", Proceedings of Protezione sismica degli edifici. Ancona, Italy.
Ciampi, V., De Angelis, M., Paolacci, F., (1995). "Design of yelding or friction-based dissipative bracings for seismic protection of buildings". Engineering Structures, Vol. 17, No.5.Pp.381-391.
Constantinou, M.C., Soong, T.T., Dargush, G.F., (1998). "Passive energy dissipation systems for structural design and retrofit". MCEER - State University of New York at Buffalo.
D'Ambrisi A., Stefano M., Tanganelli M. Use of Pushover Analysis for Predicting Seismic Response of Irregular Buildings: a Case Study. Journal of Earthquake Engineering. 2009, Vol. 13, pp. 1089-1100.
Dolce, M., Cardone, D., Marnetto, R., (2000), "Implementation and Testing of Passive Control Devices Based on Shape Memory Alloys". Earthquake Engineering and Structural Dynamics, 29 (7), 945-968.
Dolce, M., Cardone, D., Ponzo, F.C., (2001). "Retrofitting of R/C framed structures through SMA-based energy dissipating and re-centering braces". Proceedings of 7th International Seminar on Seismic Isolation, Passive Energy Dissipation and Active Control of Vibrations of Structures. Assisi, Italy, october.
Di Sarno L., Manfredi G. (2010). "Seismic retrofitting with buckling

restrained braces: Application to an existing non-ductile RC framed building". Soil Dynamics and Earthquake Engineering, 30, 1279-1297.
Engineering Center, Stanford University, Stanford, Calif. Gupta, A. and Krawinkler, H. (2000). Estimation of seismic drift demands for frame structures, Earthq. Engrg. Struc. Dyn., 29:1287-1305.
Erduran E., Ryan K. Effects of torsion on the behaviour of peripheral steel-braced frame systems. Earthquake Engineering and Structural Dynamics. 2010, DOI:10.1002/eqe.1032.
Fajfar, P. and Fischinger, M. (1988). N2—a method for nonlinear seismic analysis of regular structures, Proc., 9th World Conf. Earthq. Engrg., 5:111-116, Tokyo-Kyoto, Japan.
Fajfar P., Gaspersic P., Drobnic D. (1997). A simplified nonlinear method for seismic damage analysis of structures. Seismic design methodologies for the next generation of codes. pp. 183-194. Balkema, Rotterdam: P. Fajfar and H. Krawinkler.
Fajfar P. (1999). "Capacity spectrum method based on inelastic spectra". Earthquake Engineering and Structural Dynamics, 28, 979-993.
Fajfar P., Gaspersic P. (2000). "The N2 method for the seismic damage analysis for RC buildings". Earthquake Engineering and Structural Dynamics, 25, 23-67.
FEMA-274, (1997). "NEHRP Commentary on the Guidelines for the Seismic Rehabilitation of Buildings". Federal Emergency Management Agency Publication, U.S.A., 274.
FEMA – ASCE 356 (2000). "Prestandard and Commentary for the Seismic Rehabilitation of Buildings". Washington, DC, 2000.
Filiatrault, A., Cherry, S., (1988). "A simplified seismic design procedure for friction damped structures". Procedings of Fourth U.S. National Conference on Earthquake Engineering, 3, Palm Springs, U.S.A..
Filiatrault, A., Cherry, S., (1990). "Seismic design spectra for friction damped structures". Journal of Structural Engineering, 116(5), 1334-1355.
Freeman, S.A. (1998), "The Capacity Spectrum Method as a Tool for Seismic Design", Proceedings of the 11th European Conference on Earthquake Engineering, Paris, France, January.
Geol, R.K. and Chopra, A.K. (2004), "Evaluation of Modal and FEMA Pushover Analyses SAC Buildings", Earthquake Spectra, 20(1), 225-254.
Gupta, A. and Krawinkler, H. (1999). Seismic demands for performance evaluation of steel moment resisting frame structures (SAC Task 5.4.3),

Report No. 132, John A. Blume Earthquake.
Gupta, B. and Kunnath, S. K. (2000). Adaptive spectra-based pushover procedure for seismic evaluation of structures, Earthquake. Spectra, 16(2):367-392.
Han, S.W. and Chopra, A.K. (2006), "Approximate incremental dynamic analysis using the modal pushover analysis procedure", Earthquake Engineering & Structural Dynamics, 35(15), 1853-1873.
Kim J., Choi H. (2004). "Behavior and design of structures with buckling-restrained braces". Engineering Structures 26, 693-706.
Kim J, Choi H(2004). Energy-based seismic design of structures with buckling restrained braces. Steel Compos Struct ,4(6):437–52.
Lee D, Taylor DP. Viscous damper development and future trends. Struct Des Tall Spec 2001;10(5):311–20
Leelataviwat S, Goel SC, and Stojadinovic B (2002). Energy-based seismic design of structures using yield mechanism and target drift. J Struct Eng, 128(8): 1046–54.
Lin, J.L., Tsai, K.C. and Chuang, M.C. (2012), "Understanding the trends in torsional effects in asymmetric-plan buildings", Bulletin of Earthquake Engineering, 10(3), 955-965.
Lin YY, Tsai MH, Hwang JS, Chang KC. Direct displacement-based design for building with passive energy dissipation systems. Eng Struct 2003;25(1):25–37.
Lu XL. Seismic design guidelines for tall buildings beyond the scope of design codes. Shanghai, China: Shanghai Construction Engineering Standard Administration Office; 2009.
Luco,N and Cornell, C.A., (2007). Structure-Specific Scalar Intensity Measures for Near-Source and Ordinary Earthquake Ground Motions. Earthquake Spectra, 23(2):357-392.
Mahdi, T., and Gharaie, V. S. (2011), "Plan irregular RC frames Comparison of pushover with nonlinear dynamic analysis", Asian journal of civil engineering (building and housing), 12(6), 679-690.
Mazzolani F.M., (2006). "Seismic upgrading of RC buildings by advanced techniques". The ILVA-IDEM Research Project, Polimerica Publisher. Italy.
Mazzolani F.M., (2008). "Innovative metal systems for seismic upgrading of RC structures". Journal of Constructional Steel Research, 64, 882-895.
Mehanny, SS and Deierlein GG., (2000). Modeling and assessment of seismic performance of composite frames with reinforced concrete columns and steel beams. Report No. 136, The John A.Blume Earthquake

Engineering Center, Stanford University, Stanford.
Moghadam, A. S. and Tso, W.K. (1996), “Damage assessment of eccentric multistory buildings using 3-D pushover analysis”, Proceedings of the 11th World Conference on Earthquake Engineering, Acapulco, Mexico, June
Moghadam, A.S. and Tso, W.K. (2000). “3-D push-over analysis for damage assessment of buildings”, JSEE, 2(3), 23-31.
Ohtori, Y, Christenson, R.E., Spencer, Jr. B.F. and Dyke, S.J., (2000). Benchmark Control Problems for Seismically Excited Nonlinear Buildings, Notre Dame University, Indiana.
Palazzo G., López-Almansa F. Cahís X., Crisafulli F. (2009). “A low-tech dissipative buckling restrained brace. Design, analysis, production and testing”. Engineering Structures 31, 2152-2161.
Ponzo F.C., Dolce M., Vigoriti G., Arleo G., Di Cesare A., (2009). “Progettazione di controventi dissipativi a comportamento dipendente dagli spostamenti”. Proceedings of XIII Convegno ANIDIS L' ingegneria Sismica in Italia. Bologna, Italy.
Riddell R and Garcia JE (2001). Hysteretic energy spectrum and damage control. Earthquake Eng Struct Dyn, 30(12):1791–816.
Sabelli R., Mahin S., Chang C.(2003), “Supplemental energy dissipation: state-of-the-art and state-of-the-practice”. Engineering Structures, 25(5), 655-666.
Saiidi M., Sozen M, 1981. Simple nonlinear seismic analysis of R/C structures. Journal of Structural Division, ASCE, 107: 937-952.
Shome, N, Cornell,CA, (1999). Probabilistic seismic demand analysis of nonlinear structures. Report No. RMS-35, RMS Program, Stanford University, Stanford.
SEAOC/AISC (2005). “Recommended provisions for buckling-restrained braced frames”. Structural Engineers Assoc. of California/American Inst. Of Steel Const.
Soong T.T., Spencer Jr B.F., (2002), “Supplemental energy dissipation: state-of-the-art and state-of-the-practice”. Engineering Structures, 24, 243-259.
T.T. Soong and B.F. Spencer Jr.,2002. Supplemental energy dissipation: state-of-the-art and state-of-the practice. Engineering Structures 24:243–259
Vulcano A., Mazza F., (2002). “A simplified procedure for the seismic design of framed buildings with dissipative braces”. Proceedings of 12th

European Conference on Earthquake Engineering. London, UK.
Wen-Hsiung, L., Chopra, A.K., (2003). “Eartquake response of elastic single-degree-of-freedom systems with nonlinear visco-elastic dampers”. Journal of engineering Mechanics-ASCE, June 2003.
Whittaker, A.S., Bertero, V., Alonso, J. and Thompson, C., (1989). “Earthquake Simulator Testing of Steel Plates Added Damping and Stiffness Elements”. Technical Report EERC- 89/02, University of California, Berkeley, CA.
Xie W. (2005) “State of the art of buckling-restrained braces in Asia”. Journal of Constructional Steel Research, 61(6), 727-748.
Zhang R.H., Soong T.T. (1992). “Seismic design of viscoelastic dampers for structural applications”, ASC, J. of Structural Engineering 118(5), 1375-1392.
Yoshino T, Karino Y. Experimental study on shear wall with braces: Part 2. Summaries of technical papers of annual meeting, vol. 11. Architectural Institute of Japan, Structural Engineering Section; 1971. p. 403–4 [in Japanese].
Vamvatsikos, D. and Cornell, C.A. (2002), “Incremental dynamic analysis”, Earthquake Engineering & Structural Dynamics, 31(3), 491-514.
Yang JN, Lin S, Kim JH, Agrawal AK. Optimal design of passive energy dissipation systems based on H1 infinity and H2 performances. Earthq Eng Struct D 2002;31(4):921–36.
Y.Zhou, X.L., Lu, D.G., Weng, and R.F., Zhang(2012). A practical design method for reinforced concrete structures with viscous dampers. Engineering Structures 39: 187–198.